

**MODELING BEAM-LIKE SPACE TRUSSES WITH NONLINEAR JOINTS WITH APPLICATION TO CONTROL**

**Mark S. Webster**

M. S. Stanford University (1983)

B. S. University of Maryland (1982)

Submitted to the Department of Aeronautics and Astronautics in partial fulfillment of the requirements for the degree of

**DOCTOR OF PHILOSOPHY**

at the

**MASSACHUSETTS INSTITUTE OF TECHNOLOGY**

June, 1991

© Massachusetts Institute of Technology

Signature of Author \_\_\_\_\_  
Department of Aeronautics and Astronautics  
May 19, 1991

Certified by \_\_\_\_\_  
Professor Wallace Vander Velde, Thesis Supervisor  
Professor of Aeronautics and Astronautics

Certified by \_\_\_\_\_  
Professor John Dugundji  
Professor of Aeronautics and Astronautics

Certified by \_\_\_\_\_  
Professor Edward Crawley  
Professor of Aeronautics and Astronautics

Certified by \_\_\_\_\_  
Professor Andreas Von Flotow  
Professor of Aeronautics and Astronautics

Accepted by \_\_\_\_\_  
Professor Harold Y. Wachman  
Chairman, Department Graduate Committee

MASSACHUSETTS INSTITUTE  
OF TECHNOLOGY

JUN 12 1991

LIBRARIES

Ann

# **MODELLING BEAM-LIKE SPACE TRUSSES WITH NONLINEAR JOINTS WITH APPLICATION TO CONTROL**

**Mark S. Webster**

Submitted to the Department of Aeronautics and Astronautics in May, 1991, in  
partial fulfillment of the requirements of Doctor of Philosophy

## **ABSTRACT**

Large space structures are normally characterized by high order finite element models. In this thesis, long slender truss structures are modeled with both continuous beams and equivalent beam finite elements using an equivalent energy approach. The Timoshenko equivalent beam, which accounts for shear and rotary inertia effects, models the beam-like behavior of the truss better than the Bernoulli-Euler equivalent beam. The finite element equivalent beam has an even more accurate approach and maps the contributions of each truss element to the stiffness of the truss.

If the structure is jointed, the joints may display nonlinear force-displacement behavior. The behavior of a multi-degree of freedom structure may be modeled using describing functions as a quasi-linearization of the force-displacement relation in the joint. The results of this method agree very well with those of time integration of the nonlinear equations for a simple two-beam one joint structure. Describing functions are calculated for the force-displacement relation across an entire joint-strut-joint truss element. The resulting coefficients are used as the nonlinear stiffness and damping terms of the nonlinear truss.

The equivalent beam approach is combined with the describing function method to produce the nonlinear equivalent beam model. This is used to model simple two-dimensional truss models undergoing sinusoidal excitation. These models show typical nonlinear response characteristics and give an idea of the global behavior of structures with specific nonlinear joints.

The dual-input describing function is combined with the equivalent beam model to model nonlinear structure under gravity type pre-loads. The response of the pre-loaded structures can show marked differences from the non pre-load condition when the pre-load is large enough that the bias displacements of some of the joints lie in the nonlinear range.

Experimental sine sweeps of NASA/Langley Mini-Mast show nonlinear behavior, particularly in the vicinity of the first torsion mode. This behavior takes the form of decreasing resonant frequency and increasing damping with increasing amplitude of response. An analytical joint described as a natural joint exhibits these global dynamic characteristics when included in a simple two-dimensional truss model. This joint gives results very similar to experimental data when included in a nonlinear equivalent beam finite element model of the Mini-Mast.

The nonlinear equivalent beam finite element model is also used to analyze the response of controlled structures with control systems designed for the linear plant model. The describing function representation of the nonlinear joints is used to characterize the plant model uncertainty due to nonlinearity. These results show that disturbance rejection properties are maintained when full-state feedback is available.

## Acknowledgements

I'd like to thank my thesis advisor, Professor Wallace Vander Velde, for all the help and guidance that he has given me in doing my research and preparing this thesis. His knowledge, experience and good humor were invaluable. I'd like to thank the rest of my committee for their help with my sometimes tiresome questions. I'd like to thank Professor Paul Lagace for being my guide through my first year here and for providing a teaching role model for my future academic career.

I want to thank all the people in the Space Engineering Research Center for putting up with me for all these years and for helping me by answering some of my questions. In this last regard, I want to thank Dr. Tienie van Schoor for introducing me to the nonlinear world and helping me with the computing. Doug MacMartin helped me out with understanding the control aspects of my problems and provided the algorithms that I used. I also want to thank Bubba (who already has so many references that he won't need another) for going through this process first and beating down the path.

Even though they may not ever read this, I want to thank all the people from noon-time basketball in Dupont for providing the distraction that kept me sane through the years and improving my basketball skills at the same time. In the same vein, I want to thank Leo Tolstoy, John Barth and the other authors who also helped me keep my sanity.

I want to thank my family, who gave me the desire and abilities to succeed at the task that I had set for myself. Their initial guidance and continued support has made this whole effort a little easier.

I also thank my lovely wife, Wendy Warren. Without her love, affection, tolerance and friendship, none of this would have been possible or worthwhile.

Finally, I want to dedicate this thesis to my grandmother, Katherine Hanna.

## Table of Contents

<b>Abstract</b>	<b>1</b>
<b>Acknowledgements</b>	<b>2</b>
<b>Table of Contents</b>	<b>3</b>
<b>List of Figures</b>	<b>5</b>
<b>List of Tables</b>	<b>9</b>
<b>Nomenclature</b>	<b>10</b>
<b>Chapter 1 Introduction</b>	<b>13</b>
1.1 Introduction	13
1.2 Review of Past Work	15
1.3 Thesis Overview	16
<b>Chapter 2 Accuracy of Describing Function Models</b>	<b>19</b>
2.1 Introduction	19
2.2 Describing Function Method	19
2.3 Two-Beam Structure and Equations of Motion	21
2.4 Time Integration of Equations of Motion	22
2.5 Comparison of Models	23
<b>Chapter 3 Modeling Trusses as Beams</b>	<b>30</b>
3.1 Introduction	30
3.2 Continuum Beam Model	31
3.3 Equivalent Finite Element Beam Model	35
3.4 Determination of Truss Element Stiffness	43
3.5 Comparison of Models	44
<b>Chapter 4 Nonlinear Equivalent Beam Finite Element Model</b>	<b>50</b>
4.1 Introduction	50
4.2 Truss Element Model	51
4.3 Solution Technique	54

4.4	Simple Examples - One Bay Cantilevered Truss	57
4.5	Simple Examples - Five Bay Cantilevered Truss	68
4.6	Summary	83
<b>Chapter 5</b>	<b>Modeling Nonlinear Structures With a Pre-Load</b>	<b>85</b>
5.1	Introduction	85
5.2	Dual-Input Describing Function	85
5.3	Simple Example - Five Bay Model	89
<b>Chapter 6</b>	<b>Mini-Mast Structure and Model</b>	<b>100</b>
6.1	Introduction	100
6.2	Mini-Mast Test Facility	100
6.3	Sine Sweep Test Set-Up and Results	108
6.4	Analytical Model	109
6.5	Summary	118
<b>Chapter 7</b>	<b>Nonlinear Equivalent Beam Model for Control Design and Analysis</b>	<b>119</b>
7.1	Introduction	119
7.2	State Equations for Nonlinear System	120
7.3	Full State Feedback	121
7.4	Model Based Compensators	137
7.5	Limit Cycles	144
7.5	Summary	144
<b>Chapter 8</b>	<b>Conclusions</b>	<b>146</b>
8.1	Summary and Conclusions	146
8.2	Recommendations for Future Work	149
	<b>Bibliography</b>	<b>150</b>
	<b>Appendix A</b>	<b>153</b>
	<b>Appendix B</b>	

## List of Figures

2.1	Two beam structure with nonlinear rotary joint [Bowden(1988)]	21
2.2	Comparison of Describing Function Model and Time Integration for Cubic Spring	26
2.3	Gain Change Nonlinear Relation	26
2.4	Two Beam Structure with Gain Change Nonlinearity Frequency ResponseHardening Spring	28
2.5	Two Beam Structure with Gain Change Nonlinearity Frequency Response-Softening Spring.	28
3.1	Two Dimensional Truss Bay	32
3.2	Truss Element With Linear Joints	43
3.3	First Frequency for a Cantilevered Truss with Varying Number of Bays for Various Models	45
3.4	Percentage Error of Equivalent Beam Models From Truss Finite Element Model	46
3.5	Mode Shapes of the Finite Element Models for Cantilevered Truss with Five Bays	49
4.1	Joint-Strut-Joint Schematic	51
4.2	One Bay Cantilevered Truss With Equivalent Beam Model	57
4.4	Mode Shapes of One Bay Cantilevered Truss	59
4.5	Response of One Bay Cantilevered Truss modeled by Equivalent Beam with Linear Joints to Sinusoidal Forcing in Transverse Direction	60
4.6	Truss Element with Cubic Spring Joints in Parallel with Linear Joints	61
4.7	Response of One Bay Truss with Cubic Spring Joints to Sinusoidal Excitation with Backbone Curves	64
4.8	Response to Transverse Sinusoidal Excitation of One Bay Truss with Hardening Spring Gain Change Joints Modeled by Equivalent Beam	66
4.9	Response to Transverse Sinusoidal Excitation of One Bay Truss with Softening Spring Gain Change Joints Modeled by Equivalent Beam	67
4.10.	2-D Five Bay Cantilevered Truss with Equivalent Beam Model	68
4.11	Response at End of Bay 2 to Transverse Sinusoidal Forcing at Tip of Five Bay Truss with Linear Joints Modeled by Equivalent Finite Element Beam	69

4.12	Response at End of Truss to Transverse Sinusoidal Forcing at Tip of Five Bay Truss with Linear Joints Modeled by Equivalent Finite Element Beam	70
4.13	Response at End of Bay 2 to Transverse Sinusoidal Forcing at Tip of Five Bay Truss with Cubic Spring Joints Modeled by Nonlinear Equivalent Beam	72
4.14	Response at End of Truss to Transverse Sinusoidal Forcing at Tip of Five Bay Truss with Cubic Spring Joints Modeled by Nonlinear Equivalent Beam	73
4.15	Response at End of Bay 2 to Transverse Sinusoidal Forcing at Tip of Five Bay Truss with Hardening Gain Change Joints Modeled by Nonlinear Equivalent Beam	75
4.16	Response at End of Truss to Transverse Sinusoidal Forcing at Tip of Five Bay Truss with Hardening Gain Change Joints Modeled by Nonlinear Equivalent Beam	76
4.17	Response at End of Bay 2 to Transverse Sinusoidal Forcing at Tip of Five Bay Truss with Softening Gain Change Joints Modeled by Nonlinear Equivalent Beam	77
4.18	Response at End of Truss to Transverse Sinusoidal Forcing at Tip of Five Bay Truss with Softening Gain Change Joints Modeled by Nonlinear Equivalent Beam	78
4.19	Natural Nonlinear Joint	79
4.20	Response at End of Bay 2 to Transverse Sinusoidal Forcing at Tip of Five Bay Truss with Natural Joints Modeled by Nonlinear Equivalent Beam	80
4.21	Response at End of Truss to Transverse Sinusoidal Forcing at Tip of Five Bay Truss with Natural Joints Modeled by Nonlinear Equivalent Beam	81
4.22	Sliding Pin Nonlinearity	82
4.23	Response at End of Bay 2 to Transverse Sinusoidal Forcing at Tip of Five Bay Truss with Sliding Pin Joints Modeled by Nonlinear Equivalent Beam	84
4.24	Response at End of Truss to Transverse Sinusoidal Forcing at Tip of Five Bay Truss with Sliding Joints Modeled by Nonlinear Equivalent Beam	85
5.1	Five Bay Truss with Vertical Pre-load	90
5.2	Comparison of Response to Sinusoidal Forcing at Bay 2 of Five Bay Truss with Hardening Gain Change Joints With Pre-load (solid line) and No Pre-load (dotted line)	92
5.3	Comparison of Response to Sinusoidal Forcing at End of Five Bay Truss with Hardening Gain Change Joints With Pre-load (solid line) and No Pre-load (dotted line)	93

5.4	Comparison of Backbone Curves at Bay 2 of Five Bay Truss with Hardening Gain Change Joints With Pre-load (solid line) and No Pre-load (dotted line)	94
5.5	Comparison of Backbone Curves at End of Five Bay Truss with Hardening Gain Change Joints With Pre-load (solid line) and No Pre-load (dotted line)	95
5.6	Comparison of Backbone Curves of Five Bay Truss with Hardening Gain Change Joints With Large Pre-load (solid line) and No Pre-load (dotted line)	96
5.7	Comparison of Sinusoidal Response Curves of Five Bay Truss with Hardening Gain Change Joints With Large Pre-load (solid line) and No Pre-load (dotted line)	96
5.8	Comparison of Sinusoidal Response at Tip of Five Bay Truss with Natural Joints for Pre-Load (solid line) and No Pre-load (dotted line).	98
5.9	Comparison of Backbone Curves at Bay 2 of Five Bay Truss with Natural Joints for Pre-Load (solid line) and No Pre-load (dotted line).	99
6.1	Mini-Mast Test Facility at NASA/Langley Research Center	102
6.2	Partially Deployed Mini-Mast	103
6.3	Tip Plate of Mini-Mast with Three Torque Wheels Attached	106
6.4	Kaman Displacement Locations on Mini-Mast.	107
6.5	Transfer Function from X-Axis Torque Wheel to Tip Displacement Sensor in Vicinity of First Bending Mode, Mini-Mast Experimental Data	110
6.6	Transfer Function from Z-Axis Torque Wheel to Tip Displacement Sensor in Vicinity of First Torsion Mode, Mini-Mast Experimental Data	110
6.7	Global Static Loading Behavior of the Mini-Mast in Torque.	111
6.8	Mini-Mast Bay 1 and Equivalent Beam Model Showing Degrees of Freedom.	111
6.9	Transfer Function from Z-Axis Torque Wheel to Tip Displacement Sensor in Vicinity of First Torsion Mode, Mini-Mast Nonlinear Equivalent Beam Analytical Model with Gain Change Joints	115
6.10	Transfer Function from Z-Axis Torque Wheel to Tip Displacement Sensor in Vicinity of First Torsion Mode, Mini-Mast Nonlinear Equivalent Beam Analytical Model with Natural Joints	115
6.11	Force-Axial Displacement Curve of Mini-Mast Diagonal Truss Element with Pre-Buckling Behavior for Maximum Range of Motion Observed in Analytical Model with Axial Load Offset, $e=0.5$ cm.	117
7.1	Simple Truss for Control Evaluation	120



7.2	Transfer Function from Transverse Excitation to Tip Displacement for Structure with Gain Change Joints and LQR Control with $\rho=1$ and Full Control Authority	124
7.3	Transfer Function from Trans Excitation to Tip Displacement for Structure with Gain Change Joints and LQR Control with $\rho=.01$ and Full Control Authority	125
7.4	Transfer Function from Transverse Tip Excitation to Displacements for Structure with Gain Change Joints and LQR Control with $\rho=.01$ and Partial Control Authority	126
7.5	Transfer Function from Transverse Excitation to Tip Displacement for Structure with Gain Change Joints and LQR Integrator Control with $\rho=1$ and Partial Control Authority	127
7.6	Transfer Function from Transverse Excitation to Tip Displacement for Structure with Gain Change Joints and LQR Integrator Control with $\rho=.01$ and Partial Control Authority	128
7.7	Transfer Function from Tip Excitation to Axial Displacement for Structure with Hardening Gain Change Joints with Robust LQR Design Compared to Linear and Nonlinear LQR Control.	132
7.8	Transfer Function from Tip Excitation to Displacements for Structure with Softening Gain Change Joints with Partial Control Authority (Robust vs. Non-Robust)	133
7.9	Transfer Function from Tip Excitation to Displacements for Structure with Hardening Gain Change Joints with Partial Control Authority (Robust vs. Non-Robust)	134
7.10	Transfer Function for Tip Excitation to Axial Displacement of Structure with Gain Change Joints with Robust LQR Integrator Design Compared to Linear and Nonlinear LQR Response.	135
7.11	Transfer Functions for Linear LQR, Nonlinear Softening LQR and Linear LQR with Stiffness Properties Coinciding with Minimum Values of Nonlinear Stiffness Coefficients.	136
7.12	Transfer Function from Tip Excitation to Displacements for Structure with Gain Change Joints with LQG Compensator and Full Control Authority, $\rho=.01$ , $\mu=.01$	139
7.13	Transfer Function from Tip Excitation to Displacements for Structure with Gain Change Joints with LQG Compensator and Full Control Authority, $\rho=1$ , $\mu=1$	140
7.14	Transfer Function from Tip Excitation to Displacements for Structure with Gain Change Joints with H Infinity Compensator with Full Control	143

## **List of Tables**

6.1	Mini-Mast Strut Properties	104
6.2	Specifications for Kaman Displacement Sensors	105
6.3	Mini Mast NASTRAN Finite Element Model Frequencies and Predicted Damping.	108
6.4.	Comparison of Model Frequencies	113

## Nomenclature

$a, b$	amplitude vectors
$A$	sinusoidal amplitude, or plant matrix
$b_{NL}$	nonlinear joint force vector
$b$	joint force vector
$B$	matrix relating truss displacements to continuum strains, or bias input to nonlinear element, or control input matrix
$B_e$	matrix relating truss displacements to equivalent finite element beam
$c_p, c_q$	describing function coefficients
$C$	damping matrix
$C_{NL}$	nonlinear damping matrix of structure
$D$	matrix containing continuum equivalent beam properties, or factor matrix of parameter deviation plant matrix
$E$	factor matrix of parameter deviation plant matrix
$EA/L$	axial stiffness
$EI$	bending stiffness
$F$	force
$F_B$	second order form control input matrix
$F_J$	joint force
$F_L$	second order form disturbance input matrix
$F_{NL}$	nonlinear force
$GA_s$	shear stiffness
$h$	time step size for time integration
$h_i$	squeeze motion degree of freedom
$i_R$	rotary inertia per unit length
$\underline{k}_{ni}$	Runga-Kutta incremental derivative vector
$k$	frequency index in fourier transform

$k_1$	stiffness of gain change within linear range
$k_2$	stiffness of gain change beyond linear range
$k_1$	linear joint stiffness
$k_3$	cubic joint stiffness
$K$	stiffness matrix
$K_b$	stiffness matrix of equivalent beam finite element
$K_{NB}$	bias stiffness matrix, contains bias terms from dual-input describing function
$K_{NL}$	nonlinear stiffness matrix of structure
$K_t$	truss bay full finite element stiffness matrix
$K_T$	feedback gain matrix
$K_1$	feedback gain matrix, also $K_2$ , and $K_3$
$L$	disturbance input matrix
$m$	mass per unit length
$m^*$	modal mass matrix
$M$	mass matrix
$n$	data index in fourier transform
$N$	number of points in data
$N_B$	bias coefficient from dual-input describing function
$q$	displacement
$\dot{q}$	velocity
$Q$	non-dimensional force, or state weighting matrix
$R$	control weighting matrix
$P$	Riccati equation matrix solution
$U_t$	strain energy in one truss bay
$U_c$	strain energy per unit length in equivalent continuum beam
$v$	displacements of equivalent finite element beam

$\alpha$	a small increment
$\delta$	size of linear range in gain change joint
$\varepsilon$	strain vector
$\varepsilon_x$	extensional strain
$\varepsilon_{xy}$	shear strain
$\gamma$	H infinity bound
$\kappa$	curvature
$\mu$	noise input intensity for estimator gains calculation
$\rho$	ratio of control weighting to state weighting
$\omega$	forcing frequency
$\omega_p$	reference frequency = $EA/mL^2$
$\omega$	frequency angle = $\omega t$
$\psi$	mode shape matrix
$\xi$	modal damping matrix
$\zeta$	damping ratio



Room 14-0551  
77 Massachusetts Avenue  
Cambridge, MA 02139  
Ph: 617.253.5668 Fax: 617.253.1690  
Email: docs@mit.edu  
<http://libraries.mit.edu/docs>

## **DISCLAIMER OF QUALITY**

Due to the condition of the original material, there are unavoidable flaws in this reproduction. We have made every effort possible to provide you with the best copy available. If you are dissatisfied with this product and find it unusable, please contact Document Services as soon as possible.

Thank you.

**Some pages in the original document contain color pictures or graphics that will not scan or reproduce well.**

Pages 13-18 (Chapter 1) are missing from the original thesis submitted to the Institute Archives

## **CHAPTER 2**

### **ACCURACY OF DESCRIBING FUNCTION MODEL**

#### **2.1 INTRODUCTION**

Describing functions are a way of approximating a nonlinear input-output relation. The accuracy of this method as compared to other classical solutions for one degree of freedom nonlinear problems has been investigated in previous works. Multi-degree of freedom system with nonlinearities are more difficult to analyze with classical methods.

Bowden (1988) used the describing function method to model nonlinear joints in multi-dof structures. The material in Chapter 2 will attempt to investigate the accuracy of the describing function method by comparing time integration determination of the sinusoidal response of a structure with a nonlinear joint to Bowden's describing function models. Two types of nonlinear joints are investigated, a cubic spring in parallel with a linear spring and a gain change. The structure consists of two finite element beams connected by a nonlinear joint. The structure is multi-dimensional and therefore not easily analyzed using a classical procedure.

Chapter 4 shows how the describing function method is combined with the equivalent beam modeling procedure developed in Chapter 3 to produce the nonlinear equivalent beam finite element model to model trusses with nonlinear joints.

#### **2.2 DESCRIBING FUNCTION METHOD**

A principal part of the method described here for modeling truss structures with nonlinear joints is the use of the describing function methodology. This methodology consists of a quasi-linearization of a nonlinear input-output relation. The nonlinear relation is replaced by an analytical

function that minimizes the root-mean-square error of the output of the nonlinear element when it is excited by a sinusoidal input. This is identical to calculating the first sine and cosine coefficients of the fourier series expansion of the output of the nonlinear element and ignoring the higher harmonics.

The describing function approach requires replacing a force-state relation of the form

$$F = F_{NL}(q, \dot{q}) \quad (2.1)$$

with the approximation:

$$F = c_p(A, \omega)q + c_q(A, \omega)\dot{q} \quad (2.2)$$

By defining

$$\begin{aligned} q &= A \sin \varpi \\ \varpi &= \omega t \end{aligned} \quad (2.3)$$

the describing function coefficients become

$$\begin{aligned} c_p &= \frac{1}{\pi A} \int_0^{2\pi} F_{NL}(A \sin \varpi, A\omega \cos \varpi) \sin \varpi d\varpi \\ c_q &= \frac{1}{\omega \pi A} \int_0^{2\pi} F_{NL}(A \sin \varpi, A\omega \cos \varpi) \cos \varpi d\varpi \end{aligned} \quad (2.4)$$

This is a quasi-linearization because the coefficients  $c_p$  and  $c_q$  still depend on amplitude and frequency. For a structure these coefficients represent equivalent stiffness and damping terms respectively.

The relation for  $F_{NL}$  may be an analytical function or it may be data taken from force-displacement tests of a joint. The analytical function will either give a calculable expression or one that needs to be numerically integrated. Describing functions obtained numerically from data may be entered into a look-up table for response calculation purposes.



### 2.3 TWO BEAM STRUCTURE AND EQUATIONS OF MOTION

Bowden's (1988) thesis detailed the analytical determination of the response of a two beam structure connected with a nonlinear rotary joint using a describing function model of the nonlinear joint. The joint was represented by describing function coefficients. Figure 2.1 shows this structure.

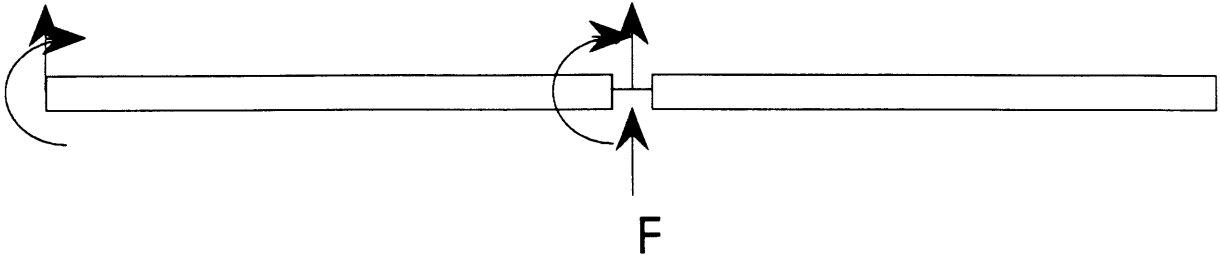


**Figure 2.1 Two beam structure with nonlinear rotary joint [Bowden(1988)]**

The mass and stiffness matrices are obtained from finite element theory using the consistent approach. The mass matrix is the consistent mass matrix. The beam element has a rotation and a transverse translation degree of freedom. The applied force makes the response of the structure symmetric about the axis of the force vector. This allows the reduction of the dof of the structure from 7 to 4. The mass and stiffness matrices for the structure are as follows:

$$M = \frac{mL}{420} \begin{bmatrix} 312 & 44L & 108 & -26L \\ 44L & 8L^2 & 26L & -6L^2 \\ 108 & 26L & 312 & -44L \\ -26L & -6L^2 & -44L & 8L^2 \end{bmatrix} \quad K = \frac{EI}{L^3} \begin{bmatrix} 24 & 12L & -24 & 12L \\ 12L & 8L^2 & -12L & 4L^2 \\ -24 & -12L & 24 & -12L \\ 12L & 4L^2 & -12L & 8L^2 \end{bmatrix}$$

where  $m$  is the mass/length,  $EI$  is the bending stiffness parameter, and  $L$  is the length of each of the beams. The matrix  $K$  does not include the properties of the joint. These properties could be linear or nonlinear and are included in a vector,  $F_J$ . These matrices are then non-dimensionalized. The displacement and force vectors used for non-dimensionalization are:

$$\underline{q}^T = \left[ \frac{q_1}{L} \quad q_2 \quad \frac{q_3}{L} \quad q_4 \right] \quad F = [Q_1L \quad Q_2 \quad Q_3L \quad Q_4]$$

Damping is assumed to originate solely from the joint. The damping matrix is then:

$$C = \begin{bmatrix} 0 & 0 & 0 & 0 \\ 0 & 0 & 0 & 0 \\ 0 & 0 & 0 & 0 \\ 0 & 0 & 0 & 8\zeta \end{bmatrix}$$

where  $\zeta$  is a non-dimensional damping factor. The equations of motion become:

$$M\ddot{\underline{q}} + C\dot{\underline{q}} + K\underline{q} + \underline{F}_j = \underline{F} \quad (2.5)$$

In the describing function approach, the vector  $\underline{F}_j$  is replaced by describing function coefficients that replace the nonlinear relations in this vector. The procedure for solving a set of equations containing describing functions is described in detail in Chapter 4. Basically it involves the use of the harmonic balance procedure combined with a Newton-Raphson iteration method. The iteration requires that new DF coefficients be calculated for each new amplitude and frequency. The DF method gives the response of the structure to an input sinusoid.

## 2.4 TIME INTEGRATION OF EQUATIONS OF MOTION

An idea of the accuracy of the describing functions in modeling the response of multi-degree of freedom structures with nonlinear joints may be obtained from comparison to the response curves determined from time integration. This requires the assumption that the time integration has some degree of accuracy in modeling the structure in question. An accurate method for this is the Runge-Kutta method.

The equations of motion (2.5) can be put into state space form by defining:

$$\underline{x} = \begin{Bmatrix} \underline{q} \\ \dot{\underline{q}} \end{Bmatrix} \quad (2.6)$$

which when substituted into equation (2.1) results in:

$$\begin{Bmatrix} \dot{\underline{q}} \\ \ddot{\underline{q}} \end{Bmatrix} = \begin{bmatrix} 0 & I \\ -M^{-1}K & -M^{-1}C \end{bmatrix} \begin{Bmatrix} \underline{q} \\ \dot{\underline{q}} \end{Bmatrix} + \begin{bmatrix} 0 \\ -M^{-1}\underline{F}_j \end{bmatrix} + \begin{bmatrix} 0 \\ M^{-1}\underline{F} \end{bmatrix} \quad (2.7)$$

or alternatively,

$$\dot{\underline{x}} = A\underline{x} + \underline{b}_{NL} + \underline{b} \quad (2.8)$$

The equations of motion are now in first order differential form. This is desirable for the Runga-Kutta integration.

The Runga-Kutta solution method is used to determine the discrete response of a system that has derivatives of the form:

$$\frac{dy}{dx} = \underline{g}(x, y) \quad (2.9)$$

The solution at the nth step for the n+1 step is:

$$\underline{y}_{n+1} = \underline{y}_n + \frac{h}{6}(\underline{k}_{n1} + 2\underline{k}_{n2} + 2\underline{k}_{n3} + \underline{k}_{n4}) \quad (2.10)$$

where

$h = \text{increment}$

$$\underline{k}_{n1} = \underline{g}(x_n, y_n)$$

$$\underline{k}_{n2} = \underline{g}\left(x_n + \frac{h}{2}, y_n + \frac{h}{2}\underline{k}_{n1}\right)$$

$$\underline{k}_{n3} = \underline{g}\left(x_n + \frac{h}{2}, y_n + \frac{h}{2}\underline{k}_{n2}\right)$$

$$\underline{k}_{n4} = \underline{g}(x_{n+1}, y_n + h\underline{k}_{n3})$$

The accuracy of the Runga-Kutta time integration algorithm is on the order of  $h^4$ .

## 2.5 COMPARISON OF MODELS

### Cubic Spring

The first type of nonlinear joint to be examined is a cubic spring in parallel with a linear spring. The vector  $F_J$  is:

$$\underline{F}_J = \left\{ \begin{array}{c} 0 \\ 0 \\ 0 \\ 4k_1 \underline{q}(4) + 4k_3 \underline{q}(4)^3 \end{array} \right\} \quad (2.11)$$

This is substituted into equation (2.7). Equation (2.7) is in the form of equation (2.9), i. e.,

$$\frac{d\underline{x}}{dt} = \underline{g}(\underline{x}, t)$$

This can be integrated using the Runge-Kutta method.

The procedure for the time integration is as follows. The equations are integrated over a large number of cycles with a time step of  $h=0.01$  at a certain frequency and value of  $F$ . This assures that any transient vibrations will have damped out. The response is calculated from the fourier transform of the data at the frequency of excitation. The equation for this is:

$$A = \left( \sum_{n=0}^N x(n) e^{-i2\pi kn/N} \right) * 2 / N \quad (2.12)$$

where  $A$  is the complex amplitude of the response,  $x(n)$  is the data for a single degree of freedom at index  $n$ ,  $k$  is the index of the frequency of interest or the driving frequency, and  $N$  is the number of time points. This is a single term of the fast fourier transform. The driving frequency is then changed and the procedure is repeated. When the driving frequency is changed, phase continuity is maintained to prevent abrupt changes in the input sinusoid. Sufficient time is again allowed for the system to reach steady state.

The FFT equation has a certain step size within the frequency domain. This step size is governed by the following equation:

$$\Delta\omega = \frac{2\pi}{hN}$$

and  $k$ , the index of the driving frequency  $\omega$ , is:

$$k = \frac{\omega h N}{2\pi}$$

The frequencies used in this analysis were chosen so that they coincided with frequencies allowable in the FFT. This gives more accurate results for the sinusoidal response at each frequency.

The DF method requires the replacement of the vector  $\underline{E}_J$  by a vector that contains DF coefficients:

$$\underline{E}_J = \left\{ \begin{array}{c} 0 \\ 0 \\ 0 \\ 4c_p q_4 + 4c_q \dot{q}_4 \end{array} \right\}$$

For the cubic spring in parallel with a linear spring,  $c_q$  would be zero. The equation for the DF coefficients for the cubic spring and others is given in Appendix A.

Figure 2.2 shows a comparison of the frequency response to a sine sweep at a certain forcing level between the time integration and the describing function models. The ratio of  $k_3/k_1$  is 0.5 for this case. The models agree very well. The lower and upper branches and the response jump indicate the multi-valued nature of the solution. For the DF approach, the initial conditions for each iteration determine whether the solution follows the lower or upper branch. The time integration response is the same for both a forward sweep of the model and a backward sweep. The transition occurs at a different frequency than for the DF response. This is not indicative of error but of the difference in the effect of initial conditions on the two models.

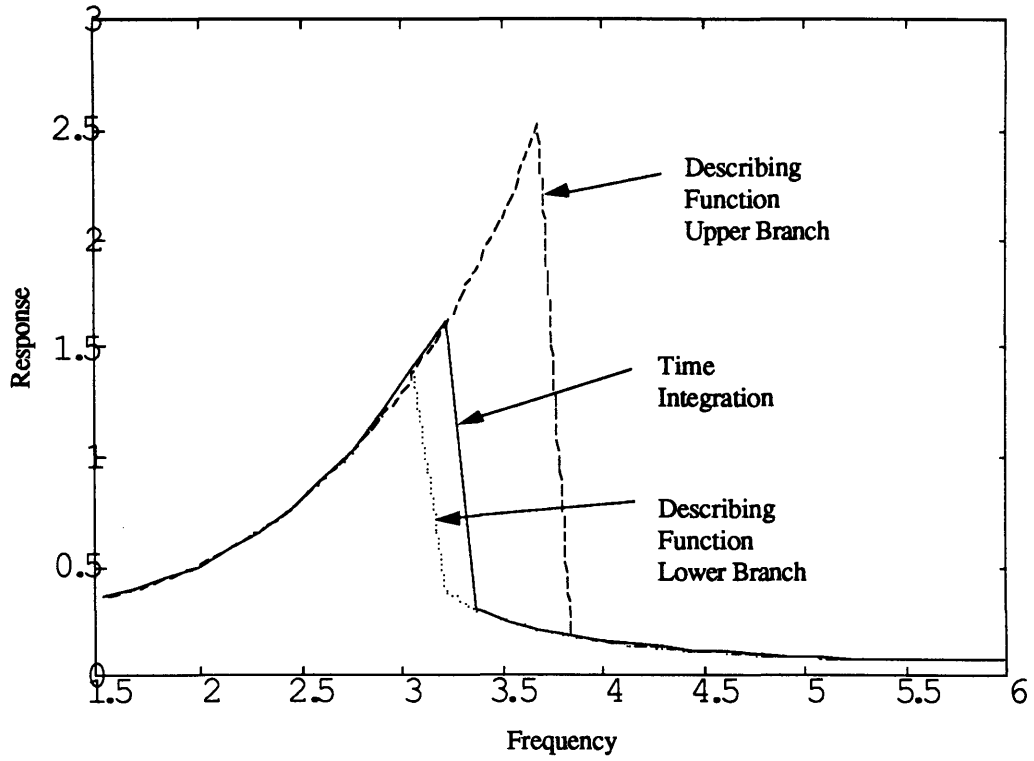


**Figure 2.2 Comparison of Describing Function Model and Time Integration for Cubic Spring**

### Gain Change

The second type of nonlinearity investigated is the gain change. A schematic of the force-displacement relation appears in Figure 2.3.

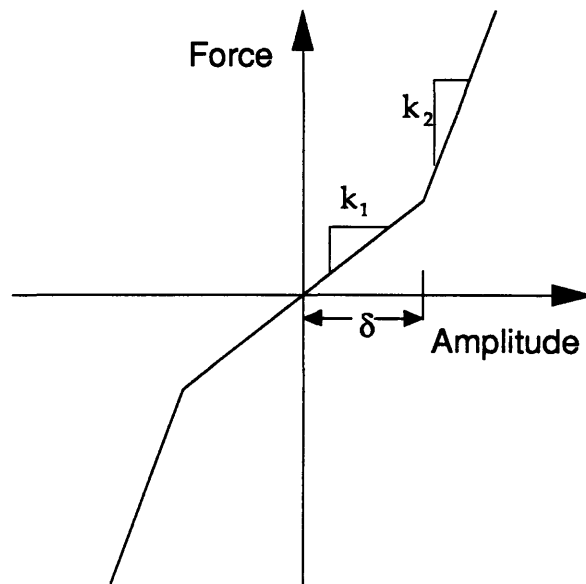


**Figure 2.3 Gain Change Nonlinear Relation**

The vector  $\underline{k}_{NL}$  for a gain change is a conditional one:

$$\text{if amp} = 2q(4) < \delta, \text{ then } \underline{F}_J = \begin{Bmatrix} 0 \\ 0 \\ 0 \\ 4k_1 q(4) \end{Bmatrix},$$

$$\text{if amp} > \delta, \text{ then } \underline{F}_J = \begin{Bmatrix} 0 \\ 0 \\ 0 \\ 2k_2 \left[ \text{amp} - 2\delta \left( 1 - \frac{k_1}{k_2} \right) \right] \end{Bmatrix}$$

where  $\delta$ ,  $k_1$ , and  $k_2$  are defined in Figure 2.3. The time integration algorithm program is of the same form as that for the cubic spring. More time is allowed for the system to reach steady-state after each increase in frequency to reduce the transients caused by the abrupt change in stiffness. Figure 2.4 shows the comparison of the frequency response calculated using the describing function technique and the time integration for a gain change with a ratio of  $k_2/k_1$  equal to 10.

The plot shows both the upper and lower branches of the multi-solution response for both models. The two branches for the time integration were obtained by sweeping frequency both forwards (increasing frequency) and backwards (decreasing frequency). The upper branch was obtained by sweeping forward and the lower branch by sweeping backward.

The agreement between the two types of modeling procedures is very good for the gain change nonlinear joint. The lower and upper branches almost exactly coincide for the two models.

It is interesting to analyze a model with a joint gain change that has a softening characteristic. The response curve is not a mirror image of the response curve for the hardening spring but has unique characteristics. Figure 2.5 shows the comparison of the two models for a softening spring gain change with  $k_2/k_1$  equal to 0.1. The response curves are nearly identical,

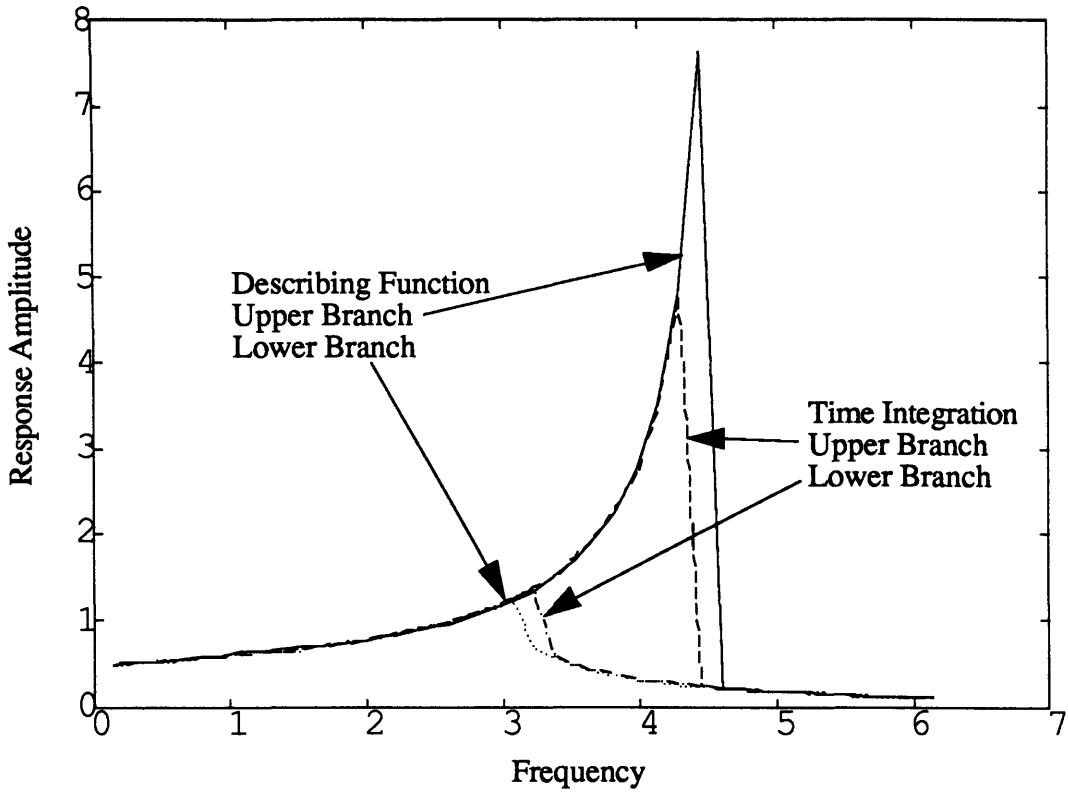


**Figure 2.4 Two Beam Structure with Gain Change Nonlinearity Frequency Response-Hardening Spring**

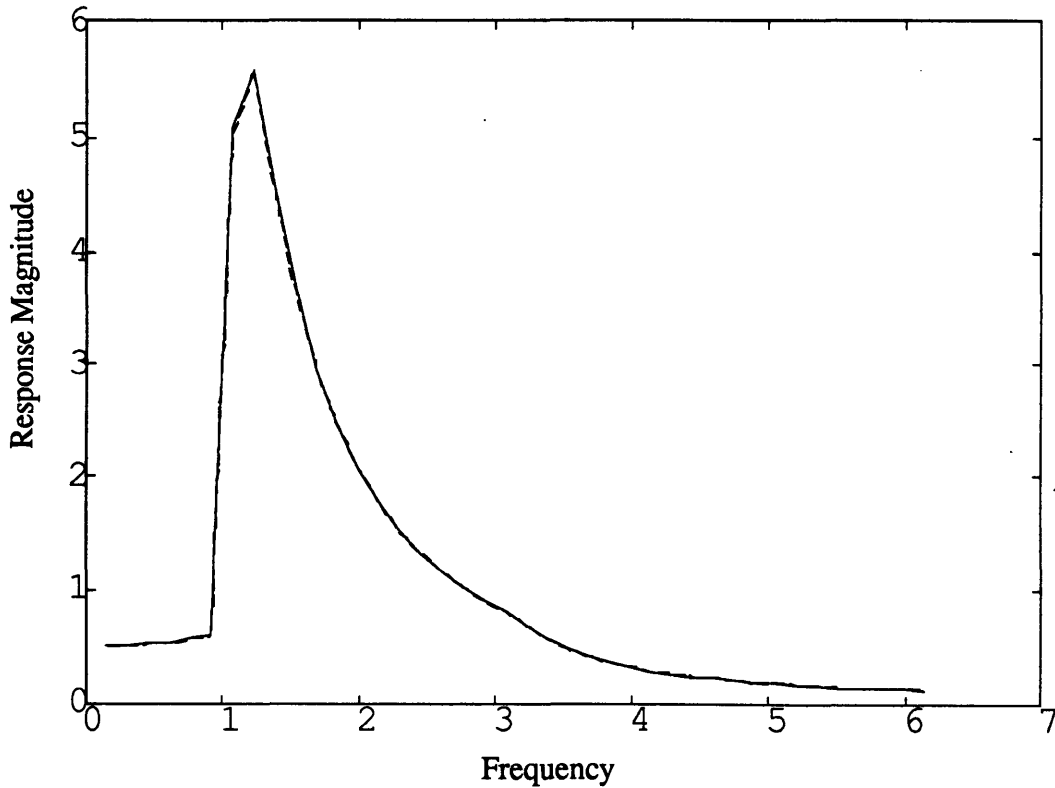


**Figure 2.5 Two Beam Structure with Gain Change Nonlinearity Frequency Response-Softening Spring.**



The response curves in Figures 2.2, 2.4, and 2.5 give an idea of the characteristics of the response of a structure with nonlinear elements. The characteristics that are obvious from the plots are jump phenomena and multi-valued solutions in the vicinity of a resonant peak. The stable solutions that exist consist of an upper branch and a lower branch. Whether a solution follows a branch depends on initial conditions at the start of determining a solution at each frequency.

For the describing function approach, the initial condition can be the linear solution to the problem or the solution without the nonlinear element present. This solution will tend to follow the lower branch. The initial condition at each iteration can be the solution at the last iteration. If the structure has a hardening spring characteristic as in Figures 2.2 and 2.4, and the sweep is in the forward direction (increasing frequency), this solution will tend to follow the upper branch. If the direction is reversed for a hardening spring, the solution will follow the lower branch. The tendency is reversed for the softening spring.

For the time integration, the initial condition at each new frequency is the final condition at the last frequency. This means that the upper and lower branches are reached by sweeping either forward or backward, depending on the nonlinear characteristic.

The drop-off point from the upper branch to the lower branch for both methods depends on the frequency step size. The smaller the step, the longer the solution will follow the upper branch when swept in the correct direction. For the softening spring shown in Figure 2.5, only one solution is present. This is probably due to the low frequency of the resonant peak. The frequency shift is bounded by zero frequency and can shift no lower.

These results show that the describing function method is a viable way of modeling nonlinear elements within simple structures and instills confidence in the method for the developments in the following chapters.

## CHAPTER 3

### MODELING TRUSSES AS BEAMS

#### 3.1 INTRODUCTION

The long slender trusses that are envisioned for use as future space structures can behave similarly to beams. The lowest structural modes of these structures appear very similar to beam modes. This can be used as a basis for modeling these trusses as beams. The advantage of this is the lower number of degrees of freedom that are retained in the analytical model, thus reducing computation time for determining response. It also serves as an inherent model reduction algorithm for control purposes. The reduction of degrees of freedom is important later in Chapter 4 when combining the method described in this chapter with the describing function method of modeling nonlinear elements described in Chapter 2 to calculate the response of a beam-like truss with nonlinear joints. Chapter 7 makes use of the model reduction characteristic for control design.

There are a number of approaches to modeling trusses as beams. The two discussed here model the complete truss as a continuum beam or model a truss cell as an equivalent finite element beam. The continuous beam method relates the displacements of a single truss bay to the strain in a continuous beam. The equivalent finite element beam relates the displacements of the truss bay to those of a single finite beam element that is the length of the bay. This equivalent finite element beam is then used to construct a finite element model of the truss. Both methods equate the energy of the single truss bay with that of a similar length beam. The displacements included in the equivalent beam model may be varied in order to accurately model the lowest global modes of the structure.

### 3.2 CONTINUUM BEAM MODEL

Both methods of modeling trusses as beams are based on the use of a finite element model of an individual truss bay or cell. The finite element model stiffness matrix of this truss cell is  $K_t$ , where the truss elements are assumed to have only axial stiffness, and the mass matrix is  $M_t$ , where the elements have consistent mass for motion in the axial direction and mass associated with the transverse direction or cable mass. This is a standard truss representation which includes no bending or shear stiffness in the truss elements. This also allows no rotational stiffness in the joints. The only stiffness is in the axial direction. This model is not as accurate as one with elements that do have bending stiffness. However, the objective of the method described here is to model the beam-like behavior of the truss. This behavior primarily consists of axial flexing of the truss members. Therefore the axial stiffness model is sufficient for this type of modeling procedure.

The strain energy of one truss bay is represented by:

$$U_t = \frac{1}{2} \mathbf{q}^T \mathbf{K}_t \mathbf{q} \quad (3.1)$$

where  $\mathbf{q}$  are the displacements of the truss nodes. The strain energy per specified length of a continuum beam may be represented as follows:

$$U_c = \frac{1}{2} \mathbf{L} \boldsymbol{\varepsilon}^T \mathbf{D} \boldsymbol{\varepsilon} \quad (3.2)$$

where  $L$  is the specified length and  $\boldsymbol{\varepsilon}$  is the strain vector for a full six DOF beam which could include extensional strains, curvature (or rate of twist) and shear strains. The continuum strains may be related to the truss displacements by the expression:

$$\boldsymbol{\varepsilon} = \mathbf{B} \mathbf{q} \quad (3.3)$$

This expression is substituted into (3.2) to give:

$$U_c = \frac{1}{2} \mathbf{L} (\mathbf{B} \mathbf{q})^T \mathbf{D} (\mathbf{B} \mathbf{q}) \quad (3.4)$$

The equation for the difference between the strain energy of the continuum beam and the truss cell is:

$$|\Delta U| = |U_c - U_t| \tag{3.5}$$

This equation is minimized or set equal to zero which, using the pseudo-inverse, gives the following relation for D:

$$D = \frac{1}{L} (BB^T)^{-1} BK_t B^T (BB^T)^{-1} \tag{3.6}$$

The diagonal elements of D are the equivalent beam properties of the continuum beam (EA, GA<sub>s</sub>, EI, GJ).

**Example**

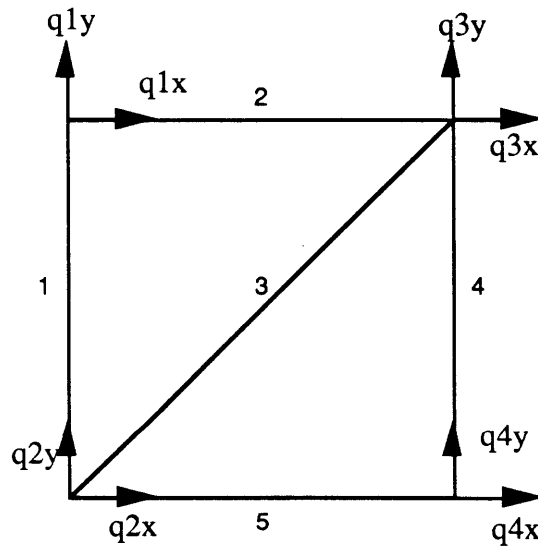


**Figure 3.1 Two Dimensional Truss Bay**

Figure 3.1 shows a two dimensional truss bay. The strain vector for the equivalent beam is:

$$[\epsilon_x \kappa \gamma]^T$$

$\epsilon_x$  = extensional strain

$\kappa$  = in - plane curvature

$\gamma$  = in - plane shear

These are the strains that capture the complete behavior of a two-dimensional beam; the axial strain for extension, the curvature for bending, and the shear for transverse displacement. The D matrix corresponding to this strain vector that would give the strain energy of the truss from equation (3.2) is:

$$D = \begin{bmatrix} EA & 0 & 0 \\ 0 & EI & 0 \\ 0 & 0 & GA_s \end{bmatrix} \quad (3.7)$$

There are off diagonal terms in this matrix that results from the condensation procedure. These terms indicate bending-extension coupling. In the analysis that follows, these terms are ignored. The stiffness matrix for this truss bay is,

$$\begin{bmatrix} k_2 & 0 & 0 & 0 & -k_2 & 0 & 0 & 0 \\ 0 & k_1 & 0 & -k_1 & 0 & 0 & 0 & 0 \\ 0 & 0 & \frac{k_3}{2} + k_5 & \frac{k_3}{2} & -\frac{k_3}{2} & -\frac{k_3}{2} & -k_5 & 0 \\ 0 & -k_1 & \frac{k_3}{2} & k_1 + \frac{k_3}{2} & -\frac{k_3}{2} & -\frac{k_3}{2} & 0 & 0 \\ -k_2 & 0 & -\frac{k_3}{2} & -\frac{k_3}{2} & k_2 + \frac{k_3}{2} & \frac{k_3}{2} & 0 & 0 \\ 0 & 0 & -\frac{k_3}{2} & -\frac{k_3}{2} & \frac{k_3}{2} & \frac{k_3}{2} + k_4 & 0 & -k_4 \\ 0 & 0 & -k_5 & 0 & 0 & 0 & k_5 & 0 \\ 0 & 0 & 0 & 0 & 0 & -k_4 & 0 & k_4 \end{bmatrix} \quad (3.8)$$

where the subscripts on the k's indicate the number of the truss element as shown in Figure 3.1.

The k's themselves refer to the stiffness of the truss strut and the joints at each end. If there are no

joints then  $k=EA/L$  with the structural properties for that truss strut. If there are joints then additional terms are needed. This is discussed in a later section.

The displacements of the truss bay must now be related to the strains of the equivalent beam. This is accomplished by displacing the truss into positions that are pure manifestations of a particular strain. For example, the average extension of the bay divided by the length gives the extensional strain. Assuming that the truss bay shown in Figure 3.1 is square with length  $L$ , the relationship between the strains of the equivalent beam and the displacements of the truss is:

$$\begin{aligned}\epsilon_x &= \frac{1}{2L}[(q_{3x} - q_{1x}) + (q_{4x} - q_{2x})] \\ \kappa &= \frac{1}{L^2}[(q_{3x} - q_{1x}) - (q_{4x} - q_{2x})] \\ \epsilon_{xy} &= \frac{1}{2L}[(q_{3y} - q_{1y}) + (q_{4y} - q_{2y}) + (q_{1x} - q_{2x}) + (q_{3x} - q_{4x})]\end{aligned}\quad (3.9)$$

This determines the elements of the B matrix. This B matrix is then substituted into equation (3.6) along with the finite element stiffness matrix for the truss bay shown in Figure 3.1. The diagonal elements of the resulting matrix correspond to the structural properties of an equivalent continuum beam as shown in equation (3.7). The properties for one truss bay are:

$$\begin{aligned}(EA)_{EQ} &= 2.35355 EA \\ (EI)_{EQ} &= \frac{1}{2} EAL^2 \\ (GA)_{EQ} &= 0.35355 EA\end{aligned}\quad (3.10)$$

where the terms  $E$ ,  $A$ , and  $L$  on the right hand side of the equations refer to the properties of the truss elements. These values have an intuitive feel. The equivalent  $EA$  contains contributions from both longerons (the factor of 2) and from the diagonal (the remaining fraction). The equivalent shear only contains a contribution from the diagonal. The equivalent bending stiffness is the areas of the upper and longerons multiplied by the distance from the center line of the truss squared. This assumes that the cell is bending in a perfect circle about the centerline and the diagonal does not deflect. The mass per unit length of the equivalent beam is simply the mass per unit length of the truss and in this case, it is equal to  $4.41421m$ , where  $m$  is the mass per unit length of the struts.

Another quantity of interest is  $i_R$ , the rotary mass moment of inertia per unit length. This becomes useful when calculating the equivalent beam frequencies with the Timoshenko beam model. This value is determined by calculating the mass moments of inertia of each strut about the centerline of the truss, adding these values together and dividing by the length of the truss bay. For the truss bay shown in Figure 3.1,  $i_R=0.7012 \text{ mL}^2$ .

In the method described above, the entire truss is modeled by a single continuous beam. The beam properties are determined from a single truss bay, in effect “smearing” truss properties throughout the continuum beam. The describing function coefficients are determined from the amplitudes of the displacements of individual elements in the truss. Therefore a method of modeling a truss as a beam for use with the describing function method must contain information about individual truss elements.

### 3.3 EQUIVALENT FINITE ELEMENT BEAM MODEL

An alternate method of modeling a truss as a beam that contains individual element information is to use an equivalent finite element beam to represent each bay of a truss. The finite element model of the truss remains the same and the strain energy of the truss is given by equation (3.1). The strain energy of an equivalent finite element beam is:

$$U_b = \frac{1}{2} \mathbf{v}^T \mathbf{K}_b \mathbf{v} \quad (3.11)$$

where  $\mathbf{v}$  is the vector containing the equivalent finite element beam displacements and  $\mathbf{K}_b$  is the finite element stiffness matrix of this beam. The equation relating truss displacements with beam displacements is:

$$\mathbf{v} = \mathbf{B}_e \mathbf{q} \quad (3.12)$$

This equation is substituted into (3.11) and the matrix  $\mathbf{K}_b$  is calculated using an equation similar to (3.6):

$$\mathbf{K}_b = (\mathbf{B}_e \mathbf{B}_e^T)^{-1} \mathbf{B}_e \mathbf{K}_t \mathbf{B}_e^T (\mathbf{B}_e \mathbf{B}_e^T)^{-1} \quad (3.13)$$

### Four Degree of Freedom Model

This method can also be applied to the structure in Figure 3.1. The structure is made to displace as a beam would. The number of degrees of freedom kept in the equivalent beam model depends on the degree of accuracy needed and the dof needed to model the complete behavior apparent in the lower modes of the truss structure. The degrees of freedom used in a consistent stiffness model of a beam are the transverse displacement and rotation at each end. For these degrees of freedom, the relation between the equivalent beam displacements and truss displacements is:

$$\begin{Bmatrix} v_1 \\ \theta_1 \\ v_2 \\ \theta_2 \end{Bmatrix} = \begin{bmatrix} 0 & \frac{1}{2} & 0 & \frac{1}{2} & 0 & 0 & 0 & 0 \\ -\frac{1}{L} & 0 & \frac{1}{L} & 0 & 0 & 0 & 0 & 0 \\ 0 & 0 & 0 & 0 & 0 & \frac{1}{2} & 0 & \frac{1}{2} \\ 0 & 0 & 0 & 0 & -\frac{1}{L} & 0 & \frac{1}{L} & 0 \end{bmatrix} \begin{Bmatrix} q_{1x} \\ q_{1y} \\ q_{2x} \\ q_{2y} \\ q_{3x} \\ q_{3y} \\ q_{4x} \\ q_{4y} \end{Bmatrix} \quad (3.14)$$

which, after substitution into equation 3.13 with the stiffness matrix for the truss cell in equation (3.7), gives the following stiffness matrix:

$$\begin{vmatrix} \frac{k_1}{2} & & \frac{k_1 L}{4} & & \frac{-k_1}{2} & & \frac{k_1 L}{4} & & \\ k_1 L & \frac{k_1 L^2}{8} + \frac{k_2 L^2}{4} + \frac{k_3 L^2}{4} & -k_1 L & & \frac{k_1 L^2}{8} - \frac{k_2 L^2}{4} - \frac{k_3 L^2}{4} & & & & \\ -k_1 & & \frac{-k_1 L}{4} & & \frac{k_1}{4} & & \frac{-k_1 L}{4} & & \\ k_1 L & \frac{k_1 L^2}{8} - \frac{k_2 L^2}{4} - \frac{k_3 L^2}{4} & -k_1 L & & \frac{k_1 L^2}{8} + \frac{k_2 L^2}{4} + \frac{k_3 L^2}{4} & & & & \end{vmatrix} \quad (3.15)$$

$$k_1 = \left( \frac{EA}{L} \right)_1 = \text{Diagonal strut stiffness}$$

$$k_2 = \left( \frac{EA}{L} \right)_2 = \text{Upper longeron stiffness}$$

$$k_3 = \left( \frac{EA}{L} \right)_3 = \text{Lower longeron stiffness}$$



The above matrix serves as a map of the effects of the various strut elements on the stiffness of the equivalent beam. Transverse displacement stiffness is due primarily to the diagonal strut, bending stiffness is due to all three struts, less so due to the diagonal strut than the upper and lower longerons. There is a noted absence of the stiffnesses of the batten truss elements. The assumption is made in this characterization that the truss behaves like a beam. This precludes the presence of squeezing motion of the top and bottom of the truss. The beam can behave like a Timoshenko beam however in that the beam faces do not have to remain perpendicular to the central line of the beam. Bending-extension coupling is not modeled in this beam model.

The mass matrix requires certain study. With no joints, the truss element stiffness matrix is of the form:

$$k_{\text{element}} = \frac{EA}{L} \begin{bmatrix} 1 & -1 \\ -1 & 1 \end{bmatrix}$$

which is the consistent formulation for purely axial motion. The element mass matrix must account for motion of the element in the transverse direction and therefore includes “cable” mass:

$$m_{\text{element}} = mL \begin{bmatrix} \frac{1}{3} & 0 & \frac{1}{6} & 0 \\ 0 & \frac{1}{2} & 0 & 0 \\ \frac{1}{6} & 0 & \frac{1}{3} & 0 \\ 0 & 0 & 0 & \frac{1}{2} \end{bmatrix}$$

This individual strut mass matrix gives the full truss cell mass matrix:

$$\begin{bmatrix}
 \frac{m_1}{2} + \frac{m_2}{3} & 0 & 0 & 0 & \frac{m_2}{6} & 0 & 0 & 0 \\
 0 & \frac{m_1}{3} + \frac{m_2}{2} & 0 & \frac{m_1}{6} & 0 & 0 & 0 & 0 \\
 0 & 0 & \frac{m_1}{2} + \frac{5m_3}{12} + \frac{m_5}{3} & \frac{m_3}{12} & \frac{m_3}{12} & \frac{m_3}{12} & \frac{m_5}{6} & 0 \\
 0 & \frac{m_1}{6} & \frac{m_3}{12} & \frac{m_1}{3} + \frac{5m_3}{12} + \frac{m_5}{2} & \frac{m_3}{12} & \frac{m_3}{12} & 0 & 0 \\
 \frac{m_2}{6} & 0 & \frac{m_3}{12} & \frac{m_3}{12} & \frac{m_2}{3} + \frac{5m_3}{12} + \frac{m_4}{2} & \frac{m_3}{12} & 0 & 0 \\
 0 & 0 & \frac{m_3}{12} & \frac{m_3}{12} & \frac{m_3}{12} & \frac{m_2}{2} + \frac{5m_3}{12} + \frac{m_4}{3} & 0 & \frac{m_4}{6} \\
 0 & 0 & \frac{m_5}{6} & 0 & 0 & 0 & \frac{m_4}{2} + \frac{m_5}{3} & 0 \\
 0 & 0 & 0 & 0 & 0 & \frac{m_4}{6} & 0 & \frac{m_4}{3} + \frac{m_5}{2}
 \end{bmatrix} \quad (3.16)$$

The subscripts again refer to the numbers on the strut elements in figure 3.1 and each m term refers to the total mass of the truss strut. The same operation is then performed on this matrix as on the truss cell stiffness matrix. This again entails the application of equation (3.13) with the transformation matrix  $B_e$  defined by equation (3.14) and the matrix  $K_t$  replaced by  $M_t$ . If it is assumed that m, the mass per unit length of the truss elements is the same for all elements, L is the length of one side of the truss bay (which is square) and the length of the diagonal is determined from geometry, then the equivalent mass matrix is:

$$\left[ \begin{array}{cccc}
\frac{5\sqrt{2}+24}{12} & -\frac{L\sqrt{2}}{24} & \frac{\sqrt{2}}{12} & -\frac{L\sqrt{2}}{24} \\
-\frac{L\sqrt{2}}{24} & \frac{120\sqrt{2}+480}{1152}L^2 & \frac{L\sqrt{2}}{24} & -\frac{12\sqrt{2}+48}{576}L^2 \\
\frac{\sqrt{2}}{12} & \frac{L\sqrt{2}}{24} & \frac{5\sqrt{2}+24}{12} & \frac{L\sqrt{2}}{24} \\
-\frac{L\sqrt{2}}{24} & -\frac{12\sqrt{2}+48}{576}L^2 & \frac{L\sqrt{2}}{24} & \frac{120\sqrt{2}+480}{1152}L^2
\end{array} \right] mL \quad (3.17)$$

The equivalent beam finite element mass and stiffness matrices in equations (3.15) and (3.17) are based on the assumption of a 4 dof equivalent beam to replace the 8 dof truss cell. This includes transverse displacement and rotation at each end of the beam. A third displacement (axial) at each end may also be included to give a 6 dof equivalent finite beam element. The comparative accuracy of these models will be compared later.

### Six Degree of Freedom Model

The six degree of freedom equivalent beam model includes the extra displacement of longitudinal translation. This results in an increase in accuracy of the model that goes beyond that which would be expected solely due to an increase in the dof. The model now captures the total beam behavior exhibited in the lower modes of a long slender truss. This will be discussed more later. The  $B_e$  transformation matrix for the 6 dof equivalent beam is:

$$\left\{ \begin{array}{c} u_1 \\ v_1 \\ \theta_1 \\ u_2 \\ v_2 \\ \theta_2 \end{array} \right\} = \left[ \begin{array}{cccccccc}
\frac{1}{2} & 0 & \frac{1}{2} & 0 & 0 & 0 & 0 & 0 \\
0 & \frac{1}{2} & 0 & \frac{1}{2} & 0 & 0 & 0 & 0 \\
-\frac{1}{L} & 0 & \frac{1}{L} & 0 & 0 & 0 & 0 & 0 \\
0 & 0 & 0 & 0 & \frac{1}{2} & 0 & \frac{1}{2} & 0 \\
0 & 0 & 0 & 0 & 0 & \frac{1}{2} & 0 & \frac{1}{2} \\
0 & 0 & 0 & 0 & -\frac{1}{L} & 0 & \frac{1}{L} & 0
\end{array} \right] \left\{ \begin{array}{c} q_{1x} \\ q_{1y} \\ q_{2x} \\ q_{2y} \\ q_{3x} \\ q_{3y} \\ q_{4x} \\ q_{4y} \end{array} \right\} \quad (3.18)$$

This is then substituted into equation (3.13) with the mass and stiffness matrices for the full truss bay to give the 6 dof stiffness matrix:

$$\begin{bmatrix}
\frac{k_3}{k_2 + \frac{k_3}{2} + k_5} & \frac{k_3}{2} & \frac{Lk_2}{2} + \frac{Lk_3}{4} + \frac{Lk_5}{2} & -\frac{k_3}{k_2 + \frac{k_3}{2} + k_5} & \frac{k_3}{2} & \frac{Lk_2}{2} + \frac{Lk_3}{4} + \frac{Lk_5}{2} \\
\frac{k_3}{2} & \frac{k_3}{2} & \frac{Lk_3}{4} & -\frac{k_3}{2} & \frac{k_3}{2} & \frac{Lk_3}{4} \\
\frac{Lk_2}{2} + \frac{Lk_3}{4} + \frac{Lk_5}{2} & \frac{Lk_3}{4} & \frac{k_2 L^2}{4} + \frac{k_3 L^2}{8} + \frac{k_5 L^2}{4} & \frac{Lk_2}{2} + \frac{Lk_3}{4} + \frac{Lk_5}{2} & \frac{Lk_3}{4} & \frac{k_2 L^2}{4} + \frac{k_3 L^2}{8} + \frac{k_5 L^2}{4} \\
-\frac{k_3}{k_2 + \frac{k_3}{2} + k_5} & -\frac{k_3}{2} & \frac{Lk_2}{2} + \frac{Lk_3}{4} + \frac{Lk_5}{2} & \frac{k_3}{k_2 + \frac{k_3}{2} + k_5} & \frac{k_3}{2} & -\frac{Lk_2}{2} - \frac{Lk_3}{4} - \frac{Lk_5}{2} \\
\frac{k_3}{2} & \frac{k_3}{2} & \frac{Lk_3}{4} & -\frac{k_3}{2} & \frac{k_3}{2} & \frac{Lk_3}{4} \\
\frac{Lk_2}{2} + \frac{Lk_3}{4} + \frac{Lk_5}{2} & \frac{Lk_3}{4} & \frac{k_2 L^2}{4} + \frac{k_3 L^2}{8} + \frac{k_5 L^2}{4} & -\frac{Lk_2}{2} - \frac{Lk_3}{4} - \frac{Lk_5}{2} & \frac{Lk_3}{4} & \frac{k_2 L^2}{4} + \frac{k_3 L^2}{8} + \frac{k_5 L^2}{4}
\end{bmatrix}$$

and the mass matrix:

$$\begin{bmatrix}
\frac{5\sqrt{2}}{12} + \frac{5}{3} & -\frac{\sqrt{2}}{12} & \frac{5L\sqrt{2}}{24} & \frac{\sqrt{2}}{12} + \frac{1}{3} & \frac{\sqrt{2}}{12} & -\frac{L\sqrt{2}}{24} \\
-\frac{\sqrt{2}}{12} & \frac{5\sqrt{2}}{12} + 2 & \frac{L\sqrt{2}}{24} & \frac{\sqrt{2}}{12} & \frac{\sqrt{2}}{12} & -\frac{L\sqrt{2}}{24} \\
\frac{5L\sqrt{2}}{24} & -\frac{L\sqrt{2}}{24} & \left(\frac{5\sqrt{2}}{48} + \frac{5}{12}\right)L^2 & \frac{L\sqrt{2}}{24} & \frac{L\sqrt{2}}{24} & \left(-\frac{\sqrt{2}}{48} + \frac{1}{12}\right)L^2 \\
\frac{\sqrt{2}}{12} + \frac{1}{3} & \frac{\sqrt{2}}{12} & \frac{L\sqrt{2}}{24} & \frac{5\sqrt{2}}{12} + \frac{5}{3} & -\frac{\sqrt{2}}{12} & -\frac{5L\sqrt{2}}{24} \\
\frac{\sqrt{2}}{12} & \frac{\sqrt{2}}{12} & \frac{L\sqrt{2}}{24} & -\frac{\sqrt{2}}{12} & \frac{5\sqrt{2}}{12} + 2 & \frac{L\sqrt{2}}{24} \\
-\frac{L\sqrt{2}}{24} & -\frac{L\sqrt{2}}{24} & \left(-\frac{\sqrt{2}}{48} + \frac{1}{12}\right)L^2 & -\frac{5L\sqrt{2}}{24} & \frac{L\sqrt{2}}{24} & \left(\frac{5\sqrt{2}}{48} + \frac{5}{12}\right)L^2
\end{bmatrix} m L$$

This model includes bending-extension coupling in the beam model. This reflects on the accuracy of the model in modeling truss motion where these effects are important.

## Restricting Squeeze Motion

There is a variation of this method of calculating these equivalent beam models that may provide some insight into the method itself. The truss displacements are related to beam displacements as in equation (3.12) except now the matrix relating the displacements is square. This is done by creating an extra degree of freedom at each end of the equivalent beam that is orthogonal to the other dof's of the beam. This can be done by creating a squeeze mode. For Figure 3.1, this could be:

$$\begin{Bmatrix} h_1 \\ h_2 \end{Bmatrix} = \begin{bmatrix} 0 & 1 & 0 & -1 & 0 & 0 & 0 & 0 \\ 0 & 0 & 0 & 0 & 0 & 1 & 0 & -1 \end{bmatrix} \begin{Bmatrix} q_{1x} \\ q_{1y} \\ q_{2x} \\ q_{2y} \\ q_{3x} \\ q_{3y} \\ q_{4x} \\ q_{4y} \end{Bmatrix} \quad (3.19)$$

If this is added to the matrix  $B_e$ , the matrix is now square and invertible. The pseudo-inverse is no longer needed and equation (3.12) becomes:

$$K_{bT} = (B_e^T)^{-1} K_T (B_e)^{-1} \quad (3.20)$$

This is an intermediate step, the matrix  $K_{bT}$  is then operated on to obtain  $K_b$ :

$$K_b = T^T K_{bT} T$$

where  $T$  is a transformation matrix that removes the rows and columns of the matrix corresponding to the squeeze motion and thus constraining that motion. This method produces the same result as the pseudo-inverse method.

## Non-Dimensionalization

To increase the generality of the examples, the equations of motion may be non-dimensionalized. Ignoring damping for now, the equations of motion of the full scale truss model, after factoring out common terms are:

$$mL[M]\ddot{\underline{x}} + \frac{EA}{L}[K]\underline{x} = \underline{F} \quad (3.21)$$

where the M and K matrices are non-dimensional. Since all the displacements are translations, they may be expressed as multiples of the length L:

$$\underline{x} = L\underline{x}' \quad (3.22)$$

The equations of motion become:

$$mL^2[M]\ddot{\underline{x}'} + EA[K]\underline{x}' = \underline{F} \quad (3.23)$$

The frequencies of the system may now be expressed in terms of multiples of  $\omega_p$  which is defined as:

$$\omega_p = \frac{EA}{mL^2}$$

and the force expressed in terms of EA. The transformation from truss to beam may be kept non-dimensional by using the non-dimensional truss displacements in equation (3.18) and using the non-dimensional displacement vector for the beam displacements:

$$\underline{v} = \begin{Bmatrix} u_1L \\ v_1L \\ \theta_1 \\ u_2L \\ v_2L \\ \theta_2 \end{Bmatrix} \quad (3.24)$$

This makes the B matrix non-dimensional and the above relations remain the same.

### 3.4 DETERMINATION OF TRUSS ELEMENT STIFFNESS

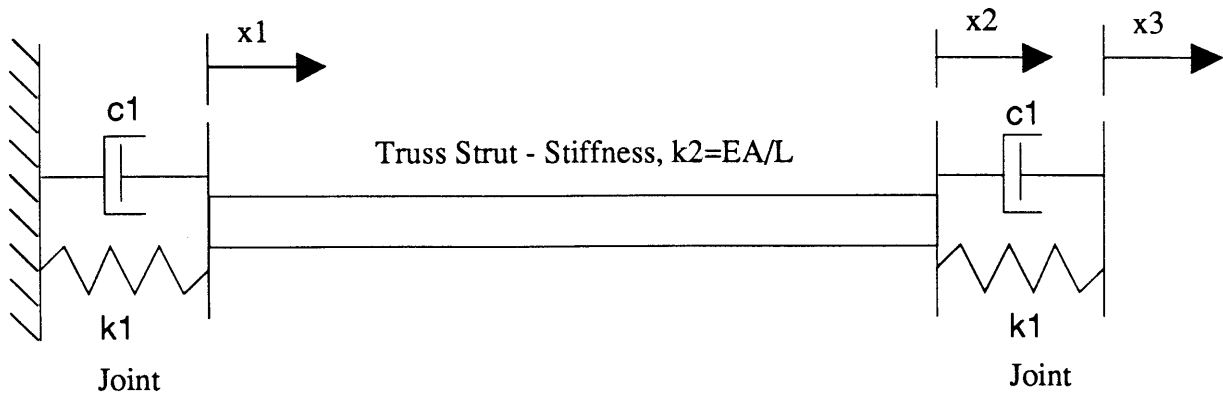


Figure 3.2 Truss Element With Linear Joints

Figure 3.2 shows a joint-strut-joint truss element that will be considered here. The strut is represented by a stiffness. The joints may have stiffness and damping. The objective is to obtain equivalent stiffness and damping terms for this structure. It is assumed that this structure will not model the mode in which the truss strut acts as a mass vibrating between the springs of the joints. This mode is at a much higher frequency than the modes of the truss that are beam-like. Because of this assumption, the force through the element is constant.

$$k_1 x_1 + c_1 \dot{x}_1 = k_2 (x_2 - x_1) = k_1 (x_3 - x_2) + c_1 (\dot{x}_3 - \dot{x}_2) = F \quad (3.25)$$

Taking the Laplace transform of the first two terms gives the relationship between  $x_1$  and  $x_2$ :

$$\left( \frac{k_1 + k_2 + c_1 s}{k_2} \right) x_1 = x_2 \quad (3.26)$$

This is substituted into the second two terms of equation (3.25) to give the relations between  $x_1$ ,  $x_2$ , and  $x_3$ :

$$\begin{aligned} x_1 &= \left( \frac{k_2}{2k_2 + k_1 + c_1 s} \right) x_3 \\ x_2 &= \left( \frac{k_1 + k_2 + c_1 s}{2k_2 + k_1 + c_1 s} \right) x_3 \end{aligned} \quad (3.27)$$

These are substituted into the middle terms of equation (3.25) to give the force-displacement relation for the displacement across the entire structure:

$$F = \left[ \frac{k_2(k_1 + c_1s)}{2k_2 + k_1 + c_1s} \right] x_3 \quad (3.28)$$

The substitution,  $s=i\omega$ , is made and the equation above is separated into real and imaginary parts. The real part signifies the equivalent stiffness and the imaginary part signifies the equivalent damping. Both of these terms are frequency dependent.

If there are no dampers in the joints, equation (3.28) simplifies to:

$$F = \left[ \frac{k_1 \frac{EA}{L}}{2 \frac{EA}{L} + k_1} \right] x_3 \quad (3.29)$$

Dividing through by  $EA/L$  gives the nondimensional  $k_{EQ}$ :

$$k_{EQ} = \frac{1}{2 \frac{EA}{k_1 L} + 1} \quad (3.30)$$

### 3.5 COMPARISON OF MODELS

A comparison of the models that have been developed here is shown in Figure 3.2. The figure shows the frequencies of the first mode for the various models as the number of bays in a cantilevered truss is increased from 1 to 10. The models shown are the continuous beam model with the frequencies calculated from Bernoulli-Euler beam theory, the continuous beam model with the frequencies calculated from Timoshenko beam theory, the finite element model of the truss (8 dof), the equivalent finite element beam model with transverse displacement and rotation at each end (4 dof) and the equivalent finite element beam model with an additional longitudinal displacement at each end (6 dof).



The Bernoulli-Euler (B-E) beam frequencies are obtained from Blevins (1979) with the equivalent beam properties calculated above. The B-E beam has bending stiffness only and the plane sections in the beam, which for a beam-truss are equivalent to the battens, remain plane. The Timoshenko beam frequencies are determined using the solution developed by Huang (1961). The Timoshenko beam includes the effects of shear and rotary inertia. Both of these effects are important in a truss-beam.

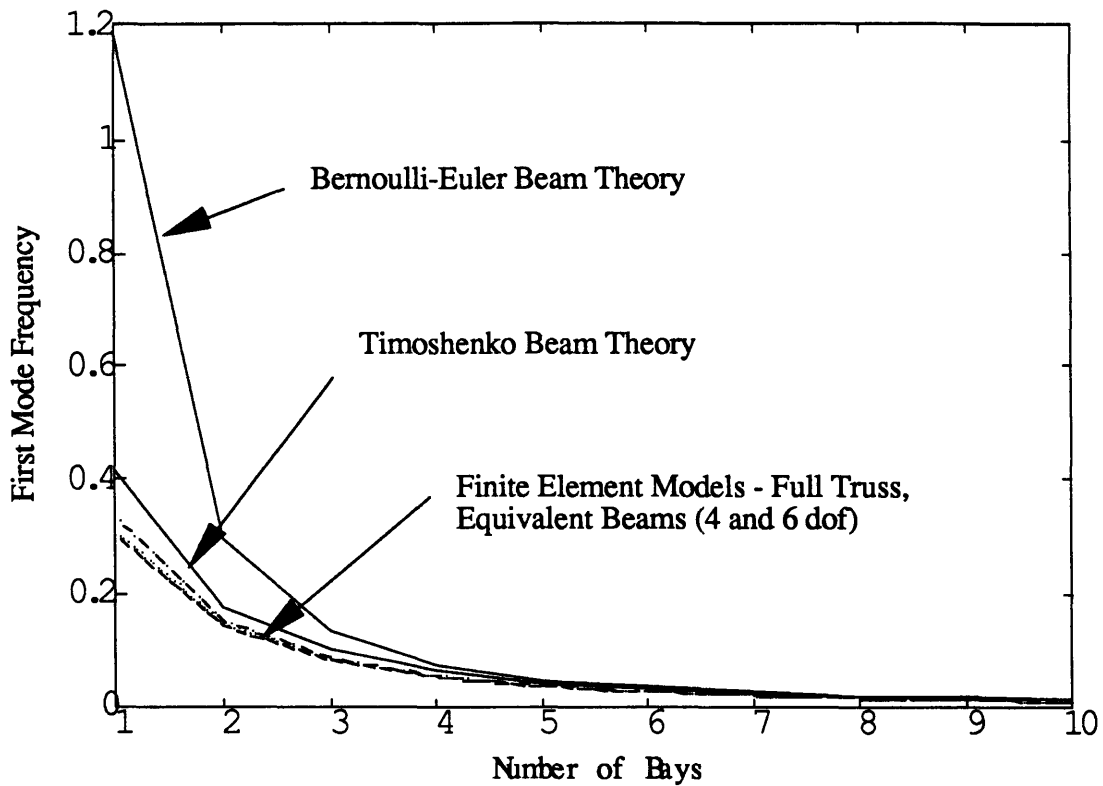


**Figure 3.3 First Frequency for a Cantilevered Truss with Varying Number of Bays for Models**

The continuous B-E beam model does not accurately model with the finite element models for trusses with a small number of bays. The Timoshenko continuous beam model is more accurate than the B-E model, particularly when there are only a few bays and shear and rotary inertia effects are predominant. Neither of the continuum beam models is as accurate as the equivalent beam finite element models. The assumption is made that the 8 dof finite element model of the truss is the most accurate representation of the truss. Therefore the continuous beam model

will be discarded to investigate the finite element equivalent beam models. Figure 3.3 shows a comparison of the percentage of the error between the six and four dof models and the eight dof model. The 6 dof model is more accurate than the 4 dof model as compared to the full 8 dof truss finite element model. This is not surprising in that the greater the number of degrees of freedom, the greater the accuracy of the model. This greater accuracy is also due to the fact that the 6 dof model models more accurately the lower beam-like modes of the truss. The 6 dof model error is below five percent even for a relatively nonbeam-like one bay truss. Both models have errors below five percent after the truss reaches about 6 bays in length.

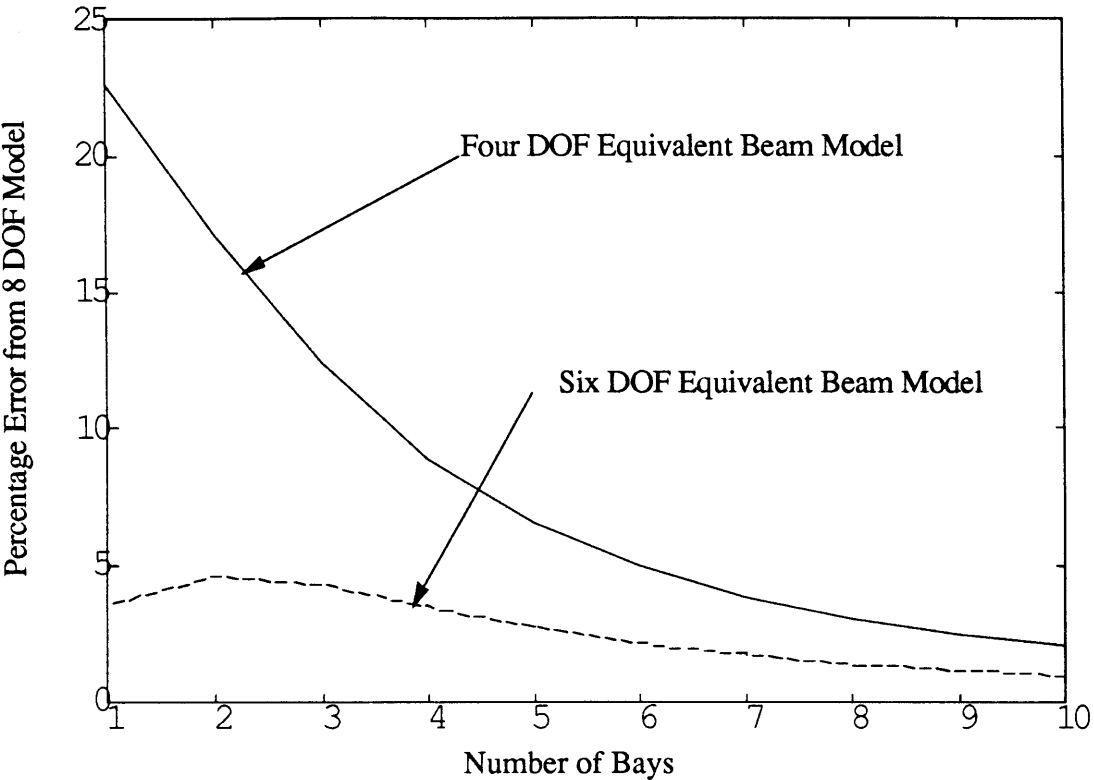


**Figure 3.4 Percentage Error of Equivalent Beam Models From Truss Finite Element Local Bending Modes**

None of the methods described above model the local bending modes of the truss members. Some indication of when these local modes become important is useful for determining the overall accuracy of the models. The truss members may be visualized as simple beams with

pinned-pinned supports. The actual supports would have some flexibility but this model serves as a lower bound on the local bending frequencies. From Blevins (1979), the equation for the first bending frequency of a beam with pinned-pinned supports is:

$$\omega_1 = \pi^2 \sqrt{\frac{EI}{mL^4}} \quad (3.31)$$

The value of EI is set to equal a multiple of  $EAL^2$ , i. e.  $EI=bEAL^2$ , and substituted into equation (3.31). The diagonal will have the lowest frequency so the length of the element is  $2^{1/2}L$ . The frequency can now be compared with the frequencies of the equivalent beam:

$$\omega_1 = \sqrt{b} \frac{\pi^2}{2} \sqrt{\frac{EA}{mL^2}} \quad (3.32)$$

A typical value of  $b=EI/EAL^2$  for a truss element is  $1.3375 \times 10^{-4}$  (Spangler, 1990). This gives  $\omega_1=0.05707\omega_p$  for the local diagonal mode frequency. For the five bay cantilevered model discussed in the next section, this is the second mode. This mode will be higher on an actual truss but the equivalent beam method has some deficiencies when used to model short 2-D trusses.

### Mode Shapes

Figure 3.4 shows a comparison of the mode shapes of the 8 dof model and the two equivalent finite element beam models for the first four modes of a cantilevered truss with five bays. The shapes for the equivalent beam models were obtained by displacing a picture of the 8 dof truss in the same way as the equivalent beam. The frequencies are non-dimensionalized as discussed previously. The 4 dof model does not have a mode comparable to mode 3 of the 6 dof and 8 dof models. This is due to the fact that mode 3 is an axial mode and the 4 dof model has no axial degree of freedom. The 4 dof model mode shapes show no axial motion, the centerpoints of the battens always intersect the line through the batten's original position. This restriction of motion also explains the fact that both equivalent beam models have higher frequencies for similar modes. The restrictions on motion serve as a stiffening effect on the model. This conclusion also holds for the continuous equivalent beam model which is the most restrictive model and therefore

has the highest frequencies. Also, the motion of the first four modes is beam-like except the axial mode is at a much lower frequency than for a normal solid beam. Finally, the 6 dof model is very accurate compared to the 8 dof model for these first four modes. This is an indication that the 'squeezing' motion that was left out is not predominant in these first beam-like modes. This observation will serve as a rule in modeling a more complex structure in that the motion that is kept in the model is the motion that defines the lower beam-like modes of the truss.

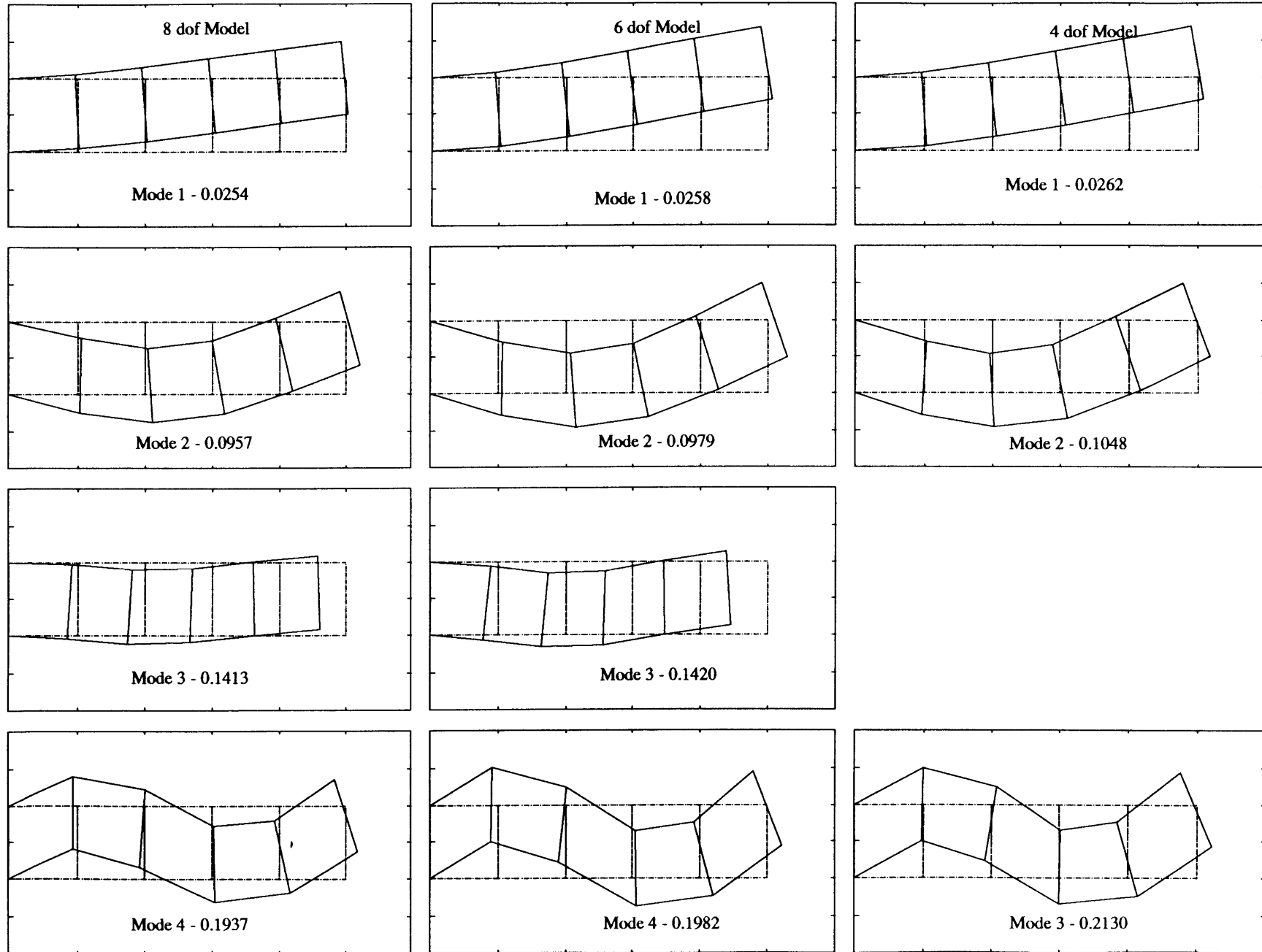


**Figure 3.5. Mode Shapes of the Finite Element Models for a Cantilevered Truss with Five Bays**

## CHAPTER 4

### NONLINEAR EQUIVALENT BEAM FINITE ELEMENT MODEL

#### 4.1 INTRODUCTION

This chapter describes how the describing function method for modelling structural nonlinearities is combined with the equivalent beam model of a beam-like truss to produce the nonlinear equivalent beam finite element. Chapter 2 showed that the describing function, for certain nonlinear elements, is an accurate representation of the response. Chapter 3 showed that the equivalent finite element beam method could accurately model the beam-like behavior of a truss. This chapter in effect combines the methods of Chapters 2 and 3 to produce the nonlinear equivalent finite element beam model for modeling trusses with nonlinear joints.

In this method each truss strut is treated as an axial linear spring in series with nonlinear elements at each end of the strut. The force-displacement relation is then calculated for the entire strut-joint structure. The describing function coefficients are calculated for this relation at certain values of amplitude and frequency. The values of  $c_p$  and  $c_q$  are then the nonlinear stiffness and damping terms, respectively, associated with that particular strut.

The types of nonlinearities that can be represented this way include any for which a force-displacement relation can be written. The DF coefficients can also be calculated numerically from experimental data. The desired experimental set-up would consist of sinusoidal response testing of the complete strut-joint structure at various amplitudes and frequencies. This would allow the

calculation of a look-up table or a curve-fitting procedure for analysis. The analysis presented here is concerned exclusively with analytical as opposed to experimentally determined nonlinear relations.

#### 4.2 TRUSS ELEMENT MODEL

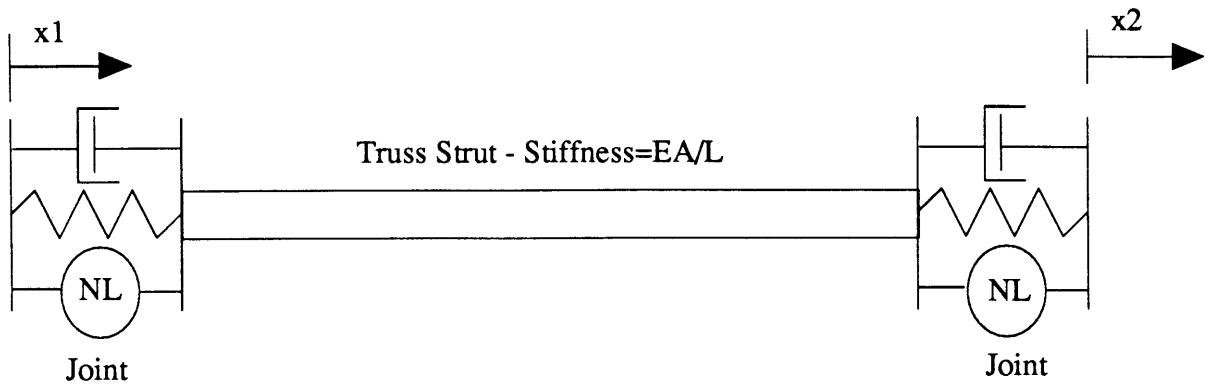


**Figure 4.1 Joint-Strut-Joint Schematic**

Figure 4.1 shows a model of the joint-strut-joint structure used to determine the describing function coefficients. The truss strut stiffness is assumed to be linear and equal to  $EA/L$ . The joints can also contain linear spring and damping elements. The element marked NL signifies the presence of nonlinear behavior. The force-state relationship for the displacement across the entire element is calculated. The describing function coefficients are calculated for this input-output relation.

The describing function coefficients are calculated for the joint-strut-joint element using the procedures outlined later in this chapter. These coefficients are the nonlinear stiffness and damping terms for that structural element. The nonlinear stiffness matrix for an individual truss element is:

$$k_{\text{strut}} = \begin{bmatrix} c_p & -c_p \\ -c_p & c_p \end{bmatrix}$$

There is a similar element matrix that gives the nonlinear damping for the single truss element.

This procedure condenses the nonlinear behavior of the truss element, which includes the joint at each end of the strut, in addition to the linear stiffness and damping contributions from the joints and the strut, into single term representations of the nonlinear stiffness and damping. The truss element nonlinear stiffness matrix shown above is used to construct the nonlinear stiffness matrix for the single truss bay in the standard finite element procedure. This matrix is exactly the same as shown in equation (3.7) except the  $k_i$ 's are replaced by  $c_{pi}$ 's. This matrix is then substituted into equation 3.12 to give the nonlinear stiffness matrix. For the structure shown in Figure 3.1, the 6 dof equivalent beam stiffness matrix is:

$$\begin{bmatrix} c_{p2} \frac{c_{p3}}{2} + c_{p5} & \frac{c_{p3}}{2} & -\frac{c_{p2}L}{2} + \frac{c_{p3}L}{4} + \frac{c_{p5}L}{2} & -c_{p2} \frac{c_{p3}}{2} c_{p5} & -\frac{c_{p3}}{2} & \frac{c_{p2}L}{2} + \frac{c_{p3}L}{4} + \frac{c_{p5}L}{2} \\ \frac{c_{p3}}{2} & \frac{c_{p3}}{2} & \frac{c_{p3}L}{4} & -\frac{c_{p3}}{2} & \frac{c_{p3}}{2} & \frac{c_{p3}L}{4} \\ \frac{c_{p2}L}{2} + \frac{c_{p3}L}{4} + \frac{c_{p5}L}{2} & \frac{c_{p3}L}{4} & \frac{c_{p2}L^2}{4} + \frac{c_{p3}L^2}{8} + \frac{c_{p5}L^2}{4} & \frac{c_{p2}L}{2} \frac{c_{p3}L}{4} \frac{c_{p5}L}{2} & -\frac{c_{p3}L}{4} & -\frac{c_{p2}L^2}{4} + \frac{c_{p3}L^2}{8} + \frac{c_{p5}L^2}{4} \\ -c_{p2} \frac{c_{p3}}{2} c_{p5} & -\frac{c_{p3}}{2} & \frac{c_{p2}L}{2} \frac{c_{p3}L}{4} \frac{c_{p5}L}{2} & c_{p2} \frac{c_{p3}}{2} + c_{p5} & \frac{c_{p3}}{2} & -\frac{c_{p2}L}{2} \frac{c_{p3}L}{4} + \frac{c_{p5}L}{2} \\ \frac{c_{p3}}{2} & \frac{c_{p3}}{2} & -\frac{c_{p3}L}{4} & \frac{c_{p3}}{2} & \frac{c_{p3}}{2} & -\frac{c_{p3}L}{4} \\ \frac{c_{p2}L}{2} + \frac{c_{p3}L}{4} + \frac{c_{p5}L}{2} & \frac{c_{p3}L}{4} & -\frac{c_{p2}L^2}{4} + \frac{c_{p3}L^2}{8} + \frac{c_{p5}L^2}{4} & -\frac{c_{p2}L}{2} \frac{c_{p3}L}{4} + \frac{c_{p5}L}{2} & -\frac{c_{p3}L}{4} & \frac{c_{p2}L^2}{4} + \frac{c_{p3}L^2}{8} + \frac{c_{p5}L^2}{4} \end{bmatrix}$$

where

$c_{p3}$ =Nonlinear diagonal strut stiffness

$c_{p2}$ =Nonlinear upper longeron stiffness

$c_{p5}$ =Nonlinear lower longeron stiffness

The subscripts refer to the numbered truss elements shown in Figure 3.1. The coefficients depend on the amplitude of the displacement of the particular joint-strut-joint element. This requires that



the individual truss element displacement be calculated to determine the nonlinear stiffness (and damping) of the truss bay. The nonlinear damping matrix is exactly the same as the stiffness matrix except the  $c_p$ 's are replaced by  $c_q$ 's. The mass matrix of course is not affected by the nonlinearity and remains as calculated for the linear equivalent beam element as shown in Chapter 3.

These nonlinear equivalent beam finite element stiffness and damping matrices may then be assembled by the standard finite element method to model repeating cell truss structures with nonlinear joints. The equations of motion for the harmonic excitation of a nonlinear structure modeled by the method described above are:

$$[M]\ddot{\underline{x}} + [C_{NL}]\dot{\underline{x}} + [K_{NL}]\underline{x} = \underline{F} \sin \omega t \quad (4.1)$$

The matrix  $C_{NL}$  also includes global linear material damping. There are many nonlinear elements which do not produce a  $c_q$  or damping term. In that case, the damping matrix would not have subscripts and it would be linear. The response is assumed to be an harmonic at the frequency of excitation, i. e.,

$$\underline{x} = \underline{a} \sin \omega t + \underline{b} \cos \omega t \quad (4.2)$$

Substituting this into equation (4.1) and separating sine and cosine terms, the equations become,

$$\begin{aligned} [K_{NL} - \omega^2 M]\underline{a} - \omega[C_{NL}]\underline{b} &= \underline{F} \\ \omega[C_{NL}]\underline{a} + [K_{NL} - \omega^2 M]\underline{b} &= \underline{0} \end{aligned} \quad (4.3)$$

This is the standard harmonic balance form. The number of equations and unknowns is  $2n$  where  $n$  is the number of degrees of freedom of the equivalent beam model. The nonlinear coefficients that make up the stiffness and damping matrices are calculated from the displacements of the individual strut members of the truss. These displacements must be calculated from the beam displacements using relationships based on the geometry of the structure.

### 4.3 SOLUTION TECHNIQUE

The solution to this set of equations is obtained by the Newton-Raphson technique. The technique stems from a truncated expansion of a set of equations. A set of equations of the form

$$f(\underline{q}) = 0 \quad (4.4)$$

may be written in expanded form:

$$f(\underline{q}) = f(\underline{q}_0) + \left[ \frac{\partial f}{\partial \underline{q}} \right]_{\underline{q}_0} d\underline{q} = 0 \quad (4.5)$$

where  $\underline{q}_0$  is the vector value about which the expansion occurs and the term in brackets is the Jacobian of system derivatives evaluated at  $\underline{q}_0$ . Treating the vector  $\underline{q}_0$  as a solution guess and  $d\underline{q}$  as the solution increment, the equation to be solved is:

$$\left[ \frac{\delta f}{\delta \underline{q}} \right]_{\underline{q}_0} \Delta \underline{q} = -f(\underline{q}_0) \quad (4.6)$$

This correction is then added to  $\underline{q}_0$ , new describing function coefficients are calculated, the nonlinear stiffness and damping matrices are constructed and the procedure is repeated until the correction becomes close to zero and the solution converges. The solution to these equations is obtained with Fortran computer codes using Linpack subroutines.

The number of degrees of freedom of the truss model combined with the complications arising from taking derivatives of the equations with respect to the equivalent beam displacements and then relating them back to the displacements across the individual struts makes it advantageous to calculate the Jacobian numerically. The most accurate way to do this is the central difference formula. The equation for the (i,j)th Jacobian matrix element is:

$$\frac{\delta f_i}{\delta x_j} = \frac{f_i(x_0 + \Delta x_j) - f_i(x_0 - \Delta x_j)}{2\alpha} \quad (4.7)$$

where  $\underline{x}_0$  is last solution guess,  $f_i$  are the equations to be solved and  $\underline{\Delta x}_j$  is a vector of zeros except for the  $j$ th element. This element is equal to  $\alpha$ , a small increment. For structural nonlinearities that have sharp discontinuities (i.e. a large change in slope), and therefore a corresponding sharp change in slope of the DF coefficients, the backward difference formula sometimes gives better results in terms of finding a solution. It also requires fewer calculations and therefore less computer time.

$$\frac{\delta f_i}{\delta x_j} = \frac{f_i(\underline{x}_0) - f_i(\underline{x}_0 - \underline{\Delta x}_j)}{\alpha} \quad (4.8)$$

The variables are the same as for the central difference formula.

The calculation of the  $f$  equations and the Jacobian requires that the solution guess in terms of the displacements of the equivalent beam be converted back into the truss displacements in order to determine the values of the DF coefficients associated with the individual struts. These are then assembled into the stiffness and damping matrices of the equivalent beam. This seems to negate the intent to reduce the truss to the equivalent beam. The reduction does save computing time however in the solution of equation (4.6). The Jacobian matrix is on the order of the reduced model and any reduction in the number of dof in the equation will result in the reduction of computing time. For the three-dimensional problem, the advantage becomes more apparent.

The locus of resonant peaks, or backbone curve, may also be calculated. With the damping set at zero, there can be a non-zero resonant response mode with no forcing function. Both  $C_{NL}$  and  $F$  are set to zero in equation (4.3) and the equation that is solved is:

$$[K_{NL} - \omega^2 M] \underline{a} = \underline{0} \quad (4.9)$$

The values of the vector  $\underline{a}$  and frequency that make the matrix in brackets singular and give a non-trivial solution to equation (4.9) correspond to the backbone curve. The solution procedure again solves equation (4.9) using the Newton-Raphson technique with a numerically calculated Jacobian. The order of the equations is now only  $n$ , the number of dofs of the beam model. The solution for

the backbone curve for a forced structure is obtained by choosing the degree of freedom of the model that is forced and varying it from a small number to large number. The frequency is set initially at the frequency of the mode of interest. The other degrees of freedom of the model are initially set at the mode shape values of the mode of interest scaled by the amplitude of the degree of freedom to be varied. The equation to be solved becomes:

$$\left[ \frac{\delta f}{\delta \underline{q}^P} \right]_{\underline{q}_0^P} \Delta \underline{q}^P = -f(\underline{q}_0^P) \quad (4.10)$$

where

$$\underline{q}^P = [\omega \ q_2 \ q_3 \ \dots]^T$$

The variable  $q_1$  is the displacement that is prescribed. The Jacobian is calculated for equation (4.9). As  $q_1$  is varied, the solution of the above equation gives the value of the frequency. Plotting frequency vs.  $q_1$  gives the backbone curve.

#### 4.4 SIMPLE EXAMPLES - ONE BAY CANTILEVERED TRUSS

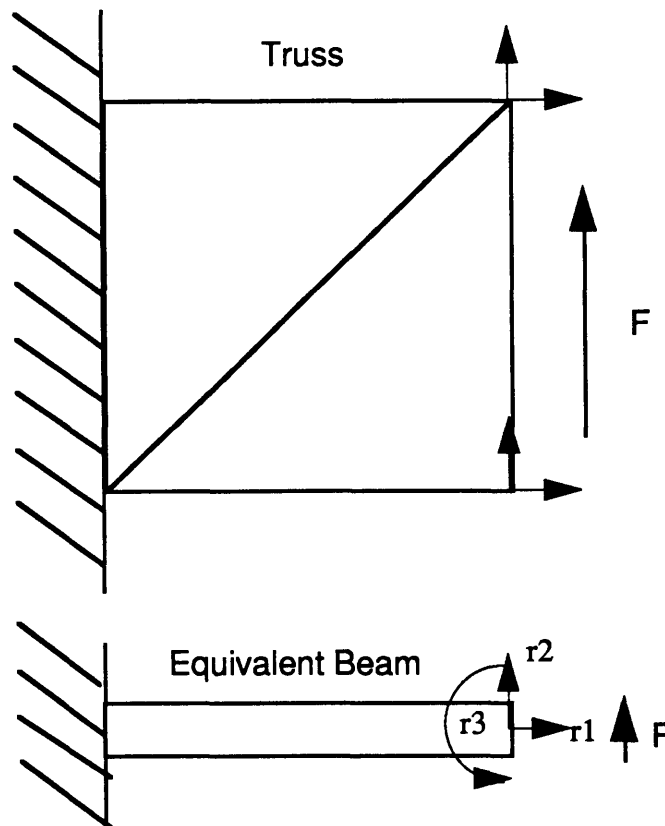


**Figure 4.2 One Bay Cantilevered Truss With Equivalent Beam Model**

To test the method and to develop the procedure algorithm, the structure shown in Figure 4.2 is analyzed using the nonlinear equivalent beam method. The structure is a single cantilevered truss bay with a force applied at one end. The equivalent beam shown below the truss will model this structure. This structure is not modeled very well by the equivalent beam procedure. However, this model will give an idea of the characteristics of the response of a truss with nonlinear joints and of the solution method. This investigation of the response of this truss structure will examine the effect of two types of joint nonlinearities, a cubic spring and a gain change.

The model that will be used is the 6 dof model. This model gives a more accurate representation of the truss than the 4 dof model. This is particularly important in this case where,

due to the cantilever and the shortness of the truss, the beam-like behavior of this truss is not as dominant.

### Linear Global Damping

The linear damping matrix still needs to be determined. First, consider a linear system of the form:

$$[M]\ddot{\underline{x}} + [C]\dot{\underline{x}} + [K]\underline{x} = \underline{0} \quad (4.11)$$

If the substitution is made:

$$\underline{x} = [\psi]\underline{q} \quad (4.12)$$

where  $\underline{q}$  is the vector of modal degrees of freedom and  $[\psi]$  is the matrix of mode shapes, and then the entire equation is premultiplied by  $[\psi]^T$ , equation (4.11) becomes:

$$[m^*]\ddot{\underline{q}} + [2\xi\omega_n m^*]\dot{\underline{q}} + [\omega_n^2 m^*]\underline{q} = \underline{0} \quad (4.13)$$

where  $m^*$ ,  $\xi_n$ , and  $\omega_n$  are diagonal matrices with the modal mass, modal damping and natural frequency for each mode distributed along the diagonal. This is in standard modal form. For the structure pictured in Figure 4.2,  $\xi$  is assumed to be 0.01 for all 3 modes. The damping matrix in equation (4.11) is then found from:

$$[C] = ([\psi]^T)^{-1} [2\xi\omega_n m^*] [\psi]^{-1} \quad (4.14)$$

This linear damping matrix, in this case is added directly to the nonlinear damping matrix in solving the nonlinear equations of motion. This linear damping is not assumed to come directly from the joints. If dampers were included in the joints, the force-displacement relation would become a complex relation. However, describing function coefficients may still be calculated for such a structure and the element would still be represented by  $c_p$ 's and  $c_q$ 's.

### Linear Joint

The procedure outlined above is first tested on the cantilevered truss with linear joints. The equivalent stiffness of the joint-strut-joint truss element was derived in Chapter 3. A schematic of the truss element is shown in Figure 3.2. For this analysis, the damping is assumed to be the global linear damping so the dampers shown in Figure 3.2 would not be present. The equation for the stiffness of the element is given by the expression in brackets in equation (3.25). The value  $k_{eq}$  corresponds directly with the values of  $k_i$  in equation (3.7). It represents the total stiffness of the truss element.

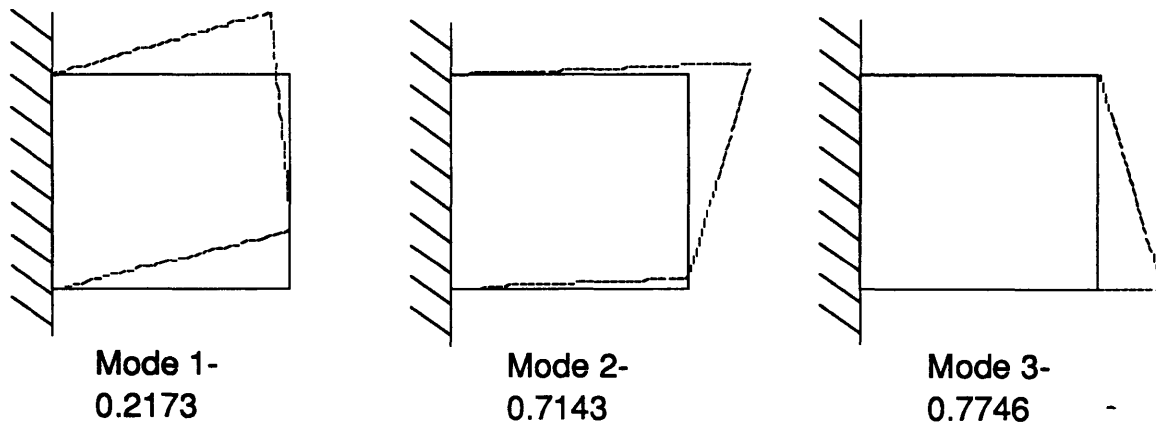


**Figure 4.4 Mode Shapes of One Bay Cantilevered Truss**

Figure 4.4 shows the mode shapes of the 6 dof equivalent model of the one bay cantilevered truss. Mode 1 is mainly transverse motion of the tip of the truss. Mode 2 is an end rotation. Mode 3 is a one strut mode consisting of the extension and contraction of the bottom

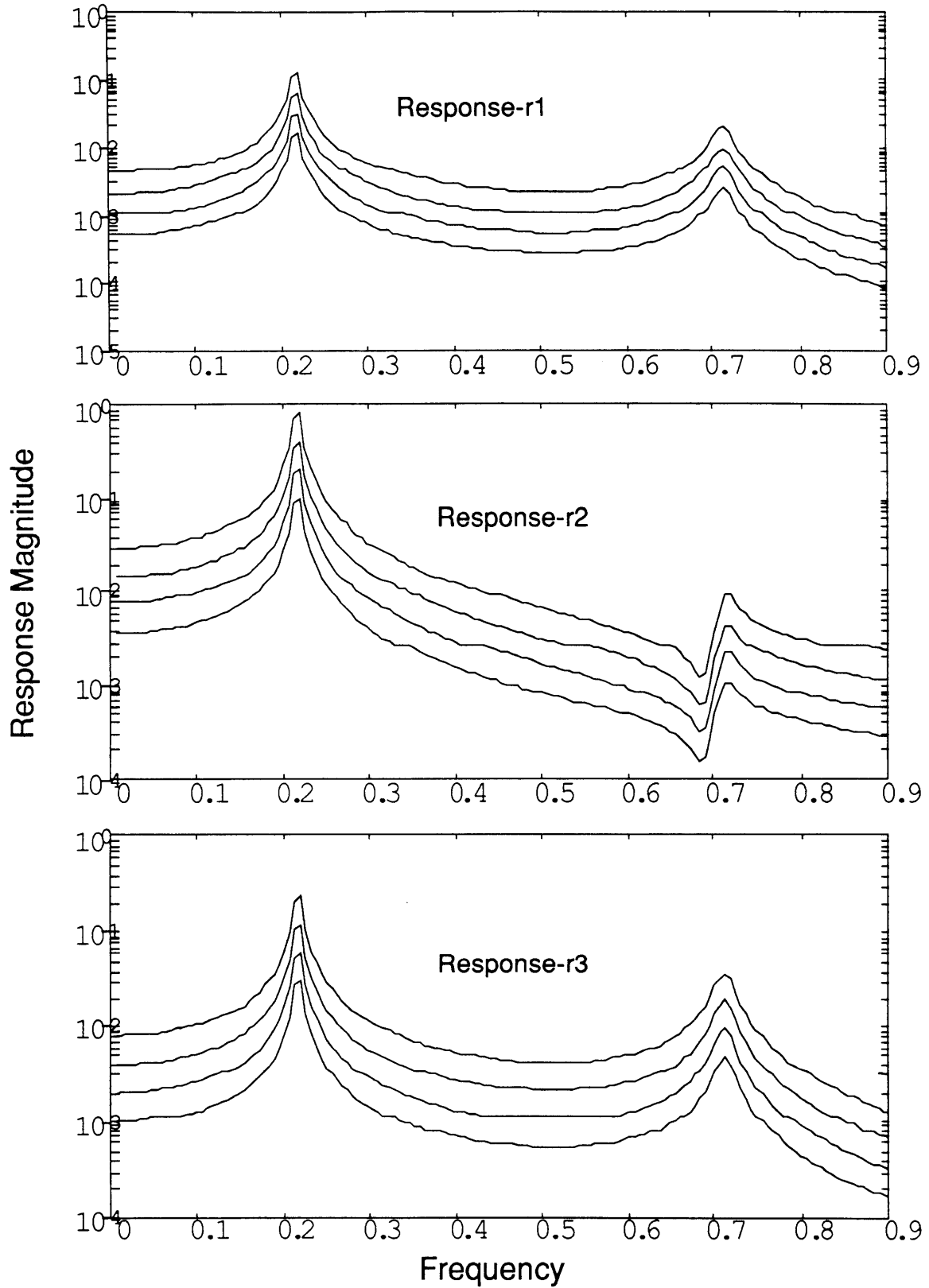


**Figure 4.5 Response of One Bay Cantilevered Truss modeled by Equivalent Beam with Linear Joints to Sinuoidal Forcing in Transverse Direction**



strut. In the 6 dof model, this mode consists of extension and rotation displacement with no transverse motion. This is significant in the analysis that follows.

Figure 4.5 shows the response of the truss structure with linear joints undergoing sinusoidal excitation by a force at the end of the truss structure acting in the transverse direction. The linear response is presented here as a reference point for the response of the later nonlinear models. The response is labeled by the degrees of freedom shown in figure 4.2. The ratio of strut stiffness to joint stiffness ( $EA/k_L L$ ) is equal to 0.5. The four different curves correspond to different levels of driving force. Each successive level of force is twice that of the preceding level. The response is shown on a logarithmic scale.

The two peaks shown on the curve correspond to the first two natural frequencies of the structure shown in Figure 4.4. The third mode is not apparent. Because the third mode does not have any transverse motion, the force at the tip does not excite this mode.

### Cubic Spring Joint

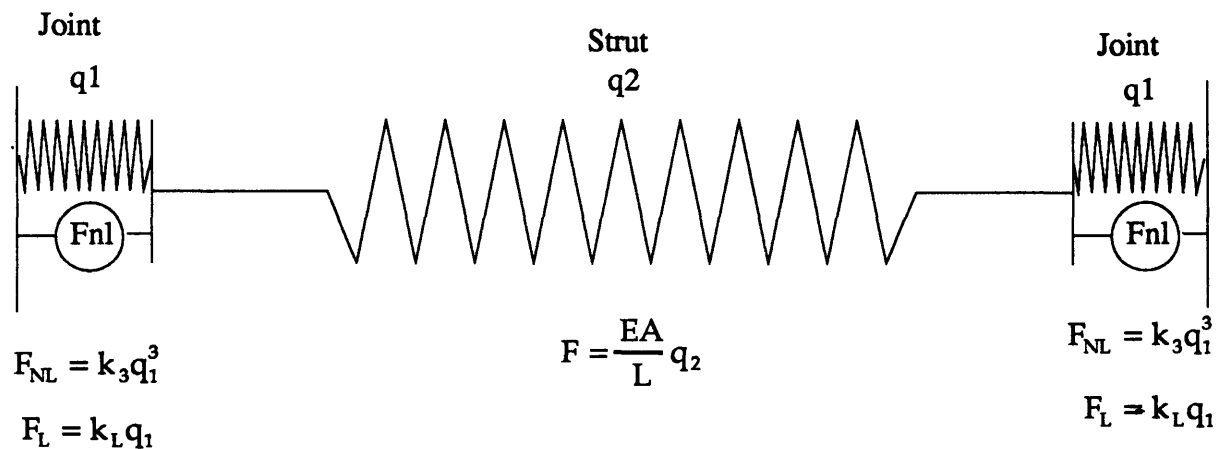


**Figure 4.6 Truss Element with Cubic Spring Joints in Parallel with Linear Joints**

The cubic spring nonlinear relationship for the joint shown in Figure 4.6 is:

$$F_{NL} = k_3 q_1^3 \quad (4.15)$$

where  $k_3$  is the coefficient of the cubic spring. The displacements across each joint are assumed to be equal. The total force in the joint is:

$$F = k_L q_1 + k_3 q_1^3 \quad (4.16)$$

The force through the structure is constant, therefore:

$$\frac{EA}{L} q_2 = k_L q_1 + k_3 q_1^3 \quad (4.17)$$

and the total displacement of the element is  $q$  which is related to the displacements of the joints and the strut by:

$$q = 2q_1 + q_2 \quad (4.18)$$

Solving this equation for  $q_2$ , substituting into equation (4.17) and dividing through by  $k_3$  gives:

$$q_1^3 + \left( \frac{k_L}{k_3} + 2 \frac{EA}{k_3 L} \right) q_1 - \frac{EA}{k_3 L} q = 0 \quad (4.19)$$

The only real-valued solution to this equation is:

$$q_1 = B_1 + B_2 \quad (4.20)$$

where

$$B_1 = \left( \frac{EA}{k_3 L} \right)^{\frac{1}{3}} \left( \frac{q}{2} + \sqrt{\frac{q^2}{4} + \left( \frac{EA}{27k_3 L} \right) \left( \frac{k_L L}{EA} + 2 \right)^2} \right)^{\frac{1}{3}}$$

$$B_2 = \left( \frac{EA}{k_3 L} \right)^{\frac{1}{3}} \left( \frac{q}{2} - \sqrt{\frac{q^2}{4} + \left( \frac{EA}{27k_3 L} \right) \left( \frac{k_L L}{EA} + 2 \right)^2} \right)^{\frac{1}{3}}$$

Equation (4.20) is then substituted into equation (4.16) to give:

$$F = k_L (B_1 + B_2) + k_3 (B_1 + B_2)^3 \quad (4.21)$$

This gives a relation for the force across the truss element in terms of the total displacement of the element. Equation (4.21) is in the form required for the calculation of the describing function equivalent stiffness coefficient which describes the truss element. Substituting (4.21) into (2.2) gives:

$$c_p = \frac{2}{\pi A} \int_0^{\pi} (k_L(B_1 + B_2) + k_3(B_1 + B_2)^3) \sin \phi \, d\phi \quad (4.22)$$

The quadrature coefficient,  $c_q$ , is zero for this non-hysteretic element.  $B_1$  and  $B_2$  now contain the substitution  $q=A \sin \phi$ , where  $\phi=\omega t$ . Because of the complexity of this equation, it is not integrated analytically. It is integrated numerically in the iteration procedure for each value of amplitude. The integration between 0 and  $\pi$  is divided into 50 intervals. This results in acceptable accuracy without a large increase in computing time.

Figure 4.7 shows the response of the one bay structure in figure 4.2 with truss elements that have cubic springs joints like those shown in figure 4.6. The force levels are the same as those for the linear structure shown in Figure 4.5. The response has the characteristics of a cubic spring nonlinear response. The solution is multivalued near the response peaks. The response curves and backbone curves have hardening spring features, i. e., the peak frequencies increase as the response amplitude increases. The zero that appears in the response in the transverse direction at the tip ( $r_2$ ), also moves to the right with an increase in response amplitude.

The backbone curve shapes are typical for a cubic spring nonlinearity. The lower end corresponds to the frequency of the structure with the linear joints discussed in an earlier section. The upper end corresponds to the frequency of the structure with completely locked joints. The truss element then has solely the stiffness of the strut.

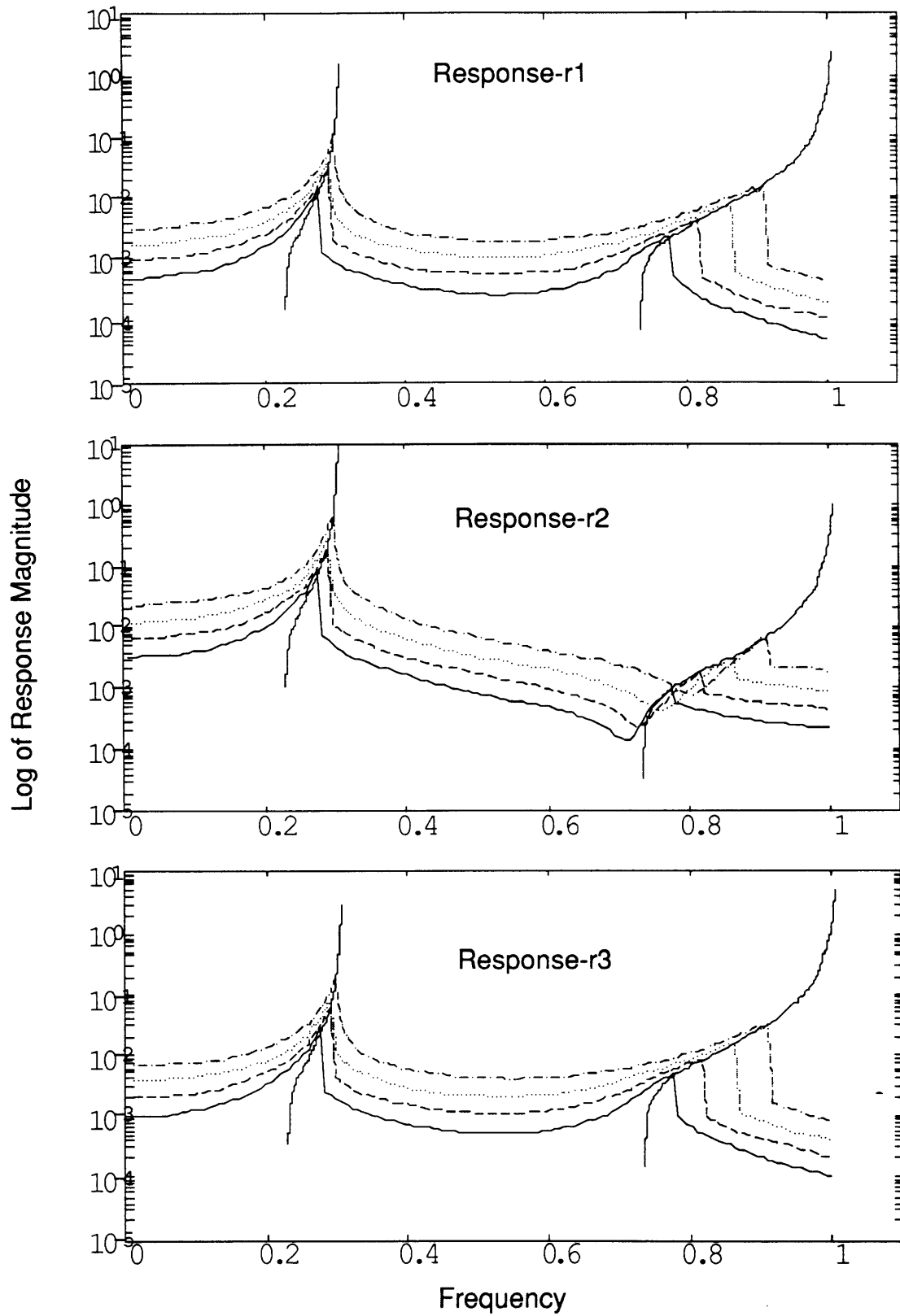


**Figure 4.7 Response of One Bay Truss with Cubic Spring Joints to Sinusoidal Excitation with Backbone Curves**

## Gain Change Joint

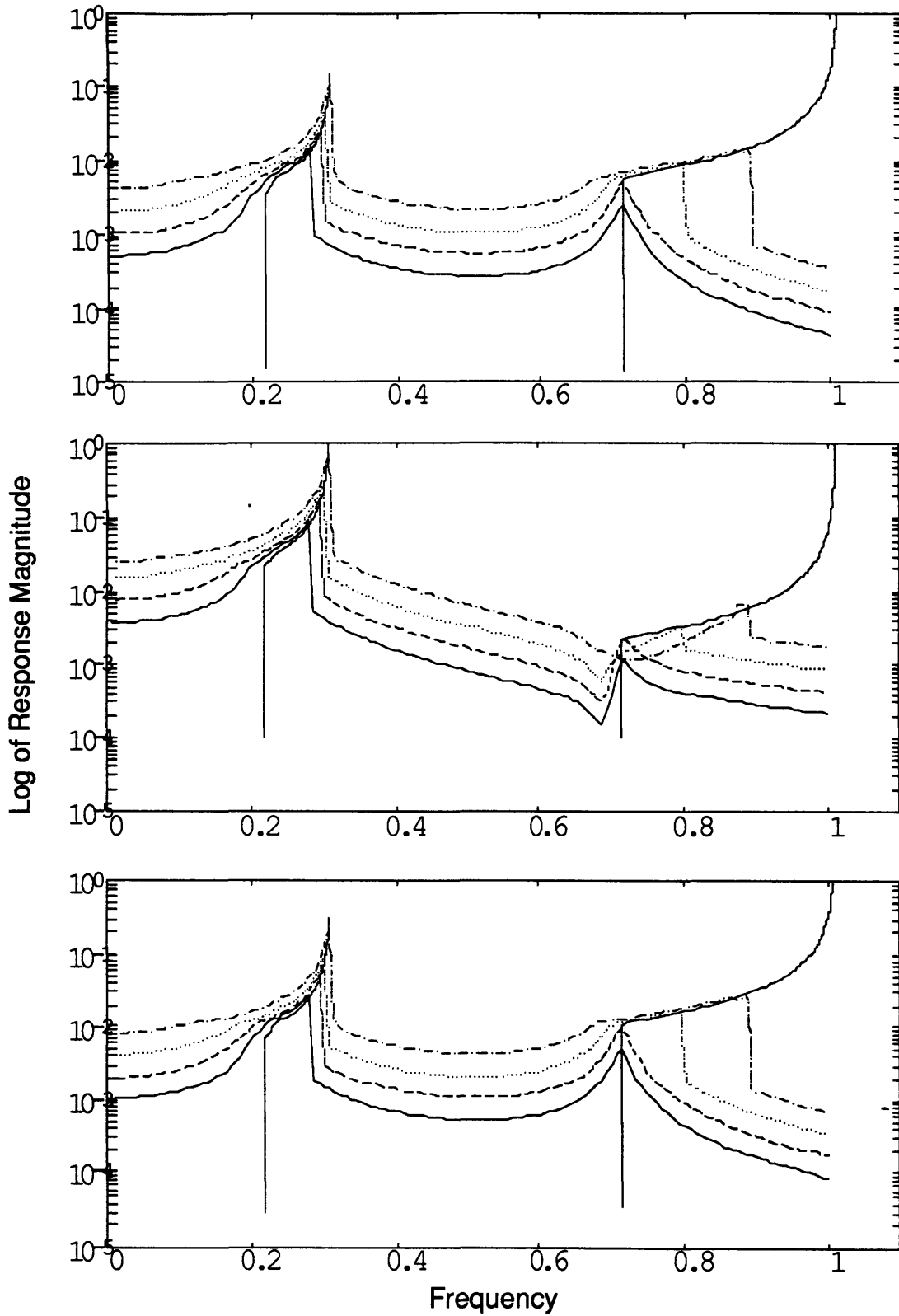
The gain change joint is similar to the linear joint in terms of the stiffness of the truss element over a certain amplitude range. The stiffness of the structure within a certain amplitude range is given by equation (3.30). Outside of that range, the stiffness is given by a similar equation that has a different stiffness term. The stiffness of the element is defined then as:

$$\begin{aligned} \text{If } |q| \leq \delta, \quad k_{eq} &= \frac{1}{2 \frac{EA}{k_1 L} + 1} \\ \text{If } |q| > \delta, \quad k_{eq} &= \frac{1}{2 \frac{EA}{k_2 L} + 1} \end{aligned} \quad (4.23)$$

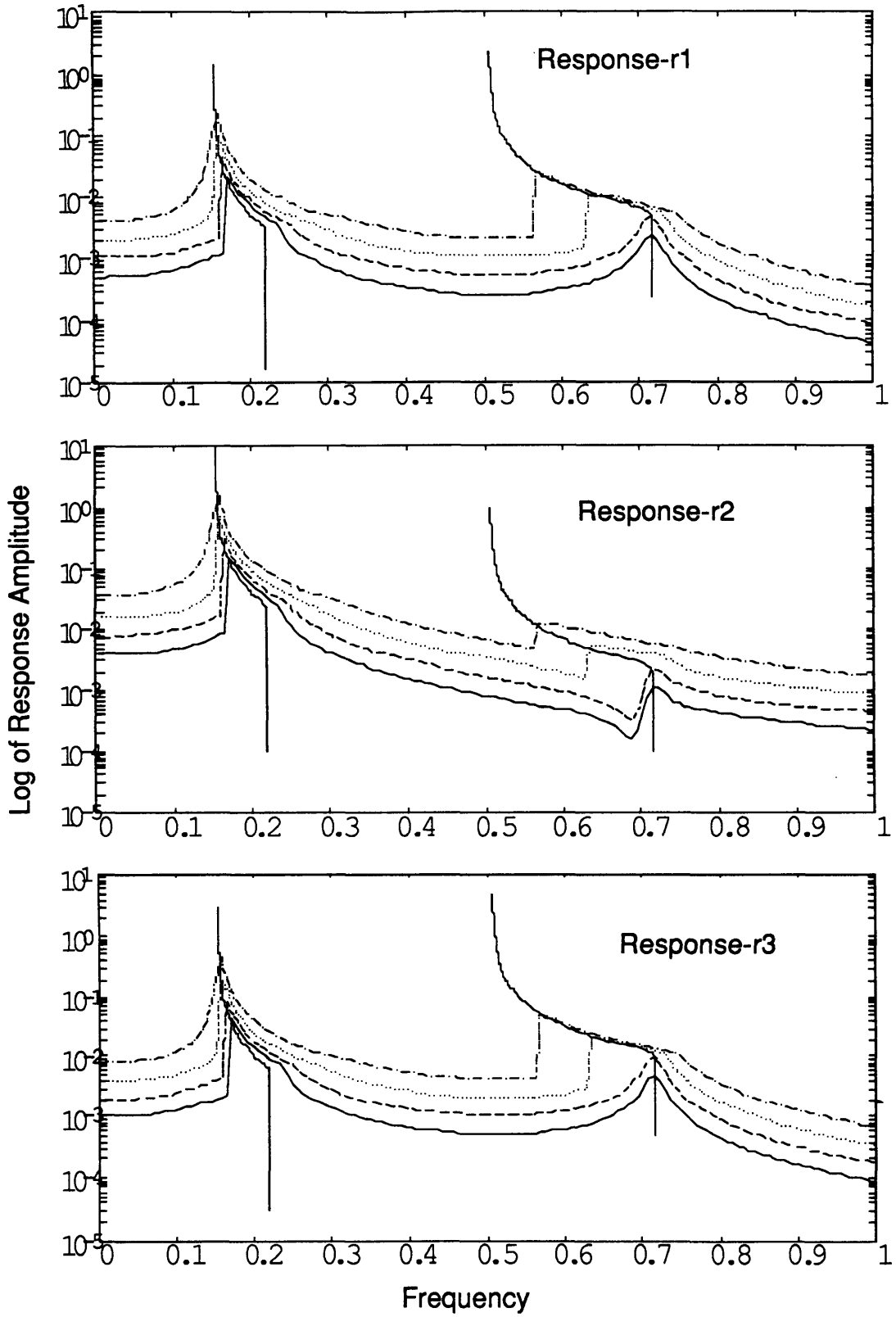
where  $q$  is the displacement across the element, and  $k_1$  and  $k_2$  are the stiffnesses of the joint within each linear range respectively. These values are used in the calculation of the DF coefficients.

Figure 4.8 shows the response of the one bay truss with gain change joints to sinusoidal excitation at the tip of the truss in the transverse direction. The sweep direction in this case is forward or from lower to higher frequency. The response has many of the characteristics of the cubic spring nonlinearity. The shape of the curve indicates a hardening spring, or peak frequency increasing with amplitude. The response is multivalued near the peak frequency with a sharp drop-off from the upper branch of the solution to the lower branch. The backbone curve has some differences. The curve veers sharply once the displacements across the joints exceed the lower stiffness range. The lower, straight part of the backbone curve corresponds to the frequency of the structure with linear joints that have the same properties that are used in the model which generated the curves shown in Figure 4.5. The upper part of the backbone curve asymptotically approaches the frequency of the structure having joints of stiffness  $k_2$ . The ratio of  $k_2/k_1$  is 2 in this case.

When the gain change is in the form of a softening spring or  $k_2/k_1 < 1$ , the response characteristics are somewhat different. Figure 4.9 shows the response of the one bay truss to sinusoidal excitation of the tip with  $k_2/k_1=0.5$ . The sweep direction in this case is backward or



**Figure 4.8 Response to Transverse Sinusoidal Excitation of One Bay Truss with Hardening Spring Gain Change Joints Modeled by Equivalent Beam.**



**Figure 4.9 Response to Transverse Sinusoidal Excitation of One Bay Truss with Softening Spring Gain Change Joints Modeled by Equivalent Beam**

from higher to lower frequency. The response peaks now shift to a lower frequency with increasing amplitude. The backbone curve asymptotes are again at frequencies defined by the two joint stiffnesses  $k$  and  $k$ . At higher force levels, the zero that appeared in the response of the cubic spring transverse displacement plot does not appear.

**4.5 SIMPLE EXAMPLES - FIVE BAY CANTILEVERED TRUSS**

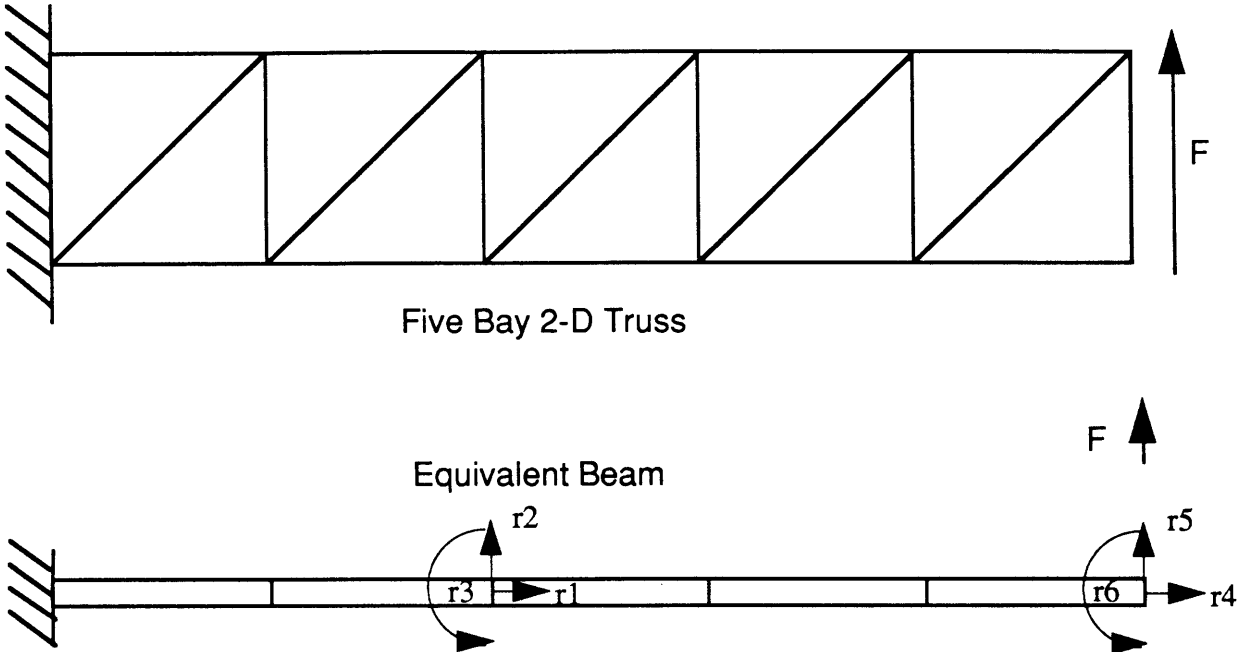


**Figure 4.10. 2-D Five Bay Cantilevered Truss with Equivalent Beam Model**

The five bay truss shown in Figure 4.10 shows more beam-like behavior than the one bay model. The following analysis and plots will apply the nonlinear equivalent beam finite element method to the truss with the two nonlinear joints that were analyzed for the one bay truss. In addition, two nonlinearities that introduce nonlinear damping into the structure will be examined.

**Linear Spring**

The stiffness coefficients and linear model were developed previously for the linear joint model. Figures 4.11 and 4.12 show the response of the five bay 6 dof model with linear springs for the degrees of freedom pictured in Figure 4.10. The value of  $EA/k_L L$  from equation (3.30) is



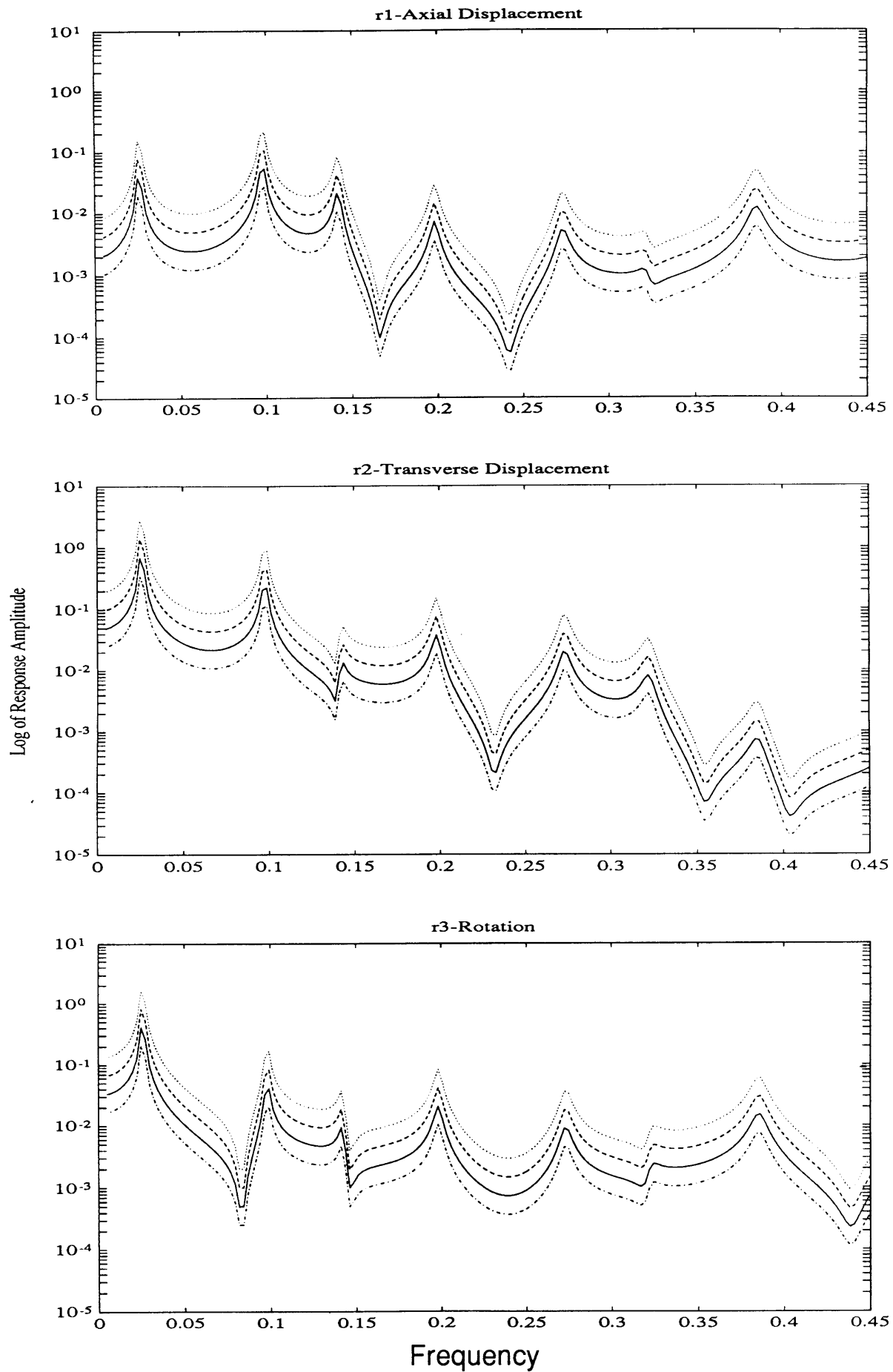


Figure 4.11 Response at End of Bay 2 to Transverse Sinusoidal Forcing at tip of Five Bay Truss with Linear Joints Modeled by Equivalent Finite Element Beam

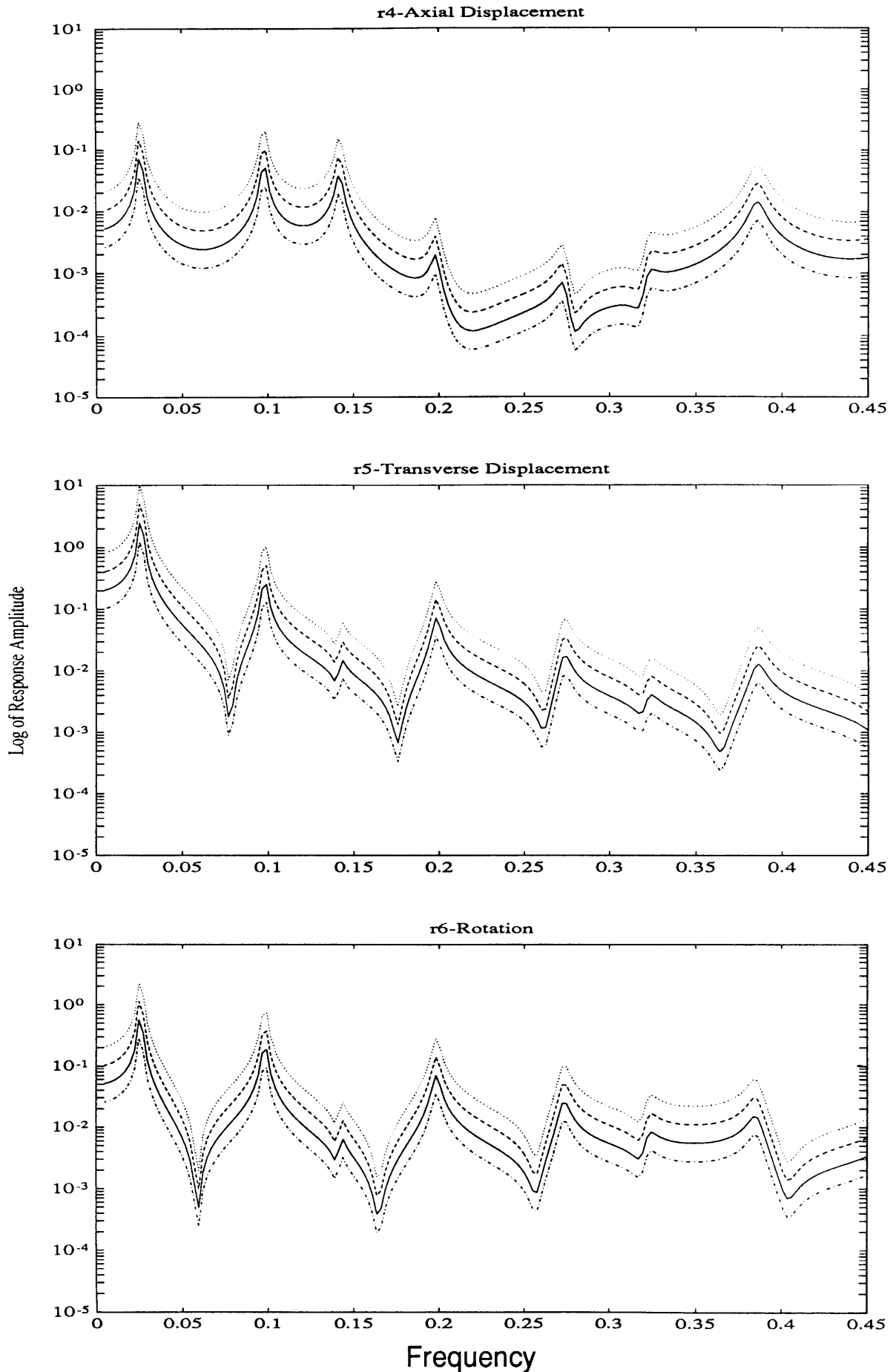


Figure 4.12 Response at End of Truss to Transverse Sinusoidal Forcing at Tip of Five Bay Truss with Linear Joints Modeled by Equivalent Finite Element Beam

0.5. The degrees of freedom were chosen to give an idea of the overall response of the model. These same dof will be shown for the nonlinear models. The first four resonant frequencies and mode shapes of the linear model are shown in Figure 3.4. The other frequencies for the five bay truss that appear on the response curves in Figures 4.11 and 4.12 are:

$$\begin{aligned}\omega &= 0.2731\omega_p, & \text{Third Bending} \\ \omega &= 0.3223\omega_p, & \text{Fourth Bending} \\ \omega &= 0.3855\omega_p, & \text{Second Axial}\end{aligned}$$

The frequency scale on the abscissa is nondimensional. The linear response is presented as a baseline for comparison to the nonlinear model responses. The four force levels are the same as those used for the one bay model;  $F = 0.0005 EA$ ,  $0.001 EA$ ,  $0.002 EA$ , and  $0.004 EA$ . These same force levels are used for all of the nonlinear analyses. Characteristics of interest include the small response of mode 3 and mode 7 to transverse excitation of the tip of the truss for dof r5. This mode is a longitudinal mode of the truss and therefore will have small response when the structure is driven in the transverse direction.

### **Cubic Spring**

Figures 4.13 and 4.14 shows the response of the truss model with cubic springs to sinusoidal forcing at four different levels. The plot spans the first seven modal frequencies and includes the backbone curves of the response peaks. The value of the cubic spring in the joints is  $k_3 = 1.0 \times 10^{-6} EA/L^3$ . The cubic spring is in parallel with a linear spring with the same value as that of the linear model discussed above. The response characteristics of this cubic spring structure are similar to those of the one bay structure. These include a hardening effect that causes a shift to higher resonant frequency with an increase in amplitude, jump phenomena, and a change in the frequency of the zeros. The zeros appear to be cancelled to a certain extent by the jump phenomenon that appears to bypass these zeros. The higher modes, with more motion of the joints, are more affected than the lower modes. Another point of interest is in Figure 4.14 on the r4-Axial Displacement curve in which the backbone curves of modes 5, 6 and 7 are very close and

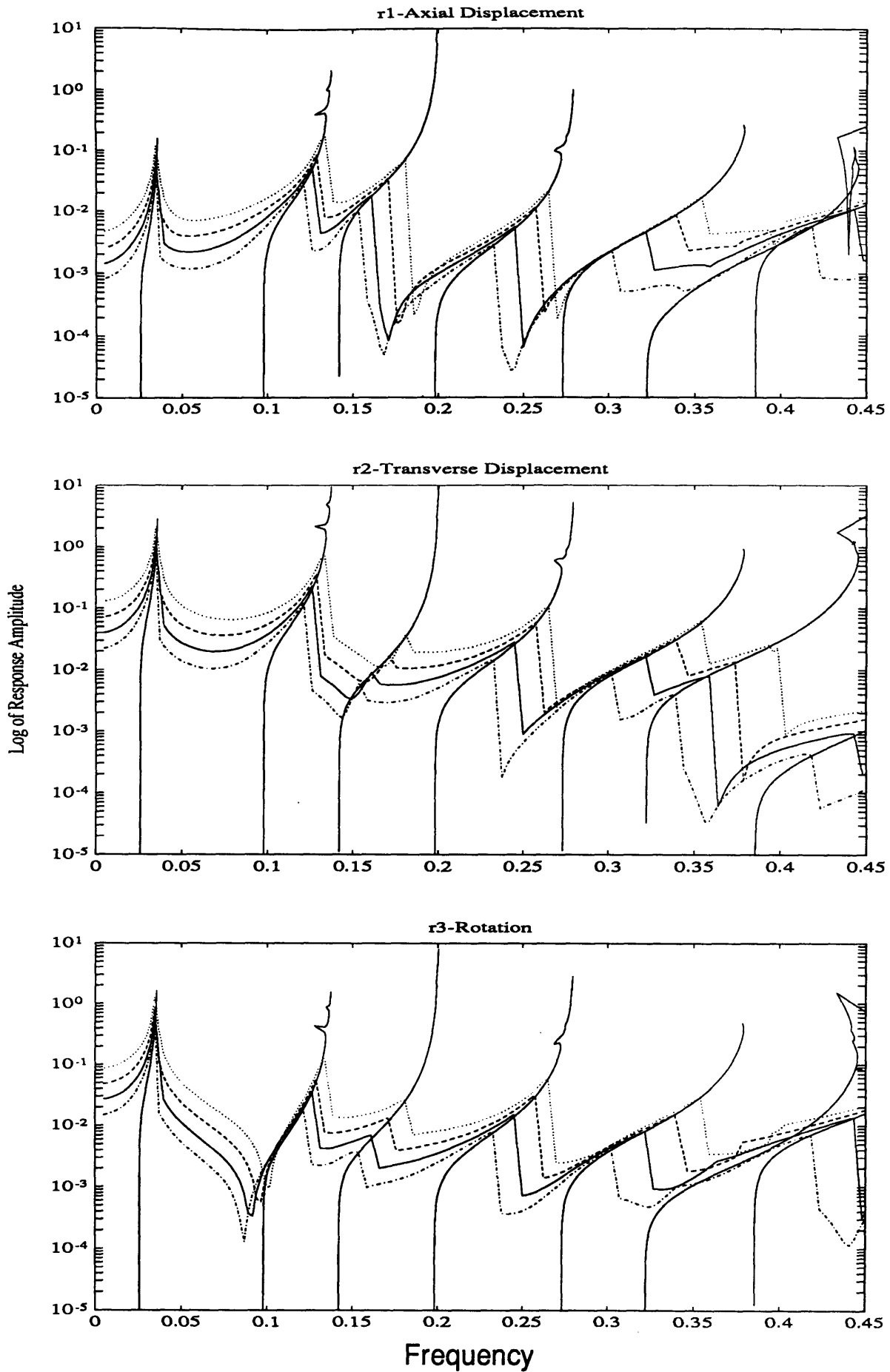


Figure 4.13 Response at End of Bay 2 to Transverse Sinusoidal Forcing at Tip of Five Bay Truss with Cubic Spring Joints Modeled by Nonlinear Equivalent Beam

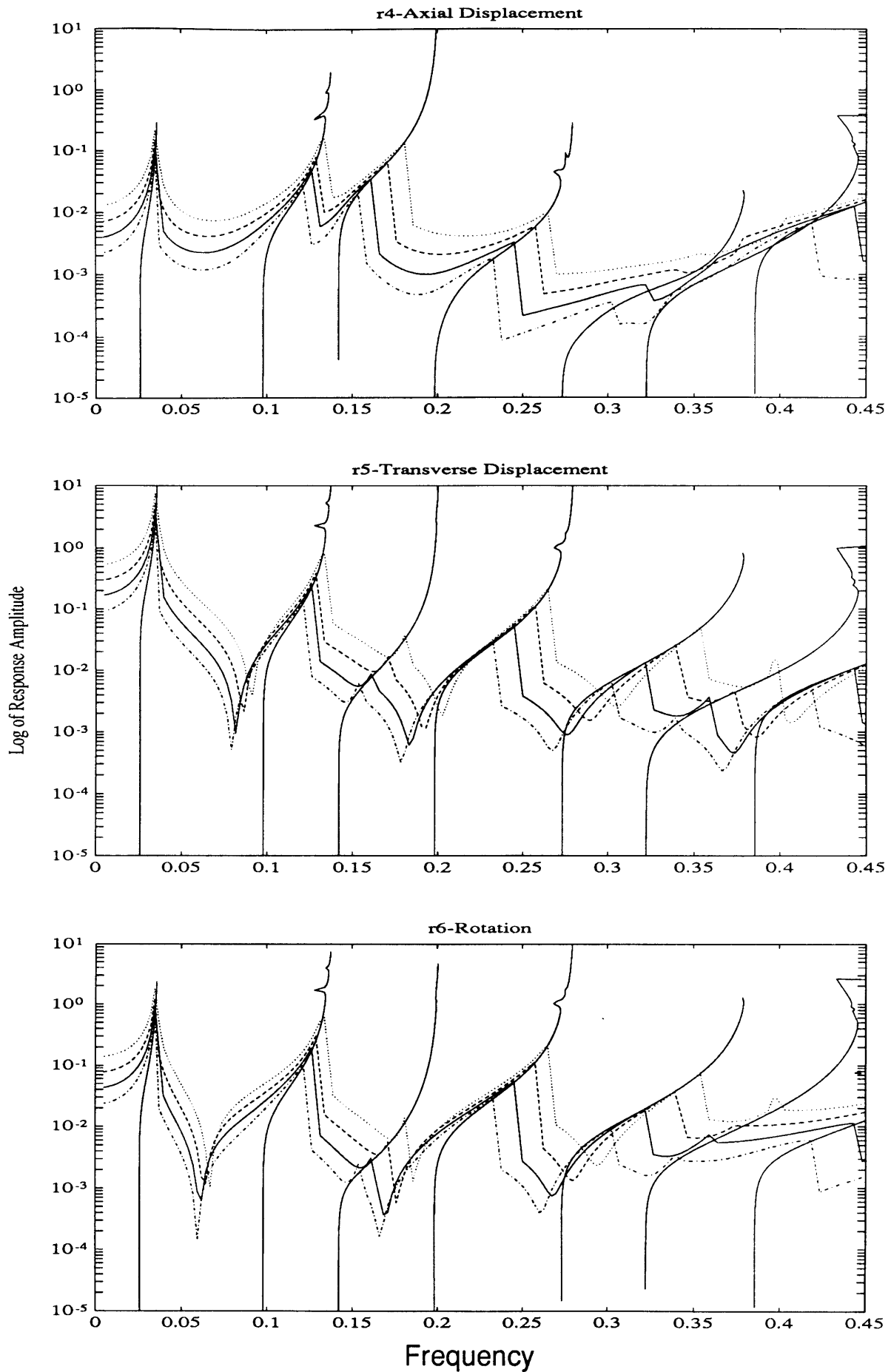


Figure 4.14 Response at End of Truss to Transverse Sinusoidal Forcing at Tip of Five Bay Truss with Cubic Spring Joints Modeled with Nonlinear Equivalent Beam

the curves for modes 6 and 7 cross. The response curve is complex in this area. The response is flat and the small resonant peaks do not occur along a backbone curve. These calculated backbone curves do not take into account cross-coupling effects, pole-zero cancellation and the effect of damping on the response peaks.

Certain backbone curves contain small “glitches” at large amplitudes. These are due to the calculation of the displacements across the truss members. The algorithm contains no limits on the size of the displacements so that rotation of the ends of one truss bay can cross and the bay inverts itself. This causes the displacement of the diagonal truss member to go to zero at one point and the backbone curve shows this effect. It is not a representation of a physical phenomenon. This occurs on other nonlinear plots as well.

### **Gain Change - Hardening**

Figures 4.15 and 4.16 show the response to sinusoidal forcing of the five bay truss model with a gain change joint that has a hardening characteristic. The value of the spring constant within the linear range is the same of that of the linear model. The stiffness ratio of the upper part of the piecewise linear curve to the lower part for the entire joint-strut-joint structure is 2. The point at which the change occurs is equal to  $0.01L$ , where  $L$  is the reference length. This plot has similar characteristics to that of the cubic spring in that it shows an increase in frequency with an increase in amplitude. The backbone curves have a similar shape as well except the gain change curves have a sharp change when the value of displacement at which the gain change occurs ( $\delta$ ) is passed. Because the zeros in the response curve are usually delineated by response at levels lower than  $\delta$ , the frequency of the zero, in general, does not change. The jump phenomena then bypasses these zeros and they do not show up in the response.

The backbone curves for this nonlinear structure also intersect for some of the frequencies. The response in the vicinity of these crossed curves is flat and the small resonant peaks do not occur along the backbone curves. As in the case of the cubic spring, the higher modes are more affected by the nonlinear joint.

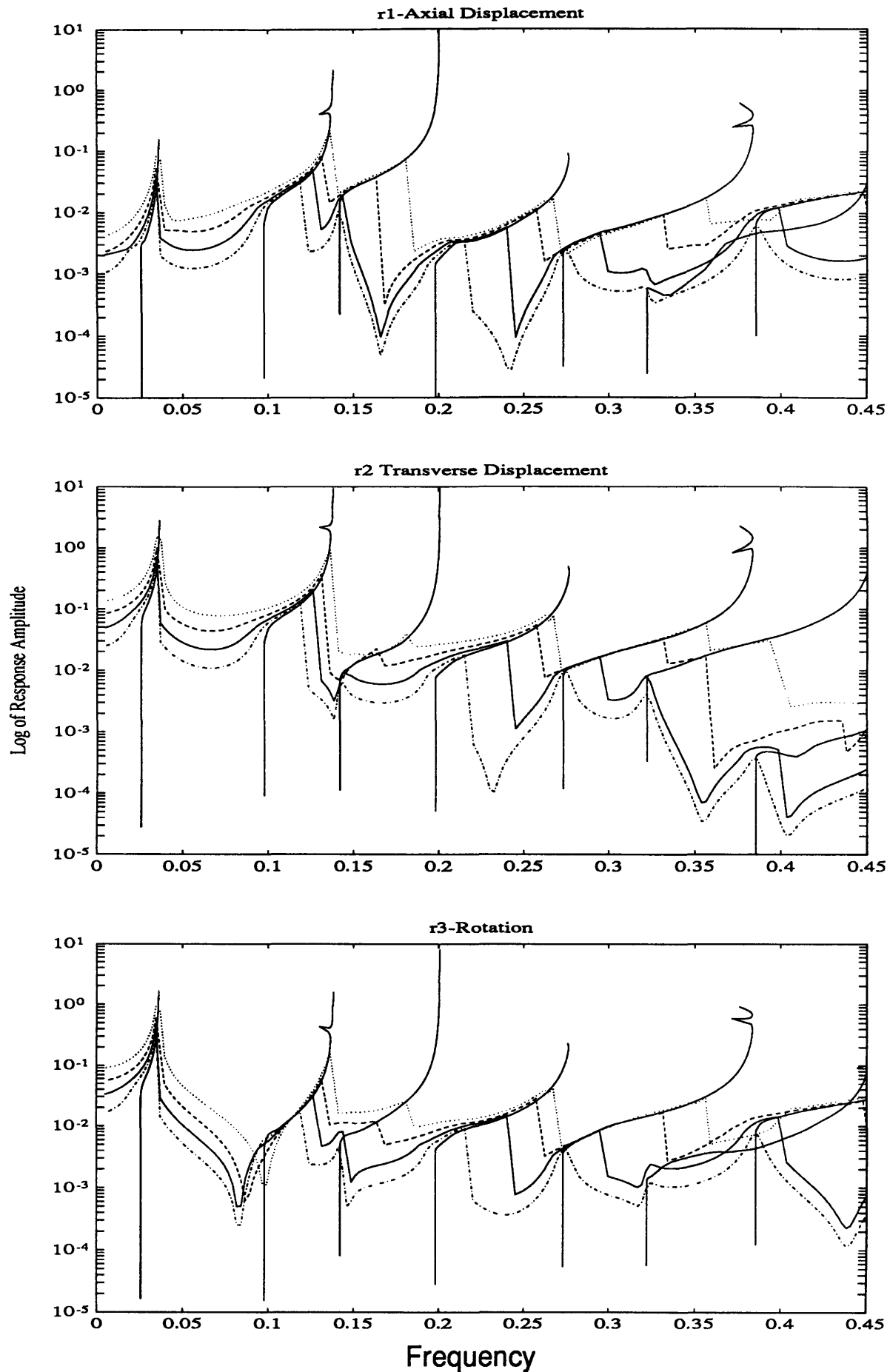


Figure 4.15 Response at End of Bay 2 to Transverse Sinusoidal Forcing at tip of Five Bay Truss with Hardening Gain Change Joints Modeled with Nonlinear Equivalent Beam

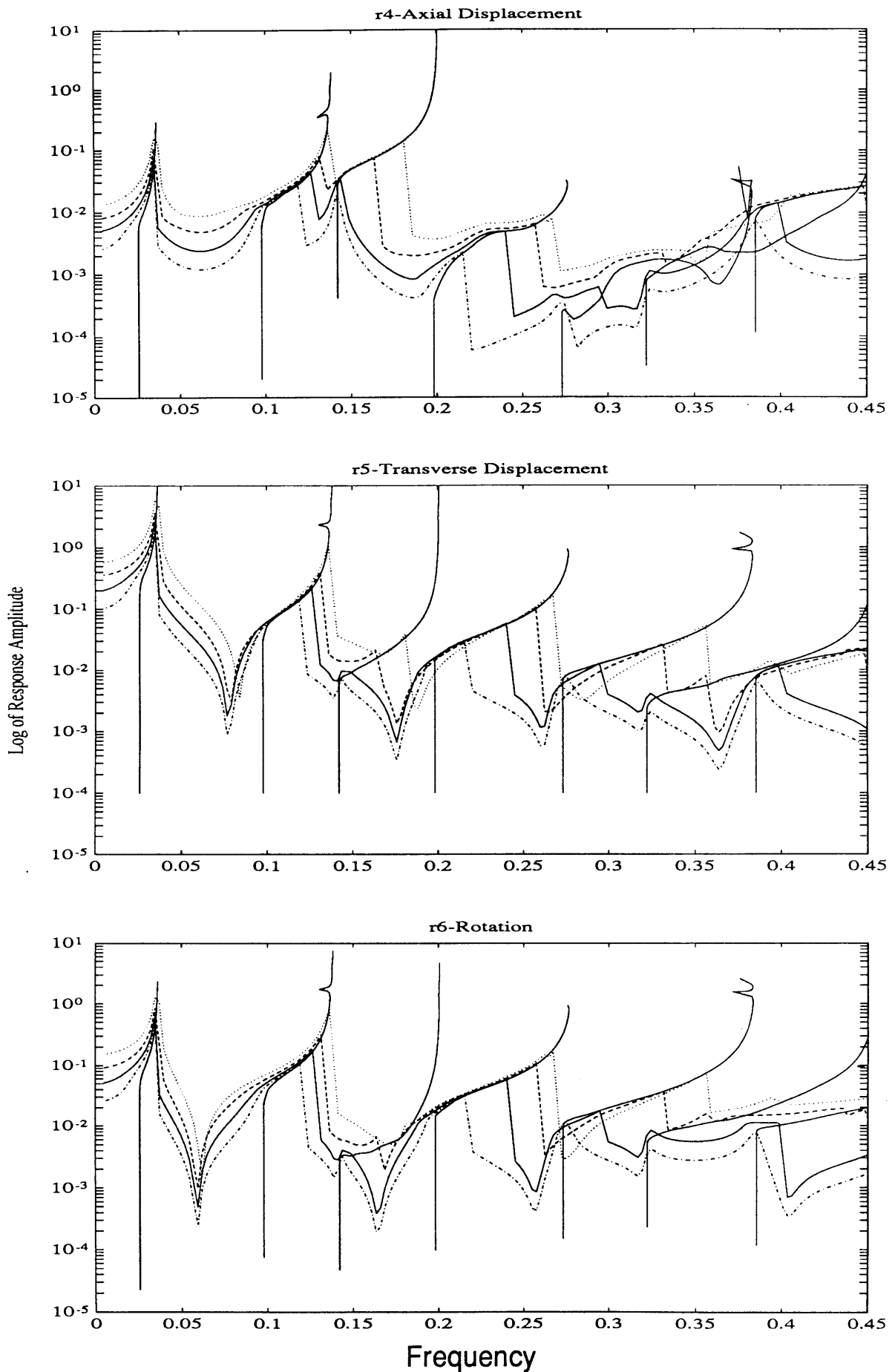


Figure 4.16 Response at End of Truss to Transverse Sinusoidal Forcing at Tip of Five Bay Truss with Hardening Gain Change Joints Modeled by Nonlinear Equivalent Beam



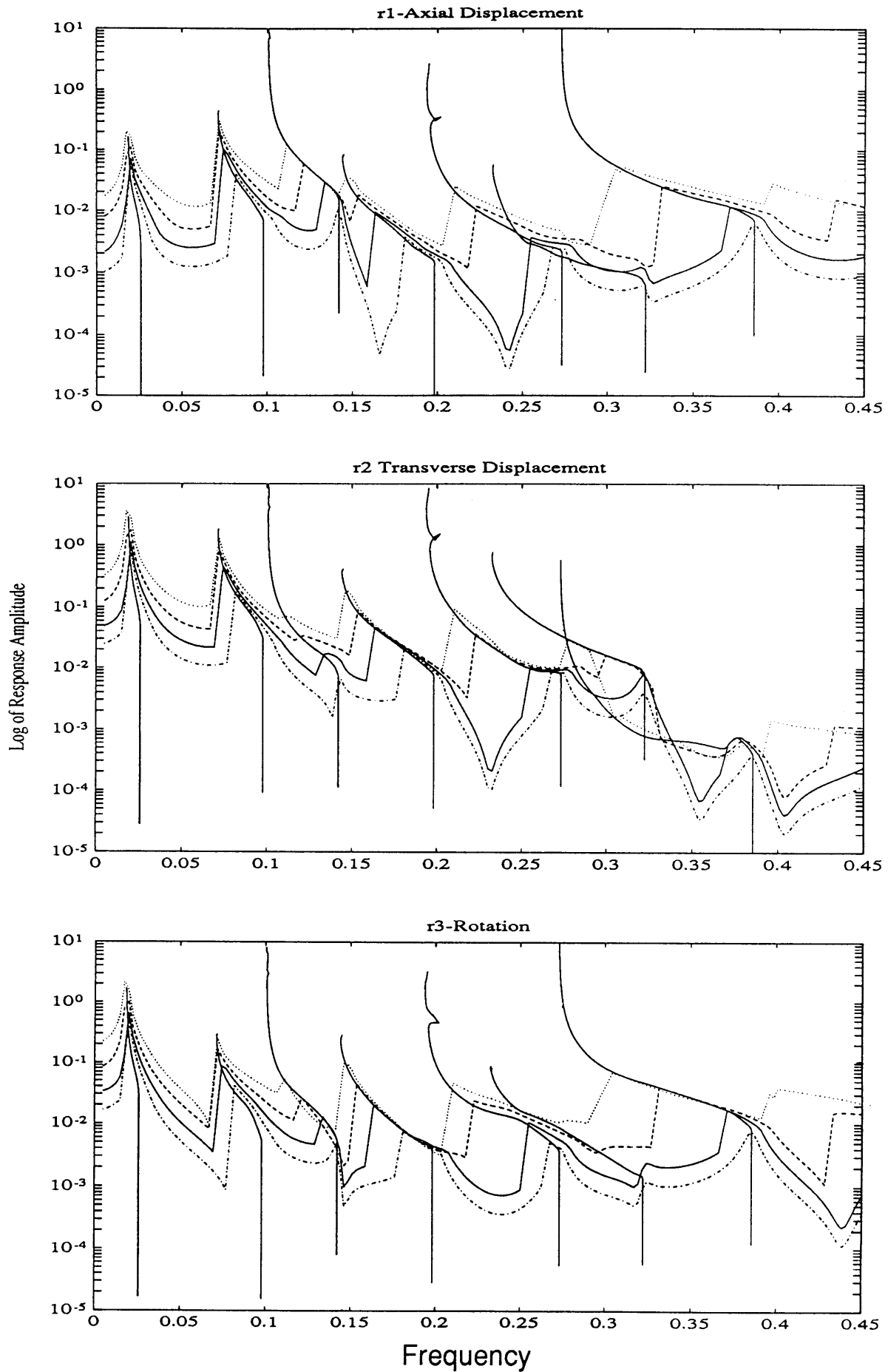


Figure 4.17 Response at End of Bay 2 to Transverse Sinusoidal Forcing at Tip of Five Bay Truss with Softening Gain Change Joints Modeled by Nonlinear Equivalent Beam

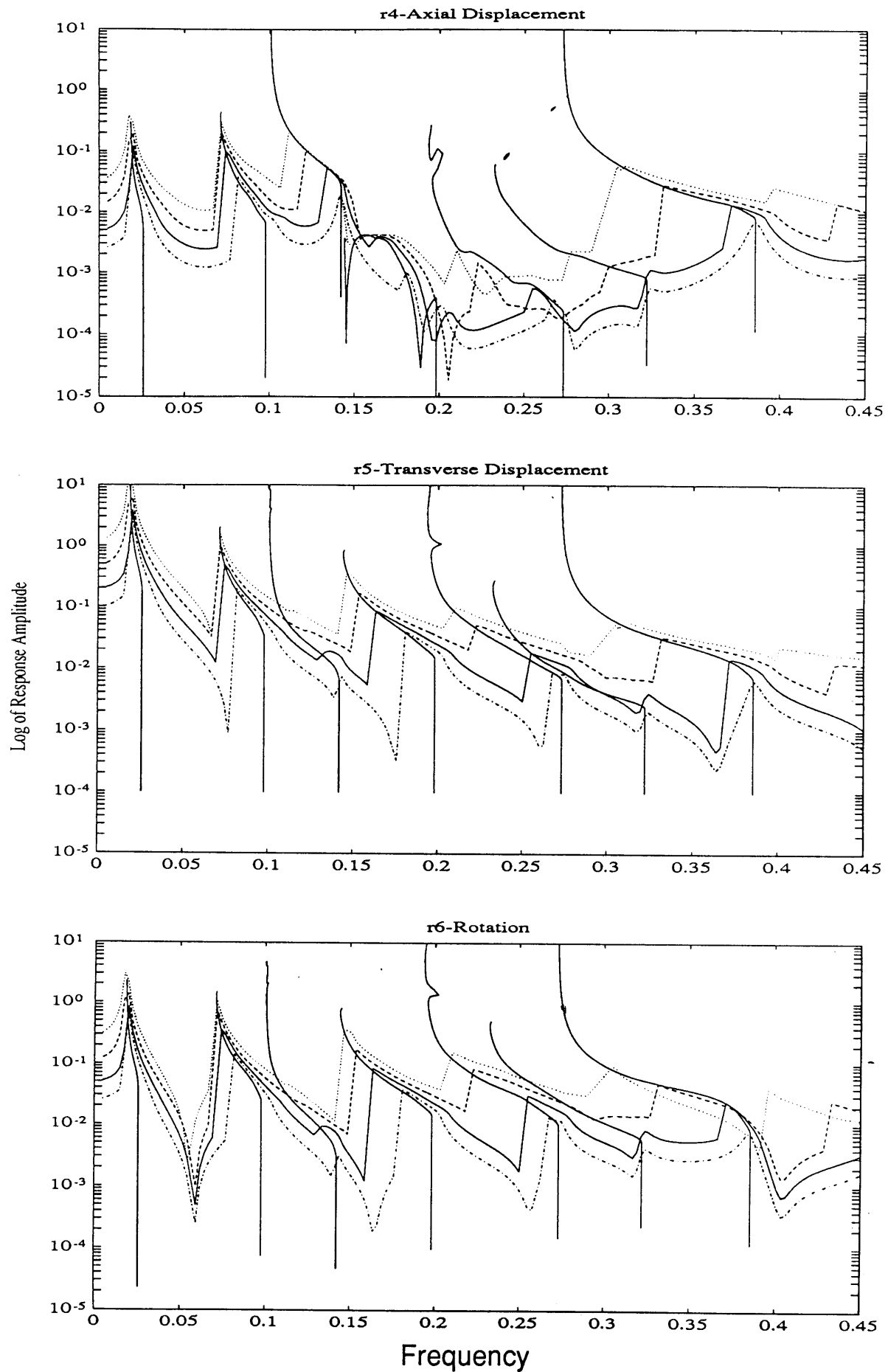


Figure 4.18 Response at End of Truss to Transverse Sinusoidal Forcing at Tip of Five Bay Truss with Softening Gain Change Joints Modeled by Nonlinear Equivalent Beam

## Gain Change - Softening

Figures 4.17 and 4.18 show the response of the five bay model with a softening spring gain change joint. The stiffness ratio is 0.5 in this case. The response is similar in character to the hardening spring but with a decrease in frequency with an increase in amplitude. The interference of one mode with another is also apparent. The crossing of backbone curves is again present at the higher frequencies. It is also present at lower frequencies. The third mode does not appear in the response in Figure 4.18 (r5-Transverse Displacement) due to the closeness of the third mode backbone curve to mode 2.

## Natural Nonlinear Joint

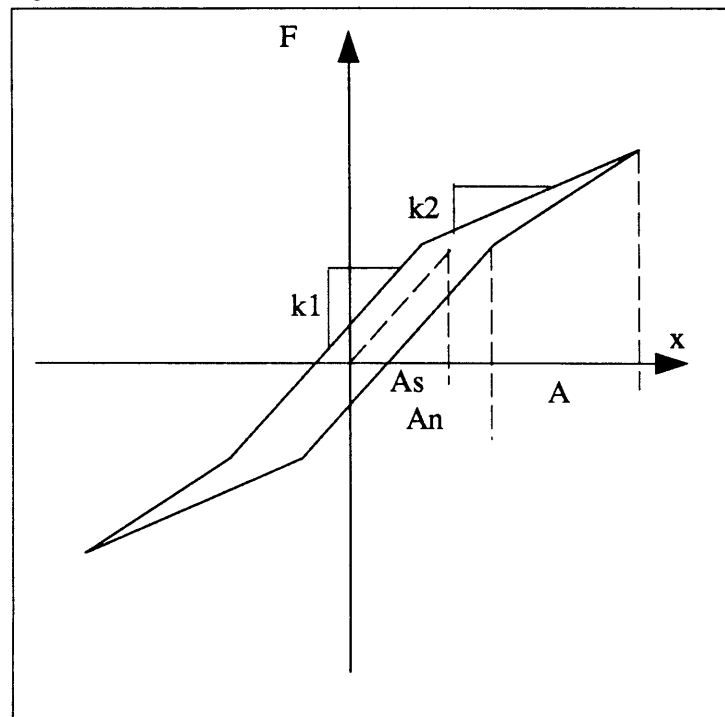


Figure 4.19 Natural Nonlinear Joint

Figure 4.19 shows a schematic of the input-output relation for a joint that is characteristic of some joint test data and is therefore called a natural joint. It has hysteresis and therefore has some nonlinear damping effects. The nonlinearity is characterized by the slopes of the two ranges of behavior, the amplitude  $A_s$  that separates linear and nonlinear behavior, the total amplitude  $A$  and  $A_n$ , the amplitude at which the slope changes on the underside of the curve. The value of  $A_n$

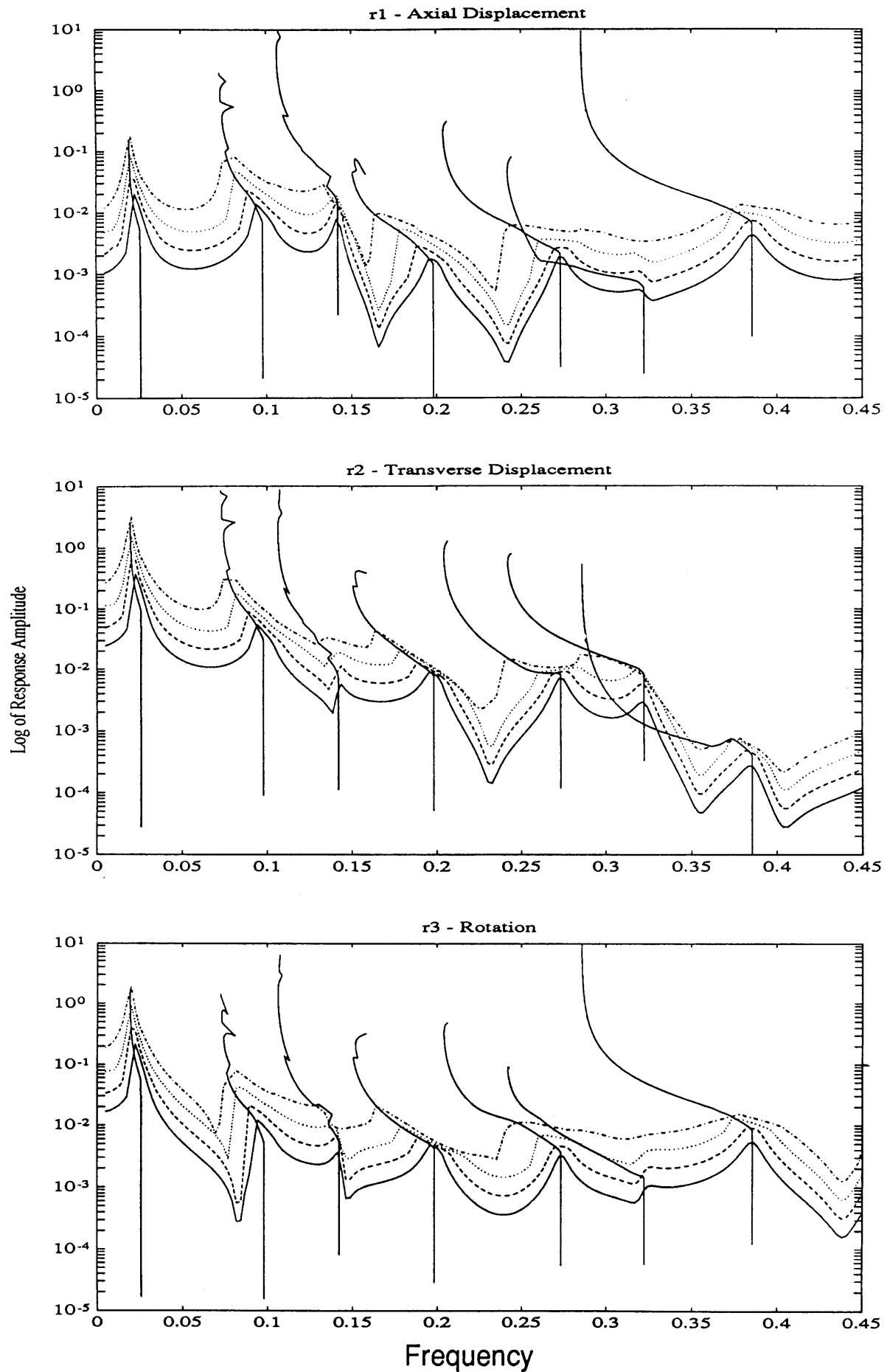


Figure 4.20 Response at End of Bay 2 to Transverse Sinusoidal Forcing at Tip of Five Bay Truss with Natural Joints Modeled by Nonlinear Equivalent Beam

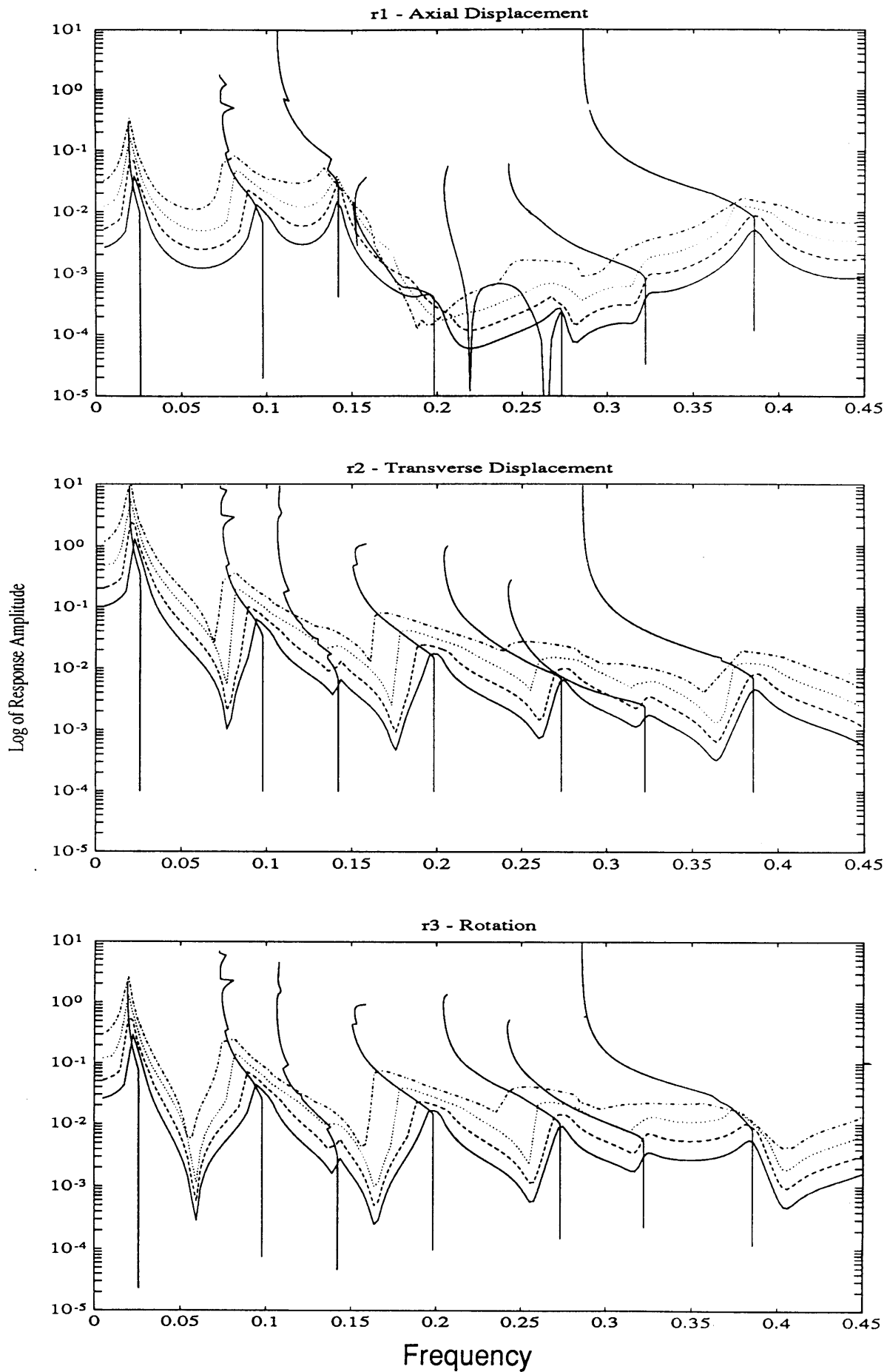
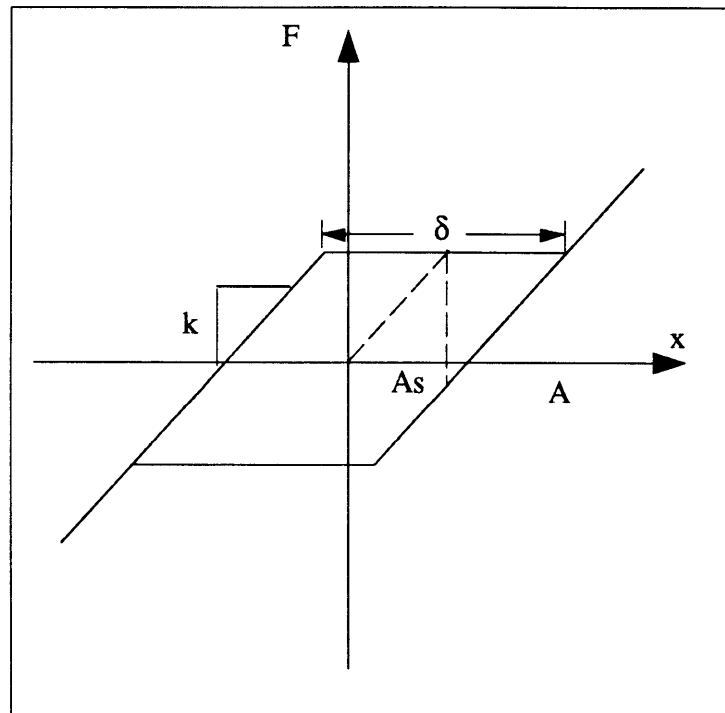


Figure 4.21 Response at End of Truss to Transverse Sinusoidal Forcing at Tip of Five Bay Truss with Natural Joints Modeled by Nonlinear Equivalent Beam

is equal to  $A_s$  plus a fixed fraction of the difference between the total amplitude and  $A_s$ , and therefore varies with total amplitude.

This is the first nonlinear element to be analyzed that produces nonlinear damping. The values for the DF coefficients are calculated using the equations shown in Appendix A. The response of the five bay truss with this type of joint is shown in Figures 4.20 and 4.21. The value of  $A_s$  is  $0.01L$ , the value of  $A_n$  is  $0.1A$  and  $k_2/k_1$  is  $0.5$ . The response shows features similar to those of the softening gain change spring. The nonlinear damping compacts the response peaks in the area of the backbone curves. The peaks do not always occur at the backbone curves as in the previous nonlinear cases. The nonlinear damping effect does not have as much effect on the location of the response peaks as one would think. The asymptotes of the backbone curves correspond to systems with stiffness  $k_1$  at the lower end and  $k_2$  at the upper end.

### Sliding Pin Joint



**Figure 4.22 Sliding Pin Nonlinearity**

Figure 4.22 shows a schematic of the sliding pin nonlinearity. The element acts as a linear spring until an amplitude is reached,  $A_s$ , after which friction is overcome and the force is constant

and the element slides until it hits a stop. The stiffness is then the same as the linear range. The behavior is governed by  $A_s$ ,  $k$  and  $\delta$ , the width of the gap.

Figures 4.23 and 4.24 show the response curves of the five bay truss with sliding pin joints. The value of  $A_s$  is  $0.01L$ , the value of  $\delta$  is  $0.05L$ , and the stiffness term is the same as that of the linear model. The backbone curves are unusual compared to previous nonlinear elements. The bottom asymptote is at the frequency of the linear model as with the previous nonlinear models. The upper asymptote, however, is also at the same frequency as the linear model. This is due to the behavior of the joint when the amplitude is very much greater than  $\delta$ . The model also shows the effect of the nonlinear damping in the compacting of resonant peaks.

#### **4.6 SUMMARY**

The preceding sections described how the nonlinear equivalent beam method may be applied to a simple two dimensional truss undergoing sinusoidal excitation for a variety of nonlinear elements. The plots of these responses give an idea of the nonlinear global characteristics that these nonlinear joints cause in the dynamics of a structure. This information may be used to determine, in Chapter 6, the type of nonlinear element that is present in the Mini-Mast.

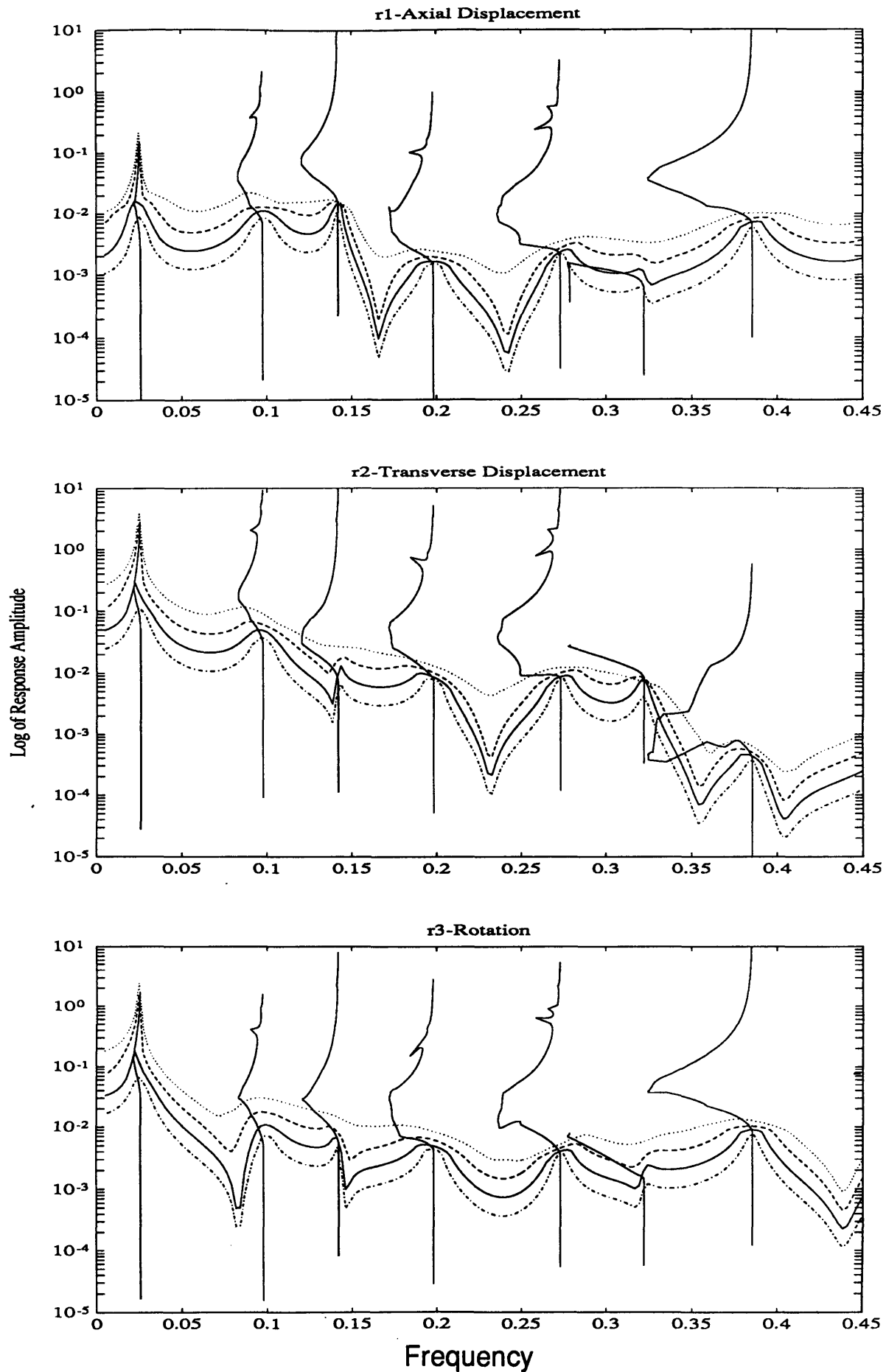


Figure 4.23 Response at End of Bay 2 to Transverse Sinusoidal Forcing at Tip of Five Bay Truss with Sliding Pin Joints Modeled by Nonlinear Equivalent Beam



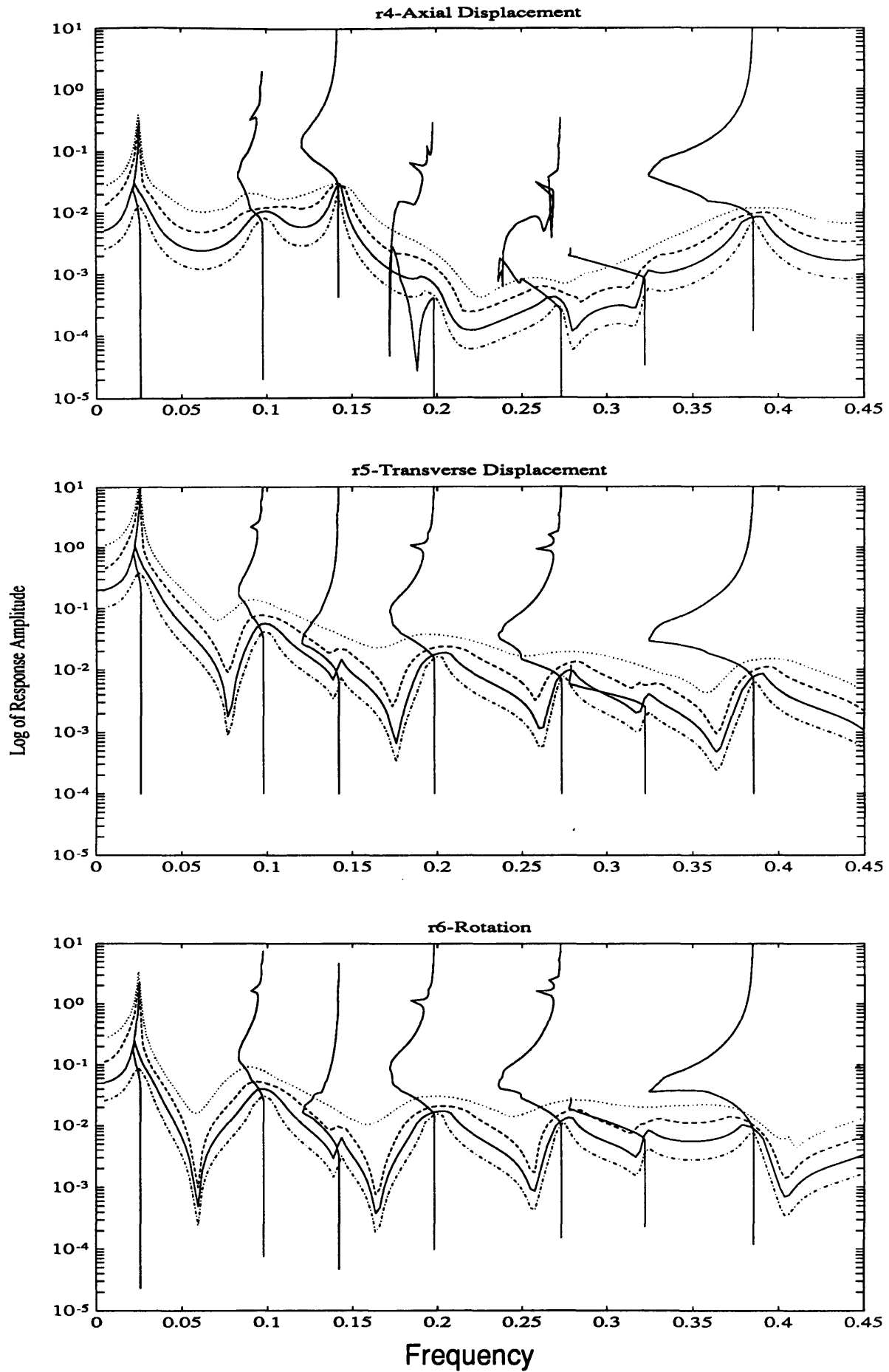


Figure 4.24 Response at End of Truss to Transverse Sinusoidal Forcing at Tip of Five Bay Truss with Sliding Pin Joints Modeled by Nonlinear Equivalent Beam

## **CHAPTER 5**

### **MODELING NONLINEAR STRUCTURES WITH A PRE-LOAD**

#### **5.1 INTRODUCTION**

One of the problems encountered when testing space-flight hardware on the ground is the effect of gravity on the dynamic behavior of structures. This is especially true in the case of structures with nonlinear characteristics. A desirable analytical model would contain information describing the change in dynamic behavior of a structure between a micro-gravity environment and a one G model. This type of model could give insight into the necessary models for designing precision control algorithms for structures.

The principal effect of gravity on a jointed structure is to introduce a pre-load in the joint. For a linear structure, this would make no difference and the stiffness of the structure would not change. For a structure with nonlinear joints, the offset introduces changes in the input-output characteristic of the joint that are not modeled by the Single Input Describing Function described in Chapter 2 and implemented in Chapter 4. The bias that the pre-load introduces can be modeled by the Dual-Input Describing Function.

#### **5.2 DUAL-INPUT DESCRIBING FUNCTION**

The Dual-Input Describing Function (DIDF) allows the introduction of a bias load and output in the quasi-linearization of a nonlinear input-output relation. The DIDF is defined as the quasi-linear function that minimizes the mean-squared error of the output of a nonlinear element driven by the sum of a bias and a sinusoid. The force-displacement-velocity relationship of the joint-truss strut element is of the form:

$$F_{NL} = F(q, \dot{q}) \quad (5.1)$$

If the displacement is assumed to be a harmonic combined with a DC bias:

$$q = B + A \sin \omega t \quad (5.2)$$

the force relationship can be quasi-linearized to:

$$F = N_B(B, A, \omega)B + c_p(B, A, \omega)q' + c_q(B, A, \omega)\dot{q}' \quad (5.3)$$

where the primes indicate the subtraction of the static displacement and,

$$\begin{aligned} N_B &= \frac{1}{2\pi B} \int_0^{2\pi} F(B + A \sin \omega t, A \omega \cos \omega t) d(\omega t) \\ c_p &= \frac{1}{\pi A} \int_0^{2\pi} F(B + A \sin \omega t, A \omega \cos \omega t) \sin \omega t d(\omega t) \\ c_q &= \frac{1}{\omega \pi A} \int_0^{2\pi} F(B + A \sin \omega t, A \omega \cos \omega t) \cos \omega t d(\omega t) \end{aligned} \quad (5.4)$$

All three coefficients are functions of the amplitude of the input bias and the amplitude and frequency of the input sinusoid.

These coefficients become again the elements of the nonlinear equivalent stiffness and damping matrices for the truss element as described in Chapter 4. The coefficients depend on the displacement across the entire joint-strut-joint structure. The  $c_q$ 's, through the equivalent beam procedure, are the elements of the nonlinear damping matrix. There are now two nonlinear stiffness matrices, a dynamic one whose elements are the  $c_p$ 's and a static one comprised of the  $N_B$ 's. The equivalent beam element nonlinear static stiffness matrix for the 6 dof model of the single two dimensional truss bay described in Chapter 4 would be:

$$\begin{bmatrix}
\frac{N_{B3}}{N_{B2} + \frac{N_{B3}}{2} + N_{B5}} & \frac{N_{B3}}{2} & \frac{N_{B2}L}{2} + \frac{N_{B3}L}{4} + \frac{N_{B5}L}{2} & -\frac{N_{B3}}{N_{B2}} - N_{B5} & \frac{N_{B3}}{2} & \frac{N_{B2}L}{2} + \frac{N_{B3}L}{4} + \frac{N_{B5}L}{2} \\
\frac{N_{B3}}{2} & \frac{N_{B3}}{2} & \frac{N_{B3}L}{4} & \frac{N_{B3}}{2} & \frac{N_{B3}}{2} & \frac{N_{B3}L}{4} \\
\frac{N_{B2}L}{2} + \frac{N_{B3}L}{4} + \frac{N_{B5}L}{2} & \frac{N_{B3}L}{4} & \frac{N_{B2}L^2}{4} + \frac{N_{B3}L^2}{8} + \frac{N_{B5}L^2}{4} & \frac{N_{B2}L}{2} + \frac{N_{B3}L}{4} + \frac{N_{B5}L}{2} & \frac{N_{B3}L}{4} & \frac{N_{B2}L^2}{4} + \frac{N_{B3}L^2}{8} + \frac{N_{B5}L^2}{4} \\
-\frac{N_{B3}}{N_{B2}} - N_{B5} & \frac{N_{B3}}{2} & \frac{N_{B2}L}{2} + \frac{N_{B3}L}{4} + \frac{N_{B5}L}{2} & \frac{N_{B3}}{N_{B2} + \frac{N_{B3}}{2} + N_{B5}} & \frac{N_{B3}}{2} & \frac{N_{B2}L}{2} + \frac{N_{B3}L}{4} + \frac{N_{B5}L}{2} \\
\frac{N_{B3}}{2} & \frac{N_{B3}}{2} & \frac{N_{B3}L}{4} & \frac{N_{B3}}{2} & \frac{N_{B3}}{2} & \frac{N_{B3}L}{4} \\
\frac{N_{B2}L}{2} + \frac{N_{B3}L}{4} + \frac{N_{B5}L}{2} & \frac{N_{B3}L}{4} & \frac{N_{B2}L^2}{4} + \frac{N_{B3}L^2}{8} + \frac{N_{B5}L^2}{4} & \frac{N_{B2}L}{2} + \frac{N_{B3}L}{4} + \frac{N_{B5}L}{2} & \frac{N_{B3}L}{4} & \frac{N_{B2}L^2}{4} + \frac{N_{B3}L^2}{8} + \frac{N_{B5}L^2}{4}
\end{bmatrix}$$

The subscripted numbers on the coefficients refer to the numbered truss elements shown in Figure 3.1. These coefficients depend on the displacements across the numbered truss elements.

The equations of motion for a nonlinear truss structure with a pre-load undergoing dynamic excitation is:

$$M\ddot{\underline{x}} + \underline{F}_{NL} = \underline{F}_s \sin \omega t + \underline{F}_B \quad (5.5)$$

The vector  $\underline{F}_{NL}$  accounts for the nonlinear stiffness and damping, the vector  $\underline{F}_s$  is the dynamic input (in this case, a sinusoid), and  $\underline{F}_B$  is a static force that introduces the preload. The conversion from truss to equivalent beam has already occurred, so  $M$  is the equivalent beam mass matrix. If we replace the vector  $\underline{x}$  using the equation:

$$\underline{x} = \underline{B} + \underline{q} \quad (5.6)$$

the equations become:

$$M\ddot{\underline{q}} + \underline{F}_{NL}(\underline{B}, \underline{q}, \dot{\underline{q}}) = \underline{F}_s \sin \omega t + \underline{F}_B \quad (5.7)$$

Now, we assume harmonic motion and replace the nonlinear force vector with the equivalent nonlinear damping and stiffness matrices:

$$\underline{F}_{NL} = \underline{C}_{NL}\dot{\underline{q}} + \underline{K}_{NB}\underline{B} + \underline{K}_{NL}\underline{q} \quad (5.8)$$

where  $K_{NB}$  is composed of the beam element nonlinear static stiffness matrices shown above, and  $K_{NL}$  and  $C_{NL}$  are the dynamic stiffness and damping matrices composed of element matrices containing the dynamic coefficients shown in equation (5.4),  $c_p$  and  $c_q$ , respectively. The vector  $\underline{q}$  may be replaced using the equation:

$$\underline{q} = \underline{a} \sin \omega t + \underline{b} \cos \omega t \quad (5.9)$$

Combining equations (5.9), (5.8) and substituting into equation (5.7) and separating like terms into the harmonic balance form gives:

$$\begin{aligned} K_{NB} \underline{B} &= \underline{F}_B \\ (K_{NL} - \omega^2 M) \underline{a} - \omega C_{NL} \underline{b} &= \underline{F}_s \\ \omega C_{NL} \underline{a} + (K_{NL} - \omega^2 M) \underline{b} &= \underline{0} \end{aligned} \quad (5.10)$$

These equations are similar to equation (4.3) in Chapter 4 except for the addition of the third set of equations involving the bias term. This nonlinear static stiffness term effectively balances the force that causes the pre-load. The number of equations is now  $3n$ , where  $n$  is the number of degrees of freedom of the structural model. They are solved as described in Chapter 4 by using a Newton-Raphson iteration technique. The Jacobian is calculated numerically.

The backbone curve may also be calculated for the nonlinear structure under pre-load. The equations to be solved are:

$$\begin{aligned} K_{NB} \underline{B} &= \underline{F}_B \\ (K_{NL} - \omega^2 M) \underline{a} &= \underline{0} \end{aligned} \quad (5.11)$$

where  $K_{NB}$  and  $K_{NL}$  are matrices that are functions of  $B$  and  $A$ , the bias and sinusoidal displacements. These equations are solved using a technique similar to that described in Chapter 4, with the element of the vector  $\underline{a}$  corresponding to the forcing vector prescribed and the frequency  $\omega$  is one of the parameters to be determined.

### 5.3 SIMPLE EXAMPLE - FIVE BAY MODEL

The five bay model developed previously may be used to determine the effect of a joint pre-load on the sinusoidal response of a truss structure with several different types of joint nonlinearities. The purpose is to determine the change in dynamic properties that occur in a

structure with and without a pre-load. The pre-load that is applied is meant to model a gravity load somewhat in that the load is applied from the top to the bottom of the structure. Figure 5.1 shows the truss model that is investigated with the equivalent beam model and the points of application of the pre-loads on the equivalent beam model. The types of nonlinear joints that are investigated are the gain change, both softening and hardening and the sliding pin joint.

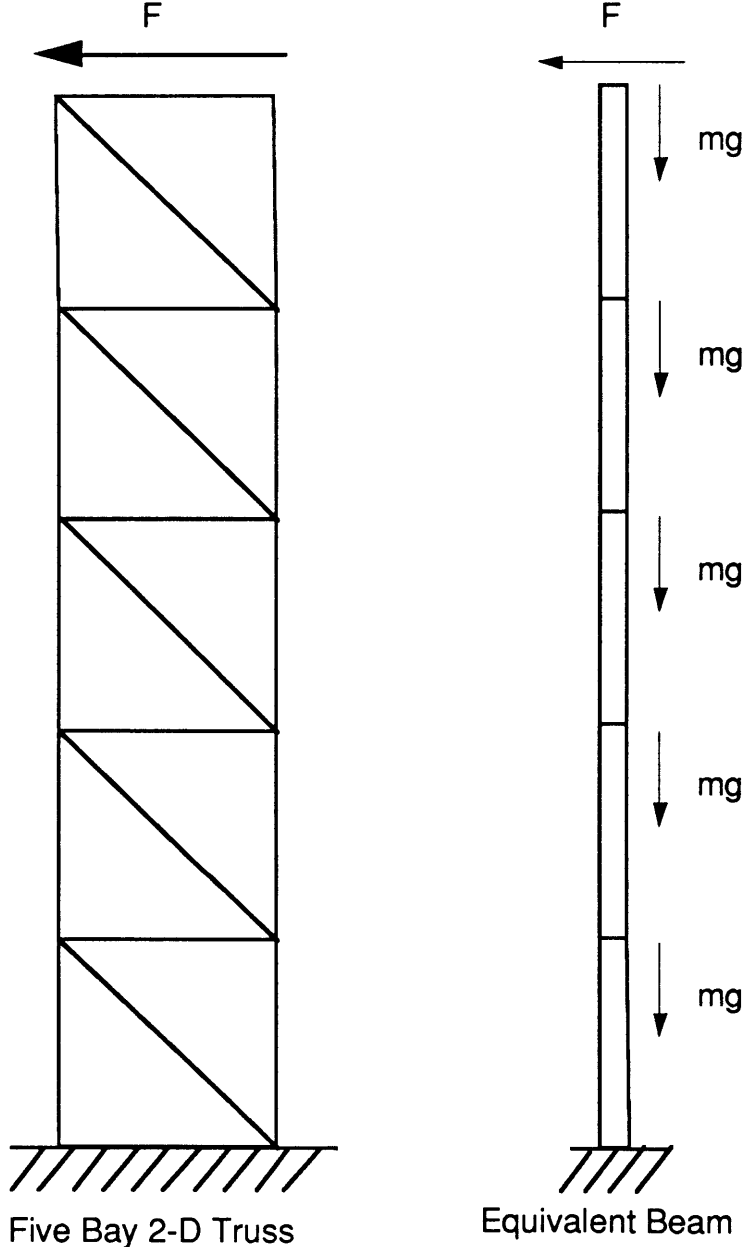


**Figure 5.1 Five Bay Truss with Vertical Pre-load**

## Gain Change - Hardening

The harmonic balance equations of motion now contain a third set of equations that are due to the bias terms. These are balanced with the gravity loading on the structure. Figures 5.2 and 5.3 show the response of a five bay 2-D truss with piecewise-linear increasing stiffness joints undergoing sinusoidal forcing in the transverse direction, with (solid line) and without (dotted line) gravity loading in the longitudinal direction. The ratio of truss element stiffness before and after gain change is  $k_2/k_1=2$ . The sinusoidal force applied is equal to  $0.001 EA$  as in it was for the gain change nonlinear element in Chapter 4. The pre-load on the structure,  $mg$  is equal to  $0.003 EA$ . This pre-load gives a bias such that the static displacement across the struts does not exceed  $\delta$ , the limit on the range of linear behavior. This has repercussions on the backbone and response curves for this structure. The curve for the non pre-load structure is taken from Chapter 4. These curves show little difference except in the vicinity of mode 6. The pre-load curve shows no response in this mode. This mode is a second axial mode, with surge mode characteristics.

Figures 5.4 and 5.5 show a comparison of the backbone curves of the modes of the structure with (solid line) and without (dotted line) pre-load. The curves for the motion at the end of the truss (Figure 5.4) show little difference. The curves for motion at the end of bay 2 (Figure 5.5) show marked differences both in shape and amplitude. The curves with and without pre-load start at the system frequencies with stiffness  $k_1$  and end at system frequencies with stiffness  $k_2$ .

Figures 5.6 and 5.7 show the a comparison between pre-load and no pre-load models with the bias causing the static displacement to lie outside of the linear range. This is true for the longerons only, the static displacement of the diagonal elements is still within the linear range. This causes a much more marked difference in the response of the models as shown in Figure 5.7 and in the backbone curves in Figure 5.6. The curves for the pre-load model start at a structure that has longerons with stiffness  $k_2$  and diagonals with stiffness  $k_1$ . The curves have upper asymptotes that are the same as the non pre-load model, the system frequencies with stiffness  $k_2$  in all truss members.

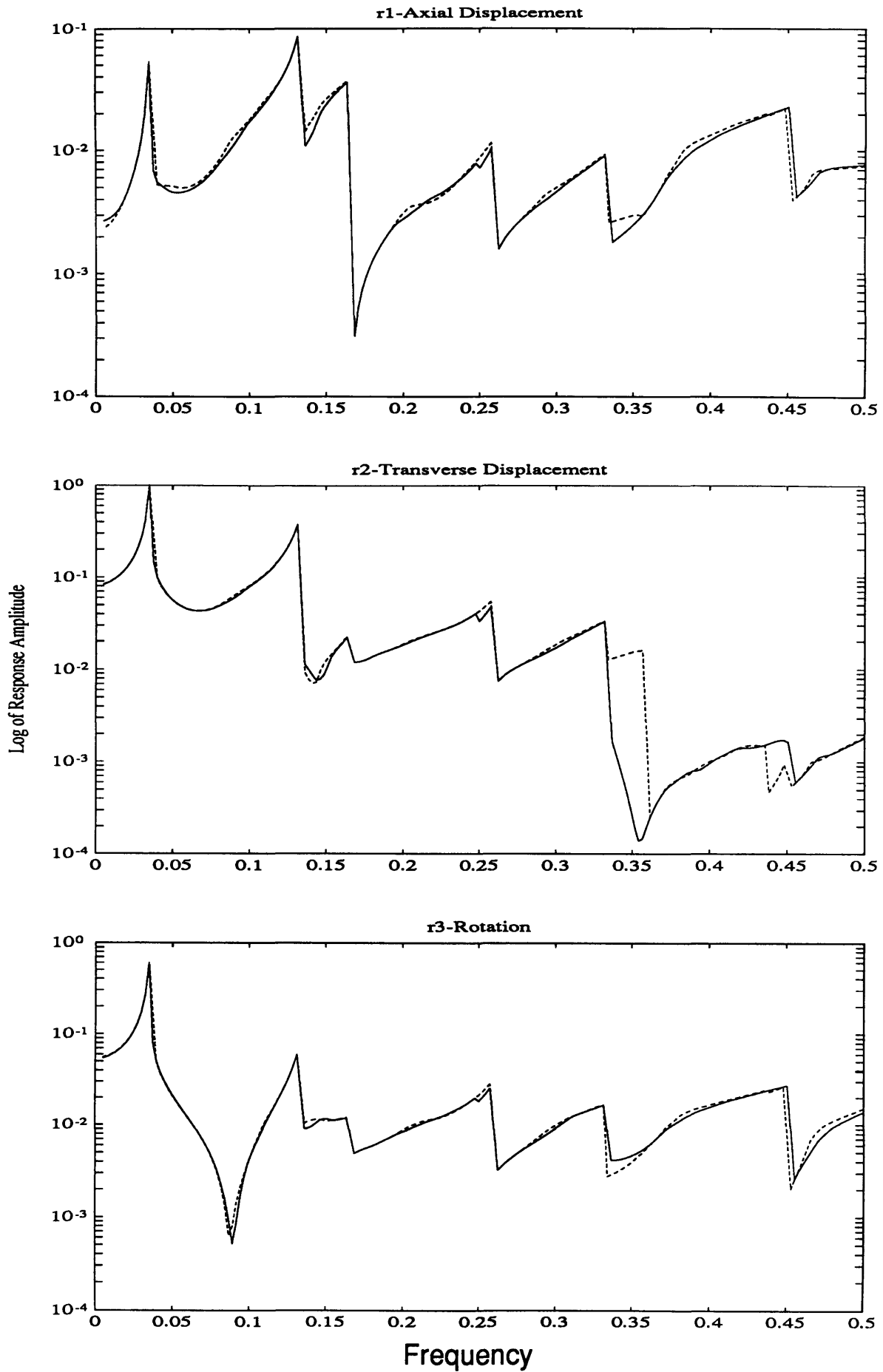


Figure 5.2 Comparison of Response to Sinusoidal Forcing at Bay 2 of Five Bay Truss with Hardening Gain Change Joints with Pre-load (solid line) and No Pre-load (dotted line)



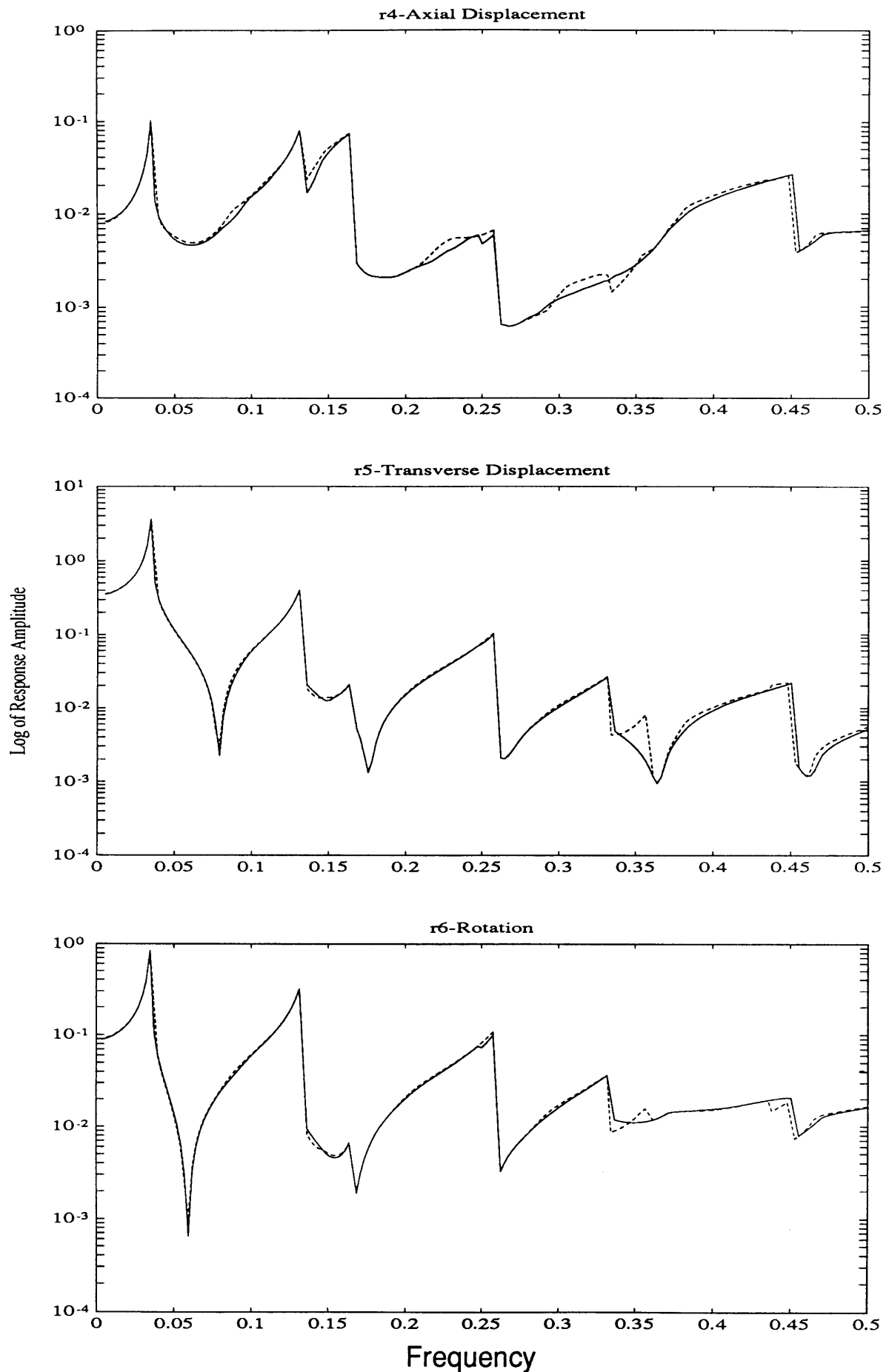


Figure 5.3 Comparison of Response to Sinusoidal Forcing at End of Five Bay Truss with Hardening Gain Change Joints with Pre-load (solid line) and No Pre-load (dotted line)

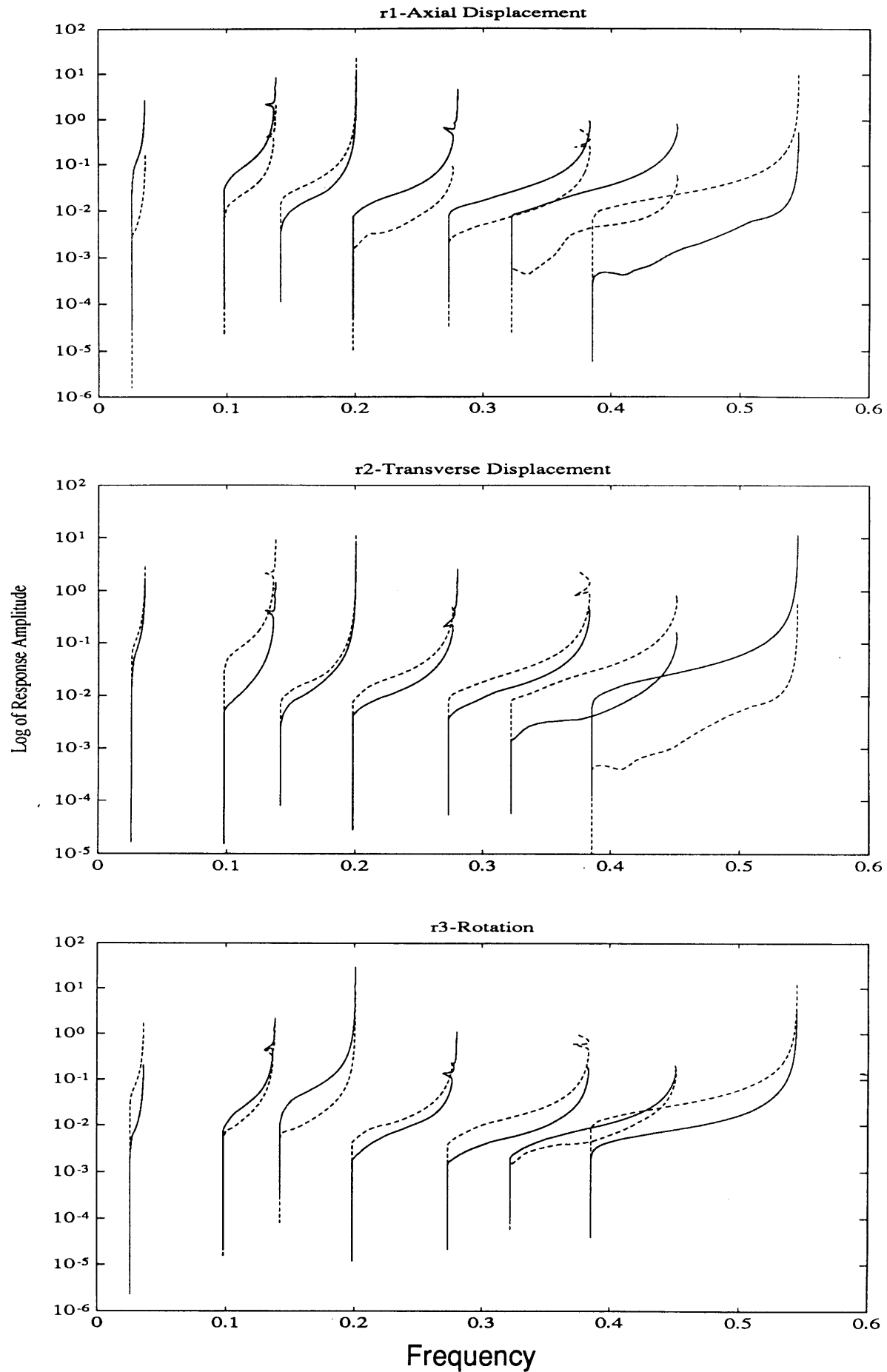


Figure 5.4 Comparison of Backbone Curves at Bay 2 of Five Bay Truss with Hardening Gain Change Joints With (solid line) and Without (dotted line) Pre-load

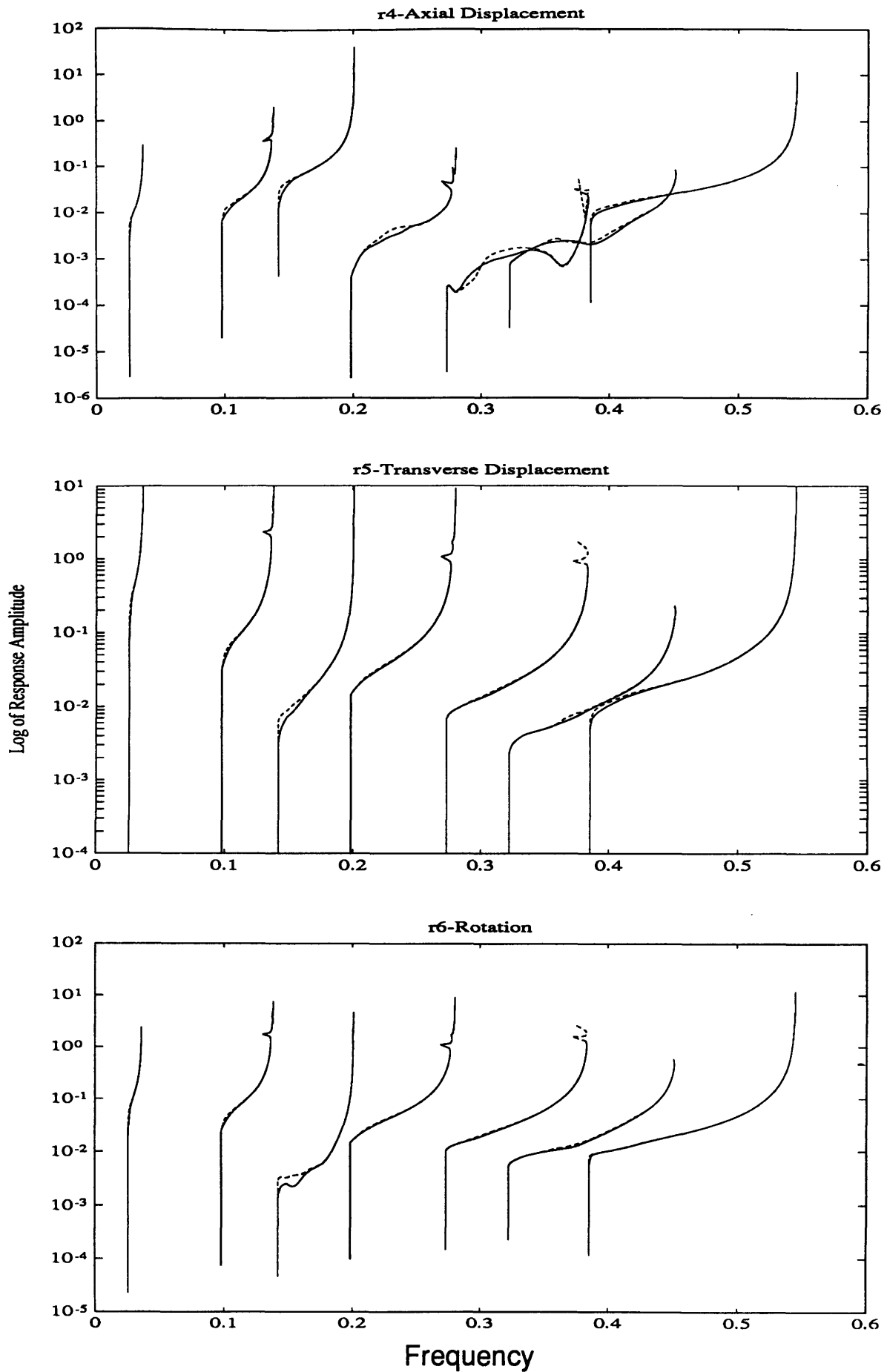


Figure 5.5 Comparison of Backbone Curves at End of Five Bay Truss With Hardening Gain Change Joints for Pre-load (solid line) and No Pre-load (dotted line)

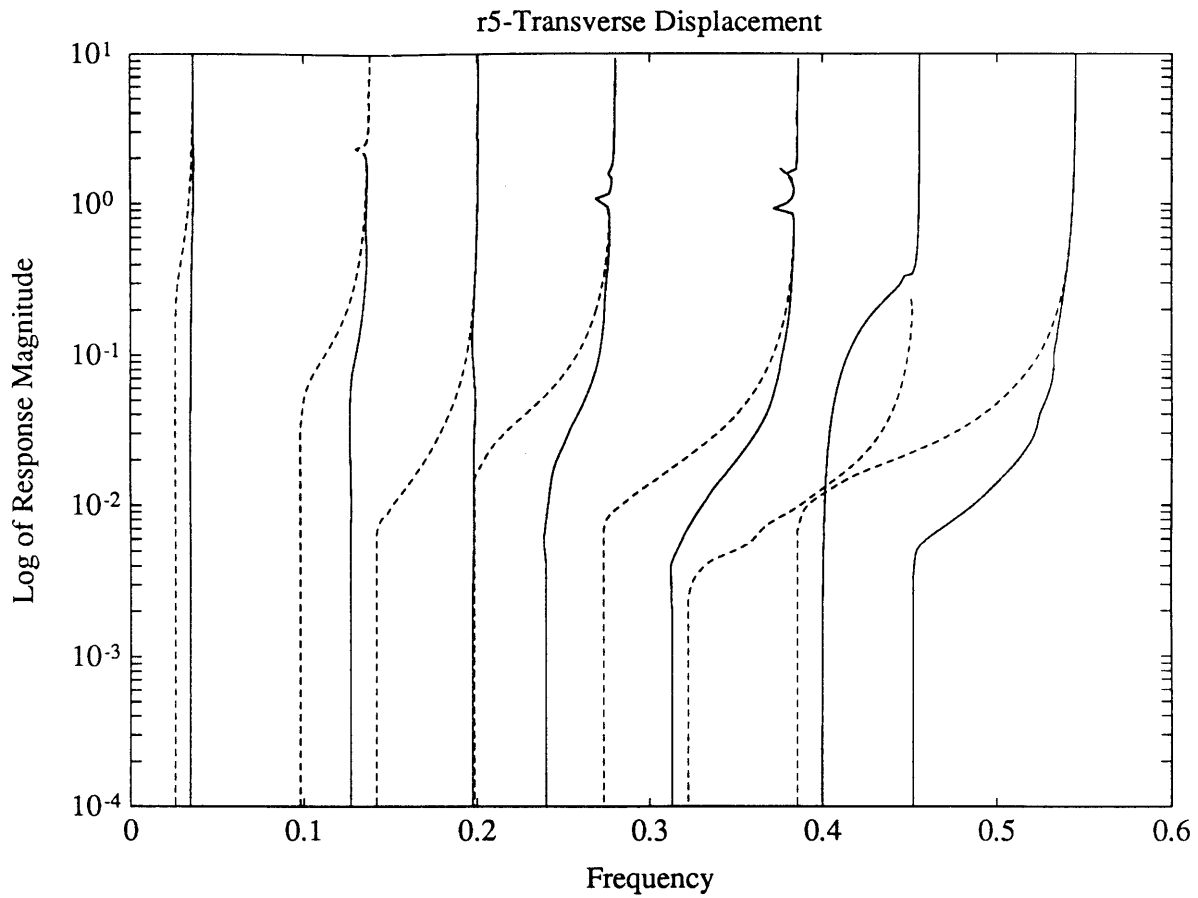


Figure 5.6 Comparison of Backbone Curves of Five Bay Truss with Hardening Gain Change Joints with Large Pre-load (solid line) and No Pre-load (dotted line)

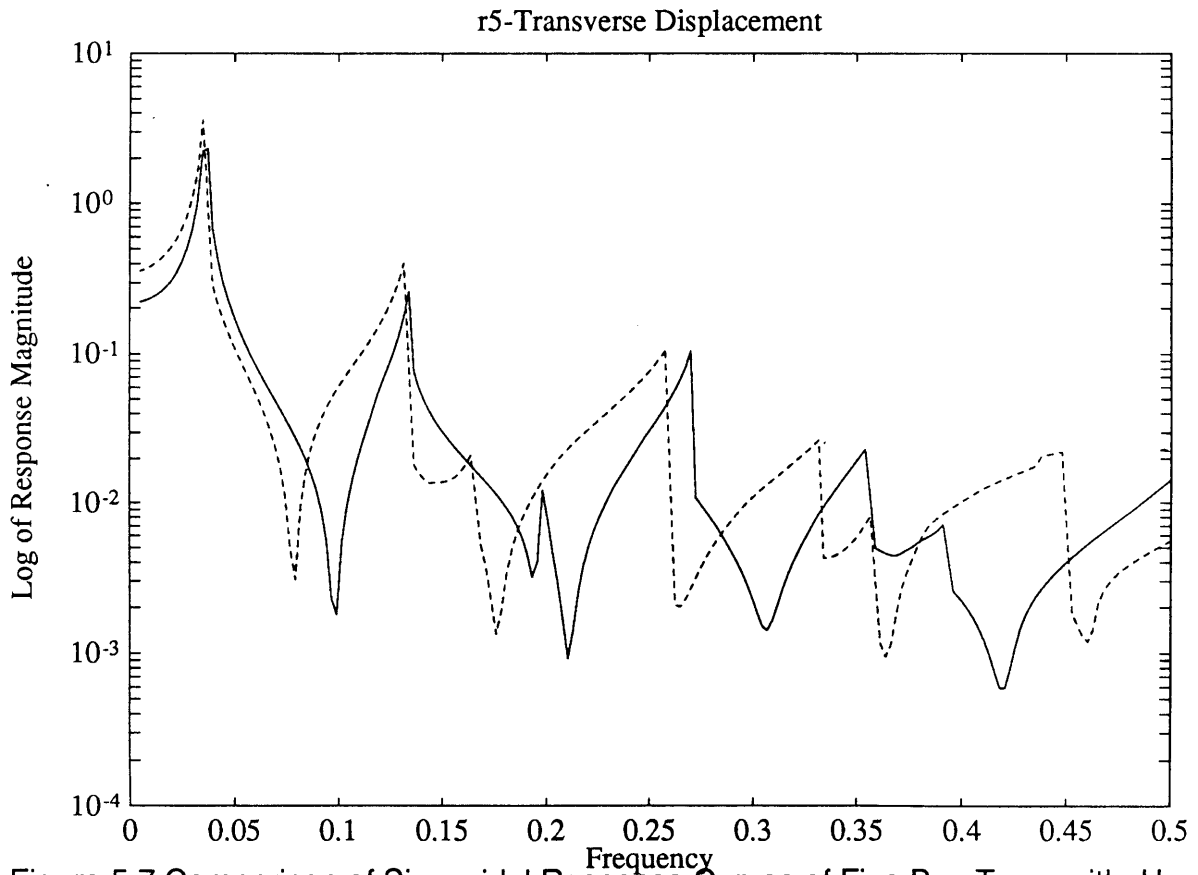


Figure 5.7 Comparison of Sinusoidal Response Curves of Five Bay Truss with Hardening Gain Change Joints with Large Pre-load (solid line) and No Pre-load (dotted line)

## **Natural Joints**

Inserting natural joints into the five bay structure allows the analysis of the effect of pre-loading or gravity loading on the sinusoidal response of structure with hysteretic joints. The parameters that describe this joint are shown in Figure 4.19. Figures 5.8 and 5.9 show comparisons of the sinusoidal response and backbone curves for the five bay truss with natural joints for the pre-load and no pre-load conditions. The sinusoidal forcing response curves are very similar for both cases. The backbone curves show larger deviations between the two models due to the fact that the added bias in the joints causes the response to enter the linear range at lower amplitudes than the no pre-load case.

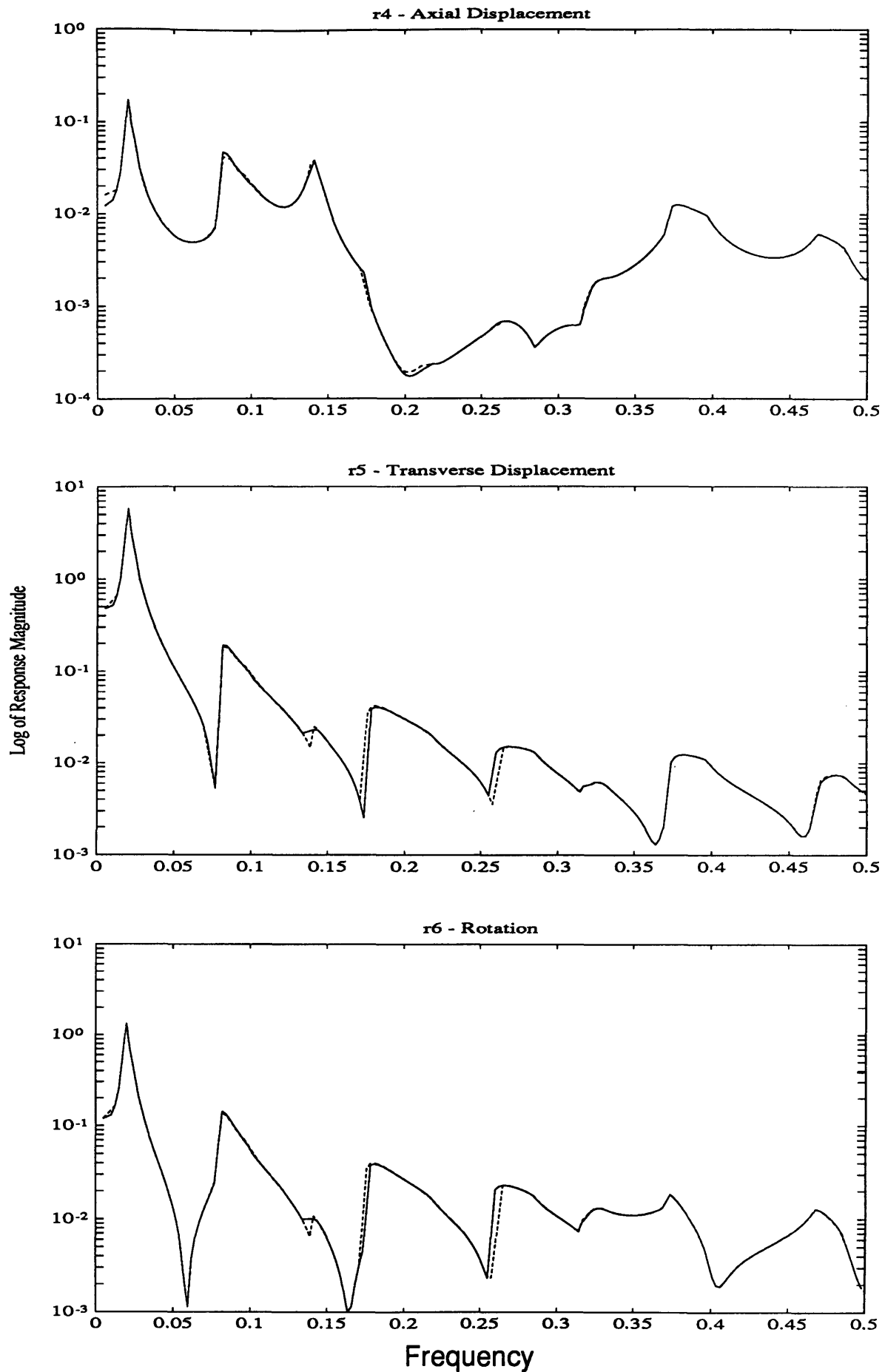


Figure 5.8 Comparison of Sinusoidal Response at Tip of Five Bay Truss with Natural Joints for Pre-load (solid line) and No Pre-load (dotted line)

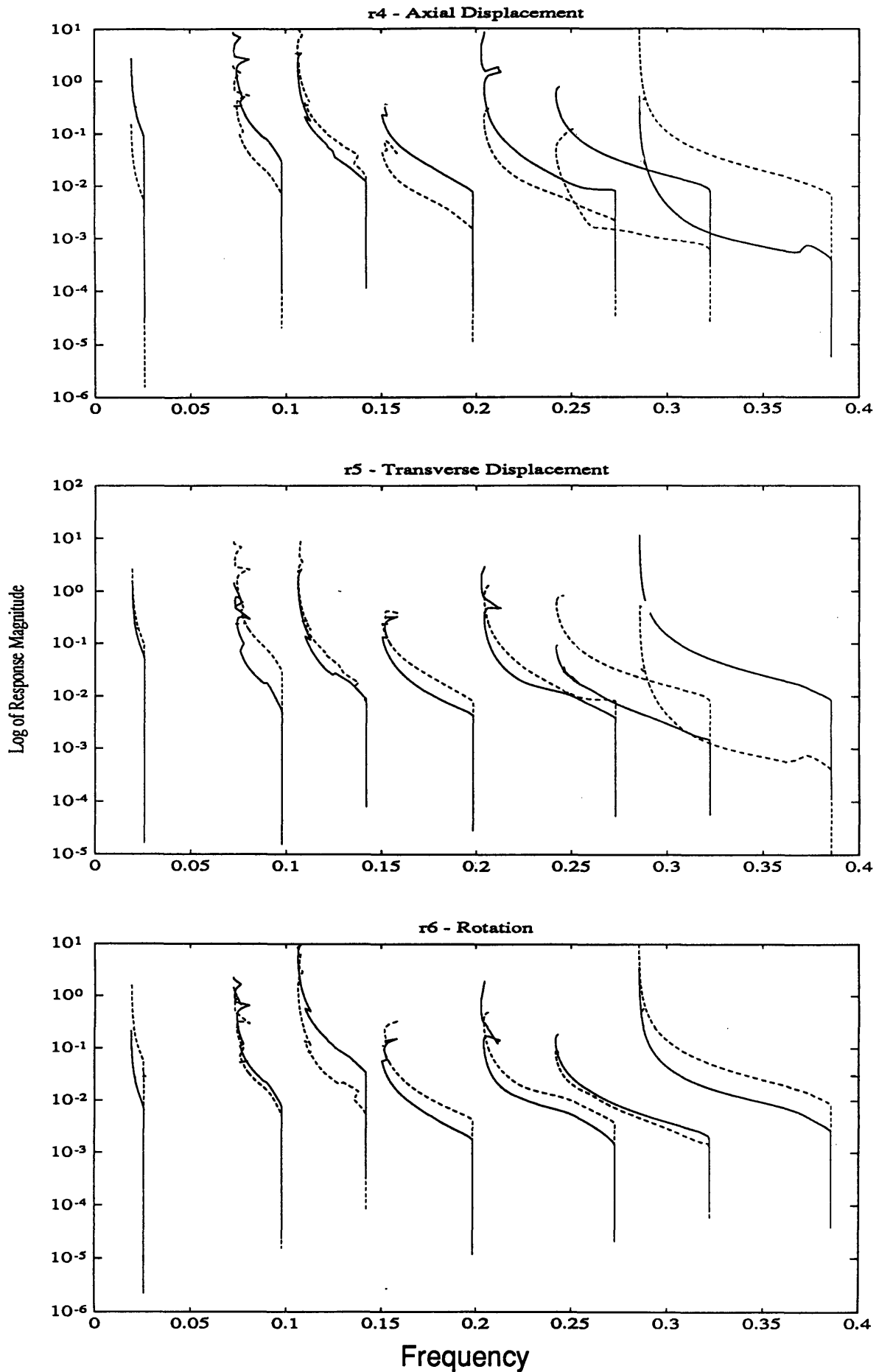


Figure 5.9 Comparison of Backbone Curves at Bay 2 of Five Bay Truss with Natural Joints for Pre-Load (solid line) and Non Pre-load (dotted line)

## **CHAPTER 6**

### **MINI-MAST STRUCTURE AND MODEL**

#### **6.1 INTRODUCTION**

The Mini-Mast at NASA/Langley Research Center is an example of the type of structure that may be used in space applications. It is a deployable structure that is very flexible. It is long and has a high aspect ratio, exhibiting beam-like behavior in its lowest modes. It is built using space flight quality hardware and assembly techniques and yet it displays nonlinear behavior. This structure is a good example of a beam-like truss to analyze with the modeling procedure developed in previous chapters.

The Mini-Mast CSI Guest Investigator Program is designed to give researchers a test-bed for developing modeling procedures, control algorithms, failure detection schemes and other techniques for the control of structures. Part of the program was to determine the extent of nonlinear behavior in the structure and to possibly model this behavior. This chapter describes in detail the Mini-Mast structure, the experiments that were conducted upon the structure to determine the nonlinear behavior, the Mini-Mast equivalent beam analytical model, both linear and nonlinear, and compares the results that were obtained from test and analysis.

#### **6.2 MINI-MAST TEST FACILITY**

The Mini-Mast is a 20 meter, 18 bay deployable space truss at the Structural Dynamics Research Laboratory at Langley. It is deployed vertically inside a high tower with a fixed base.



The truss has a three-longeron triangular construction with the corners of the triangle fitting inside a circle of 1.4 meters diameter. The three types of structural members that make up the truss are longerons, battens, and diagonals. The truss members are made of graphite epoxy with the corner bodies and mid-diagonal hinges made of titanium with stainless steel pins. The diagonal members fold inward when the truss is retracted. The truss has been heavily instrumented along its length. Displacement proximity sensors have been carefully placed and calibrated. Stops have been placed to prevent the Mast from displacing more than a specified amplitude. The diagonal members of the truss could buckle if the structure twists by more than a certain amount. All of these instruments and stops prevent the Mini-Mast from being retracted and it is therefore permanently deployed.

Figure 6.1 is a picture of the Mini-Mast deployed inside the test building at Langley. The tower contains a stairway that provides access to all of the deployed structure. As stated, the geometry of the truss is triangular. The diagonals are in an alternating arrangement as shown in a picture of the partially deployed Mast in Figure 6.2. The structure is attached at the top by a line through a pulley to a 300 lb. weight that simulates some degree of weightlessness. Most of the mass of the structure is concentrated in the tip plate assembly which is mounted with three torque wheels.

The properties of the struts are shown in Table 6.1. Note the small value of the buckling parameter,  $P_{CR}$  for the diagonal elements.

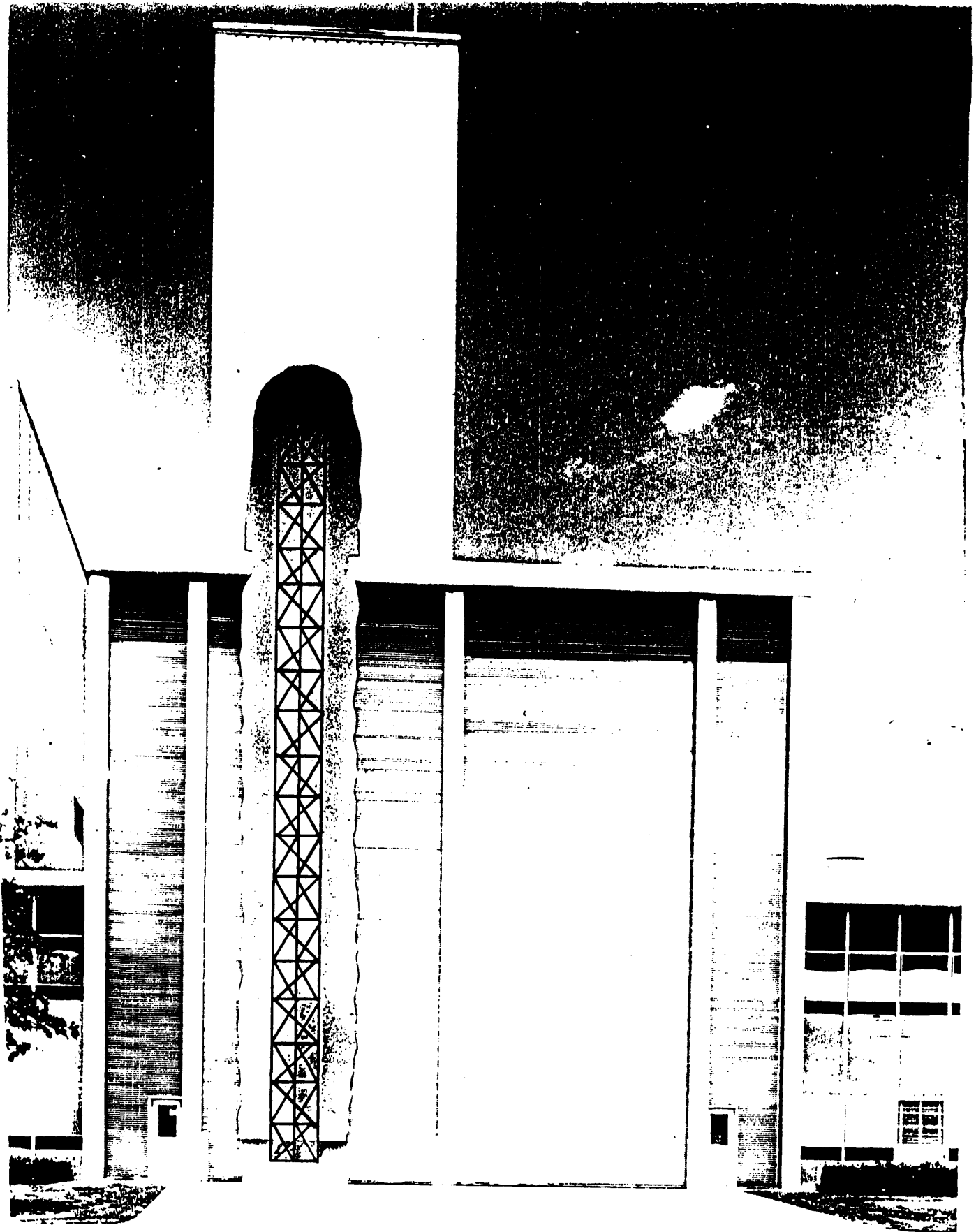


Figure 6.1 Mini-Mast Test Facility at NASA/Langley Research Center

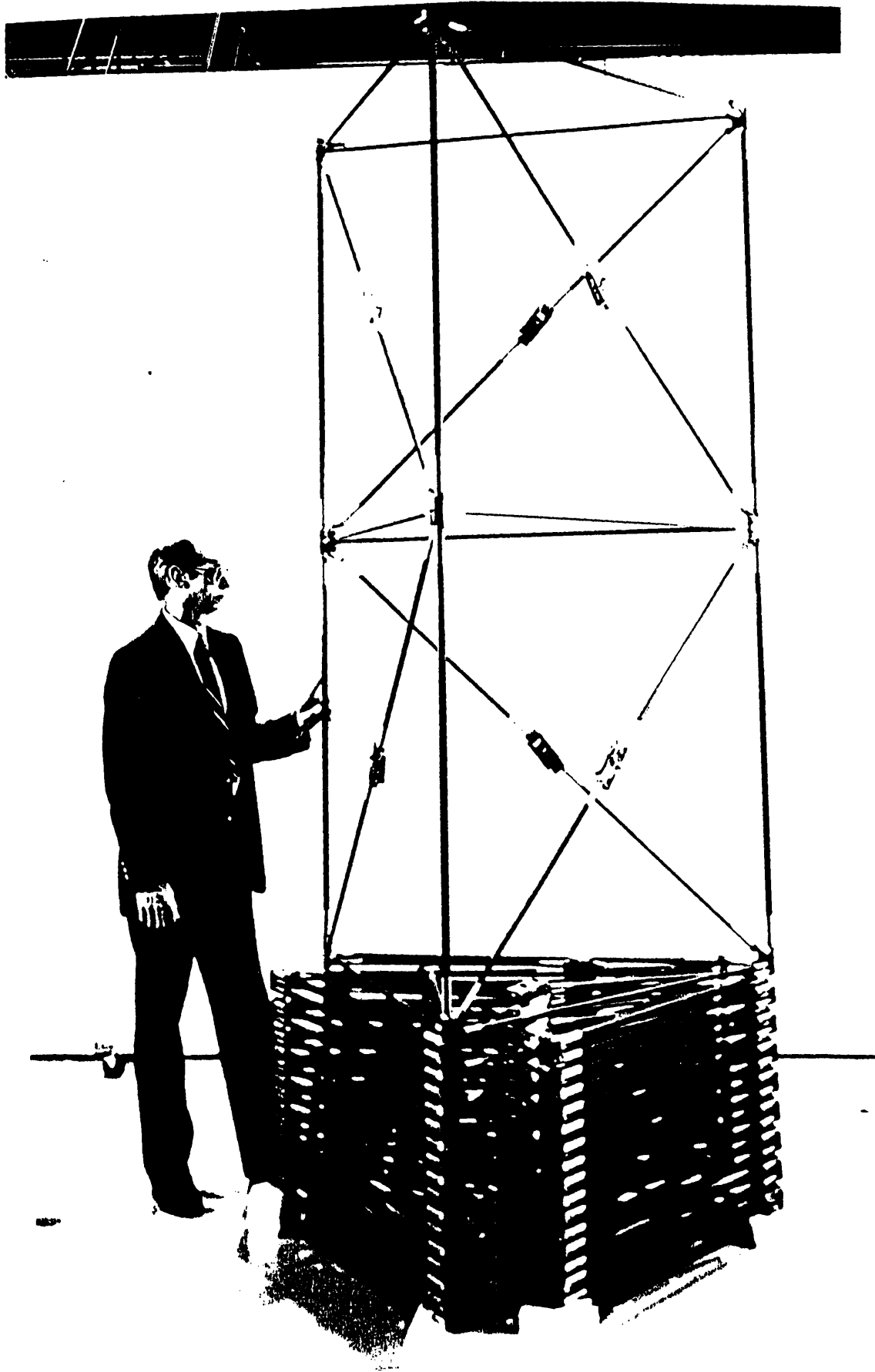


Figure 6.2 Partially Deployed Mini-Mast

	<b>Longerons</b>	<b>Battens</b>	<b>Diagonals</b>
Length (m)	1.092	1.2124	1.6225
OD (mm)	20.2	15.1	15.1
ID (mm)	14.9	11.9	11.2
A (m <sup>2</sup> )	1.461x10 <sup>-4</sup>	6.786x10 <sup>-5</sup>	8.056x10 <sup>-5</sup>
I (m <sup>4</sup> )	5.763x10 <sup>-9</sup>	1.568x10 <sup>-9</sup>	1.780x10 <sup>-9</sup>
E (N/m <sup>2</sup> )	1.240x10 <sup>11</sup>	1.240x10 <sup>11</sup>	1.240x10 <sup>11</sup>
P <sub>cr</sub> (N)	5904.8	1305.2	827.3
P <sub>cr</sub> (lbs)	1327.4	293.4	186.0

**Table 6.1 Mini-Mast Strut Properties**

### **Strut Testing**

The truss elements used in constructing the Mini-Mast were taken by another guest investigator to be tested to determine the stiffness characteristics of the structural elements and the pinned joints. These tests were difficult to conduct and inconclusive. Free play within the corner bodies and the angle of the pins caused three dimensional response under axial load. Axial only measurement failed to capture the properties of the strut-joint structure. Stiffness properties varied widely from test to test and little viable data became available. This analysis therefore will not use experimental data on the truss elements. Instead, nonlinear joint properties will be inferred from the global properties exhibited by sine sweep tests.

An examination of the corner body joints, at which the longerons, battens, and diagonals are connected to the truss bay apexes, has indicated some amount of movement along the pins that connect the struts to the corner bodies. The low buckling load could indicate pre-buckling behavior as well. These effects could account for nonlinear behavior and will be addressed later.

## Sensors and Actuators

There are steel instrumentation platforms at bays 10 and 18. The platform at bay 10 holds two accelerometers, two rate gyros, and three shakers. Bay 18 holds four accelerometers, one rate gyro and three torque wheel actuators, one for each direction. Figure 6.3 shows the three torque wheels attached to the tip platform. The torque wheels are the main actuators for the structure for control systems that are applied to control the structure. The shakers are used primarily as disturbance sources.

Fifty-one Kaman proximity probes are installed at locations along the Mini-Mast. The probes are positioned as indicated in Figure 6.4. The specs for these sensors are shown in Table 6.2.

Linear Range	2.00 inches
Frequency Range	DC-50 kHz
Sensitivity	0.5 mV/mil
Threshold/Resolution	0.2 mil

**Table 6.2 Specifications for Kaman Displacement Sensors**

The torque wheels on the Mini-Mast have a maximum output of 50 ft-lbs at 50 volts and 9.6 amps. The X and Y axis torque wheels weigh 85 pounds each and the Z axis torque wheel weighs 72.5 pounds. There are some dynamics associated with the torque wheels. The transfer function associated with each of the torque wheels is as follows:

$$\text{X-axis Torque Wheel: } \frac{\text{Torque(Nm)}}{\text{Input Voltage}} = \frac{34861.3s}{(s + 23.50)(s + 336.90)}$$

$$\text{Y-axis Torque Wheel: } \frac{\text{Torque(Nm)}}{\text{Input Voltage}} = \frac{38508.9s}{(s + 23.56)(s + 401.31)}$$

$$\text{Z-axis Torque Wheel: } \frac{\text{Torque(Nm)}}{\text{Input Voltage}} = \frac{36433.0s}{(s + 23.44)(s + 372.34)}$$

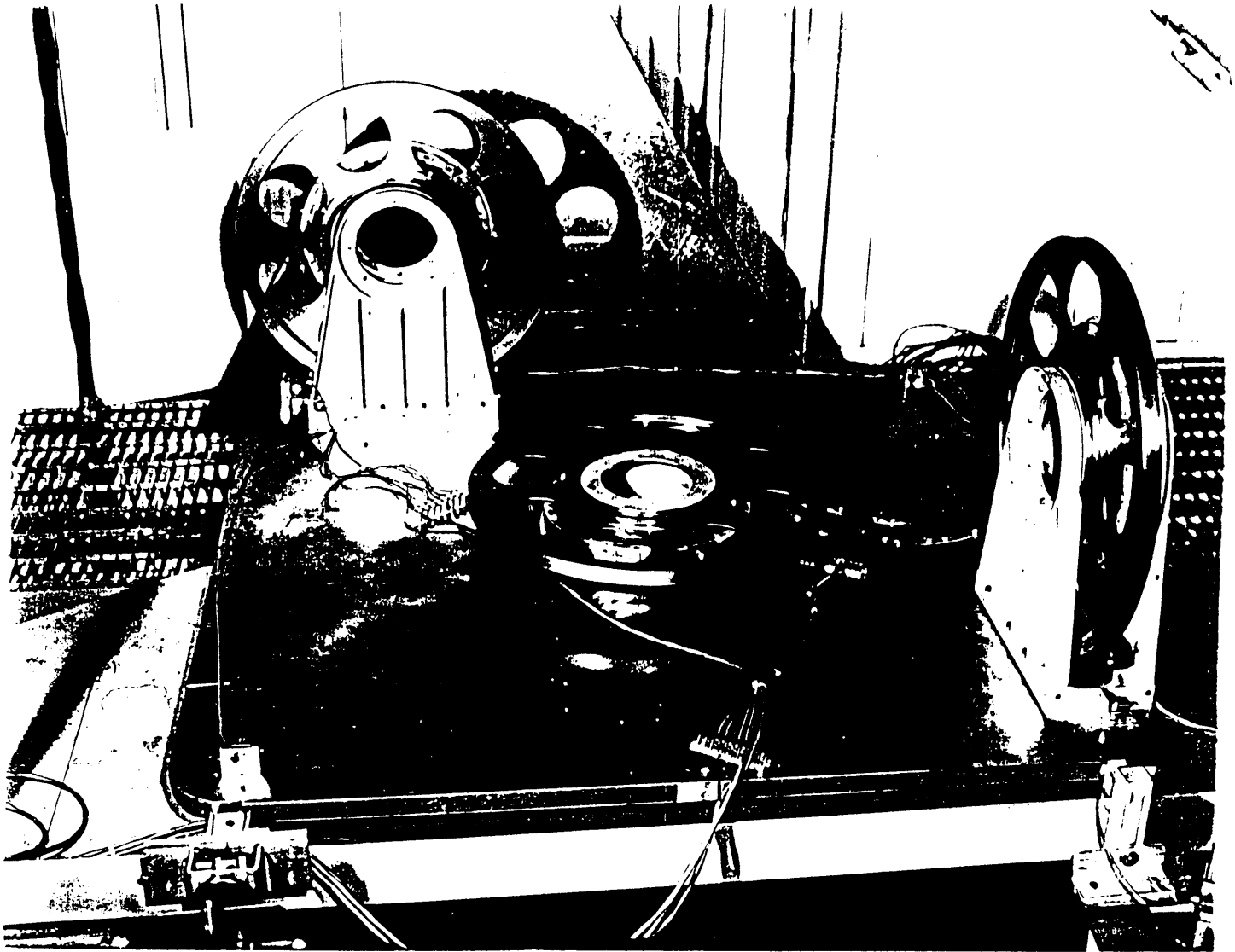


Figure 6.3 Tip Plate of Mini-Mast with Three Torque Wheels Attached

## NASA Finite Element Model Modes

A NASTRAN finite element model of the Mini-Mast was assembled at Langley to determine the dynamic characteristics of the structure. The frequencies that were obtained are shown in Table 6.2. The first two modes of the structure are orthogonal bending modes with motion primarily in either the x or y axis but with some motion in both axes for both modes. The third mode is the first torsion mode with very little coupling with bending. The next two modes obtained were the second bending modes. Due to the position of the X and Y torque wheel actuators, the axes of bending for these two modes are rotated away from the reference axes. The next modes include tip plate flexure modes, the first axial mode at 15.42 Hz and 108 local modes that consist primarily of the first bending modes of the 58 diagonal truss members. All these modes contain motion of all the diagonal struts. The next mode after these is the second torsion mode. These figures are for the latest model available. This model is continually being upgraded to match changes to the structure and to match experimental data.

### SENSOR POSITIONS

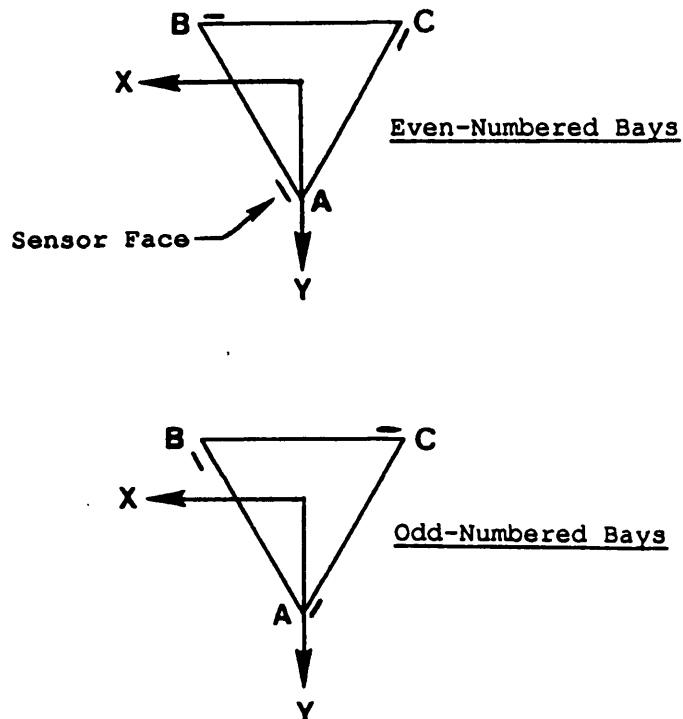


Figure 6.4 Kaman Displacement Sensor Locations on Mini-Mast.

Mode Number	Predicted Frequency (Hz)	Predicted Damping	Description
1	0.83	.018	1st Y Bending
2	0.83	.018	1st X Bending
3	4.37	.012	1st Torsion
4	6.38	.01	2nd X Bending
5	6.44	.01	2nd Y Bending
6	14.72	.005	Tip Plate
7	14.83	.005	Diagonal
8	15.42	.005	1st Axial
9	15.57	.005	Tip Plate
10	15.60	.005	Tip Plate
11-116	15.7-19.8	.005	Diagonal modes
117	20.29	.005	Tip Plate
118	21.8	.005	Second Torsion

**Table 6.3 Mini Mast NASTRAN Finite Element Model Frequencies and Predicted Damping.**

### 6.3 SINE SWEEP TEST SET-UP AND RESULTS

An HP 3562A dynamic signal analyzer served as both signal source and data analyzer. The analyzer swept through a certain frequency range (in the vicinity of a mode of interest) and determined the magnitude and phase of the response at the frequency of excitation. The analyzer determined these parameters through a direct integration scheme. The time of integration at each frequency point was lengthened until there was no change in the transfer function that was measured. The output magnitude was given in terms of a transfer function. The torque wheels mounted on the tip plate were the actuators used in the experimental runs. The HP 3562A has only a single input channel so a single Kaman displacement sensor at the tip was used to measure the



response. The output of this sensor is 0.00127 m/Volt.

The tests that were conducted were sine sweeps both forward and backward in a frequency range that brackets modes of interest. This procedure captures the nonlinear characteristics of the structure for later comparison to analytical results.

Figure 6.5 shows the transfer function of the Mini-Mast vs frequency for a sine sweep in the vicinity of the first mode using the X-axis torque wheel actuator. The data shows that with an increase in forcing level, the response peak shifts to the left (softening) and the damping decreases.

Figure 6.6 shows the transfer function for sinusoidal excitation using the Z-torque wheel actuator (torsional motion of the truss) in the vicinity of the first torsional mode. For increasing force level, the response peak shifts left (softening) and the damping increases. There was no difference between the forward or backward sweeps for either set of data shown in Figures 6.5 and 6.6.

As stated, reliable data on the truss elements was not available. However, full scale static testing of the Mini-Mast by Taylor (1987) gave the force-state relationship shown in Figure 6.7. This data is for the entire truss structure. The data needed is the force-displacement relation for the individual strut-joint elements. However this data served as the inspiration for the natural joint model developed in Chapter 4.

## **6.4 ANALYTICAL MODEL**

### **Beam reduction**

The construction of the Mini-Mast analytical model followed the procedures outlined in Chapters 3 and 4. Figure 6.8 shows a schematic of a Mini-Mast bay and the corresponding equivalent beam model. There are two types of bays on the Mini-Mast, with an alternating diagonal pattern. The configuration in Figure 6.8 corresponds to Bay 1. Stiffness and mass properties were deduced from the Mini-Mast NASTRAN model obtained from NASA/Langley.

The degrees of freedom chosen in the equivalent beam fully model the beam behavior of the lowest modes of the truss. The reduction ratio between the truss model and the equivalent beam

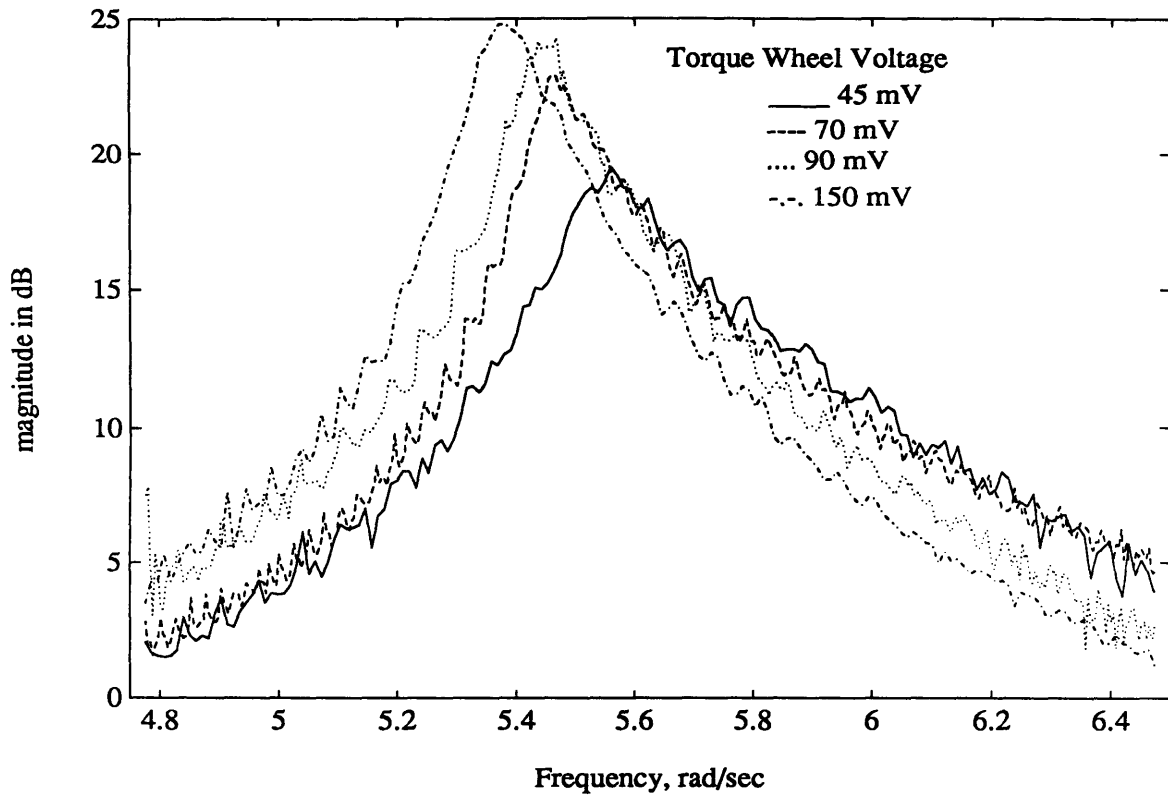


Figure 6.5 Transfer Function from X-Axis Torque Wheel to Tip Displacement Sensor in Vicinity of First Bending Mode, Mini-Mast Experimental Data

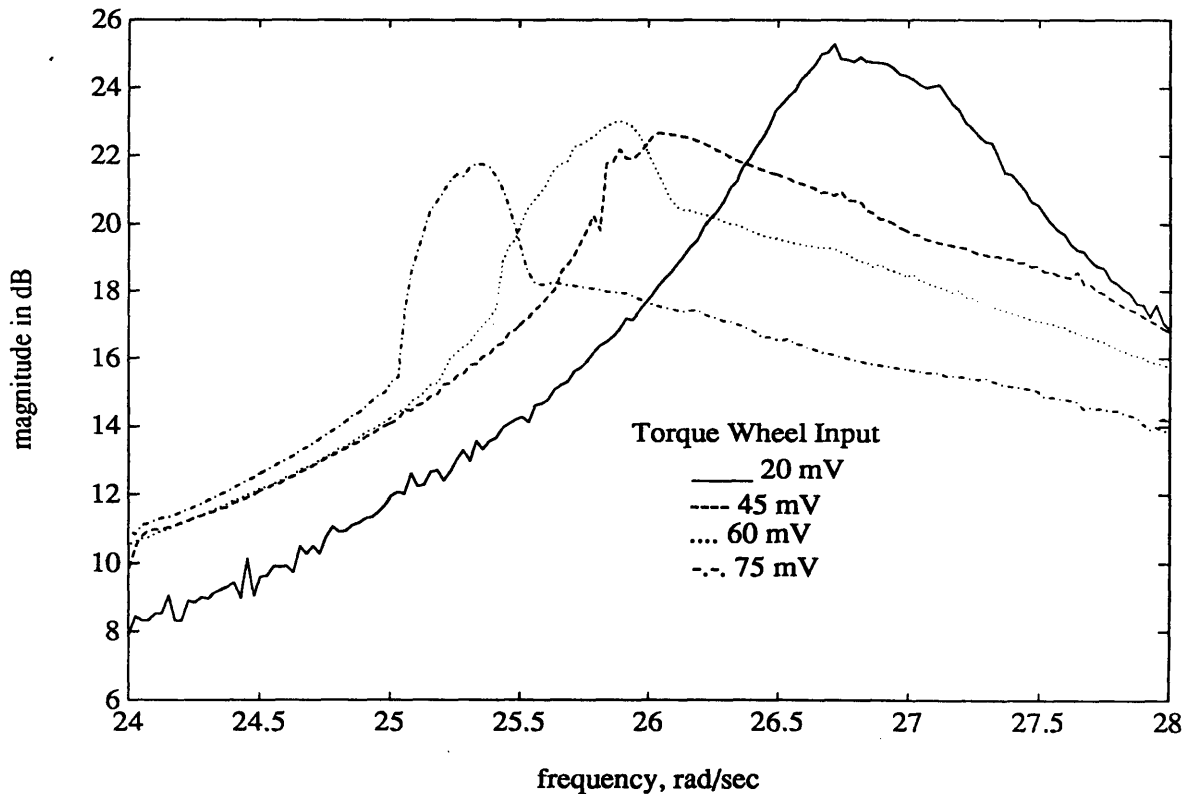


Figure 6.6 Transfer Function from Z-Axis Torque Wheel to Tip Displacement Sensor in Vicinity of First Torsion Mode, Mini-Mast Experimental Data

model is 2/3.

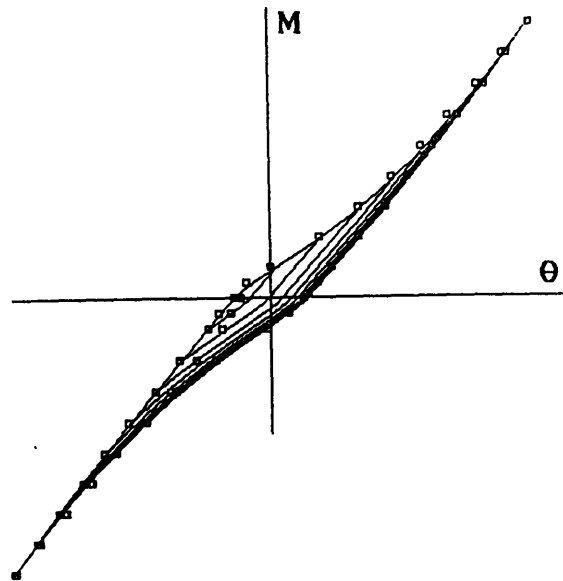


Figure 6.7 Global Static Loading Behavior of the Mini-Mast in Torque (Taylor, 1987)

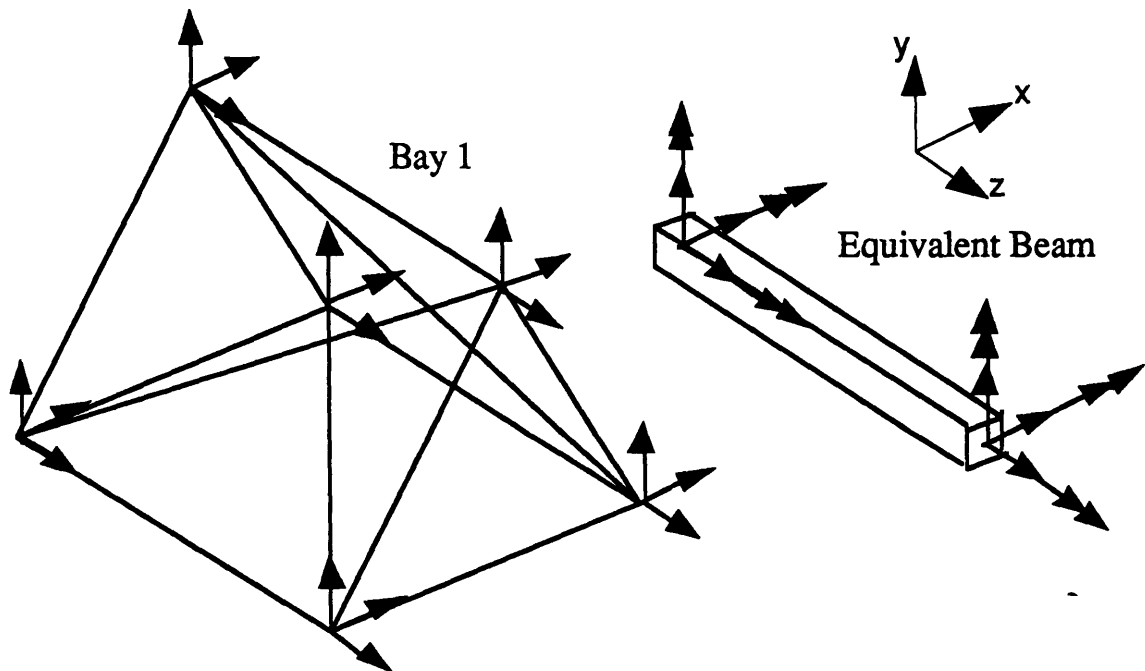


Figure 6.8. Mini-Mast Bay 1 and Equivalent Beam Model Showing Degrees of Freedom.

The  $B_e$  matrix from equation (3.12) is determined by assuming that the truss bends and twists about its center axis. This axis intersects the plane of the end of the truss bay at  $0.5d$  in the

x direction and  $1/3d$  in the y direction from the lower left corner of the truss shown in figure 6.8.

The constant  $d$  is the length in meters of the batten from the centers of the corner bodies. The

upper left corner of the matrix  $B_e$  is:

$$B_p = \begin{bmatrix} \frac{1}{3} & 0 & 0 & \frac{1}{3} & 0 & 0 & \frac{1}{3} & 0 & 0 \\ 0 & \frac{1}{3} & 0 & 0 & \frac{1}{3} & 0 & 0 & \frac{1}{3} & 0 \\ 0 & 0 & \frac{1}{3} & 0 & 0 & \frac{1}{3} & 0 & 0 & \frac{1}{3} \\ 0 & 0 & -\frac{1}{\sqrt{3}d} & 0 & 0 & \frac{2}{\sqrt{3}d} & 0 & 0 & -\frac{1}{\sqrt{3}d} \\ 0 & 0 & \frac{1}{d} & 0 & 0 & 0 & 0 & 0 & \frac{1}{d} \\ \frac{1}{2\sqrt{3}d} & -\frac{1}{2d} & 0 & -\frac{1}{\sqrt{3}d} & 0 & 0 & \frac{1}{2\sqrt{3}d} & \frac{1}{2d} & 0 \end{bmatrix} \quad (6.1)$$

This matrix forms the  $B_e$  matrix:

$$B_e = \begin{bmatrix} B_p & 0 \\ 0 & B_p \end{bmatrix} \quad (6.2)$$

The truss bay stiffness matrix is determined with the struts modeled by axial stiffness elements.

The  $B_e$  matrix and the truss bay stiffness matrix are substituted into equation (3.13) to give the equivalent beam finite element stiffness matrix. A similar operation gives the mass matrix. There are two element mass matrices and stiffness matrices due to the two types of bays. These are then combined to form the finite element model of the Mini-Mast.

### Linear Model Modes

Table 6.3 shows a comparison of the first seven beam-like modes of the Mini-Mast from several sources. The 18 dof model corresponds to a full truss element (axial stiffness) model with no reduction to an equivalent beam model. The 12 dof model is the equivalent beam model (reduced from the 18 dof model). The other two models are the Langley NASTRAN model and experimental results from Schenk and Pappa (1990). The equivalent beam model is more accurate than the Langley finite element model for the first three modes when compared with experimental results. The 108 local diagonal modes and the tip plate modes aren't modeled by the 18 dof and 12 dof models. Local bending modes are not modeled due to the axial only stiffness in the truss

elements. The tip and bay 10 platforms are modeled by concentrated masses. The mass of the corner bodies, diagonal hinges and other hardware are included in the truss element mass matrices and thereby distributed throughout the structure for the 18 dof and 12 dof models. These two models show the first axial and second torsion modes in opposite order from the other two modes.

Also shown in the table is the experimentally determined damping ratios for the modes. The experimental data does not have a value for the 1st axial mode frequency or damping ratio as it is difficult to excite this mode with the actuators that are available. The ranges on the figures in the experimental columns for the frequency of the first two bending modes and the damping of the first five modes are due to nonlinear behavior.

<b>Mode</b>	<b>18 DOF Truss (Hz)</b>	<b>12 Dof Beam (Hz)</b>	<b>Langley FE (Hz)</b>	<b>Exper (Hz)</b>	<b>Damping Ratio (Exper-%)</b>
<b>1st Bend</b>	<b>0.86</b>	<b>0.86</b>	<b>0.83</b>	<b>0.856- 0.870</b>	<b>1.0-4.0</b>
<b>1st Bend</b>	<b>0.86</b>	<b>0.86</b>	<b>0.83</b>	<b>0.862- 0.868</b>	<b>1.0-4.0</b>
<b>1st Tors</b>	<b>4.0</b>	<b>4.19</b>	<b>4.37</b>	<b>4.19</b>	<b>1.3-1.9</b>
<b>2nd Bend</b>	<b>6.70</b>	<b>6.72</b>	<b>6.38</b>	<b>6.11</b>	<b>2.0-2.5</b>
<b>2nd Bend</b>	<b>6.71</b>	<b>6.73</b>	<b>6.44</b>	<b>6.18</b>	<b>1.1-1.14</b>
<b>1st Axial</b>	<b>19.22</b>	<b>19.2</b>	<b>15.42</b>		
<b>2nd Tors</b>	<b>13.37</b>	<b>15.15</b>	<b>21.80</b>	<b>22.89</b>	<b>0.82</b>

**Table 6.4. Comparison of Model Frequencies**

### **Nonlinear Model and Results**

The lack of reliable data for strut-joints caused problems with a main objective of this research, namely to match analytical models with experimental data. The approach that was adopted was to use analytical nonlinearities that would give the characteristics that were observed in the experimental data. These analytical models would be based to a certain extent on past

observations and experience with nonlinear behavior in joints. There are an infinite number of ways that the nonlinear behavior shown in figures 6.5 and 6.6 could be modeled. Once a nonlinear element is chosen, it can be implemented in the model in a various configurations; in only one joint, in only the diagonal joints, etc. More than one nonlinear element can be chosen and these can be spread throughout the structure in various patterns. These types of arrangements most likely reflect the mechanism at work within a structure as extensive and complex as the Mini-Mast. However, to reduce the complexity of the model, the assumptions are made that only one nonlinear element is chosen and it is implemented in all of the truss elements.

An example of the computer codes used in this thesis is given in Appendix B. These five codes are similar in structure to all of the codes used to obtain the solutions to the harmonic response of the structures analyzed in chapters 4 and 5. The nonlinear model of the Mini-Mast has 216 degrees of freedom. The code calculates a Jacobian of this size and solves the iteration equations for each step. These codes were run on the Cray Supercomputer at MIT and took approximately 6 minutes of cpu time.

The first part of the analysis focused on the data in Figure 6.6 that shows the transfer function from the Z-axis torque wheel to the Kaman displacement sensor 49. The global behavior of this mode indicates a nonlinear joint or strut-joint that is a softening spring with an increase in damping accompanying an increase in amplitude or forced response.

The first nonlinear element that was analyzed was a gain change with a softening spring characteristic. This element was chosen to test the model and the procedure. The results of this analysis is shown in Figure 6.9. This is a transfer function from the Z-axis torque wheel location to the Kaman sensor position in the vicinity of the first torsion mode. The displacements and rotations of the model at the end of the truss are combined in such a way to determine the displacement at the sensor. Torque wheel dynamics and sensor scalings are included in the model.

This type of nonlinear joint nearly matches the behavior observed in figure 6.6. The resonant peak shifts downward in frequency with an increase in amplitude. There is also a certain relative amplitude change as the amplitude decreases.

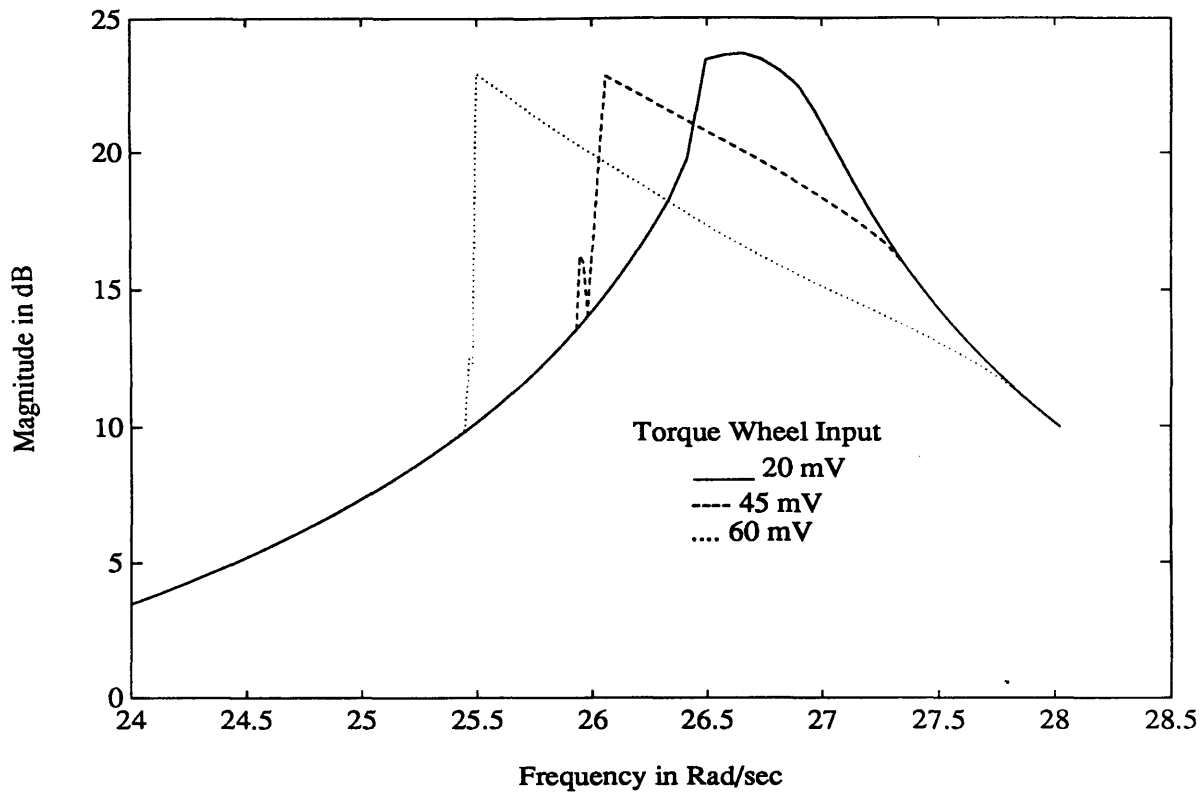


Figure 6.9 Transfer Function from Z-Axis Torque Wheel to Tip Displacement Sensor in Vicinity of First Torsion Mode, Mini-Mast Nonlinear Equivalent Beam Analytical Model with Gain Change Joints

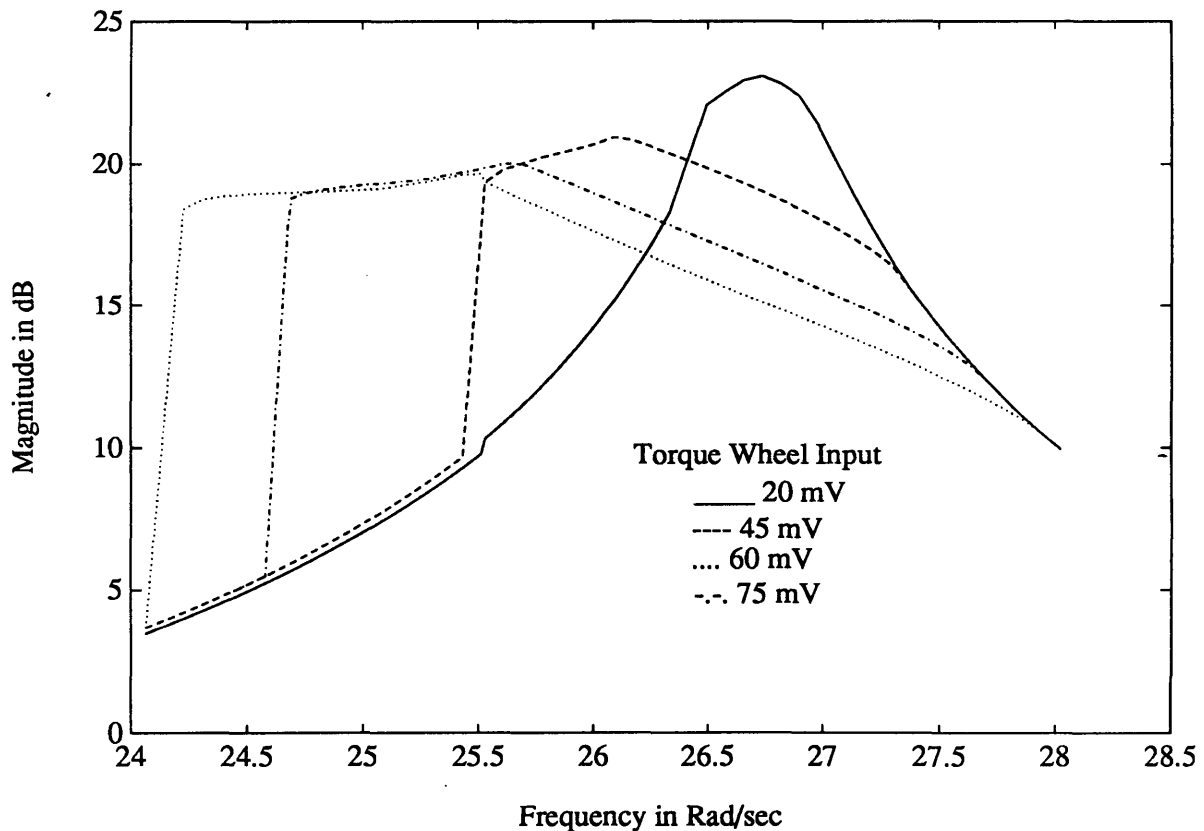


Figure 6.10 Transfer Function from Z-Axis Torque Wheel to Tip Displacement Sensor in Vicinity of First Torsion Mode, Mini-Mast Nonlinear Equivalent Beam Analytical Model with Natural Joints

The forcing levels cover the same range as those shown in Figure 6.6. Damping was set at one percent and the ratio of  $k_2/k_1$  is 0.7.

The second type of nonlinear element analyzed was described in Chapter 4 as a natural joint. It has a softening spring characteristic with a hysteresis effect. A schematic of this joint is shown in Figure 4.19. The transfer function of the Mini-Mast analytical model with this joint is shown in Figure 6.10. These plots compare very well with the plots in Figure 6.6. There is a lowering of peak frequency with amplitude and an increase in damping. The plots show the results of sine sweeps in the backwards direction. The forward sweeps caused the sharp jumps for each of the curves to shift to the right so that the jump occurs just to the left of the peak on each curve. These curves were not added to avoid confusion.

Both analytical models have very sharp jumps that the experimental data does not have. The solution is multi-valued around the resonant peaks and the analytical makes sudden transitions from one solution to the other. The experimental data is smoother. A likely reason is that noise and disturbances in the actual apparatus tend to obscure distinction between response modes.

### **Pre-Buckling Behavior in Diagonals**

A possible explanation for the softening effect shown in the experimental data is pre-buckling behavior in the diagonals. The buckling load of the diagonals, from Table 6.1, is 827.3 N. The loading of these diagonals in compression results in axial deflection and fore-shortening due to the load offset induced bowing of the element. Figure 6.11 shows this behavior for an amplitude range that represents the average range of displacements of the diagonals along the length of the Mini-Mast in the vicinity of the torsion mode resonant peak. The range of motion is small. The offset of the axial loading to induce the behavior shown in the figure is 0.5 cm. This softening behavior occurs only in the compressive range of the truss element. The overall effect, however, is a softening spring. This softening effect combined with hysteresis could also give the behavior shown in the experimental data. Such an element would not have a finite asymptotic stiffness as buckling would occur for large axial displacements.



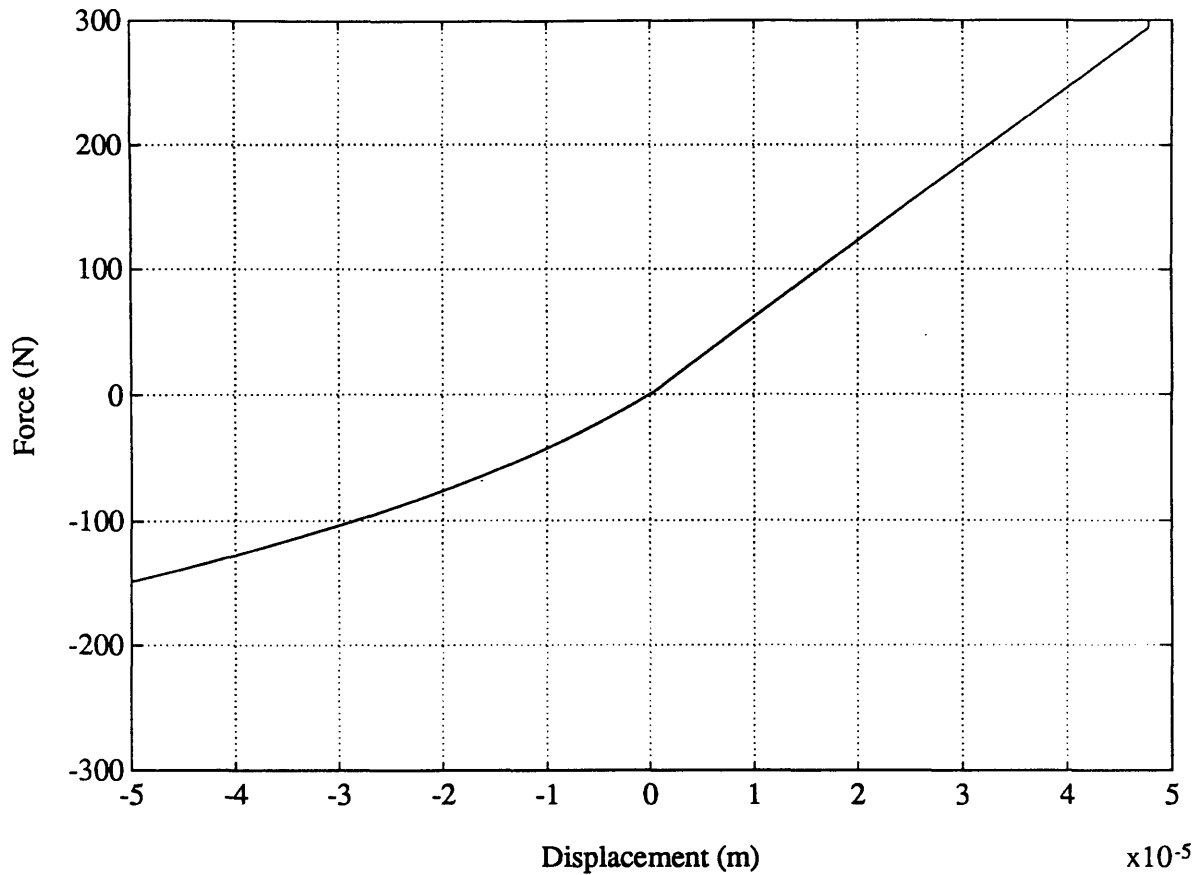


Figure 6.11 Force-Axial Displacement Curve of Mini-Mast Diagonal Truss Element with Pre-Buckling Behavior for Maximum Range of Motion Observed in Analytical Model with Axial Load Offset  $e = 0.5$  cm

## 6.5 SUMMARY

The method developed in the preceding chapters has been shown to model physical global nonlinear behavior very well. The natural joint gives a viable model of the nature of the response of the Mini-Mast. The softening characteristics of the element could be explained in part by pre-buckling behavior of the diagonal truss elements. The linear equivalent beam model gives a reasonably accurate model of the lowest global structural dynamic modes of the structure.

## **CHAPTER 7**

### **NONLINEAR EQUIVALENT BEAM MODEL FOR CONTROL DESIGN AND ANALYSIS**

#### **7.1 INTRODUCTION**

Nonlinearities within a structure present problems for designing a controller. The standard control design methodologies assume a linear model. The presence of nonlinear joints could possibly have an effect on the stability of the controlled system. This could also lead to instabilities such as limit cycles within the controlled structure.

The presence of nonlinear elements also causes degradation in the performance of the controlled structure. In terms of disturbance rejection, this degradation could lead to unacceptably large response to a disturbance input.

This chapter will use the method developed in the previous chapters to model a nonlinear structure with a control system. The linear controlled model response is compared to the nonlinear model response to show the differences in disturbance rejection between the design model and the actual model. Both full-state feedback designs and model-based compensator with limited measurements and estimators are analyzed. The effect of a robust full-state feedback design on performance is also investigated.

## 7.2 STATE EQUATIONS FOR NONLINEAR SYSTEM

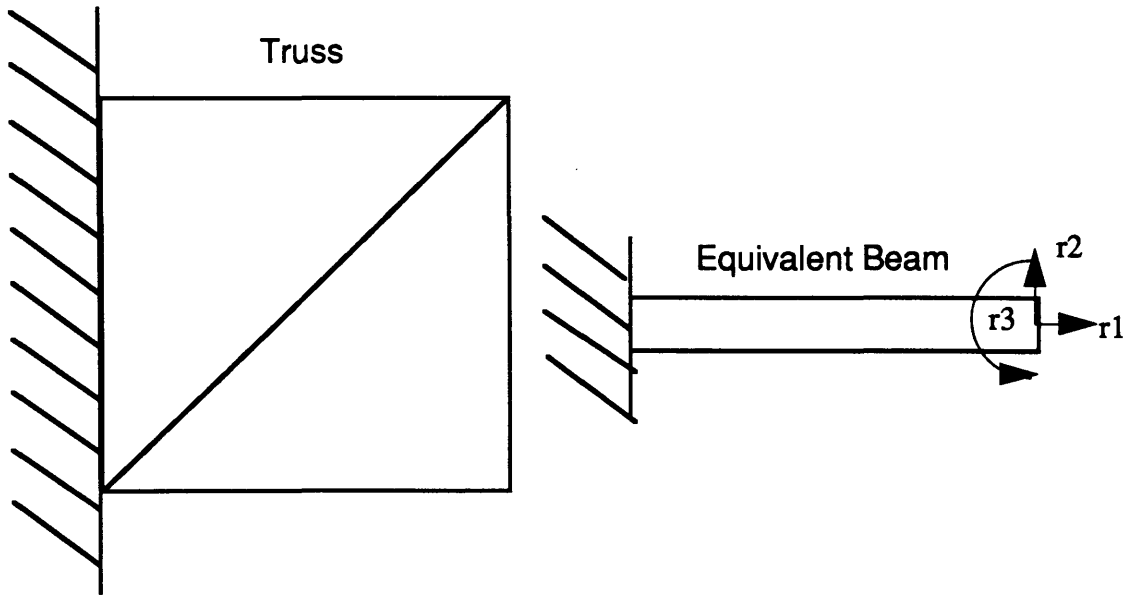


**Figure 7.1 Simple Truss for Control Evaluation**

Figure 7.1 shows the one bay 2-D truss and the equivalent beam model that will be used for control evaluation. It is identical to the one bay structure analyzed in Chapter 4 with the exception that there is a mass at the tip of this structure.

The equations of motion in state space form for a linear structure are, with a disturbance input:

$$\begin{Bmatrix} \dot{\underline{x}} \\ \ddot{\underline{x}} \end{Bmatrix} = \begin{bmatrix} 0 & I \\ -M^{-1}K_{NL} & -M^{-1}C_{NL} \end{bmatrix} \begin{Bmatrix} \underline{x} \\ \dot{\underline{x}} \end{Bmatrix} + \begin{bmatrix} 0 \\ M^{-1}F_B \end{bmatrix} \underline{u} + \begin{bmatrix} 0 \\ M^{-1}F_L \end{bmatrix} \underline{w} \quad (7.1)$$

or

$$\dot{\underline{q}} = A\underline{q} + B\underline{u} + L\underline{w} \quad (7.2)$$

where  $\underline{u}$  is the control and  $\underline{w}$  is the disturbance input. The  $K$  and  $C$  matrices for the structure in figure 7.1 are constructed using the nonlinear equivalent finite element beam method developed in previous chapters. One percent damping is assumed in all three modes of the structure.

If integrators are present in the control loop, the augmented state-space model is:

$$\begin{Bmatrix} \dot{\underline{z}} \\ \dot{\underline{x}} \\ \ddot{\underline{x}} \end{Bmatrix} = \begin{bmatrix} 0 & \mathbf{I} & 0 \\ 0 & 0 & \mathbf{I} \\ 0 & -\mathbf{M}^{-1}\mathbf{K}_{NL} & -\mathbf{M}^{-1}\mathbf{C}_{NL} \end{bmatrix} \begin{Bmatrix} \underline{z} \\ \underline{x} \\ \dot{\underline{x}} \end{Bmatrix} + \begin{bmatrix} 0 \\ 0 \\ \mathbf{M}^{-1}\mathbf{F}_B \end{bmatrix} \underline{u} + \begin{bmatrix} 0 \\ 0 \\ \mathbf{M}^{-1}\mathbf{F}_L \end{bmatrix} \underline{w} \quad (7.3)$$

The vector  $\underline{z}$  is the state of the integrator.

The nonlinear element investigated in the following analysis is the gain change, both hardening and softening. Non-dimensional values of the nonlinear joint parameters are  $\delta=0.01$  and  $k_2/k_1=0.6, 2.0$ .

### 7.3 FULL STATE FEEDBACK

#### Linear Quadratic Regulator

The Linear Quadratic Regulator control design assumes full state feedback. The feedback matrix is determined by solving the following Riccati equation:

$$0 = \mathbf{A}^T\mathbf{P} + \mathbf{P}\mathbf{A} + \mathbf{Q} - \mathbf{P}\mathbf{B}\mathbf{R}^{-1}\mathbf{B}^T\mathbf{P} \quad (7.4)$$

to give

$$\mathbf{K}_T = \mathbf{R}^{-1}\mathbf{B}^T\mathbf{P} \quad (7.5)$$

where  $\mathbf{A}$  and  $\mathbf{B}$  are defined from equation (7.1) or (7.3) with linear stiffness and damping matrices,  $\mathbf{Q}$  is the state weighting matrix,  $\mathbf{R}$  is control weighting matrix and  $\mathbf{K}_T$  is the full state feedback gain matrix. The weighting matrices,  $\mathbf{Q}$  and  $\mathbf{R}$  are taken as the identity matrices with the control matrix multiplied by  $\rho$ , which serves as a measure of the ratio of control weighting to state weighting.

The full state feedback gain matrix from equation (7.5) is divided into the components multiplying each element in the state vector:

$$\underline{u} = -\mathbf{K}_1\underline{x} - \mathbf{K}_2\dot{\underline{x}} \quad (7.6)$$

The closed loop state space equations of motion are:

$$\begin{Bmatrix} \dot{\underline{x}} \\ \ddot{\underline{x}} \end{Bmatrix} = \begin{bmatrix} 0 & \mathbf{I} \\ -\mathbf{M}^{-1}(\mathbf{K}_{NL} + \mathbf{F}_B\mathbf{K}_1) & -\mathbf{M}^{-1}(\mathbf{C}_{NL} + \mathbf{F}_B\mathbf{K}_2) \end{bmatrix} \begin{Bmatrix} \underline{x} \\ \dot{\underline{x}} \end{Bmatrix} + \begin{bmatrix} 0 \\ \mathbf{M}^{-1}\mathbf{F}_L \end{bmatrix} \underline{w} \quad (7.7)$$

The nonlinear stiffness and damping matrices are dependent on the amplitude across the nonlinear elements and the frequency. If the disturbance input is sinusoidal, i. e.,

$$\underline{w} = \underline{e} \sin \omega t \quad (7.8)$$

the response can be assumed to be harmonic as in equation (4.2) and the equations of motion are written in harmonic balance form similar to equation (4.3) with the added gain matrices. In matrix form, these are:

$$\begin{bmatrix} K_{NL} + F_B K_1 - \omega^2 M & -\omega(C_{NL} + F_B K_2) \\ \omega(C_{NL} + F_B K_2) & (K_{NL} + F_B K_1 - \omega^2 M) \end{bmatrix} \begin{Bmatrix} \underline{a} \\ \underline{b} \end{Bmatrix} = \begin{Bmatrix} F_L \underline{e} \\ 0 \end{Bmatrix} \quad (7.9)$$

These equations are solved to determine the disturbance rejection properties of the controlled system with nonlinear joints.

If an integrator is included in the control design, the feedback gain matrix is now broken into three components.

$$\underline{u} = -K_1 \underline{z} - K_2 \underline{x} - K_3 \dot{\underline{x}} \quad (7.10)$$

And if a sinusoidal disturbance and response is assumed,  $\underline{x}$  has the same form as before. The state  $\underline{z}$  is the integral of the displacement vector.

$$\underline{z} = -\frac{1}{\omega} \underline{a} \cos \omega t + \frac{1}{\omega} \underline{b} \sin \omega t \quad (7.11)$$

The harmonic balance equations of motion for the nonlinear system in matrix form are:

$$\begin{bmatrix} K_{NL} + F_B K_1 - \omega^2 M & \frac{1}{\omega} F_B K_1 - \omega(C_{NL} + F_B K_2) \\ \omega(C_{NL} + F_B K_2) - \frac{1}{\omega} F_B K_1 & (K_{NL} + F_B K_1 - \omega^2 M) \end{bmatrix} \begin{Bmatrix} \underline{a} \\ \underline{b} \end{Bmatrix} = \begin{Bmatrix} F_L \underline{e} \\ 0 \end{Bmatrix} \quad (7.12)$$

Both equation (7.9) and (7.12) are solved using the Newton-Raphson iteration algorithm used to solve the nonlinear equations of motion in previous chapters. The Jacobian is calculated numerically as before.

Equations (7.9) and (7.12) will be used to determine the disturbance rejection properties of

the nonlinear truss structure shown in Figure 7.1 with an LQR controller. The disturbance input is at the tip of the structure in the transverse direction.

Figure 7.2 shows the transfer functions from the disturbance input to the displacements of the structure with full control and  $\rho=1$ , or relatively expensive control. The linear transfer function is the solid line and the plots for a softening and hardening gain change are shown. The disturbance input is large so that the nonlinear stiffness coefficients are near their maximum values. The nonlinear transfer function serves as an approximate edge of the envelope of amplitude dependent nonlinear responses. The linear response is the other edge of the envelope. The nonlinear transfer function for the transverse direction shows a small deviation from the linear, whereas the axial displacement and rotation show large fluctuations in response, particularly at low frequencies. One point of interest is that the control is more robust to a softening gain change than to a hardening gain change.

Figure 7.3 shows the same transfer functions with cheap control ( $\rho=0.01$ ). There is no discernible difference between linear and nonlinear response in this case. This is due to the fact that the controller limits the displacements of the structure to the linear range.

Figure 7.4 shows the transfer functions for the structure with only one degree of freedom being controlled. The ratio of control to state weighting is 1, i. e. expensive control. The dynamics of the structure are more apparent here than in the full control case. The softening spring moves the dynamics to the left to a lower frequency and the hardening spring moves them to the right. The control is relatively robust for the transfer function to the transverse displacement in terms of an average response. However, the nonlinear structure causes the zeros in the transfer function to move away from the linear locations.

Figures 7.5 and 7.6 show the transfer functions for the controlled structure with and without an integrator in the loop. The high authority control is very robust and shows no significant deviation from the linear response for the softening or hardening gain change. The low authority control shown in Figure 7.6 shows that the nonlinearity has more effect on the response of the system with this control.

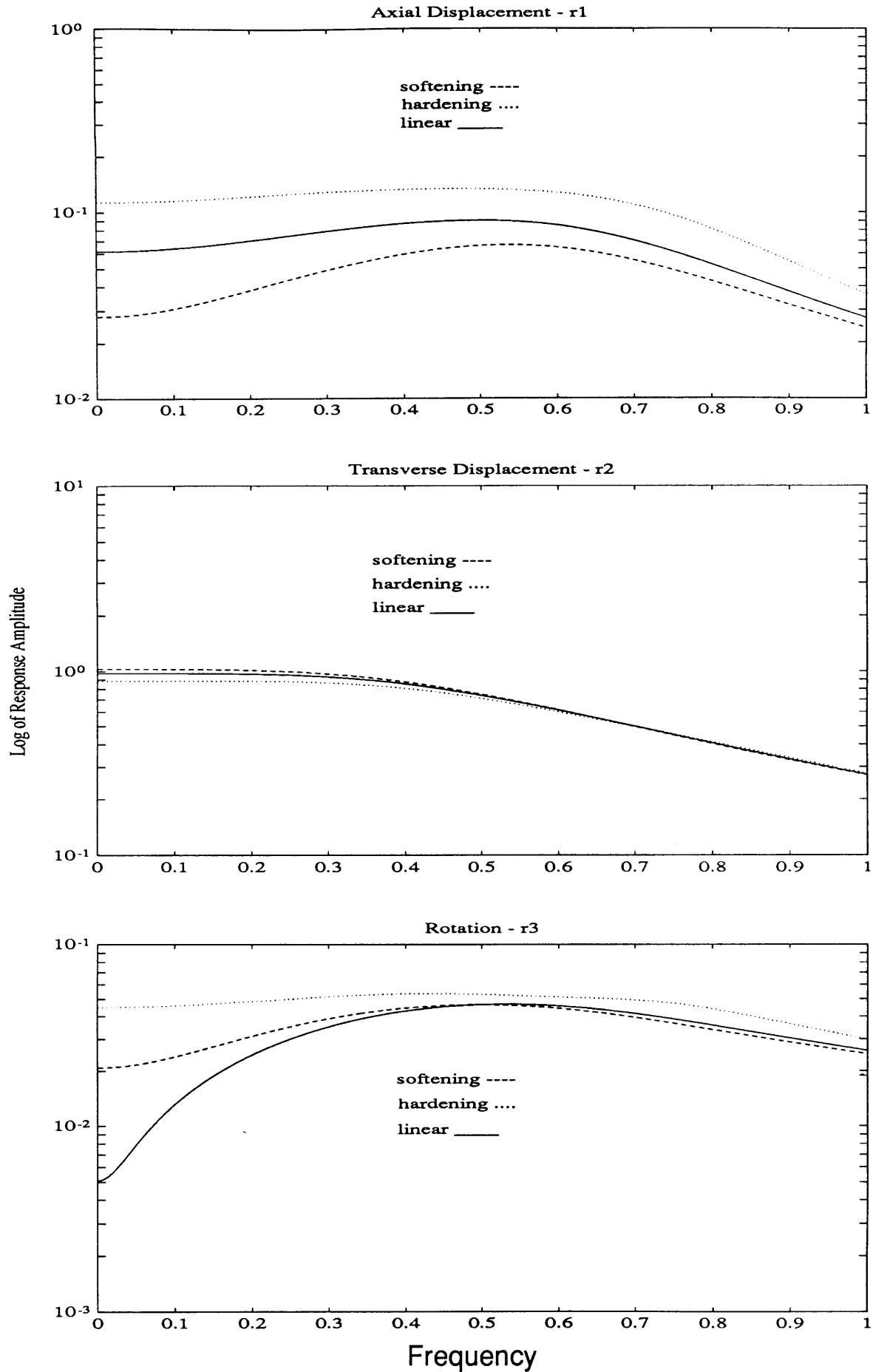


Figure 7.2 Transfer Function from Transverse Excitation to Tip Disp. for Structure With Gain Change Joints and LQR Control with  $\rho = 1$  and Full Control Authority



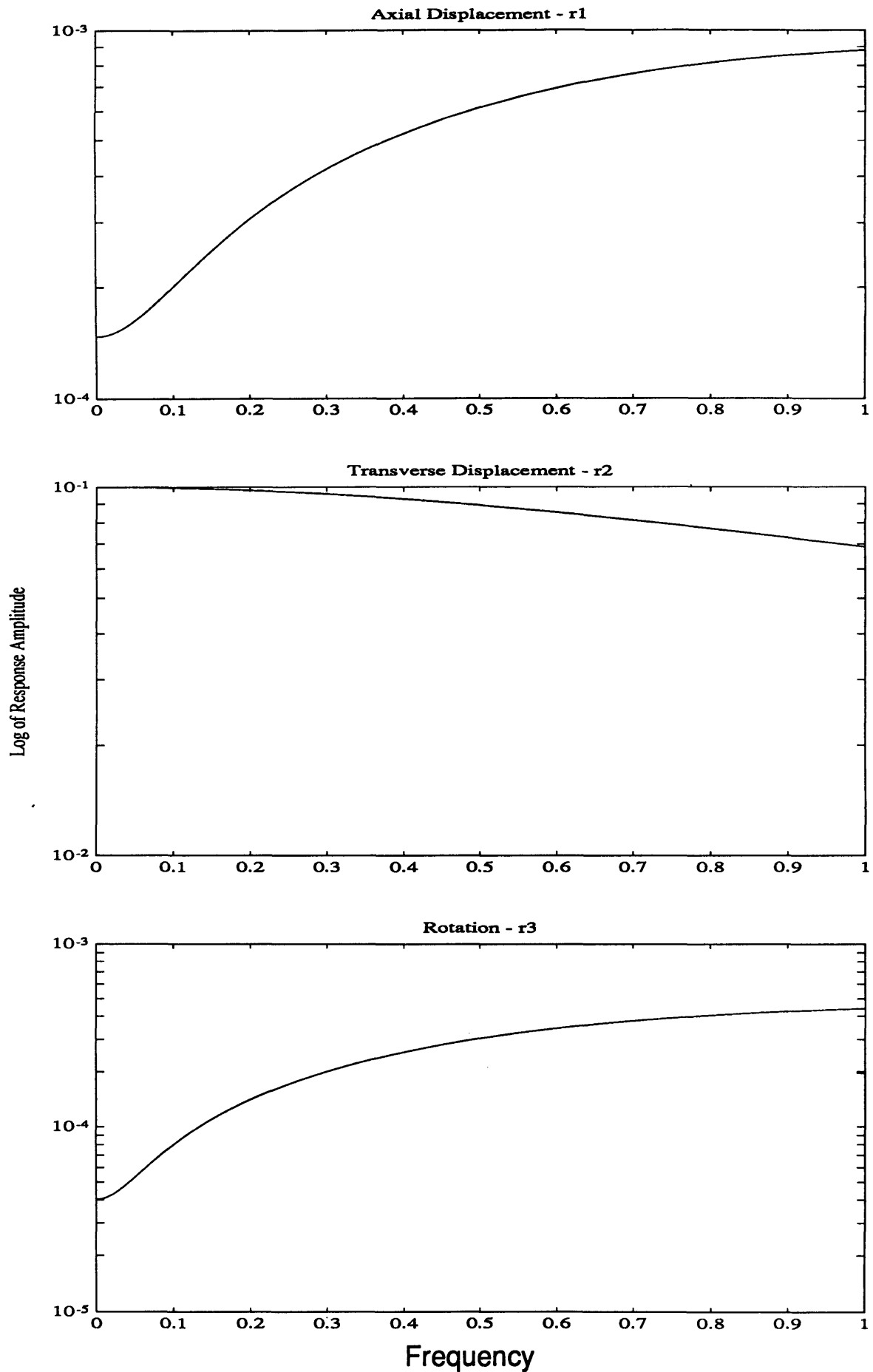


Figure 7.3 Transfer Function from Trans Excitation to Tip Displacements for Structure with Gain Change Joints and LQR Control with  $\rho = .01$ , Full Control Authority

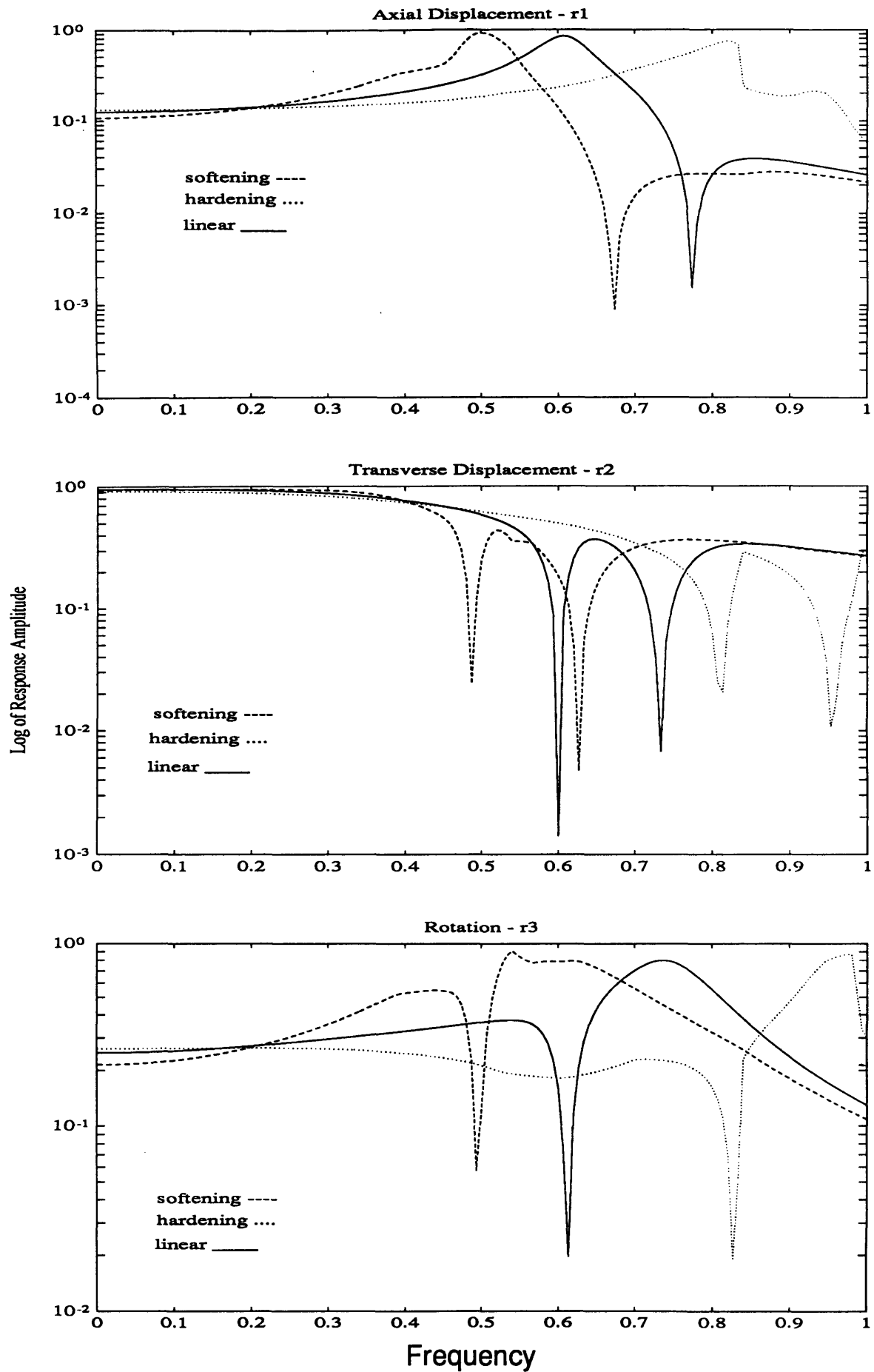


Figure 7.4 Transfer Function from Transverse Tip Excitation to Displacements for Structure with Gain Change Joints and LQR Control with  $\rho = .01$  and Partial Control Authority

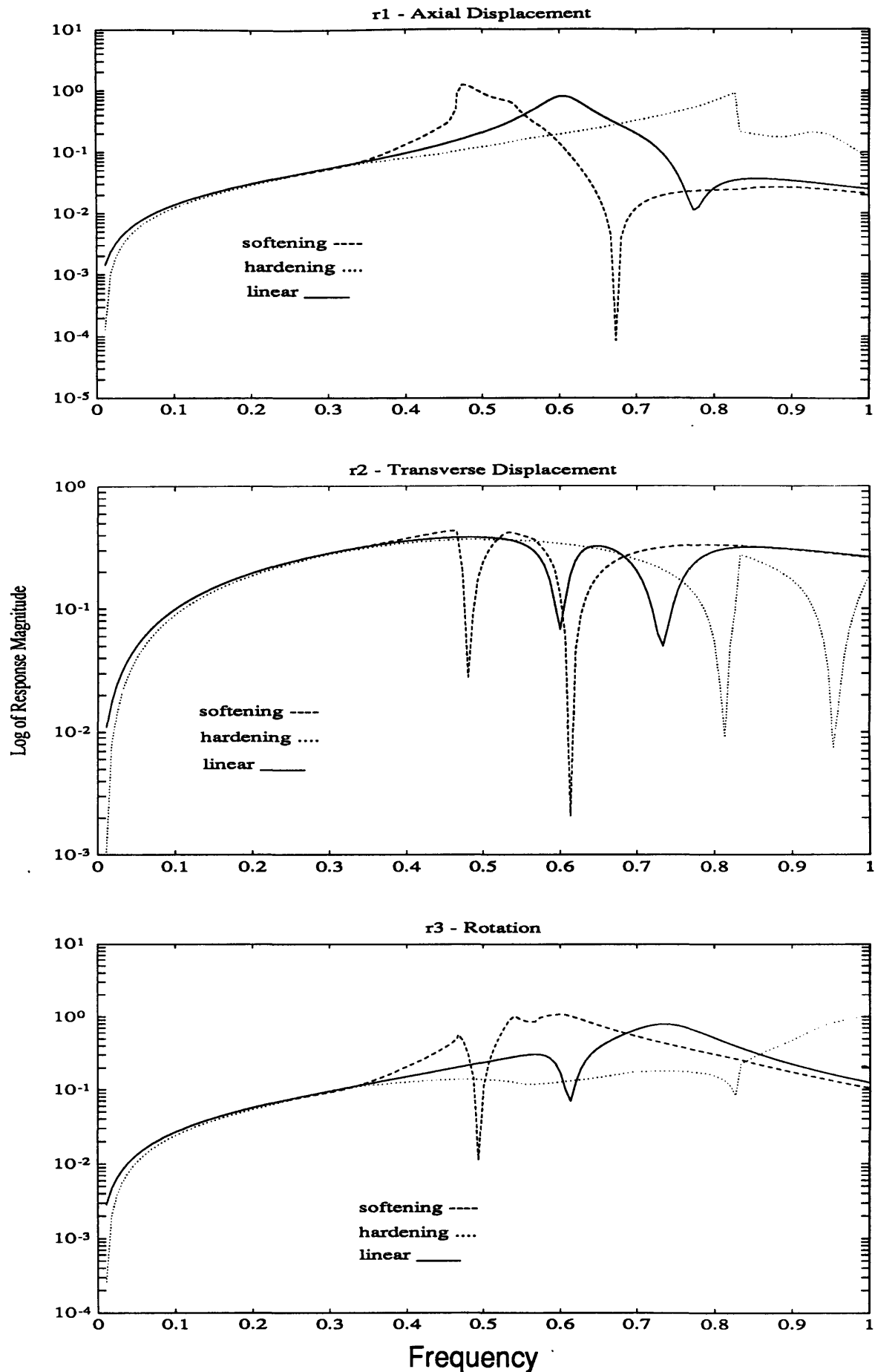


Figure 7.5 Transfer Function from Tip Excitation to Displacements for Structure with Gain Change Joints and LQR Integrator Control with  $\rho = 1$  and Partial Control Authority

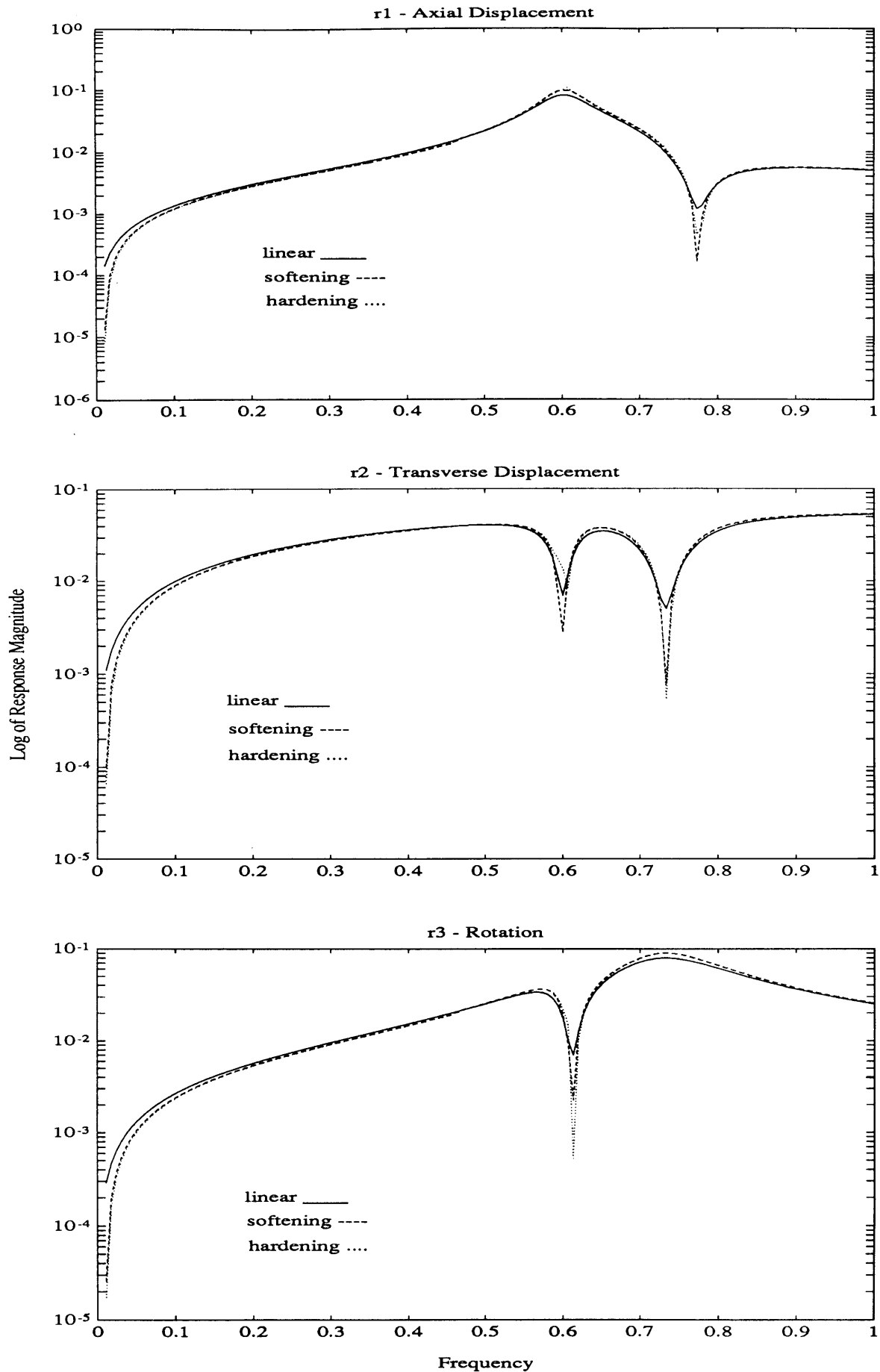


Figure 7.6 Transfer Function from Tip Excitation to Displacements for Structure with Gain Change Joints and LQR Integrator Control with  $\rho = .01$  and Partial Control Authority

## Robust LQR

None of the designs investigated in the previous section proved to be unstable when applied to a nonlinear model. However, the disturbance rejection properties of these designs were somewhat degraded by the presence of nonlinearities. It is interesting to investigate the effect that a robust control design has on the response of a controlled nonlinear structure and to determine if there is an improvement in performance over a non-robust design.

The robust control design approach considered here was developed by Peterson and Hollot (1985) for a state equation of the form:

$$\dot{q}(t) = \left[ A_o + \sum_{i=1}^k A_i r_i(t) \right] q(t) + \left[ B_o + \sum_{i=1}^k B_i s_i(t) \right] u(t) \quad (7.13)$$

The summation terms represent the independent deviations from the nominal model. These deviations are factored into rank one matrices of the form:

$$A_i = d_i e_i^T, \quad B_i = f_i g_i^T \quad (7.14)$$

and the multiplying terms  $r_i$  and  $s_i$ , are scalar parameters that indicate the magnitude of uncertainty. This is used to develop a control system design for full state feedback with a quadratic Lyapunov bound on the closed loop system. Bernstein (1987) adapts this approach to allow factor matrices with rank greater than one.

$$A_i = D_i E_i \quad (7.15)$$

The present model has no uncertainty in the B matrix, so related terms will be disregarded.

The feedback gain matrix for the robust controller is:

$$K_T = R^{-1} B^T P$$

which is the same as equation (7.5). The P matrix is obtained from the Riccati equation:

$$0 = A^T P + P A + P D P + Q + E - P B R^{-1} B^T P \quad (7.16)$$

where the state (Q) and control weighting (R) matrices are the same as the standard LQR and

$$D = \sum_{i=1}^k \delta D_i D_i^T, \quad E = \sum_{i=1}^k \delta E_i^T E \quad (7.17)$$

The parameter  $\delta$  is a measure of the magnitude of uncertainty and is determined from:

$$\delta \geq |r_i(t)|, \quad i = 1, \dots, k; \quad \delta \geq 0$$

The value of the stiffness and damping of the nonlinear structure most likely will approach some asymptotic or extreme value. If this is not the case, a maximum amplitude may be prescribed and the stiffness properties at that value may be treated as maximum or minimum values. These values may be used to determine the extent of parameter variation in the plant model of the structure. The state equations of the above structure may be written as:

$$\begin{Bmatrix} \dot{x} \\ \ddot{x} \end{Bmatrix} = \begin{bmatrix} 0 & I \\ -M^{-1}K_{NLm} & -M^{-1}C_{NLm} \end{bmatrix} \begin{Bmatrix} x \\ \dot{x} \end{Bmatrix} + \begin{bmatrix} 0 \\ M^{-1}F_B \end{bmatrix} \underline{u} \quad (7.18)$$

The values in the matrices  $K_{NLm}$  and  $C_{NLm}$  are determined from the extremum values of the describing function coefficients that compose these matrices. These matrices are divided into a linear part and a variation:

$$\begin{aligned} K_{NLm} &= K + \Delta K \\ C_{NLm} &= C + \Delta C \end{aligned} \quad (7.19)$$

The state equations for the system of equation (7.13) are now:

$$\begin{Bmatrix} \dot{x} \\ \ddot{x} \end{Bmatrix} = \begin{bmatrix} 0 & I \\ -M^{-1}K & -M^{-1}C \end{bmatrix} \begin{Bmatrix} x \\ \dot{x} \end{Bmatrix} + \begin{bmatrix} 0 & 0 \\ -M^{-1}\Delta K & -M^{-1}\Delta C \end{bmatrix} \begin{Bmatrix} x \\ \dot{x} \end{Bmatrix} + \begin{bmatrix} 0 \\ M^{-1}F_B \end{bmatrix} \underline{u} \quad (7.20)$$

which is in the form,

$$\dot{q} = (A + \Delta A)q + Bu \quad (7.21)$$

These equations are in the form required for the robust LQR design described above where  $A_1 = \Delta A$  and there is only one independent uncertainty. The particular nonlinearity under investigation is a gain change so only the stiffness varies. Therefore the variation in the plant is

represented by:

$$\Delta A = \begin{bmatrix} 0 & 0 \\ -M^{-1}\Delta K & 0 \end{bmatrix} \quad (7.22)$$

The factorization of  $\Delta A$  is not unique. An obvious choice is:

$$D_i = \begin{bmatrix} 0 \\ -M^{-1} \end{bmatrix} \quad E_i = [\Delta K \quad 0] \quad (7.23)$$

where  $\Delta K$  is determined from equation (7.19). This represents the maximum deviation from the linear for the nonlinear structure. In the analysis that follows, the D and E matrices calculated from equation (7.23) and (7.17), is multiplied by the scaling factor  $\delta$ .

The first case investigated is that with response shown in Figure 7.2; expensive control, full control authority. Only the hardening spring element is investigated. The value of  $\delta$ , the measure of the uncertainty, was varied to give control gains that were similar in magnitude to those for the non-robust problem. Figure 7.7 shows that the disturbance rejection properties for the axial displacement of the truss at higher frequencies are improved by the implementation of the robust control design, albeit only in small way. At low frequencies, the response does not change.

The next case is the partial control case with control effort only available in the direction of the disturbance. Obtaining a solution to equation (7.16) is somewhat more problematic in this case. The highest uncertainty bound that gave a viable solution was  $\delta=0.004$ . The algorithm did give a solution at  $\delta=0.005$ , but the gains that resulted were two orders of magnitude higher than those given for the non-robust design. Any higher value results in no solution. The allowable bound is not large. The variation in stiffness from the gain change models as indicated by equation (7.19) is much larger for the cases that are investigated. However, the robust design does result in some performance improvement as shown in Figure 7.8 and 7.9. This is particularly true of the rotation degree of freedom for the hardening spring model at high frequencies. At some points, the robust control produces better performance than the linear model.

The final robust control case is the control with an integrator in the loop. This system also

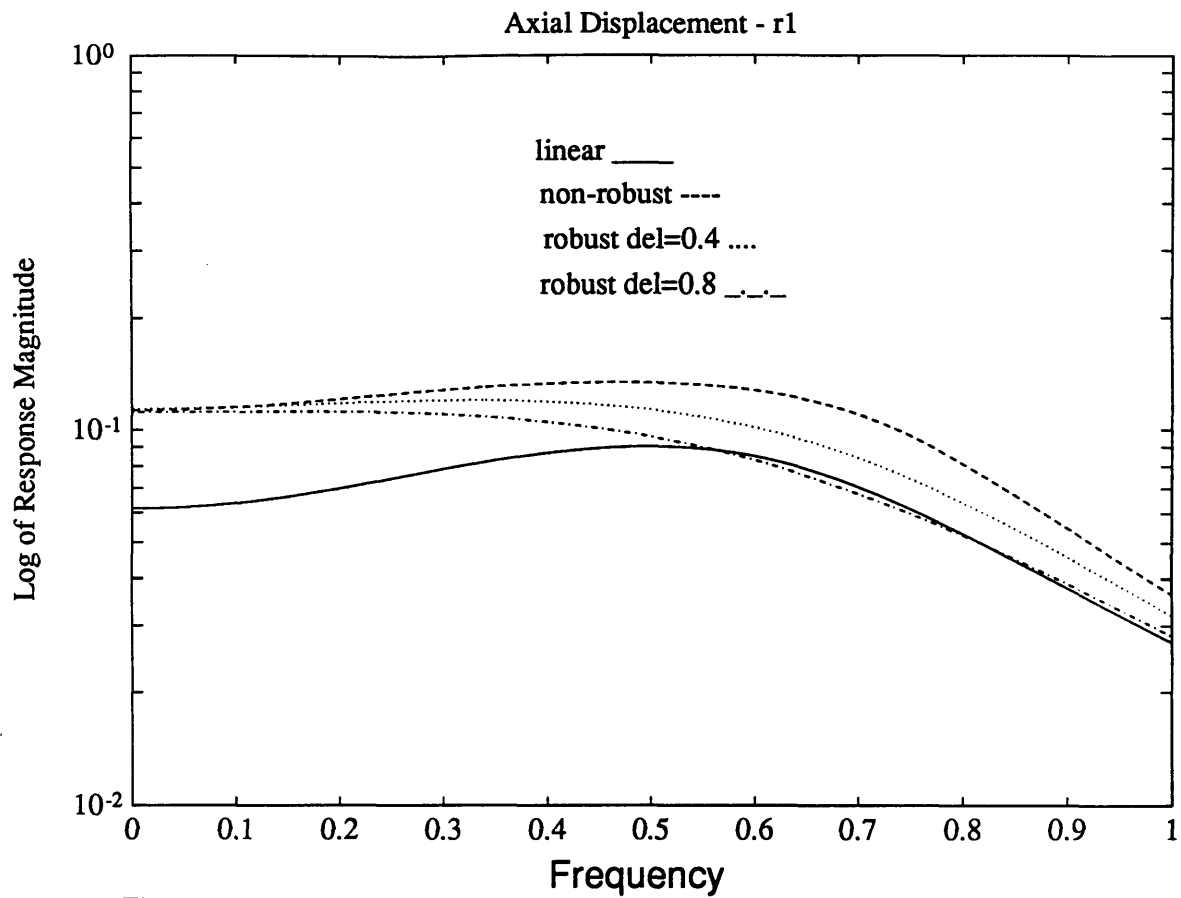


**Figure 7.7 Transfer Function From Tip Excitation to Axial Displacement  
 for Structure with Hardening Gain Change Joints with Robust LQR Design  
 Compared to Linear and Nonlinear LQR Control**



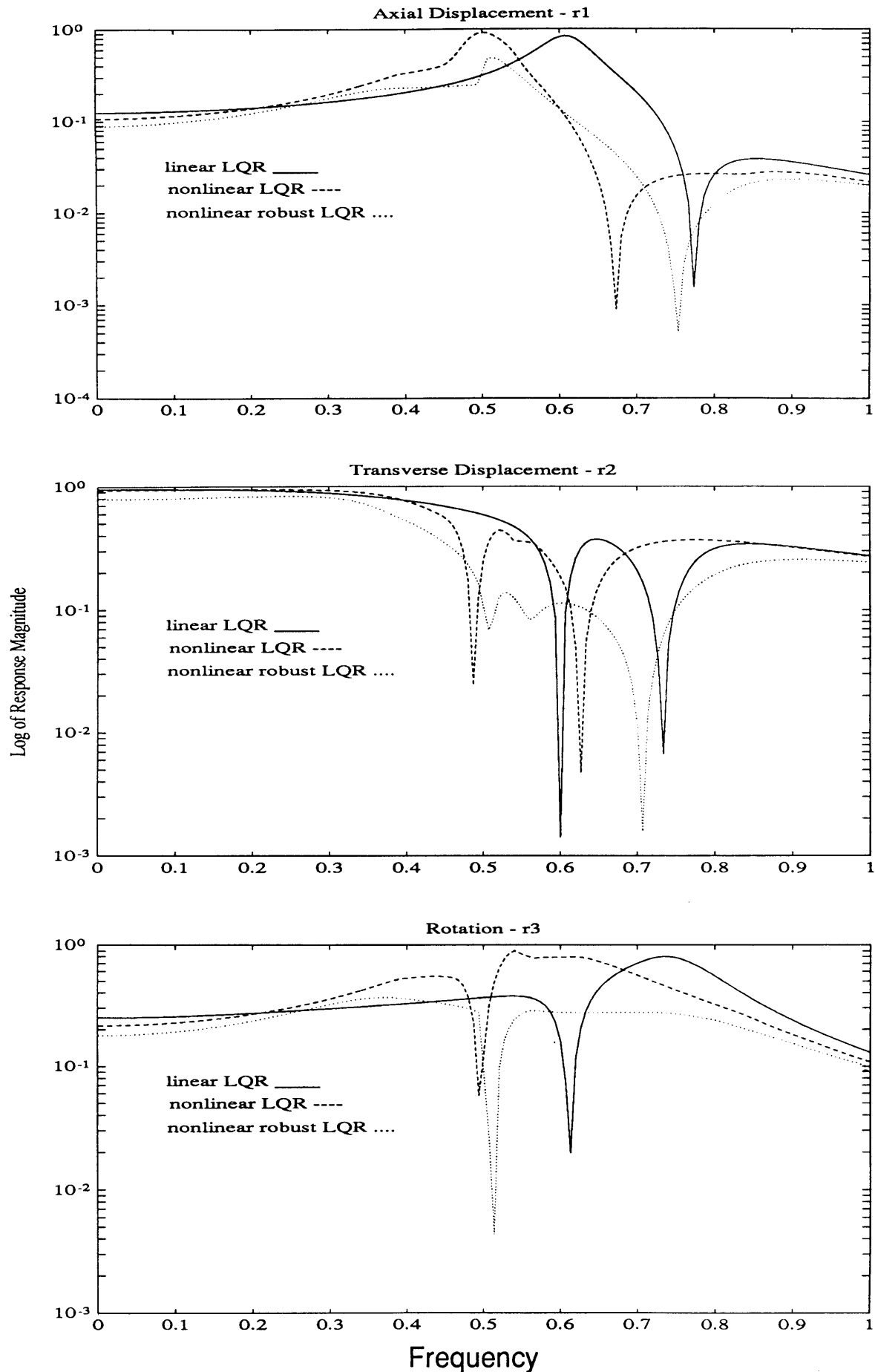


Figure 7.8 Transfer Functions from Tip Excitation to Displacements for Structure with Softening Gain Change Joints with Partial Control Authority

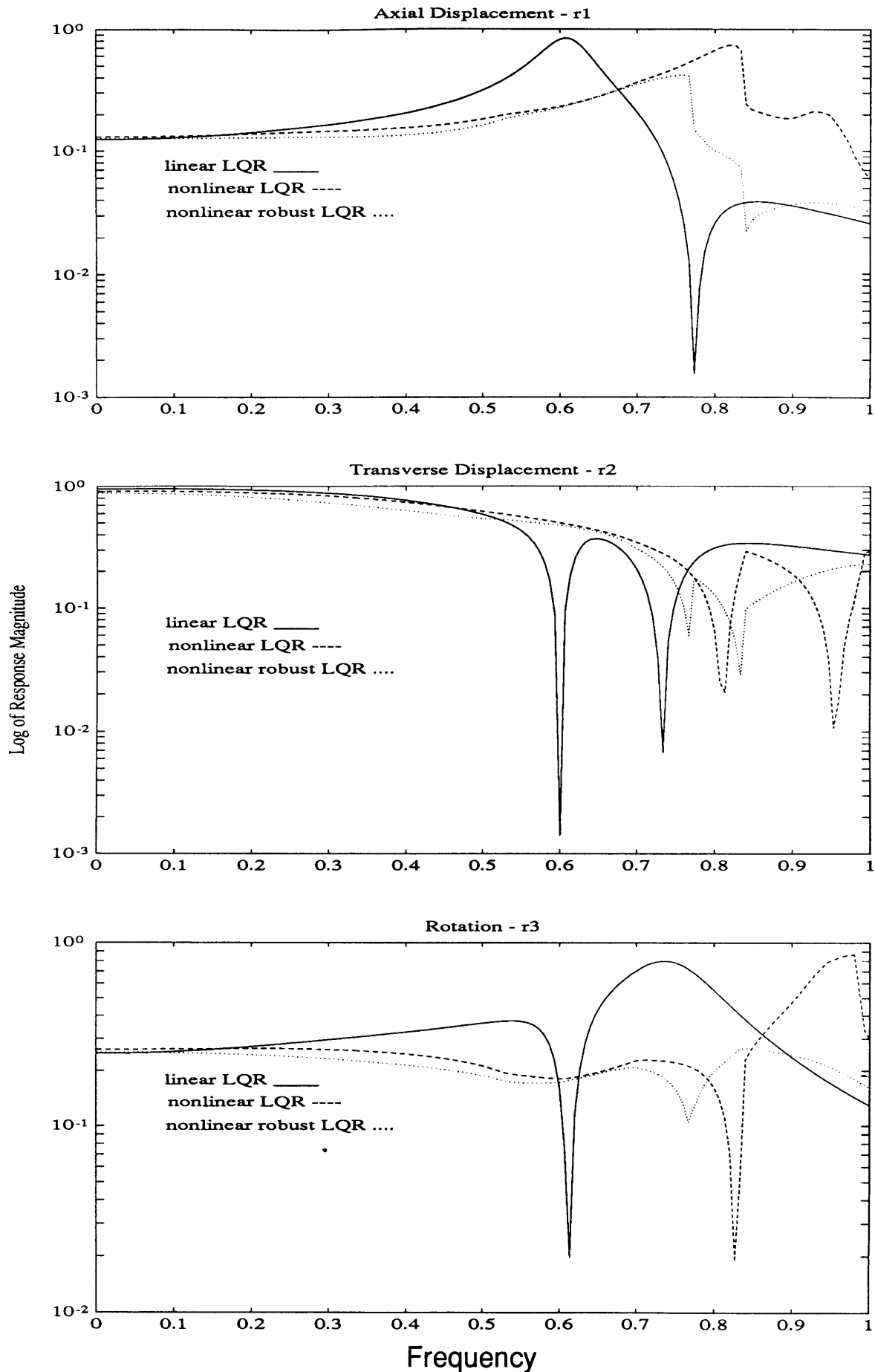


Figure 7.9 Transfer Functions from Tip Excitation to Displacements for Structure with Hardening Gain Change Joints with Partial Control Authority

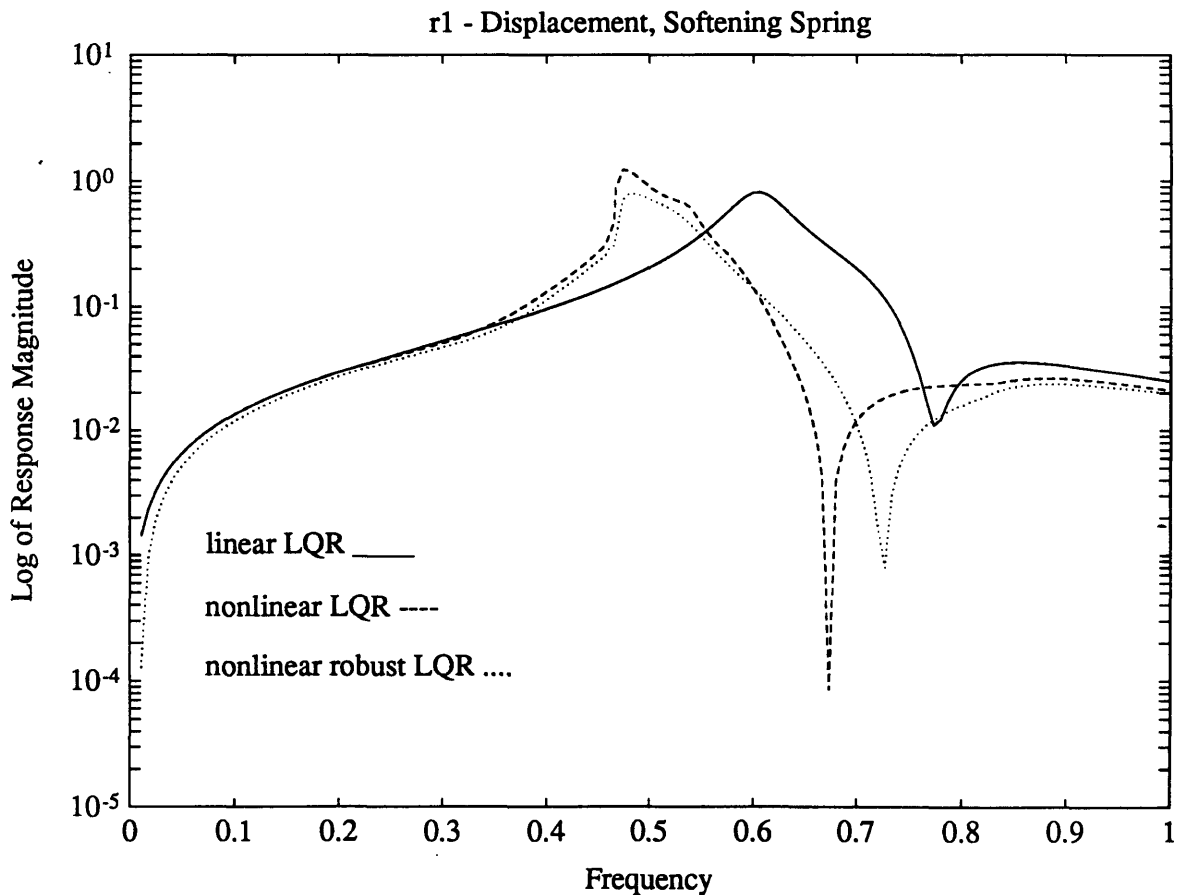
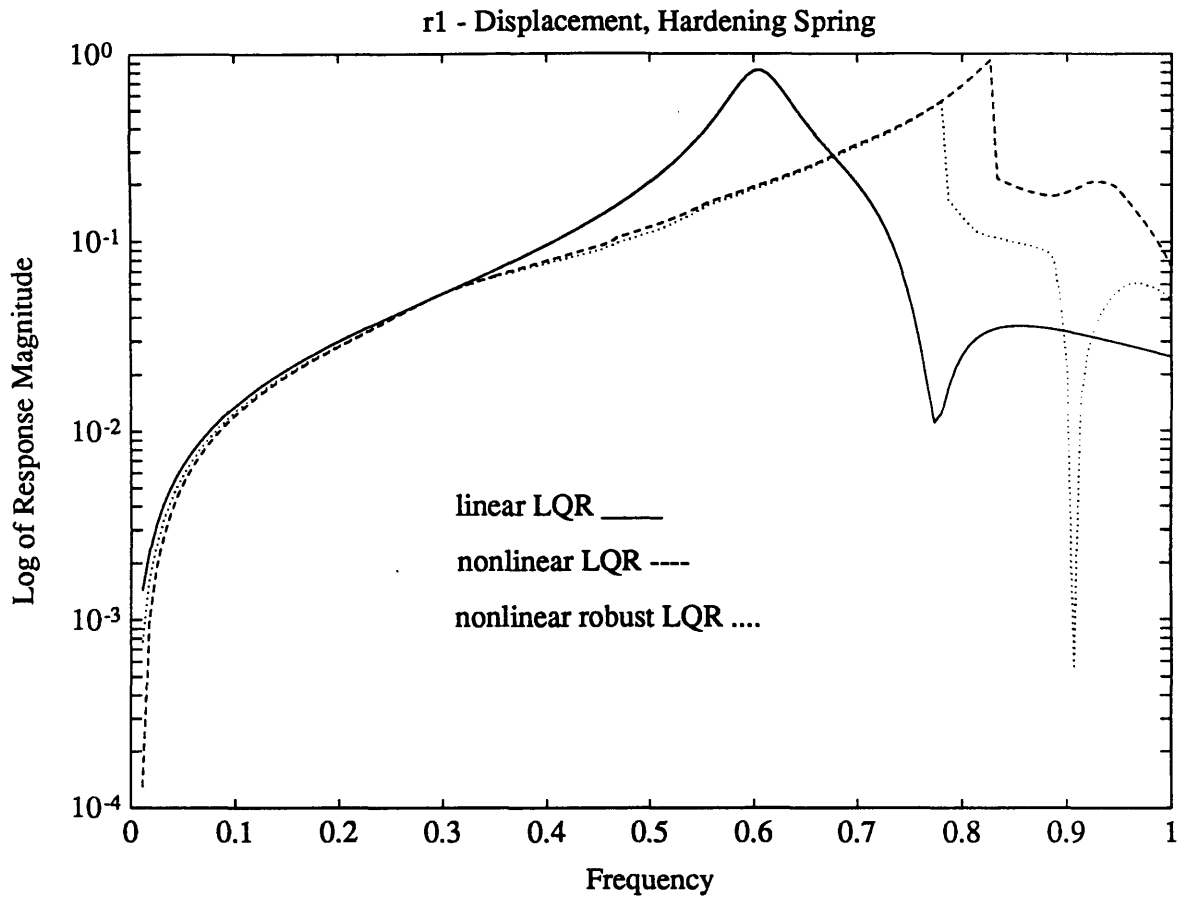


Figure 7.10 Transfer Function for Tip Excitation to Axial Displacement of Structure with Gain Change Joints with Robust LQR Integrator Design Compared to Linear and Nonlinear LQR Control Design

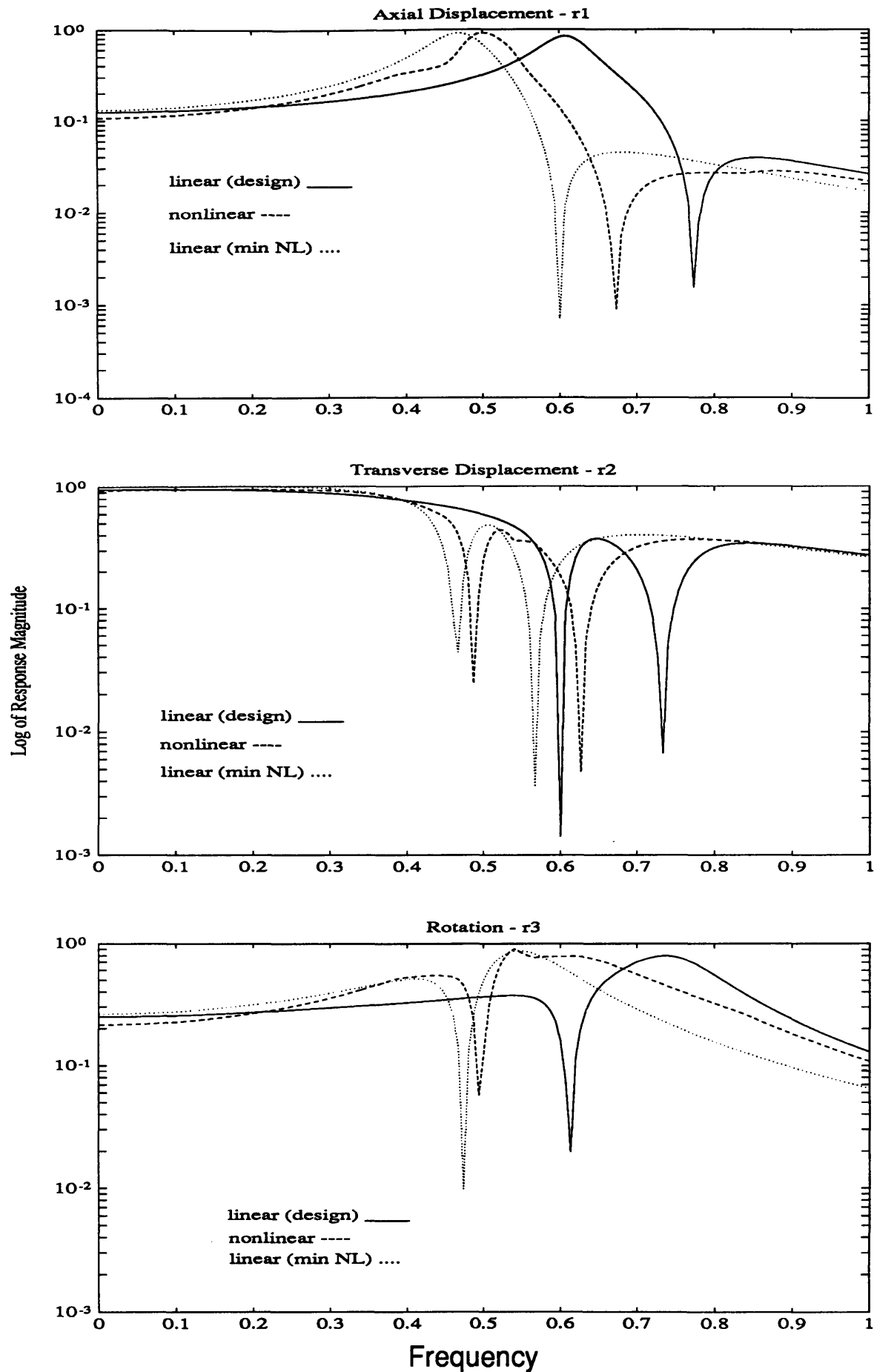


Figure 7.11 Transfer Functions for Linear LQR, Nonlinear Softening LQR and Linear LQR with Stiffness Properties Coinciding with Minimum Values of Nonlinear Stiffness Coefficients

did not produce a solution to equation (7.16) for high values of uncertainty . The allowable bound in this case is  $\delta=0.003$ . Again there is a very high gain solution at a slightly higher value and no solution at the next value. The gains in performance with this design are not as large as the case with no integrator as shown in Figure 7.10. This figure shows the results for the axial degree of freedom.

A final figure for this section compares the response of the linear and nonlinear models with single dof LQR control with a linear model with the minimum value of the describing function nonlinear stiffness model for the softening gain change control. Figure 7.11 shows that the extremum linear model could serve as a lower bound for the design model. Some of the nonlinear plant dynamics, however, are not modeled.

### 7.3 MODEL BASED COMPENSATORS

Model based compensators such as the Linear Quadratic Gaussian control design or an H infinity design with an estimator are very dependent on an accurate model of the plant. An investigation into the effect of plant nonlinearities on the response of a controlled structure using these designs could give some insight into the nature of their robustness to these nonlinearities.

#### Linear Quadratic Gaussian

The Linear Quadratic Gaussian (LQG) compensator is of the form:

$$\begin{aligned}\dot{\underline{z}} &= (\underline{A}_p - \underline{B}\underline{G} - \underline{H}\underline{C})\underline{z} + \underline{H}\underline{y} \\ \underline{u} &= -\underline{G}\underline{z}\end{aligned}\tag{7.24}$$

where  $\underline{A}_p$  is the design or linear plant model. The gain matrices are found using the following formulae:

$$\begin{aligned}0 &= \underline{A}_p^T \underline{P} + \underline{P} \underline{A}_p + \underline{Q} - \underline{P} \underline{B} \underline{B}^T \underline{P} / \rho \\ \underline{G} &= \frac{1}{\rho} \underline{B}^T \underline{P}\end{aligned}\tag{7.25}$$

for the control gains and

$$0 = A_p X + X A_p^T + L L^T - \left(\frac{1}{\mu}\right) X C^T C X$$

$$H = \frac{1}{\mu} X C^T \quad (7.26)$$

for the estimator gains. The factors  $\rho$  and  $\mu$  govern the size of the control gains. The matrices  $L$  and  $B$  are given by equation (7.1). If the compensator is combined with the plant, the equations of motion for a disturbance input are:

$$\dot{\underline{z}} = (A_p - B G - H C) \underline{z} + H C \underline{q}$$

$$\dot{\underline{q}} = -B G \underline{z} + A \underline{q} + L \underline{w} \quad (7.27)$$

If the input disturbance is sinusoidal, the states of the plant and of the compensator are assumed harmonic (the plant equations returned to second order form);

$$\underline{x} = \underline{a} \sin \omega t + \underline{b} \cos \omega t \quad \dim(\underline{x}) = n$$

$$\underline{z} = \underline{c} \sin \omega t + \underline{d} \cos \omega t \quad \dim(\underline{z}) = 2n \quad (7.28)$$

and the equations are written in harmonic balance form:

$$\begin{bmatrix} K_{NL} - \omega^2 M & -\omega C & M(BG)_L & 0 \\ \omega C & K_{NL} - \omega^2 M & 0 & M(BG)_L \\ -(HC)_L & \omega(HC)_R & -A_c & -\omega I \\ -\omega(HC)_R & -(HC)_L & \omega I & -A_c \end{bmatrix} \begin{Bmatrix} \underline{a} \\ \underline{b} \\ \underline{c} \\ \underline{d} \end{Bmatrix} = \begin{Bmatrix} \underline{e} \\ 0 \\ 0 \\ 0 \end{Bmatrix} \quad (7.29)$$

where the matrix  $BG$  has been partitioned so the only the lower non-zero part appears. The  $HC$  matrix also has been partitioned into terms multiplying displacement (subscript  $L$ ) and velocity (subscript  $R$ ).  $A_c$  is the compensator state matrix given by equation (7.24). The subscript  $NL$  only appears on the  $K$  since the nonlinearity investigated here is the gain change which only affects the stiffness.

Figure 7.12 shows the response of the one bay structure with the LQG compensator with  $\rho=0.01$  and  $\mu=0.01$ . The control exerts effort in all directions and the measurement available is the

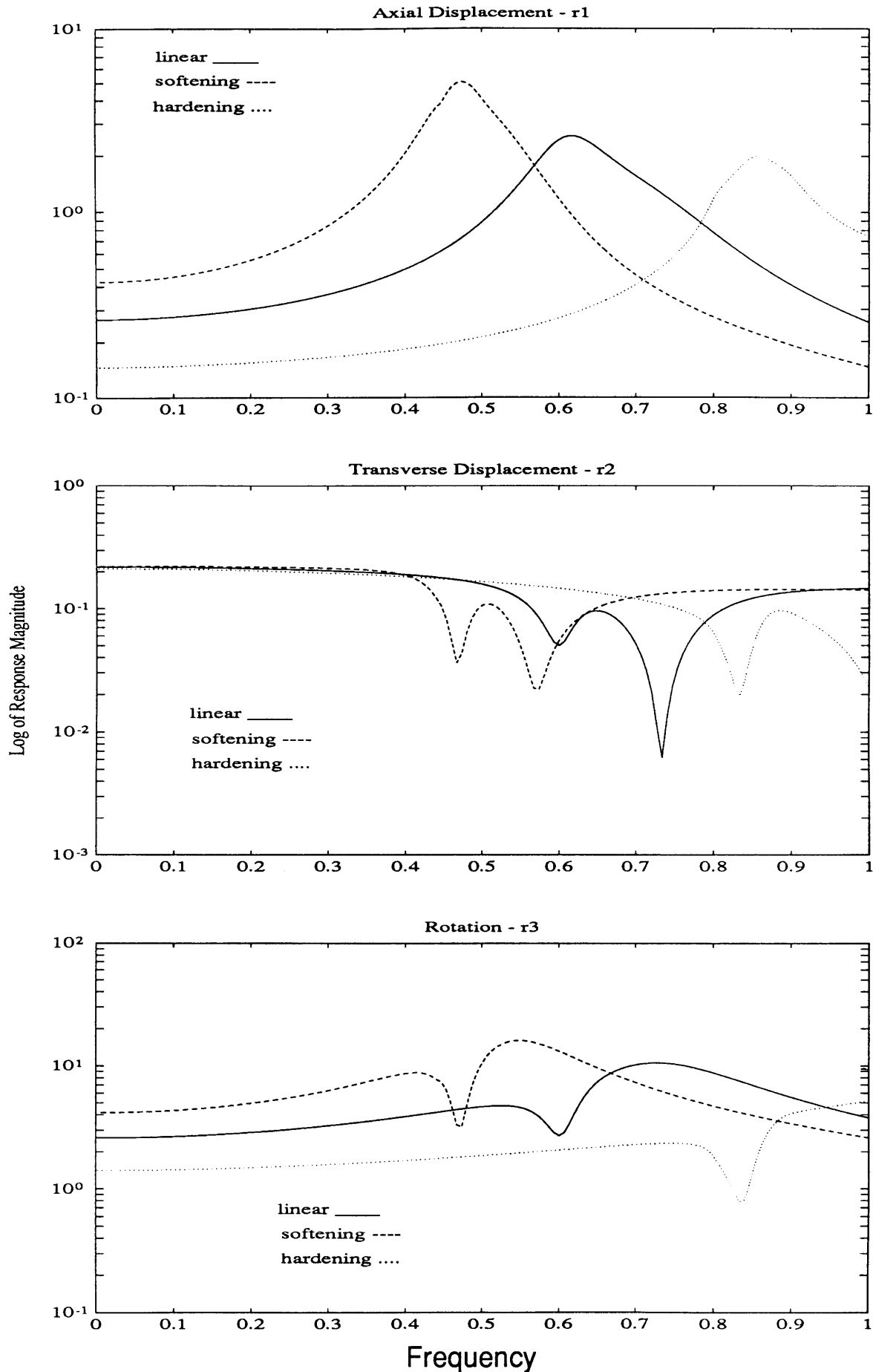


Figure 7.12 Transfer Function from Tip Excitation to Displacements for Structure with Gain Change Joints with LQG Compensator with Full Control Authority,  $\rho=0.01$ ,  $\mu=0.01$

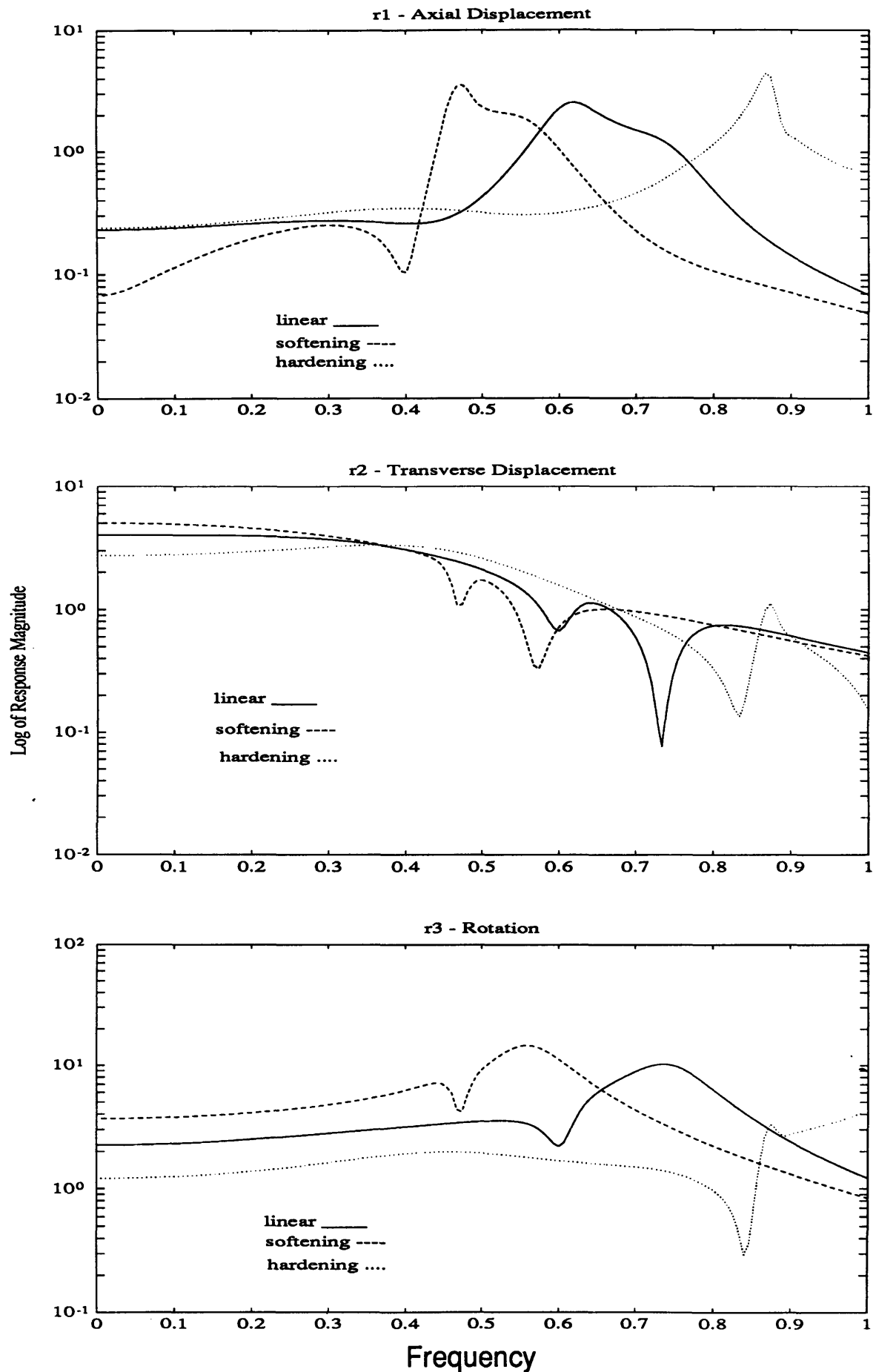


Figure 7.13 Transfer Function from Tip Excitation to Displacements for Structure with Gain Change Joints with LQG Compensator with Full Control Authority,  $\rho=1$ ,  $\mu=1$



displacement in the transverse direction. The figure shows that performance is degraded in the directions other than that of the disturbance for both the softening and hardening spring. The case with  $\rho=1$  and  $\mu=1$  in Figure 7.13 shows degraded disturbance rejection to a somewhat greater extent. The dynamics of the structure are more apparent. However there is not a large improvement in performance between the two designs. Performance in general is far worse than with full state feedback design.

## H Infinity Compensator

The H infinity compensator is based on the following plant model:

$$\begin{Bmatrix} \dot{\underline{q}} \\ \underline{e} \\ \underline{y} \end{Bmatrix} = \begin{bmatrix} A_p & B_1 & B_2 \\ C_1 & 0 & D_{12} \\ C_2 & D_{21} & 0 \end{bmatrix} \begin{Bmatrix} \underline{q} \\ \underline{d} \\ \underline{u} \end{Bmatrix} \quad (7.30)$$

where  $e$  and  $d$  are the error vector of the states and controls and disturbance vector respectively. The disturbance vector includes the disturbance as discussed in previous sections plus a noise in the measurement. The values of the various matrices in the terms of the previous section are:

$$\begin{aligned} B_1 &= [L \quad 0] & B_2 &= B \\ C_1 &= \begin{bmatrix} I \\ 0 \end{bmatrix} & C_2 &= C \\ D_{12} &= \begin{bmatrix} 0 \\ I \end{bmatrix} & D_{21} &= [0 \quad I] \end{aligned} \quad (7.31)$$

The measurement available is the displacement in the transverse direction of the structure. The compensator has the form:

$$\begin{aligned} \dot{\underline{z}} &= (A_p + \gamma^{-2} B_1 B_1^T X_{\text{inf}} + B_2 F_{\text{inf}} + Z_{\text{inf}} L_{\text{inf}} C_2) \underline{z} - Z_{\text{inf}} L_{\text{inf}} \underline{y} \\ \underline{u} &= F_{\text{inf}} \underline{z} \end{aligned} \quad (7.32)$$

where,

$$F_{\text{inf}} = -B_2^T X_{\text{inf}}, \quad L_{\text{inf}} = -Y_{\text{inf}} C_2^T, \quad Z_{\text{inf}} = (I - \gamma^{-2} Y_{\text{inf}} X_{\text{inf}})^{-1} \quad (7.33)$$

and the matrices  $X$  and  $Y$  are obtained from the algebraic Riccati equations:

$$\begin{aligned} 0 &= A_p^T X_{\text{inf}} + X_{\text{inf}} A_p + X_{\text{inf}} (\gamma^{-2} B_1 B_1^T - B_2 B_2^T) X_{\text{inf}} + C_1^T C_1 \\ 0 &= A_p Y_{\text{inf}} + Y_{\text{inf}} A_p^T + Y_{\text{inf}} (\gamma^{-2} C_1^T C_1 - C_2^T C_2) Y_{\text{inf}} + B_1 B_1^T \end{aligned} \quad (7.34)$$

The set of equations is solved by varying the parameter  $\gamma$  until the following conditions are satisfied:

$$Y_{\text{inf}} > 0, \quad X_{\text{inf}} > 0, \quad \text{eig}(X_{\text{inf}} Y_{\text{inf}}) < \gamma^2$$

Once a solution is obtained, the equations of motion including the controller are arranged in harmonic balance form in much the same way as the LQG design was. The harmonic balance equations of motion are:

$$\begin{bmatrix} K_{\text{NL}} - \omega^2 M & -\omega C & -M(BF_{\text{inf}})_L & 0 \\ \omega C & K_{\text{NL}} - \omega^2 M & 0 & -M(BF_{\text{inf}})_L \\ (Z_{\text{inf}} L_{\text{inf}} C_2)_L & -\omega (Z_{\text{inf}} L_{\text{inf}} C_2)_R & -A_{\text{inf}} & -\omega I \\ \omega (Z_{\text{inf}} L_{\text{inf}} C_2)_R & (Z_{\text{inf}} L_{\text{inf}} C_2)_L & \omega I & -A_{\text{inf}} \end{bmatrix} \begin{Bmatrix} \underline{a} \\ \underline{b} \\ \underline{c} \\ \underline{d} \end{Bmatrix} = \begin{Bmatrix} \underline{d} \\ 0 \\ 0 \\ 0 \end{Bmatrix} \quad (7.35)$$

where the matrices are partitioned in the same way as in equation (7.29) and  $A$  is given in equation (7.32)

Figure 7.13 shows the response of the system with the H infinity controller that uses the same plant model used in the LQG design. The solution procedure converged with  $\gamma = 15.65$ . This control design has low gains. The transfer functions show some degradation in the disturbance rejection with both the softening and hardening spring nonlinearities. The choice of the  $C$  and  $D$  matrices implies a relative weighting between the state and control in the error vector. This can be changed by scaling to get higher or lower gain matrices and possibly better performance.

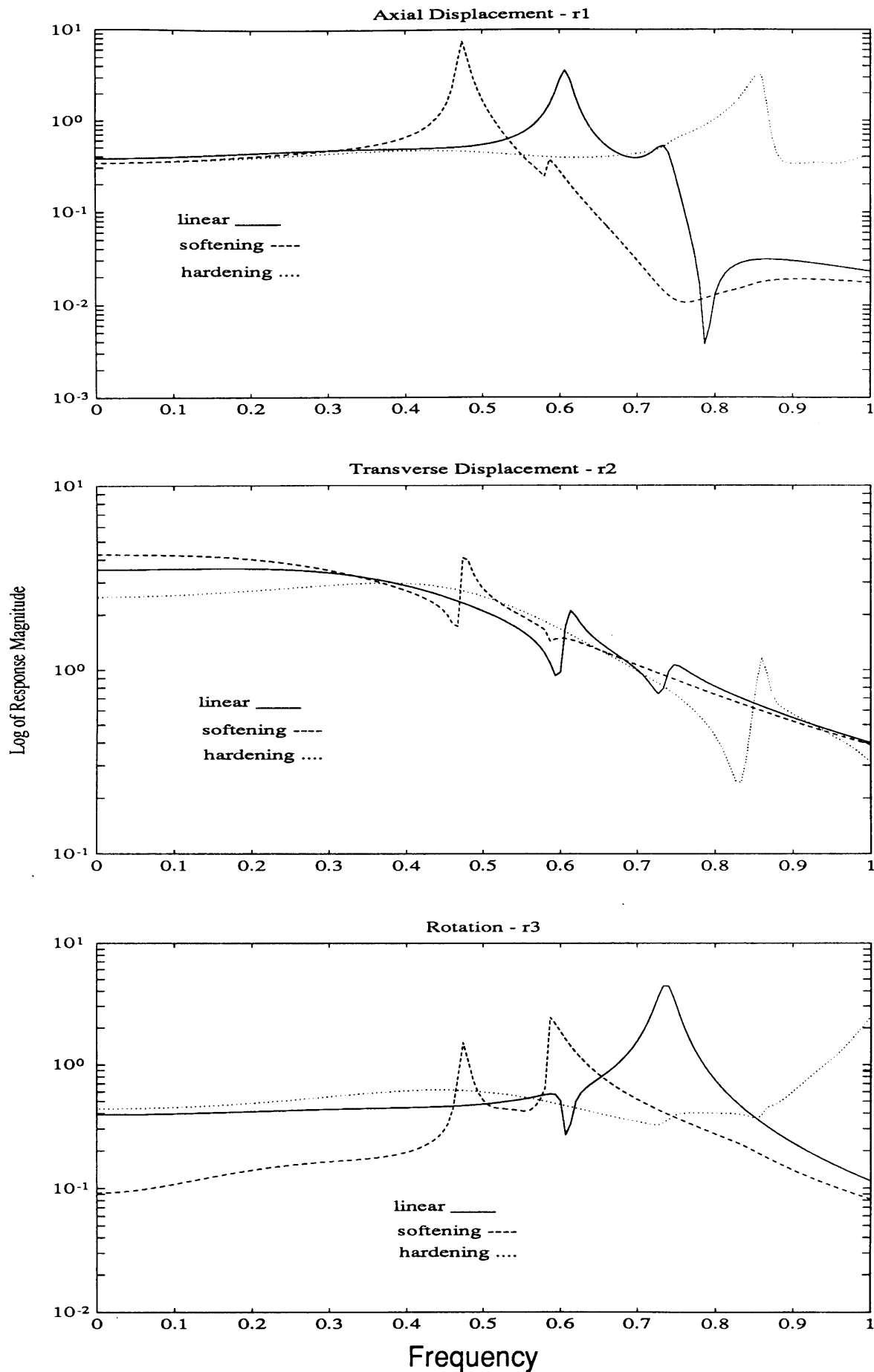


Figure 7.14 Transfer Function from Tip Excitation to Displacements for Structure with Gain Change Joints with H Infinity Compensator with Full Control

## 7.4 LIMIT CYCLES

Equations (7.9), (7.12), (7.29) and (7.35) may be used to determine limit cycles. If the right hand side of these equations is set equal to zero and a certain frequency and non-zero response vector gives a solution to these equations, a limit cycle is present. To find limit cycles, a sine or cosine component of one variable in the response vector element is set equal to zero and the frequency is allowed to vary and the equations solved. The success is very dependent on the initial conditions that are input.

Although there is no guarantee of the absence of limit cycles, none of the controllers discussed above were determined to have a limit cycle. To test the solution procedure, a limit cycle was induced in the structure by the use of an eigenstructure assignment control algorithm with full control and full state feedback with integrators in all channels. The first mode of the structure was lowered in frequency while adding a small amount of damping. This mode is assigned a purely axial shape. The other two modes are moved far to the left of the imaginary axis. The joints in the model were sliding pins. This rather unrealistic eigenstructure assignment led to a high gain controller which did exhibit a limit cycle.

## 7.6 SUMMARY

The effectiveness of the equivalent beam model with a describing function model of structural nonlinearities for analysis of controlled structures is demonstrated. The model is used to analyze full state feedback with and without a robust design and a structure controlled using a model based compensator.

Results from this analysis indicate that for an amplitude dependent nonlinear plant, high control authority will keep the nonlinear model within the small displacement linear range and no problems with performance robustness should arise. This is only useful if stability robustness is preserved with a high gain controller. If, for a LQR design, control authority is limited both in gain or direction, a robust control design does result in improved performance.

Model based compensators do not maintain disturbance rejection properties when

implemented with a nonlinear plant.

## CHAPTER 8

### CONCLUSIONS

#### 8.1 SUMMARY AND CONCLUSIONS

A method of modeling long thin truss structures with nonlinear joints undergoing sinusoidal excitation was developed. The method consists of determining the force-displacement relationship for the total axial displacement across a truss element. These elements include the joints at each end which can have nonlinear properties and damping as well as stiffness. This information is used to determine equivalent linear stiffness and damping terms when there are no nonlinear elements present and equivalent nonlinear stiffness and damping terms when they are. The nonlinear terms are calculated using the describing function quasi-linearization technique. The coefficients depend on amplitude and frequency and are used to construct a nonlinear finite element model of the truss. This model is reduced to a nonlinear equivalent beam finite element model or the linear equivalent beam model if no nonlinearities are present.

Chapter 2 shows that the describing function method of modeling nonlinear elements within a multi-degree of freedom structure compares very well with a time integration analysis of the same structure. This is subject to the inaccuracies inherent in the analytical model of the linear structure but indicates accuracy in the quasi-linearization approach.

Two types of linear equivalent beam models were investigated, a continuous model and an equivalent beam finite element. The accuracy of linear equivalent beam structural dynamic models of a long slender two dimensional truss depend on the ability of the model to mimic the first beam-like modes of the truss. The Bernoulli-Euler continuous beam model does not account for shear or rotary inertia effects that are important in truss bending behavior and gives correspondingly

inaccurate results for first mode frequency when compared with the full truss model from which it was derived. The Timoshenko continuous beam model which does account for these effects gives results that are more accurate. The highest degree of accuracy is obtained from the equivalent beam finite elements models. The two models developed differ in the degrees of freedom that the beam is allowed to have. The model with only transverse displacement (shear) and rotation about the mid-plane (bending) is less accurate than the model that has, in addition to these, axial displacement. This is due to the fact that for a truss, the axial mode is one of the first few modes as opposed for a solid beam. The equivalent beam procedures are based on an axial element model and do not model the local bending modes of the truss members. For a two-dimensional five bay truss, the first local diagonal mode can occur as low as the second mode. However for the three dimensional Mini-Mast, the first local diagonal mode occurs after the 5th beam-like mode.

The nonlinear equivalent beam finite element model was used to investigate the behavior of one and five bay 2-D trusses with various types of nonlinear joints. These include a cubic spring, both hardening and softening gain change, sliding pin, a sliding gain change, and a joint that was designed to give a certain global characteristic nonlinear response that was observed in the experimental response of the Mini-Mast. These results show the classic characteristics of nonlinear response (jump phenomena, nonproportional increase in response with increase in force, multiple solutions, change in resonant frequencies and damping with change in amplitude and frequency of excitation). These results established the efficacy of the procedure and the describing functions used to model the nonlinear joints. These models also determined the particular global response characteristics that the various nonlinear joints produce in the structure.

The nonlinear equivalent beam finite element model was also used to model the change in behavior between a structure with nonlinear joints under stationary gravitational loading (pre-loaded joints) and a micro-gravity environment (no pre-load) through the use of the dual input describing function. The structure that was investigated is the same five bay structure that was analyzed with the single input describing function. Comparing the two models shows that the differences can be significant for certain large pre-loads but for smaller pre-loads the difference can

be small. The asymptotic frequency which the models approach at large amplitudes remains the same.

The model of the Mini-Mast that was built using the techniques developed in this thesis matched the lower linear beam-like modal frequencies very well when compared with experimentally determined modes and the NASA/Langley finite element model modes. This is particularly true for the first bending modes and the first torsion modes. The second bending modes are not as accurate. The axial and second torsion modes that occur after the first local diagonal mode are switched for both the full axial element truss model and the equivalent beam reduction. This would indicate that some local motion is involved with one or both of these modes that the two models cannot simulate.

The nonlinear model of the truss 'natural' joints developed in Chapter 4 gives the response that most closely matches the experimental data obtained in sine sweep excitations of the Mini-Mast. This nonlinear element contains hysteretic behavior with a softening characteristic. A possible physical explanation for this characteristic is pre-buckling behavior in the diagonal elements.

The nonlinear equivalent beam model was then used to model a controlled structure. The amplitude dependent structural properties from the equivalent model were used to set bounds on the parameter variations of the structure. These bounds were used to design a robust control system for the nonlinear structure. The algorithm to determine the feedback gains had a solution for small values of  $\delta$ , the measure of the maximum parameter variation. The controller that results from this robust design gives a significant of disturbance rejection improvement for the nonlinear plant as compared to the nonlinear plant with the non-robust control design.

The modeling procedure also is effective in modeling the dynamics of controlled structures with model-based compensators.



## **8.2 RECOMMENDATIONS FOR FUTURE WORK**

Future work in determining the response of nonlinear structures could include several investigations that build on the present work:

- More complex finite element models that can model local bending modes while retaining the describing function coefficients to model the axial nonlinear force displacement relation.
- Obtaining an actual Mini-Mast truss element and testing it to determine nonlinear characteristic. This data could be used to calculate the DF coefficients numerically for input into the Mini-Mast nonlinear model.
- Further investigation into the use of the Dual-Input Describing Function and Single-Input Describing Function to model structures in earth gravity and micro-gravity, with experimental verification from on-orbit and ground testing.
- Investigate the possibility of using the information inherent in the describing function methodology to design controlled structures that are robust to nonlinearities in the plant.

## Bibliography

1. Belvin, K. W., "Vibration of Joints for the Dynamic Analysis of Truss Structures", M. S. Thesis, School of Engineering and Applied Science, George Washington University, December 1985.
2. Ludwigsen, J. S., "An Assessment of the Effects of Nonlinear Behavior on the Dynamic Performance of Large Orbiting Space Structures," PhD. Thesis, Dept. of Civil Engineering, MIT, Sept. 1987.
3. Sarver, G. L., "Energy Transfer and Dissipation in Structures with Discrete Nonlinearities," PhD. Thesis, Dept. of Aeronautics and Astronautics, MIT, November 1987.
4. Bowden, M. L., "Dynamics of Space Structures With Nonlinear Joints," Ph.D thesis, Dept. Aeronautics and Astronautics, MIT, May 1988.
5. van Schoor, M. C. "The Coupled Nonlinear Dynamics of Spacecraft with Fluids in Tanks of Arbitrary Geometry", PhD. Thesis, Dept. of Aeronautics and Astronautics, MIT, March 1989.
6. Mercadal, M., "Joint Nonlinearity Effects in the Design of a Flexible Truss Structure Control System," Master's thesis, Dept. of Aeronautics and Astronautics, MIT, December 1986.
7. Noor, A. K., Anderson, M. S., and Greene, W. H., "Continuum Models for Beam- and Platelike Lattice Structures," *AIAA Journal*, Vol. 16, No. 12, December 1978, pp. 1219-1228.
8. Barton, O., Anderson, M. S., and Reiss, R., "A Simple Method to Model Truss-Beams as Equivalent Continua," Proceedings of the 20th Midwestern Mechanics Conference, Sept. 1987.
9. Noor, A. K., and Nemeth, M. P., "Micropolar Beam Models for Lattice Grids with Rigid Joints," *Computer Methods in Applied Mechanics and Engineering* 21, 1980, pp.249-263.

10. Noor, A. K., and Nemeth, M. P., "Analysis of Spatial Beamlike Lattices with Rigid Joints," *Computer Methods in Applied Mechanics and Engineering* 24, 1980, pp. 35-59.
11. Mills, R. A., "Natural Vibrations of Beam-Like Trusses," Master's thesis, Aeronautics and Astronautics, Massachusetts Institute of Technology, June 1985.
12. Thomas, S., and Stubbs, N., "Dynamic analysis of the Space Station Truss Structure Based on a Continuum Representation," AIAA paper 89-1280, presented at the 30th Structures, Structural Dynamics and Materials Conference, April, 1989.
13. Stubbs, N. and Fluss, H., "Continuum Modeling of Discrete Structures," Recent Advances in Engineering Mechanics, Vol 1, Editors W. F. Chen, and A. Lewis, ASCE, 1983, pp. 475-478.
14. Gelb, A. and Vander Velde, W. E., Multiple-Input Describing Functions and Nonlinear System Design, McGraw-Hill, 1968.
15. Chapman, J. M., "Nonlinear Modeling of Joint Dominated Structures," Year End Report, CSI-GI Contract, NASA-Langley Research Center, January 1990.
16. Taylor, Jr., L. W., "Nonlinear and Distributed Parameter Models of the Mini-Mast Truss," Third NASA/DOD Controls-Structures Interaction Technology Conference, January 1989.
17. Pappa, R., Miserentino, B., Bailey, J., Elliott, K., Perez, S., Cooper, P., and Williams, B., Sulla, J., Ghosh, D., Montgomery, R., "Mini-Mast CSI Testbed User's Guide," NASA Langley Research Center, March 1989.
18. Huang, T. C., "The Effect of Rotatory Inertia and of Shear Deformation on the Frequency and Normal Mode Equations of Uniform Beams With Simple End Conditions", *Journal of Applied Mechanics*, December 1961, pp. 579-584.
19. Spangler, R., "Two-Dimensional Optical Interferometer Sample Problem", MIT Space Engineering Research Center Report 11-90-I.
20. Blevins, R. D., Formulas for Natural Frequency and Mode Shape, Krieger, 1979.

21. Schenk, A. and Pappa, R. S., "Modal Identification of a Deployable Space Truss," NASA TM 102720, Langley Research Center, September 1990.
22. Lee, R. Y., "Assessment of Linear and Nonlinear Joint Effects on Space Truss Booms," Master's thesis, Dept. of Aeronautics and Astronautics, MIT, June 1985.
23. Press, W. H., Flannery, B. P., Teukolsky, S. A., and Vetterling, W. T., Numerical Recipes - The Art of Scientific Computing, Cambridge University Press, 1986.
24. Webster, M., and Vander Velde, W., "Modelling Beam-Like Space Trusses with Nonlinear Joints," Proceedings of the 32nd AIAA Structures, Dynamics and Materials Conference, April 1991, Baltimore, MD. Vol. 4, pp. 2744-2753.
25. Webster, M., and Vander Velde, W., "Application of Robust Linear Control Design to a Truss Structure With Nonlinear Joints," to be given at 1991 AIAA Guidance, Navigation and Control Conference, August, 1991, New Orleans, La.
26. Doyle, J. C., Glover, K., Khargonekar, P., Francis, B. A., "State-Space Solution to Standard  $H_2$  and  $H_\infty$  Control Problems," *IEEE Transactions on Automatica Control*, Vol. 34, No. 8, August 1989, pp. 831-846.
27. Peterson, I. R., and Hollot, C. V., "A Riccati Equation Approach to the Stabilization of Uncertain Linear Systems," *Automatica*, Vol. 22, No. 4, April 1986, pp. 397-411.
28. Bernstein, D. S., "Robust Static and Dynamic Output-Feedback Stabilization: Deterministic and Stochastic Perspectives," *IEEE Transactions on Automatic Control*, Vol. AC-32, No. 12, December 1987, pp. 1076-1084.

## Appendix A

### Single and Dual Input Describing Function Formulas Used in This Thesis

These formulas use the following functions:

$$f(\lambda) = -1 \quad \lambda < -1$$

$$f(\lambda) = \frac{2}{\pi} \left( \sin^{-1} \lambda + \lambda \sqrt{1 - \lambda^2} \right) \quad |\lambda| \leq 1$$

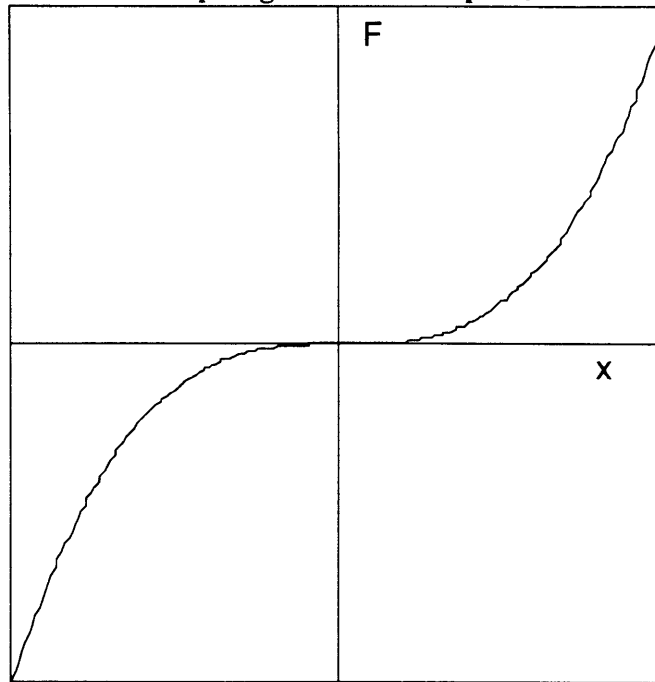
$$f(\lambda) = 1 \quad \lambda > 1$$

and

$$g(\lambda) = \frac{2}{\pi} \left( \lambda \sin^{-1} \lambda + \sqrt{1 - \lambda^2} \right) \quad |\lambda| \leq 1$$

$$g(\lambda) = |\lambda| \quad |\lambda| > 1$$

### Cubic Spring SIDF - Simple Joint



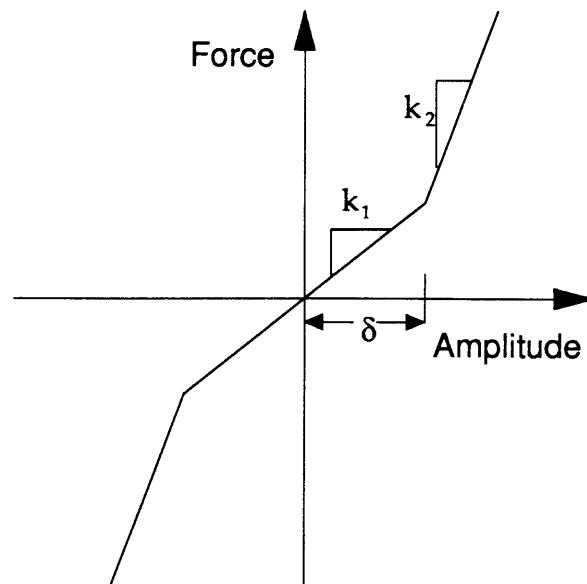
$$F = k_3 x^3$$

$$x = A \sin \omega t$$

$$c_p = \frac{3}{4} k_3 A$$

$$c_q = 0$$

### Gain Change Simple Joint



$$\text{if amp} = 2q(4) < \delta, \text{ then } \underline{F}_J = \begin{Bmatrix} 0 \\ 0 \\ 0 \\ 4k_1q(4) \end{Bmatrix},$$

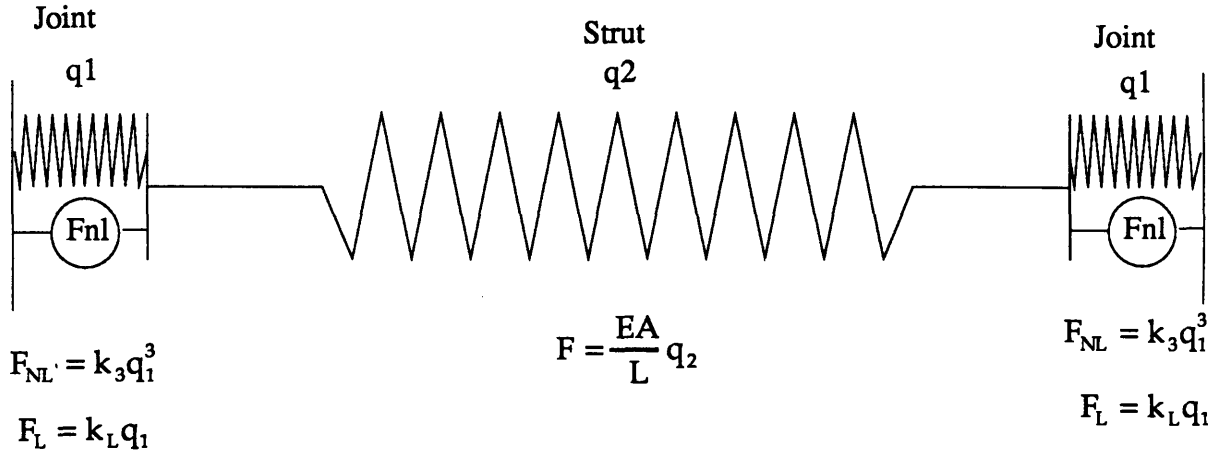
$$\text{if amp} > \delta, \text{ then } \underline{F}_J = \begin{Bmatrix} 0 \\ 0 \\ 0 \\ 2k_2 \left[ \text{amp} - 2\delta \left( 1 - \frac{k_1}{k_2} \right) \right] \end{Bmatrix}$$

$$x = A \sin \omega t$$

$$c_p = (k_1 - k_2) f \left( \frac{\delta}{A} \right) + k_2$$

$$c_q = 0$$

### Truss Element with Cubic Spring in Parallel with Linear Spring Joints



$$B_1 = \left( \frac{EA}{k_3 L} \right)^{\frac{1}{3}} \left( \frac{q}{2} + \sqrt{\frac{q^2}{4} + \left( \frac{EA}{27 k_3 L} \right) \left( \frac{k_L L}{EA} + 2 \right)^2} \right)^{\frac{1}{3}}$$

$$B_2 = \left( \frac{EA}{k_3 L} \right)^{\frac{1}{3}} \left( \frac{q}{2} - \sqrt{\frac{q^2}{4} + \left( \frac{EA}{27 k_3 L} \right) \left( \frac{k_L L}{EA} + 2 \right)^2} \right)^{\frac{1}{3}}$$

$$c_p = \frac{2}{\pi A} \int_0^{\pi} \left( k_L (B_1 + B_2) + k_3 (B_1 + B_2)^3 \right) \sin \phi \, d\phi$$

$$c_q = 0$$

### Truss Element with Gain Change Joints

$$\text{If } |q| \leq \delta, \quad k_{eq1} = \frac{1}{2 \frac{EA}{k_1 L} + 1}$$

$$\text{If } |q| > \delta, \quad k_{eq2} = \frac{1}{2 \frac{EA}{k_2 L} + 1}$$

$$q = A \sin \omega t$$

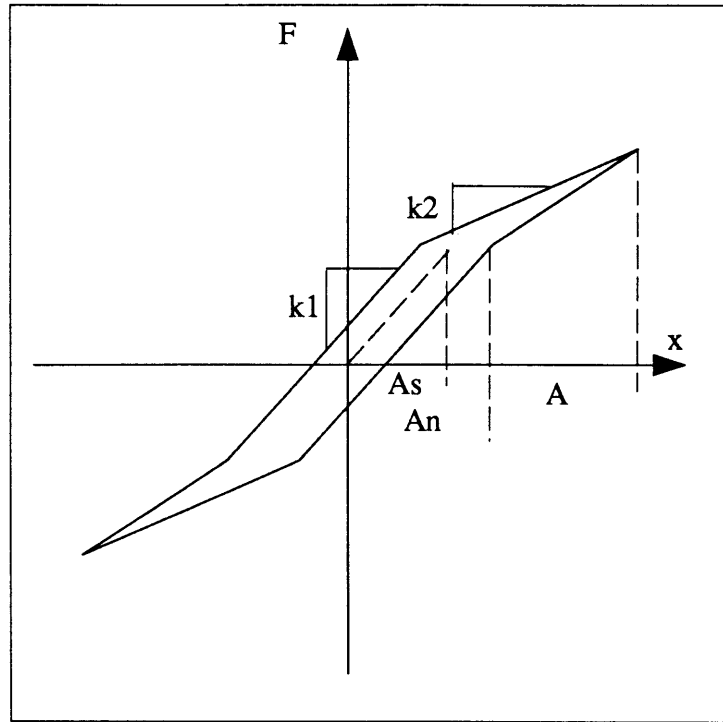
$$c_p = (k_{eq1} - k_{eq2}) f\left(\frac{\delta}{A}\right) + k_{eq2}$$

$$c_q = 0$$

$$\delta = \text{Twice } \delta \text{ of joint}$$



### Truss Element with Natural Joint



$$A_n = A_s + (A - A_s) a_n$$

$$k_3 = \left( \frac{1 + a_n}{1 - a_n} \right) k_2$$

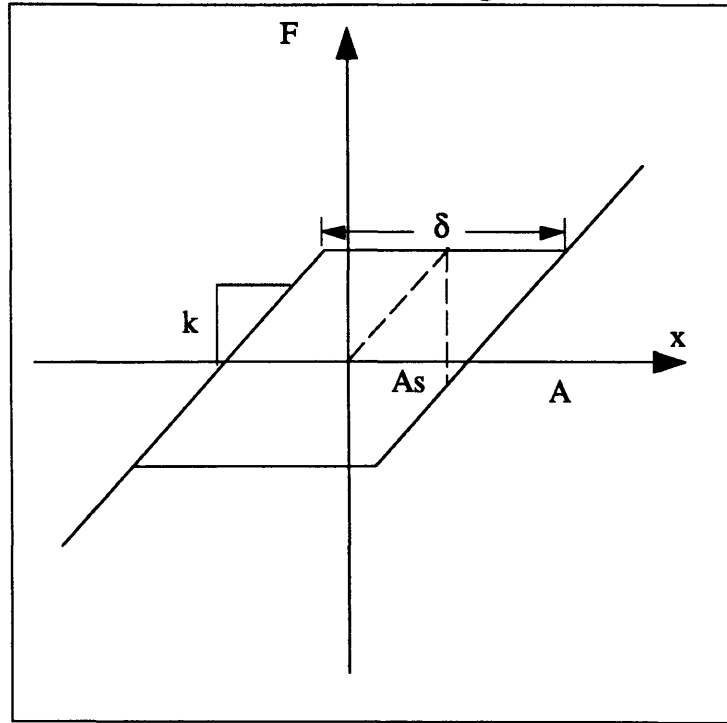
$$b_1 = \frac{A_s - (A - A_s) a_n}{A}$$

$$b_2 = \frac{A_s + (A - A_s) a_n}{A}$$

$$c_p = \frac{1}{2} \left\{ (k_1 - k_2) f(b_1) + (k_3 - k_1) f(b_2) + k_1 + \frac{k_2}{2} - \frac{k_3}{2} \right\}$$

$$c_q = \frac{2}{\omega \pi} \left\{ \frac{1}{2} (k_2 - k_1) b_1^2 + \frac{1}{2} (k_1 - k_3) b_2^2 + (k_2 - k_3) \left( \frac{1}{2} - \frac{A_s}{A} \right) + (k_2 + k_3) \left( 1 - \frac{A_s}{A} \right) a_n \right\}$$

### Truss Element with Sliding Pin Joints



if  $A < A_s$ ,

$$c_p = k$$

$$c_q = 0$$

if  $A_s < A < \delta$ ,

$$c_p = \frac{k}{2} \left[ 1 + f \left( \frac{2A_s - A}{A} \right) \right]$$

$$c_q = \frac{4k}{\omega\pi} \left( \frac{A_s}{A} \right) \left( 1 - \frac{A_s}{A} \right)$$

if  $A > \delta$ ,

$$b_1 = \frac{A_s - \frac{\delta}{2}}{A}, \quad b_2 = \frac{A_s - \frac{\delta}{2}}{A}$$

$$c_p = \frac{k}{2} [2 - f(b_2) + f(b_1)]$$

$$c_q = \frac{2k\delta A_s}{\omega\pi A^2}$$

**Truss Element with Gain Change Joint**  
**Dual Input Describing Function**

(see above figure)

$$x = B + A \sin \omega t$$

$$b_1 = \frac{\delta + B}{A}, \quad b_2 = \frac{\delta - B}{A}$$

$$N_B = \frac{A}{2B}(k_1 - k_2)[g(b_1) - g(b_2)] + k_2$$

$$c_p = \frac{1}{2}(k_1 - k_2)[f(b_1) + f(b_2)] + k_2$$

$$c_q = 0$$

**Truss Element with Natural Joint**  
**Dual Input Describing Function**

(see above figure)

$$k_4 = \left( \frac{1 + a_n}{1 - a_n} \right) k_2$$

$$A_B = \left( \frac{A - B - A_s}{A} \right) a_n$$

$$k_3 = \left( \frac{A + B + A_B - A_s}{A + B - A_B - A_s} \right) k_2$$

$$b_1 = \frac{A_s - B - A_B}{A}, \quad b_2 = \frac{A_B + A_s - B}{A}, \quad b_3 = \frac{A_s + B - A_B}{A}, \quad b_4 = \frac{A_B + A_s + B}{A}$$

$$N_B = \frac{A}{4B} \left\{ (k_2 - k_1)g(b_1) + (k_3 - k_1)g(b_2) + (k_1 - k_2)g(b_3) + (k_1 - k_4)g(b_4) - k_3 b_2 + k_4 b_4 \right\} + \frac{k_2}{2}$$

$$c_p = \frac{1}{4} \left\{ (k_1 - k_2)f(b_1) + (k_1 - k_3)f(b_2) + (k_1 - k_2)f(b_3) + (k_1 - k_4)f(b_4) + k_3 + k_4 \right\} + \frac{k_2}{2}$$

$$c_q = \frac{1}{\omega\pi} \left\{ \begin{array}{l} (k_2 - k_1) \frac{b_1^2}{2} + (k_1 - k_3) \frac{b_2^2}{2} + (k_2 - k_1) \frac{b_3^2}{2} + (k_1 - k_4) \frac{b_4^2}{2} - \\ k_2 b_1 + k_3 b_2 - k_2 b_3 + k_4 b_4 + \frac{1}{2}(2k_2 - k_3 - k_4) \end{array} \right\}$$

## **Appendix B**

This appendix contains some sample program listings. These programs determine the nonlinear response of the Mini-Mast model with natural joints. The programs listed are:

MASC - Data generation program, generates mass and damping matrices for input to main program.

MMRESPS - Main program, calls other subroutines, enters data, calls Linpack routines, calculates solution.

STFDMPS - Calculates nonlinear stiffness and damping matrices from amplitude vector and frequency, uses output from NATDF.

JCOBDS - calculates the Jacobian numerically using the backwards difference formula, calls STFDMPS

NATDF - Determines the values of the describing functions for each truss bay

```

C*****
C*   Program masc.f
C*   Calculates mass matrix and damping matrix for 1.0% damping
C*   for the Mini-Mast equivalent beam nonlinear finite element
C*   model.
C*
C*   Created 11 June 1990
C*
C*   Mark Webster
C*
C*****
      implicit real*8 (a-h,o-z)
      integer i,j,ij,ji
      integer ipvt(108),info,job
      real*8 me1(12,12),me2(12,12),ke1(12,12),ke2(12,12)
      real*8 m(108,108),k(108,108),mt(18,18),kt(18,18)
      real*8 fv1(108),fv2(108),k1,k2,k3,mdl(108,10)
      real*8 w(108),z(108,108),work(108),zt(108)
      real*8 det(2),temp,mp(108,108),mst(10)
      real*8 zeta,c(108,108),cd1(10,108)
C* Input Sine and Cosine of Diagonals
      so=0.734832d0
      co=0.678223d0
C* Mass per unit length of Truss Elements
      x1=0.492926d0
      x2=0.454952d0
      x3=0.6708010d0
      to=so/co
      so2=so**2
      co2=co**2
      tsqr=3.0d0**(0.5d0)
      t=tsqr
C* Stiffness of Longerons and Diagonals
      k2=1.61898d7*1.033d0
      k3=6.054573d6*1.033d0
      d=1.2124d0
      zeta=.01d0
C*input element mass matrix
      do 10 i=1,12
      do 10 j=1,12
         ke1(i,j)=0.0d0
         ke2(i,j)=0.0d0
         me1(i,j)=0.0d0
10      me2(i,j)=0.0d0
      me1(1,1)=3.0d0*x1+1.5d0*x2+x3*(1.25d0+0.25d0*co2)
      me1(1,4)=d*so*co*x3/(-8.0d0*t)
      me1(1,5)=d*so*co*x3/(-8.0d0)
      me1(1,7)=x3*so2/4.0d0
      me1(1,10)=d*x3*co*so/(8.0d0*t)
      me1(1,11)=d*x3*co*so/(-8.0d0)
      me1(2,2)=3.0d0*x1+1.5d0*x2+x3*(1.25d0+0.25d0*co2)
      me1(2,4)=d*x3*co*so/(8.0d0)
      me1(2,5)=t*d*x3*co*so/(-24.0d0)
      me1(2,8)=x3*so2/4.0d0
      me1(2,10)=d*x3*co*so/(8.0d0)
      me1(2,11)=t*d*x3*co*so/(24.0d0)
      me1(3,3)=3.0d0*x1+x2+x3*(1.0d0+so2/2.0d0)
      me1(3,6)=d*x3*co*so/(4.0d0*t)
      me1(3,9)=(x2+x3*co2)/2.0d0
      me1(3,12)=d*x3*co*so/(-4.0d0*t)
      me1(4,4)=d**2*(x1*6.0d0+2.0d0*x2+x3*(2.0d0+so2))/12.0d0
      me1(4,7)=d*x3*co*so/(8.0d0*t)
      me1(4,8)=d*x3*co*so/(-8.0d0)
      me1(4,10)=d**2*(-2.0d0*x2+x3*co2)/(-24.0d0)
      me1(4,11)=x3*co2*d**2/(-8.0d0*t)
      me1(5,5)=d**2*(x1*6.0d0+2.0d0*x2+x3*(2.0d0+so2))/12.0d0

```

```

me1(5,7)=d*x3*co*so/(8.0d0)
me1(5,8)=t*d*x3*co*so/(24.0d0)
me1(5,10)=x3*co2*d**2/(8.0d0*t)
me1(5,11)=d**2*(-2.0d0*x2+x3*co2)/(-24.0d0)
me1(6,6)=d**2*(x1+x2/2.0d0+x3*(0.458333d0+co2/24.0d0))
me1(6,9)=d*x3*co*so/(-4.0d0*t)
me1(6,12)=d**2*x3*so2/24.0d0
me1(7,7)=3.0d0*x1+1.5d0*x2+x3*(1.25d0+0.25d0*co2)
me1(7,10)=d*so*co*x3/(-8.0d0*t)
me1(7,11)=d*so*co*x3/(8.0d0)
me1(8,8)=3.0d0*x1+1.5d0*x2+x3*(1.25d0+0.25d0*co2)
me1(8,10)=d*so*co*x3/(-8.0d0)
me1(8,11)=t*d*x3*co*so/(-24.0d0)
me1(9,9)=3.0d0*x1+x2+x3*(1.0d0+so2/2.0d0)
me1(9,12)=d*x3*co*so/(4.0d0*t)
me1(10,10)=d**2*(x1*6.0d0+2.0d0*x2+x3*(2+so2))/12.0d0
me1(11,11)=d**2*(x1*6.0d0+2.0d0*x2+x3*(2+so2))/12.0d0
me1(12,12)=d**2*(x1+x2/2.0d0+x3*(0.458333d0+co2/24.0d0))
do 20 i=1,12
do 20 j=1,12
20     me2(i,j)=me1(i,j)
c* Bay 2 changes
me2(1,4)=-1.0d0*me1(1,4)
me2(1,10)=-1.0d0*me1(1,10)
me2(2,5)=-1.0d0*me1(2,5)
me2(2,11)=-1.0d0*me1(2,11)
me2(3,6)=-1.0d0*me1(3,6)
me2(3,12)=-1.0d0*me1(3,12)
me2(4,7)=-1.0d0*me1(4,7)
me2(4,11)=-1.0d0*me1(4,11)
me2(5,8)=-1.0d0*me1(5,8)
me2(5,10)=-1.0d0*me1(5,10)
me2(5,12)=-1.0d0*me1(5,12)
me2(6,9)=-1.0d0*me1(6,9)
me2(7,10)=-1.0d0*me1(7,10)
me2(8,11)=-1.0d0*me1(8,11)
me2(9,12)=-1.0d0*me1(9,12)
do 30 i=2,12
do 30 j=1,i-1
30     me2(i,j)=me2(j,i)
30     me1(i,j)=me1(j,i)
c* Input Element Stiffness Matrix
kel(1,1)=3.0d0*k3*so2/2.0d0
kel(1,4)=3.0d0*d*k3*co*so/(4.0d0*tsqr)
kel(1,5)=3.0d0*d*k3*co*so/4.0d0
kel(1,7)=-3.0d0*k3*so2/2.0d0
kel(1,10)=-3.0d0*d*k3*co*so/(4.0d0*tsqr)
kel(1,11)=3.0d0*d*k3*co*so/4.0d0
kel(2,2)=3.0d0*k3*so2/2.0d0
kel(2,4)=-3.0d0*d*k3*co*so/4.0d0
kel(2,5)=t*d*k3*co*so/(4.0d0)
kel(2,8)=-3.0d0*k3*so2/2.0d0
kel(2,10)=-3.0d0*d*k3*co*so/4.0d0
kel(2,11)=t*d*k3*co*so/(-4.0d0)
kel(3,3)=3.0d0*(k2+k3*co2)
kel(3,6)=-3.0d0*d*k3*co*so/(2.0d0*tsqr)
kel(3,9)=-3.0d0*(k2+k3*co2)
kel(3,12)=3.0d0*d*k3*co*so/(2.0d0*tsqr)
kel(4,4)=d**2*(k2+k3*co2)/2.0d0
kel(4,7)=-3.0d0*d*k3*co*so/(4.0d0*tsqr)
kel(4,8)=3.0d0*d*k3*co*so/4.0d0
kel(4,10)=d**2*(-2.0d0*k2+k3*co2)/4.0d0
kel(4,11)=3.0d0*d**2*k3*co2/(4.0d0*t)
kel(5,5)=d**2*(k2+k3*co2)/2.0d0
kel(5,7)=-3.0d0*d*k3*co*so/4.0d0
kel(5,8)=t*d*k3*co*so/(-4.0d0)

```

```

kel(5,10)=-3.0d0*d**2*k3*co2/(4.0d0*t)
kel(5,11)=d**2*(-2.0d0*k2+k3*co2)/4.0d0
kel(6,6)=d**2*k3*so2/4.0d0
kel(6,9)=3.0d0*d*k3*co*so/(2.0d0*t)
kel(6,12)=d**2*k3*so2/(-4.0d0)
kel(7,7)=3.0d0*k3*so2/2.0d0
kel(7,10)=3.0d0*d*k3*co*so/(4.0d0*t)
kel(7,11)=-3.0d0*d*k3*co*so/4.0d0
kel(8,8)=3.0d0*k3*so2/2.0d0
kel(8,10)=3.0d0*d*k3*co*so/4.0d0
kel(8,11)=t*d*k3*co*so/4.0d0
kel(9,9)=3.0d0*(k2+k3*co2)
kel(9,12)=-3.0d0*d*k3*co*so/(2.0d0*t)
kel(10,10)=d**2*(k2+k3*co2)/2.0d0
kel(11,11)=d**2*(k2+k3*co2)/2.0d0
kel(12,12)=d**2*k3*so2/4.0d0
do 40 i=1,12
do 40 j=1,12
40     ke2(i,j)=kel(i,j)
c* Bay 2 changes
ke2(1,4)=-1.0d0*kel(1,4)
ke2(1,10)=-1.0d0*kel(1,10)
ke2(2,5)=-1.0d0*kel(2,5)
ke2(2,11)=-1.0d0*kel(2,11)
ke2(3,6)=-1.0d0*kel(3,6)
ke2(3,12)=-1.0d0*kel(3,12)
ke2(4,7)=-1.0d0*kel(4,7)
ke2(4,11)=-1.0d0*kel(4,11)
ke2(5,8)=-1.0d0*kel(5,8)
ke2(5,10)=-1.0d0*kel(5,10)
ke2(6,9)=-1.0d0*kel(6,9)
ke2(7,10)=-1.0d0*kel(7,10)
ke2(8,11)=-1.0d0*kel(8,11)
ke2(9,12)=-1.0d0*kel(9,12)
ick=1
open (unit=8,file='masc.d',access='sequential')
do 50 i=2,12
do 50 j=1,i-1
50     kel(i,j)=kel(j,i)
50     ke2(i,j)=ke2(j,i)
c*construct complete mass and stiffness matrices
do 60 i=1,108
do 60 j=1,108
mp(i,j)=0.0d0
mst(i)=0.0d0
c(i,j)=0.0d0
k(i,j)=0.0d0
60     m(i,j)=0.0d0
do 63 i=1,6
do 63 j=1,6
k(i,j)=kel(i+6,j+6)
63     m(i,j)=me1(i+6,j+6)
do 65 i=1,12
do 65 j=1,12
k(i,j)=k(i,j)+ke2(i,j)
65     m(i,j)=m(i,j)+me2(i,j)
do 67 i=1,18
do 67 j=1,18
kt(i,j)=0.0d0
67     mt(i,j)=0.0d0
do 70 i=1,12
do 70 j=1,12
kt(i,j)=kel(i,j)
70     mt(i,j)=me1(i,j)
do 75 i=7,18
do 75 j=7,18

```

```

      kt(i,j)=kt(i,j)+ke2(i-6,j-6)
75      mt(i,j)=mt(i,j)+me2(i-6,j-6)
      ik=6
      do 85 ij=1,8
      do 80 i=1,18
      do 80 j=1,18
      m(ik+i,ik+j)=m(ik+i,ik+j)+mt(i,j)
      k(ik+i,ik+j)=k(ik+i,ik+j)+kt(i,j)
80      continue
      ik=ik+12
85      continue
c*input tip and bay 10 plate masses and moments of inertia
      m(55,55)=m(55,55)+41.042d0
      m(56,56)=m(56,56)+41.042d0
      m(57,57)=m(57,57)+41.042d0
      m(58,58)=m(58,58)+4.93d0
      m(59,59)=m(59,59)+4.93d0
      m(60,60)=m(60,60)+9.84d0
      m(103,103)=m(103,103)+129.525d0
      m(104,104)=m(104,104)+129.525d0
      m(105,105)=m(105,105)+129.525d0
      m(106,106)=m(106,106)+39.48d0
      m(107,107)=m(107,107)+45.539d0
      m(108,108)=m(108,108)+58.93d0
c* write mass matrix
      write(8,101)' m'
      do 90 i=1,108
90      write(8,104)(m(i,j),j=1,108)
      do 95 ij=1,108
      do 95 ji=1,108
      mp(ij,ji)=m(ij,ji)
95      continue
c* write stiffness matrix
      write(8,101)' k matrix'
      do 150 i=1,108
150      write(8,104)(k(i,j),j=1,108)
      i11 = 108
      i22 = 1
c* calculate eigenvalues
      write(6,*)'Just before rsg'
      call rsg(i11,i11,k,m,w,i22,z,fv1,fv2,ierr)
      write(6,*)'Just after rsg'
      write(6,104)(w(j),j=1,10)
      write(8,101)' mode'
      write(8,104)(z(i,3),i=1,108)
c* Calculate discrete damping matrix that gives 1 percent
c* damping in first 10 modes
      do 130 ij=1,108
      do 130 ji=1,10
      mdl(ij,ji)=0.0d0
      do 130 i=1,108
      mdl(ij,ji)=mdl(ij,ji)+mp(ij,i)*z(i,ji)
130      continue
      do 132 ij=1,10
      mst(ij)=0.0d0
      do 132 i=1,108
      mst(ij)=mst(ij)+mdl(i,ij)*z(i,ij)
132      continue
      do 134 i=1,10
134      mst(i)=mst(i)*2.0d0*zeta*w(i)**(.5d0)
c* invert eigenvectors
      call dgeco(z,108,108,ipvt,rcond,zt)
      job=11
      call dgedi(z,108,108,ipvt,det,work,job)
      do 136 i=1,10
      do 136 j=1,108

```



```
136      cdl(i,j)=mst(i)*z(i,j)
      do 138 ij=1,108
      do 138 ji=1,108
      c(ij,ji)=0.0d0
      do 138 i=1,10
138      c(ij,ji)=c(ij,ji)+cdl(i,ji)*z(i,ij)
c* write damping matrix
      write(8,101)' c matrix'
      do 140 i=1,108
140      write (8,104) (c(i,j),j=1,108)
104 format (6(1x,g12.6))
101 format (a20)
      stop
      end
```

```

*****
c*   Program mmresps2.f
c*   This program calculates the response of the Mini-
c*   Mast equivalent beam finite element model with nonlinear
c*   joints to sinusoidal excitation by z torque wheel (torsion
c*   of the mast).
c*
c*   Created 16 October 1990
c*
c*   Mark Webster
c*
c*****
      implicit real*8 (a-h,o-z)
      integer i,j,icnt,ipas,flag
      integer ipvt(216),job
      real*8 x(216),xi(216)
      real*8 m(108,108),k(108,108),xold(216)
      real*8 k2,k3,f(216),dyn(108,108),an
      real*8 c(108,108),dx(216),hold(216),resp(12)
      real*8 dfdx(216,216),z(216),omd2
      real*8 delta(108),dum(108,108),ct(108,108)
      common pi,as,an,t,k2,k3,xl,dia,d,slp
      pi=4.0*atan(1.0)
      t=3.0**(0.5)
c* System Parameters
c* Structural parameters
      k2=1.61898e7
      k3=6.054573e6
      d=1.2124
      xl=1.119
      dia=sqrt(xl**2+d**2)
c* Nonlinear Joint Parameters
      an=0.035
      slp=0.6
      as=.000015
c* Frequency range and voltage input to torque wheels
      wmin=24.0
      wmax=28.023
      f0=60.0e-3
c* Torque wheel dynamics parameters
      anp=36433.0
      bn=23.44
      cn=372.34
c* Program parameters
      yerr=1.0d-7
      imax=28
      ichk=1
      flag=0
c* Read in mass, mode shape, and damping matrices
      open (unit=9,file='masc.d',access='sequential')
      read(9,101)
      do 5 i=1,108
5         read (9,104) (m(i,j),j=1,108)
          read(9,101)
          do 10 i=1,108
10         read(9,104) (dum(i,j),j=1,108)
           read(9,101)
           read(9,104) (xi(i),i=1,108)
           read(9,101)
           do 15 i=1,108
15         read(9,104) (ct(i,j),j=1,108)
          open (unit=10,file='mminit.d',access='sequential')
          read (10,104) (xi(i),i=1,216)
          do 20 i=1,216
20         hold(i)=xi(i)
c* Open file for output

```

```

        open (unit=8,file='ersp6.d',access='sequential')
c* Set up frequency range
        omd=(wmax-wmin)/50.0
        omg=wmax
        omd2=omd/5.0
        omg2=omg
c* Begin run
        do 100 ipas=1,imax
        write(6,*)ipas,'pass'
        ist=1
        do 3 i=1,216
        x(i)=hold(i)
25      dx(i)=0.0
        icnt=0
c* Torque Wheel dynamics
        fs=(f0*anp*(bn+cn)*omg**2)/((bn*cn-omg**2)**2+(omg**2)*
        +(cn+bn)**2)
        fc=(f0*anp*omg*(bn*cn-omg**2))/((bn*cn-omg**2)**2+
        +(omg**2)*(cn+bn)**2)
c* Check if converged, if not, first time take smaller step
c* second time move on
        30 if (icnt.gt.10) then
        do 35 i=1,12
35      resp(i)=0.0
        if (flag.eq.1)then
        do 40 i=1,216
40      hold(i)=xi(i)
        flag=0
        go to 110
        endif
        omg=omg2+omd2
        do 45 i=1,216
45      x(i)=xold(i)
        icnt=0
        flag=1
        go to 30
        endif
c* Increment solution
        do 50 i=1,216
50      x(i)=x(i)+dx(i)
        write(6,*)icnt,' pass'
c* Determine nonlinear stiffness and damping
        call stfdmps(x,k,c,omg)
        do 55 i=1,108
        do 55 j=1,108
        c(i,j)=c(i,j)+ct(i,j)
55      dyn(i,j)=k(i,j)-omg*omg*m(i,j)
        do 60 i=1,108
        f(i)=0.0
        f(i+108)=0.0
        do 60 j=1,108
        f(i)=f(i)+dyn(i,j)*x(j)-omg*c(i,j)*x(j+108)
        f(i+108)=f(i+108)+dyn(i,j)*x(j+108)+omg*c(i,j)*x(j)
60      continue
c* calculate the jacobian matrix for this system
        call jcobds(x,dfdx,omg,m,ct,f)
c* Apply forcing components
        f(108)=f(108)-fs
        f(216)=f(216)-fc
        do 65 i=1,216
        f(i)=-1.0*f(i)
65      continue
c* Solve (df/dx)*dx=-f using linpack
        call sgeco(dfdx,216,216,ipvt,rcond,z)
        job=0
        call sgesl(dfdx,216,216,ipvt,f,job)

```

```

c* Can now get new estimate for dx
  do 70 i=1,216
    dx(i)=f(i)
    icnt=icnt+1
c* Check for convergence
  do 75 i=1,108
    delta(i)=sqrt(dx(i)*dx(i)+dx(108+i)*dx(108+i))
75  if (delta(i).gt.yerr) go to 30
    do 80 i=1,216
      x(i)=x(i)+dx(i)
80  hold(i)=x(i)
    do 85 i=1,6
      resp(i)=x(i+102)
      resp(i+6)=x(i+210)
85  continue
c* Output frequency and response
110 write (8,104) omg
    write (8,104) (resp(i),i=1,6)
    write (8,104) (resp(i),i=7,12)
    if(ipas.eq.imax)then
      write (8,104) (x(i),i=1,216)
    endif
    do 90 i=1,216
90  xold(i)=x(i)
      flag=0
      omg2=omg
      omg=omg+omd
100 continue
      stop
    104 format (6(1x,g12.6))
    101 format (a20)
      end

```

```

c*****
c* Subroutine stfdmp
c* Calculates stiffness and damping matrix of the Mini-
c* Mast equivalent beam finite element model with nonlinear
c* joints - Natural Joint
c*
c* Created February 12, 1991
c*
c* Mark Webster
c*
c*****
subroutine stfdmps(x,k,c,wfw0)
implicit real*8 (a-h,o-z)
integer i,j
real*8 kel(12,12),cel(12,12),x(216),a1(6)
real*8 k(108,108),c(108,108),a2(6),b1(6)
real*8 b2(6),cp(6),cq(6),k2,k3,an,slp
common pi,as,an,t,k2,k3,xl,dia,d,slp
c* Geometric properties for calculating the stiffness and
c* damping matrices
so=0.734832
co=0.678223
to=so/co
so2=so**2
co2=co**2
ds=d**2
c* Zero stiffness and damping
do 60 i=1,108
do 60 j=1,108
c(i,j)=0.0
60 k(i,j)=0.0
c* calculate DF coefficients at each bay
do 20 i=1,6
a1(i)=0.0
20 b1(i)=0.0
ibt=1
do 32 ibay=1,18
ik=6*(ibay-1)
ikb=108+6*(ibay-1)
do 25 j=1,6
a2(j)=x(ik+j)
25 b2(j)=x(ikb+j)
call natdf(a1,b1,a2,b2,wfw0,cp,cq,ibt)
do 10 i=1,12
do 10 j=1,12
cel(i,j)=0.0
10 kel(i,j)=0.0
c* Use DF coefficients to calculate nonlinear stiffness matrix
kel(1,1)=(cp(4)+cp(5)+4.0*cp(6))*so2/4.0
kel(1,2)=t*(cp(4)-cp(5))*so2/4.0
kel(1,3)=(cp(4)+cp(5)-2.0*cp(6))*so*co/2.0
kel(1,4)=(2.0*cp(5)-cp(4)+2.0*cp(6))*d*co*so/(4.0*t)
kel(1,5)=(cp(4)+2.0*cp(6))*d*co*so/4.0
kel(1,6)=d*(2.0*cp(6)-cp(4)-cp(5))*so2/(4.0*t)
kel(1,7)=(cp(4)+cp(5)+4.0*cp(6))*so2/(-4.0)
kel(1,8)=t*(cp(5)-cp(4))*so2/4.0
kel(1,9)=(2.0*cp(6)-cp(4)-cp(5))*so*co/2.0
kel(1,10)=(cp(5)-2.0*cp(4)-2.0*cp(6))*d*co*so/(4.0*t)
kel(1,11)=(cp(5)+2.0*cp(6))*d*co*so/4.0
kel(1,12)=d*(cp(4)+cp(5)-2.0*cp(6))*so2/(4.0*t)
kel(2,2)=3.0*(cp(4)+cp(5))*so2/4.0
kel(2,3)=t*(cp(4)-cp(5))*so*co/2.0
kel(2,4)=(cp(4)+cp(5)*2.0)*d*co*so/(-4.0)
kel(2,5)=t*d*cp(4)*co*so/(4.0)
kel(2,6)=d*(cp(5)-cp(4))*so2/4.0
kel(2,7)=t*(cp(5)-cp(4))*so2/4.0

```

```

kel(2,8)=3.0*(cp(4)+cp(5))*so2/(-4.0)
kel(2,9)=t*(cp(5)-cp(4))*so*co/2.0
kel(2,10)=(2.0*cp(4)+cp(5))*d*co*so/(-4.0)
kel(2,11)=t*d*cp(5)*co*so/(-4.0)
kel(2,12)=d*(cp(4)-cp(5))*so2/4.0
kel(3,3)=cp(1)+cp(2)+cp(3)+(cp(4)+cp(5)+cp(6))*co2
kel(3,4)=d*(cp(2)*2.0-cp(1)-cp(3)+(cp(5)*2.0-cp(4)-cp(6))
1*co2)/(t*2.0)
kel(3,5)=d*(cp(1)-cp(3)+(cp(4)-cp(6))*co2)/2.0
kel(3,6)=(cp(4)+cp(5)+cp(6))*d*co*so/(-2.0*t)
kel(3,7)=(2.0*cp(6)-cp(4)-cp(5))*so*co/2.0
kel(3,8)=t*(cp(5)-cp(4))*so*co/2.0
kel(3,9)=-1.0*(cp(1)+cp(2)+cp(3)+(cp(4)+cp(5)+cp(6))*co2)
kel(3,10)=d*(cp(1)-2.0*cp(2)+cp(3)+(cp(5)-2.0*cp(4)+cp(6))
1*co2)/(2.0*t)
kel(3,11)=d*(cp(3)-cp(1)+(cp(5)-cp(6))*co2)/2.0
kel(3,12)=(cp(4)+cp(5)+cp(6))*d*co*so/(2.0*t)
kel(4,4)=ds*(cp(1)+4.0*cp(2)+cp(3)+(cp(6)+4.0*cp(5)+
1cp(4))*co2)/12.0
kel(4,5)=ds*(cp(3)-cp(1)+(cp(6)-cp(4))*co2)/(4.0*t)
kel(4,6)=ds*(cp(4)-2.0*cp(5)+cp(6))*so*co/12.0
kel(4,7)=(cp(4)-2.0*cp(5)-2.0*cp(6))*d*co*so/(4.0*t)
kel(4,8)=(cp(4)+2.0*cp(5))*d*co*so/4.0
kel(4,9)=d*(cp(1)-2.0*cp(2)+cp(3)+(cp(4)-2.0*cp(5)+cp(6))
1*co2)/(2.0*t)
kel(4,10)=ds*((2.0*cp(4)+2.0*cp(5)-cp(6))*co2-cp(1)-4.0
1*cp(2)-cp(3))/12.0
kel(4,11)=ds*(cp(1)-cp(3)+(2.0*cp(5)+cp(6))*co2)/(4.0*t)
kel(4,12)=ds*(2.0*cp(5)-cp(4)-cp(6))*so*co/12.0
kel(5,5)=ds*(cp(1)+cp(3)+(cp(4)+cp(6))*co2)/4.0
kel(5,6)=ds*(cp(6)-cp(4))*so*co/(4.0*t)
kel(5,7)=(cp(4)+2.0*cp(6))*d*co*so/(-4.0)
kel(5,8)=t*d*cp(4)*co*so/(-4.0)
kel(5,9)=d*(cp(3)-cp(1)+(cp(6)-cp(4))*co2)/2.0
kel(5,10)=ds*(cp(1)-cp(3)-(2.0*cp(4)+cp(6))*co2)/(4.0*t)
kel(5,11)=ds*(cp(6)*co2-cp(1)-cp(3))/(4.0)
kel(5,12)=ds*(cp(4)-cp(6))*so*co/(4.0*t)
kel(6,6)=ds*(cp(4)+cp(5)+cp(6))*so2/12.0
kel(6,7)=d*(cp(4)+cp(5)-2.0*cp(6))*so2/(4.0*t)
kel(6,8)=d*(cp(4)-cp(5))*so2/4.0
kel(6,9)=(cp(4)+cp(5)+cp(6))*d*co*so/(2.0*t)
kel(6,10)=ds*(2.0*cp(4)-cp(5)-cp(6))*so*co/12.0
kel(6,11)=ds*(cp(6)-cp(5))*so*co/(4.0*t)
kel(6,12)=ds*(cp(4)+cp(5)+cp(6))*so2/(-12.0)
kel(7,7)=(cp(4)+cp(5)+4.0*cp(6))*so2/4.0
kel(7,8)=t*(cp(4)-cp(5))*so2/4.0
kel(7,9)=(cp(4)+cp(5)-2.0*cp(6))*so*co/2.0
kel(7,10)=(2.0*cp(4)-cp(5)+2.0*cp(6))*d*co*so/(4.0*t)
kel(7,11)=-1.0*(cp(5)+2.0*cp(6))*d*co*so/4.0
kel(7,12)=d*(-2.0*cp(4)-2.0*cp(5)+4.0*cp(6))*so2/(8.0*t)
kel(8,8)=3.0*(cp(4)+cp(5))*so2/4.0
kel(8,9)=t*(cp(4)-cp(5))*so*co/2.0
kel(8,10)=(cp(5)+cp(4)*2.0)*d*co*so/(4.0)
kel(8,11)=t*d*cp(5)*co*so/(4.0)
kel(8,12)=d*(cp(5)-cp(4))*so2/4.0
kel(9,9)=cp(1)+cp(2)+cp(3)+(cp(4)+cp(5)+cp(6))*co2
kel(9,10)=d*(2.0*cp(2)-cp(1)-cp(3)+(2.0*cp(4)-cp(5)-cp(6))
1*co2)/(2.0*t)
kel(9,11)=d*(cp(1)-cp(3)+(cp(6)-cp(5))*co2)/2.0
kel(9,12)=(cp(4)+cp(5)+cp(6))*d*co*so/(-2.0*t)
kel(10,10)=ds*(cp(1)+4.0*cp(2)+cp(3)+(cp(6)+4.0*cp(4)+
1cp(5))*co2)/12.0
kel(10,11)=ds*(cp(3)-cp(1)+(cp(5)-cp(6))*co2)/(4.0*t)
kel(10,12)=ds*(2.0*cp(4)-cp(5)-cp(6))*co*so/(-12.0)
kel(11,11)=ds*(cp(1)+cp(3)+(cp(5)+cp(6))*co2)/4.0
kel(11,12)=ds*(cp(5)-cp(6))*co*so/(4.0*t)

```

```

kel(12,12)=ds*(cp(4)+cp(5)+cp(6))*so2/12.0
c*Calculate nonlinear damping element matrix
cel(1,1)=(cq(4)+cq(5)+4.0*cq(6))*so2/4.0
cel(1,2)=t*(cq(4)-cq(5))*so2/4.0
cel(1,3)=(cq(4)+cq(5)-2.0*cq(6))*so*co/2.0
cel(1,4)=(2.0*cq(5)-cq(4)+2.0*cq(6))*d*co*so/(4.0*t)
cel(1,5)=(cq(4)+2.0*cq(6))*d*co*so/4.0
cel(1,6)=d*(2.0*cq(6)-cq(4)-cq(5))*so2/(4.0*t)
cel(1,7)=(cq(4)+cq(5)+4.0*cq(6))*so2/(-4.0)
cel(1,8)=t*(cq(5)-cq(4))*so2/4.0
cel(1,9)=(2.0*cq(6)-cq(4)-cq(5))*so*co/2.0
cel(1,10)=(cq(5)-2.0*cq(4)-2.0*cq(6))*d*co*so/(4.0*t)
cel(1,11)=(cq(5)+2.0*cq(6))*d*co*so/4.0
cel(1,12)=d*(cq(4)+cq(5)-2.0*cq(6))*so2/(4.0*t)
cel(2,2)=3.0*(cq(4)+cq(5))*so2/4.0
cel(2,3)=t*(cq(4)-cq(5))*so*co/2.0
cel(2,4)=(cq(4)+cq(5)*2.0)*d*co*so/(-4.0)
cel(2,5)=t*d*cq(4)*co*so/(4.0)
cel(2,6)=d*(cq(5)-cq(4))*so2/4.0
cel(2,7)=t*(cq(5)-cq(4))*so2/4.0
cel(2,8)=3.0*(cq(4)+cq(5))*so2/(-4.0)
cel(2,9)=t*(cq(5)-cq(4))*so*co/2.0
cel(2,10)=(2.0*cq(4)+cq(5))*d*co*so/(-4.0)
cel(2,11)=t*d*cq(5)*co*so/(-4.0)
cel(2,12)=d*(cq(4)-cq(5))*so2/4.0
cel(3,3)=cq(1)+cq(2)+cq(3)+(cq(4)+cq(5)+cq(6))*co2
cel(3,4)=d*(cq(2)*2.0-cq(1)-cq(3)+(cq(5)*2.0-cq(4)-cq(6)
1*co2)/(t*2.0)
cel(3,5)=d*(cq(1)-cq(3)+(cq(4)-cq(6))*co2)/2.0
cel(3,6)=(cq(4)+cq(5)+cq(6))*d*co*so/(-2.0*t)
cel(3,7)=(2.0*cq(6)-cq(4)-cq(5))*so*co/2.0
cel(3,8)=t*(cq(5)-cq(4))*so*co/2.0
cel(3,9)=-1.0*(cq(1)+cq(2)+cq(3)+(cq(4)+cq(5)+cq(6))*co2
cel(3,10)=d*(cq(1)-2.0*cq(2)+cq(3)+(cq(5)-2.0*cq(4)+cq(6)
1*co2)/(2.0*t)
cel(3,11)=d*(cq(3)-cq(1)+(cq(5)-cq(6))*co2)/2.0
cel(3,12)=(cq(4)+cq(5)+cq(6))*d*co*so/(2.0*t)
cel(4,4)=ds*(cq(1)+4.0*cq(2)+cq(3)+(cq(6)+4.0*cq(5)+
1cq(4))*co2)/12.0
cel(4,5)=ds*(cq(3)-cq(1)+(cq(6)-cq(4))*co2)/(4.0*t)
cel(4,6)=ds*(cq(4)-2.0*cq(5)+cq(6))*so*co/12.0
cel(4,7)=(cq(4)-2.0*cq(5)-2.0*cq(6))*d*co*so/(4.0*t)
cel(4,8)=(cq(4)+2.0*cq(5))*d*co*so/4.0
cel(4,9)=d*(cq(1)-2.0*cq(2)+cq(3)+(cq(4)-2.0*cq(5)+cq(6)
1*co2)/(2.0*t)
cel(4,10)=ds*((2.0*cq(4)+2.0*cq(5)-cq(6))*co2-cq(1)-4.0
1*cq(2)-cq(3))/12.0
cel(4,11)=ds*(cq(1)-cq(3)+(2.0*cq(5)+cq(6))*co2)/(4.0*t)
cel(4,12)=ds*(2.0*cq(5)-cq(4)-cq(6))*so*co/12.0
cel(5,5)=ds*(cq(1)+cq(3)+(cq(4)+cq(6))*co2)/4.0
cel(5,6)=ds*(cq(6)-cq(4))*so*co/(4.0*t)
cel(5,7)=(cq(4)+2.0*cq(6))*d*co*so/(-4.0)
cel(5,8)=t*d*cq(4)*co*so/(-4.0)
cel(5,9)=d*(cq(3)-cq(1)+(cq(6)-cq(4))*co2)/2.0
cel(5,10)=ds*(cq(1)-cq(3)-(2.0*cq(4)+cq(6))*co2)/(4.0*t)
cel(5,11)=ds*(cq(6)*co2-cq(1)-cq(3))/(4.0)
cel(5,12)=ds*(cq(4)-cq(6))*so*co/(4.0*t)
cel(6,6)=ds*(cq(4)+cq(5)+cq(6))*so2/12.0
cel(6,7)=d*(cq(4)+cq(5)-2.0*cq(6))*so2/(4.0*t)
cel(6,8)=d*(cq(4)-cq(5))*so2/4.0
cel(6,9)=(cq(4)+cq(5)+cq(6))*d*co*so/(2.0*t)
cel(6,10)=ds*(2.0*cq(4)-cq(5)-cq(6))*so*co/12.0
cel(6,11)=ds*(cq(6)-cq(5))*so*co/(4.0*t)
cel(6,12)=ds*(cq(4)+cq(5)+cq(6))*so2/(-12.0)
cel(7,7)=(cq(4)+cq(5)+4.0*cq(6))*so2/4.0
cel(7,8)=t*(cq(4)-cq(5))*so2/4.0

```

```

cel(7,9)=(cq(4)+cq(5)-2.0*cq(6))*so*co/2.0
cel(7,10)=(2.0*cq(4)-cq(5)+2.0*cq(6))*d*co*so/(4.0*t)
cel(7,11)=-1.0*(cq(5)+2.0*cq(6))*d*co*so/4.0
cel(7,12)=d*(-2.0*cq(4)-2.0*cq(5)+4.0*cq(6))*so2/(8.0*t)
cel(8,8)=3.0*(cq(4)+cq(5))*so2/4.0
cel(8,9)=t*(cq(4)-cq(5))*so*co/2.0
cel(8,10)=(cq(5)+cq(4)*2.0)*d*co*so/(4.0)
cel(8,11)=t*d*cq(5)*co*so/(4.0)
cel(8,12)=d*(cq(5)-cq(4))*so2/4.0
cel(9,9)=cq(1)+cq(2)+cq(3)+(cq(4)+cq(5)+cq(6))*co2
cel(9,10)=d*(2.0*cq(2)-cq(1)-cq(3)+(2.0*cq(4)-cq(5)-cq(6))
1*co2)/(2.0*t)
cel(9,11)=d*(cq(1)-cq(3)+(cq(6)-cq(5))*co2)/2.0
cel(9,12)=(cq(4)+cq(5)+cq(6))*d*co*so/(-2.0*t)
cel(10,10)=ds*(cq(1)+4.0*cq(2)+cq(3)+(cq(6)+4.0*cq(4)+
1cq(5))*co2)/12.0
cel(10,11)=ds*(cq(3)-cq(1)+(cq(5)-cq(6))*co2)/(4.0*t)
cel(10,12)=ds*(2.0*cq(4)-cq(5)-cq(6))*co*so/(-12.0)
cel(11,11)=ds*(cq(1)+cq(3)+(cq(5)+cq(6))*co2)/4.0
cel(11,12)=ds*(cq(5)-cq(6))*co*so/(4.0*t)
cel(12,12)=ds*(cq(4)+cq(5)+cq(6))*so2/12.0
c* Bay 2 adjustments
  if(ibt.eq.2)then
c*Stiffness matrix
  kel(1,3)=-1.0*kel(1,3)
  kel(1,4)=(cp(5)-2.0*cp(4)-2.0*cp(6))*d*so*co/(4.0*t)
  kel(1,5)=d*(cp(5)+2.0*cp(6))*so*co/4.0
  kel(1,6)=(2.0*cp(6)-cp(4)-cp(5))*so2*d/(4.0*t)
  kel(1,9)=-1.0*kel(1,9)
  kel(1,10)=(2.0*cp(5)-cp(4)+2.0*cp(6))*so*co*d/(4.0*t)
  kel(1,11)=d*(cp(4)+2.0*cp(6))*so*co/4.0
  kel(2,3)=-1.0*kel(2,3)
  kel(2,4)=d*(2.0*cp(4)+cp(5))*so*co/(-4.0)
  kel(2,5)=t*d*cp(5)*so*co/(-4.0)
  kel(2,9)=-1.0*kel(2,9)
  kel(2,10)=d*(cp(4)+2.0*cp(5))*so*co/(-4.0)
  kel(2,11)=t*d*cp(4)*so*co/4.0
  kel(3,4)=(2.0*cp(2)-cp(1)-cp(3)+(2.0*cp(4)-cp(5)-cp(6))
1*co2)/(2.0*t)
  kel(3,5)=d*(cp(1)-cp(3)+(cp(6)-cp(5))*co2)/2.0
  kel(3,6)=-1.0*kel(3,6)
  kel(3,7)=-1.0*kel(3,7)
  kel(3,8)=-1.0*kel(3,8)
  kel(3,10)=(cp(1)-2.0*cp(2)+cp(3)+(cp(4)-2.0*cp(5)+cp(6))
1*co2)/(2.0*t)
  kel(3,11)=d*(cp(3)-cp(1)+(cp(6)-cp(4))*co2)/2.0
  kel(3,12)=-1.0*kel(3,12)
  kel(4,4)=ds*(cp(1)+4.0*cp(2)+cp(3)+(4.0*cp(4)+cp(5)+cp(6))
1*co2)/12.0
  kel(4,5)=ds*(cp(3)-cp(1)+(cp(5)-cp(6))*co2)/(4.0*t)
  kel(4,6)=ds*(2.0*cp(4)-cp(5)-cp(6))*so*co/12.0
  kel(4,7)=d*(2.0*cp(4)-cp(5)+2.0*cp(6))*so*co/(4.0*t)
  kel(4,8)=d*(2.0*cp(4)+cp(5))*so*co/4.0
  kel(4,9)=d*(cp(1)-2.0*cp(2)+cp(3)+(cp(5)-2.0*cp(4)+cp(6))
1*co2)/(2.0*t)
  kel(4,11)=ds*(cp(1)-cp(3)-(2.0*cp(4)+cp(6))*co2)/(4.0*t)
  kel(4,12)=ds*(cp(5)-2.0*cp(4)+cp(6))*so*co/12.0
  kel(5,5)=ds*(cp(1)+cp(3)+(cp(5)+cp(6))*co2)/4.0
  kel(5,6)=ds*(cp(6)-cp(5))*so*co/(4.0*t)
  kel(5,7)=d*(cp(5)+cp(6)*2.0)*so*co/(-4.0)
  kel(5,8)=t*d*cp(5)*so*co/4.0
  kel(5,9)=d*(cp(3)-cp(1)+(cp(5)-cp(6))*co2)/2.0
  kel(5,10)=ds*(cp(1)-cp(3)+(2.0*cp(5)+cp(6))*co2)/(4.0*t)
  kel(5,12)=ds*(cp(5)-cp(6))*so*co/(4.0*t)
  kel(6,9)=-1.0*kel(6,9)
  kel(6,10)=ds*(cp(4)-2.0*cp(5)+cp(6))*so*co/12.0

```



```

kel(6,11)=ds*(cp(6)-cp(4))*so*co/(4.0)
kel(7,9)=-1.0*kel(7,9)
kel(7,10)=d*(cp(4)-2.0*cp(5)-2.0*cp(6))*so*co/(4.0*t)
kel(7,11)=d*(cp(4)+2.0*cp(6))*so*co/(-4.0)
kel(8,9)=-1.0*kel(8,9)
kel(8,10)=d*(cp(4)+2.0*cp(5))*so*co/4.0
kel(8,11)=t*d*cp(4)*so*co/(-4.0)
kel(9,10)=d*(2.0*cp(2)-cp(1)-cp(3)+(cp(5)*2.0-cp(4)-cp(6))
1*co2)/(2.0*t)
kel(9,11)=d*(cp(1)-cp(3)+(cp(4)-cp(6))*co2)/2.0
kel(9,12)=-1.0*kel(9,12)
kel(10,10)=ds*(cp(1)+4.0*cp(2)+cp(3)+(cp(4)+4.0*cp(5)+cp(6))
1*co2)/12.0
kel(10,11)=ds*(cp(3)-cp(1)+(cp(6)-cp(4))*co2)/(4.0*t)
kel(10,12)=ds*(2.0*cp(5)-cp(4)-cp(6))*so*co/12.0
kel(11,11)=ds*(cp(1)+cp(3)+(cp(4)+cp(6))*co2)/4.0
kel(11,12)=ds*(cp(4)-cp(6))*so*co/(4.0*t)
c*Damping matrix
cel(1,3)=-1.0*cel(1,3)
cel(1,4)=(cq(5)-2.0*cq(4)-2.0*cq(6))*d*so*co/(4.0*t)
cel(1,5)=d*(cq(5)+2.0*cq(6))*so*co/4.0
cel(1,6)=(2.0*cq(6)-cq(4)-cq(5))*so2*d/(4.0*t)
cel(1,9)=-1.0*cel(1,9)
cel(1,10)=(2.0*cq(5)-cq(4)+2.0*cq(6))*so*co*d/(4.0*t)
cel(1,11)=d*(cq(4)+2.0*cq(6))*so*co/4.0
cel(2,3)=-1.0*cel(2,3)
cel(2,4)=d*(2.0*cq(4)+cq(5))*so*co/(-4.0)
cel(2,5)=t*d*cq(5)*so*co/(-4.0)
cel(2,9)=-1.0*cel(2,9)
cel(2,10)=d*(cq(4)+2.0*cq(5))*so*co/(-4.0)
cel(2,11)=t*d*cq(4)*so*co/4.0
cel(3,4)=(2.0*cq(2)-cq(1)-cq(3)+(2.0*cq(4)-cq(5)-cq(6))
1*co2)/(2.0*t)
cel(3,5)=d*(cq(1)-cq(3)+(cq(6)-cq(5))*co2)/2.0
cel(3,6)=-1.0*cel(3,6)
cel(3,7)=-1.0*cel(3,7)
cel(3,8)=-1.0*cel(3,8)
cel(3,10)=(cq(1)-2.0*cq(2)+cq(3)+(cq(4)-2.0*cq(5)+cq(6))
1*co2)/(2.0*t)
cel(3,11)=d*(cq(3)-cq(1)+(cq(6)-cq(4))*co2)/2.0
cel(3,12)=-1.0*cel(3,12)
cel(4,4)=ds*(cq(1)+4.0*cq(2)+cq(3)+(4.0*cq(4)+cq(5)+cq(6))
1*co2)/12.0
cel(4,5)=ds*(cq(3)-cq(1)+(cq(5)-cq(6))*co2)/(4.0*t)
cel(4,6)=ds*(2.0*cq(4)-cq(5)-cq(6))*so*co/12.0
cel(4,7)=d*(2.0*cq(4)-cq(5)+2.0*cq(6))*so*co/(4.0*t)
cel(4,8)=d*(2.0*cq(4)+cq(5))*so*co/4.0
cel(4,9)=d*(cq(1)-2.0*cq(2)+cq(3)+(cq(5)-2.0*cq(4)+cq(6))
1*co2)/(2.0*t)
cel(4,11)=ds*(cq(1)-cq(3)-(2.0*cq(4)+cq(6))*co2)/(4.0*t)
cel(4,12)=ds*(cq(5)-2.0*cq(4)+cq(6))*so*co/12.0
cel(5,5)=ds*(cq(1)+cq(3)+(cq(5)+cq(6))*co2)/4.0
cel(5,6)=ds*(cq(6)-cq(5))*so*co/(4.0*t)
cel(5,7)=d*(cq(5)+cq(6)*2.0)*so*co/(-4.0)
cel(5,8)=t*d*cq(5)*so*co/4.0
cel(5,9)=d*(cq(3)-cq(1)+(cq(5)-cq(6))*co2)/2.0
cel(5,10)=ds*(cq(1)-cq(3)+(2.0*cq(5)+cq(6))*co2)/(4.0*t)
cel(5,12)=ds*(cq(5)-cq(6))*so*co/(4.0*t)
cel(6,9)=-1.0*cel(6,9)
cel(6,10)=ds*(cq(4)-2.0*cq(5)+cq(6))*so*co/12.0
cel(6,11)=ds*(cq(6)-cq(4))*so*co/(4.0)
cel(7,9)=-1.0*cel(7,9)
cel(7,10)=d*(cq(4)-2.0*cq(5)-2.0*cq(6))*so*co/(4.0*t)
cel(7,11)=d*(cq(4)+2.0*cq(6))*so*co/(-4.0)
cel(8,9)=-1.0*cel(8,9)
cel(8,10)=d*(cq(4)+2.0*cq(5))*so*co/4.0

```

```

cel(8,11)=t*d*cq(4)*so*co/(-4.0)
cel(9,10)=d*(2.0*cq(2)-cq(1)-cq(3)+(cq(5)*2.0-cq(4)-cq(6))
1*co2)/(2.0*t)
cel(9,11)=d*(cq(1)-cq(3)+(cq(4)-cq(6))*co2)/2.0
cel(9,12)=-1.0*cel(9,12)
cel(10,10)=ds*(cq(1)+4.0*cq(2)+cq(3)+(cq(4)+4.0*cq(5)+cq(6))
1*co2)/12.0
cel(10,11)=ds*(cq(3)-cq(1)+(cq(6)-cq(4))*co2)/(4.0*t)
cel(10,12)=ds*(2.0*cq(5)-cq(4)-cq(6))*so*co/12.0
cel(11,11)=ds*(cq(1)+cq(3)+(cq(4)+cq(6))*co2)/4.0
cel(11,12)=ds*(cq(4)-cq(6))*so*co/(4.0*t)
endif
if(ibt.eq.1)then
  ibt=2
else
  ibt=1
endif
45  do 50 i=2,12
    do 50 j=1,i-1
      cel(i,j)=cel(j,i)
50   kel(i,j)=kel(j,i)
c*construct complete stiffness and damping matrices
  if(ibay.eq.1)then
    do 63 i=1,6
    do 63 j=1,6
      c(i,j)=cel(i+6,j+6)
63   k(i,j)=kel(i+6,j+6)
    go to 33
  endif
  ibc=6*(ibay-2)
  do 65 i=1,12
  do 65 j=1,12
    c(ibc+i,ibc+j)=c(ibc+i,ibc+j)+cel(i,j)
65   k(ibc+i,ibc+j)=k(ibc+i,ibc+j)+kel(i,j)
33  do 70 i=1,6
    a1(i)=a2(i)
70   b1(i)=b2(i)
32  continue
101 format(a20)
    return
  end

```

```

c*****
c*   SUBROUTINE jacobds-
c*
c*       This subroutine calculates the jacobian numerically
c*       with a backward-difference formula for the Mini-Mast truss
c*
c*       20 December 1990
c*
c*       Mark Webster
c*****
      subroutine jacobds(x,dfdx,wfw0,m,ct,f)
      implicit real*8 (a-h,o-z)
      integer i,j,ijk
      real*8 wfw0,k2,k3,an,slp
      real*8 k(108,108),f(216),cn(108,108)
      real*8 x(216),dfdx(216,216)
      real*8 xt(216),delt(216),ct(108,108)
      real*8 dyn(108,108),m(108,108),c(108,108)
      common pi,as,an,t,k2,k3,xl,dia,d,slp
      alf=0.0001
c* Zero Jacobian
      do 17 i=1,216
        do 17 j=1,216
          17 dfdx(i,j)=0.0
c* Progressively vary each parameter of equations and determine
c* Jacobian numerically
      do 100 ijk=1,216
        do 9 i=1,216
          9 delt(i)=0.0
          delt(ijk)=alf
          do 13 i=1,216
            c 13 xt(i)=x(i)-delt(i)
            13 xt(i)=x(i)-delt(i)*x(i)
c* calculate stiffness and damping matrices
            call stfdmps(xt,k,cn,wfw0)
c* calculate matrices for Jacobian
            do 30 i=1,108
              do 30 j=1,108
                c(i,j)=ct(i,j)+cn(i,j)
            30 dyn(i,j)=k(i,j)-wfw0*wfw0*m(i,j)
            do 80 i=1,216
              dfdx(i,ijk)=f(i)
            80 continue
            do 81 i=1,108
              do 81 j=1,108
                dfdx(i,ijk)=dfdx(i,ijk)-dyn(i,j)*xt(j)+wfw0*c(i,j)*xt(j+108)
                dfdx(i+108,ijk)=dfdx(i+108,ijk)-dyn(i,j)*xt(j+108)-wfw0*c(i,j)
                1*xt(j)
            81 continue
            100 continue
            do 84 i=1,216
              do 84 j=1,216
                dfdx(i,j)=dfdx(i,j)/(alf*x(j))
            84 continue
            return
            end

```

```

c*****
c*   SUBROUTINE natdf.f -
c*
c*       This subroutine calculates the describing function
c*       coefficients for the Mini-Mast truss with natural nonlinear
c*       joints for input into program mmresp.f.
c*
c*       January 11, 1991
c*
c*       Mark Webster
c*****
      subroutine natdf(a1,b1,a2,b2,wfw0,cp,cq,ibt)
      implicit real*8 (a-h,o-z)
      integer i,j
      real*8 k2,k3,xk3,xk2,phil,phi2,qb1(9),qb2(9)
      real*8 qa1(9),qa2(9),cp(6),cq(6),asdm,asdp
      real*8 di(6),a1(6),b1(6),d1(6),d2(6)
      real*8 a2(6),b2(6),pi,an,slp
      common pi,as,an,t,k2,k3,xl,dia,d,slp
      do 5 i=1,6
      di(i)=0.0
      d1(i)=0.0
      d2(i)=0.0
5      continue
      do 6 i=1,9
      qa1(i)=0.0
      qa2(i)=0.0
      qb1(i)=0.0
      qb2(i)=0.0
6      continue
c* Calculate absolute magnitude of the displacements of the bay
c* truss vertices
      qa1(1)=a1(1)+a1(6)*d*t/6.0
      qa1(2)=a1(2)-a1(6)*d/2.0
      qa1(3)=a1(3)-a1(4)*t*d/6.0+a1(5)*d/2.0
      qa1(4)=a1(1)-a1(6)*t*d/3.0
      qa1(5)=a1(2)
      qa1(6)=a1(3)+a1(4)*t*d/3.0
      qa1(7)=a1(1)+a1(6)*t*d/6.0
      qa1(8)=a1(2)+a1(6)*d/2.0
      qa1(9)=a1(3)-a1(4)*t*d/6.0-a1(5)*d/2.0
      qa2(1)=a2(1)+a2(6)*d*t/6.0
      qa2(2)=a2(2)-a2(6)*d/2.0
      qa2(3)=a2(3)-a2(4)*t*d/6.0+a2(5)*d/2.0
      qa2(4)=a2(1)-a2(6)*t*d/3.0
      qa2(5)=a2(2)
      qa2(6)=a2(3)+a2(4)*t*d/3.0
      qa2(7)=a2(1)+a2(6)*t*d/6.0
      qa2(8)=a2(2)+a2(6)*d/2.0
      qa2(9)=a2(3)-a2(4)*t*d/6.0-a2(5)*d/2.0
      qb1(1)=b1(1)+b1(6)*d*t/6.0
      qb1(2)=b1(2)-b1(6)*d/2.0
      qb1(3)=b1(3)-b1(4)*t*d/6.0+b1(5)*d/2.0
      qb1(4)=b1(1)-b1(6)*t*d/3.0
      qb1(5)=b1(2)
      qb1(6)=b1(3)+b1(4)*t*d/3.0
      qb1(7)=b1(1)+b1(6)*t*d/6.0
      qb1(8)=b1(2)+b1(6)*d/2.0
      qb1(9)=b1(3)-b1(4)*t*d/6.0-b1(5)*d/2.0
      qb2(1)=b2(1)+b2(6)*d*t/6.0
      qb2(2)=b2(2)-b2(6)*d/2.0
      qb2(3)=b2(3)-b2(4)*t*d/6.0+b2(5)*d/2.0
      qb2(4)=b2(1)-b2(6)*t*d/3.0
      qb2(5)=b2(2)
      qb2(6)=b2(3)+b2(4)*t*d/3.0
      qb2(7)=b2(1)+b2(6)*t*d/6.0

```

```

qb2(8)=b2(2)+b2(6)*d/2.0
qb2(9)=b2(3)-b2(4)*t*d/6.0-b2(5)*d/2.0
c* Calculate displacement of rods in truss
d1(1)=qa2(3)-qa1(3)
d1(2)=qa2(6)-qa1(6)
d1(3)=qa2(9)-qa1(9)
d2(1)=qb2(3)-qb1(3)
d2(2)=qb2(6)-qb1(6)
d2(3)=qb2(9)-qb1(9)
if(ibt.eq.1)then
p1=d/2.0+qa2(4)-qa1(1)
p2=t*d/2.0+qa2(5)-qa1(2)
p3=x1+qa2(6)-qa1(3)
d1(4)=sqrt(p1*p1+p2*p2+p3*p3)-dia
p1=d/2.0+qa2(7)-qa1(4)
p2=t*d/2.0+qa1(5)-qa2(8)
p3=x1+qa2(9)-qa1(6)
d1(5)=sqrt(p1*p1+p2*p2+p3*p3)-dia
p1=d+qa1(7)-qa2(1)
p2=x1+qa2(3)-qa1(9)
d1(6)=sqrt(p1*p1+p2*p2)-dia
p1=d/2.0+qb2(4)-qb1(1)
p2=t*d/2.0+qb2(5)-qb1(2)
p3=x1+qb2(6)-qb1(3)
d2(4)=sqrt(p1*p1+p2*p2+p3*p3)-dia
p1=d/2.0+qb2(7)-qb1(4)
p2=t*d/2.0+qb1(5)-qb2(8)
p3=x1+qb2(9)-qb1(6)
d2(5)=sqrt(p1*p1+p2*p2+p3*p3)-dia
p1=d+qb1(7)-qb2(1)
p2=x1+qb2(3)-qb1(9)
d2(6)=sqrt(p1*p1+p2*p2)-dia
go to 15
endif
p1=d/2.0+qa1(4)-qa2(1)
p2=t*d/2.0+qa1(5)-qa2(2)
p3=x1+qa2(3)-qa1(6)
d1(4)=sqrt(p1*p1+p2*p2+p3*p3)-dia
p1=d/2.0+qa1(7)-qa2(4)
p2=t*d/2.0+qa2(5)-qa1(8)
p3=x1+qa2(6)-qa1(9)
d1(5)=sqrt(p1*p1+p2*p2+p3*p3)-dia
p1=d+qa2(7)-qa1(1)
p2=x1+qa2(9)-qa1(3)
d1(6)=sqrt(p1*p1+p2*p2)-dia
p1=d/2.0+qa1(4)-qa2(1)
p2=t*d/2.0+qa1(5)-qa2(2)
p3=x1+qa2(3)-qa1(6)
d2(4)=sqrt(p1*p1+p2*p2+p3*p3)-dia
p1=d/2.0+qa1(7)-qa2(4)
p2=t*d/2.0+qa2(5)-qa1(8)
p3=x1+qa2(6)-qa1(9)
d2(5)=sqrt(p1*p1+p2*p2+p3*p3)-dia
p1=d+qa2(7)-qa1(1)
p2=x1+qa2(9)-qa1(3)
d2(6)=sqrt(p1*p1+p2*p2)-dia
15 do 10 i=1,6
10 di(i)=sqrt(d1(i)*d1(i)+d2(i)*d2(i))
c*calculate coefficients for six values of d
xk2=slp*k2
xk3=(1.0+an)*xk2/(1.0-an)
do 50 i=1,6
cq(i)=0.0
50 cp(i)=0.0
do 30 i=1,6
if(di(i).le.as)then

```

```

cp(i)=k2
cq(i)=0.0
go to 20
endif
asdm=as/di(i)-(1.0-as/di(i))*an
asdp=as/di(i)+(1.0-as/di(i))*an
phi1=asin(asdm)
phi2=pi-asin(asdp)
cp(i)=2.0*((k2-xk2)*(phi1/2.0-sin(2.0*phi1)/4.0+
+asdm*cos(phi1))+(xk3-k2)*(phi2/2.0-sin(2.0*phi2)/
+4.0+asdp*cos(phi2))+pi*(xk2-xk3+2.0*k2)/4.0)/pi
cq(i)=2.0*((xk2-k2)*(asdm**2)/2.0+(k2-xk3)*(asdp**2)
+/2.0+(xk2-xk3)*(0.5-as/di(i))+(xk2+xk3)*(1.0-
+as/di(i))*an)/(pi*wfw0)
20  if(i.gt.3)then
      cp(i)=cp(i)*k3/k2
      cq(i)=cq(i)*k3/k2
    endif
30  continue
    return
    end

```